A Theoretical and Computational Study on Active Wake Control

Thesis by

Luca Cortelezzi

In Partial Fulfillment of the Requirements

for the Degree of

Doctor of Philosophy

California Institute of Technology

Pasadena, California

1993

(Submitted September 15, 1992)

In memory of my uncle,

Piero Cortelezzi

1913–1992

Acknowledgements

I would like to express my sincere gratitude to my advisors, Dr. A. Leonard and Dr. J.C. Doyle, for their guidance, patience and availability. The many enlightening discussions, the crucial suggestions, and the opportunity to conduct this research in my own way, were greatly appreciated. Special thanks to Dr. A. Roshko, Dr. D.I. Pullin, and Dr. F.E. Marble, my thesis committee, for the valuable discussions and continuous encouragement. Thanks also to Dr. A. Prosperetti, who first introduced me to fluid mechanics during my undergraduate studies, for inspiring and encouraging my adventure at Caltech.

I am greatly indebted to Dr. R. Camassa for his guidance, moral support, patience, and sense of humor which have been invaluable throughout my graduate studies. I am also thankful to Dr. D.D. Holm who kindly sponsored my pleasant and instructive visit to the Center for Nonlinear Studies at the Los Alamos National Laboratories.

Special thanks to the system managers, Mr. P. Hardy, Dr. J.D. Melvin, and Mr. T.E. Welmers, for their help with the computer animation which complements the results obtained in the present dissertation. Thanks also to Mrs. J. Anderson and Mrs. P. Gladson, at the Aeronautical Library, for their assistance and availability.

This investigation would not have been possible without the financial support provided by the Office of Naval Research, the Air Force Office of Scientific Research, and Rockwell International.

Abstract

In the first part of this dissertation a two-dimensional unsteady separated flow past a semi-infinite plate with transverse motion is considered. The flow is assumed incompressible and at high Reynolds number. The rolling-up of the separated shear-layer is modelled by a point vortex whose time dependent circulation is predicted by an unsteady Kutta condition. A power-law starting flow is assumed along with a power-law for the transverse motion. The effects of the motion of the plate on the starting vortex circulation and trajectory are presented. A suitable vortex shedding mechanism is introduced and a class of flows involving several vortices is presented. Subsequently, a control strategy able to maintain constant circulation when a vortex is present is derived. An exact solution for the non-linear controller is then obtained. Dynamical system analysis is used to explore the performance of the controlled system. Finally, the control strategy is applied to a class of flows and the results are discussed.

In the second part of this dissertation the previous results are extended to the case of a two-dimensional unsteady separated flow past a plate of variable length. Again the rolling-up of the separated shear-layer is modelled by a vortex pair whose time dependent circulation is predicted by an unsteady Kutta condition. A power-law starting flow is assumed while the plate length is kept constant. The results of the simulations are presented and the model validated. A time-dependent scaling which unveils the universality of the phenomenon is discussed. The previous vortex shedding mechanism is implemented and a vortex merging scheme is tested in a class of flows involving several vortices and is shown to be highly accurate. Subsequently, a control strategy able to maintain constant circulation when a vortex pair is present is derived. An exact solution for the non-linear controller is obtained in the form of an ordinary differential equation. Dynamical system analysis is used to explore the performance of the controlled system and the existence of a controllability region is discussed. Finally, the control strategy is applied to two classes of flows and the results are presented.

Contents

Chapter 1

The semi-infinite forced plate

1.1 Introduction

Two-dimensional unsteady separation of an incompressible flow past a semi-infinite plate at high Reynolds number has been extensively studied in literature. Basically two different inviscid models have been used to predict this phenomenon. In the simpler case the rolling-up of the separated shear-layer is modelled by a point vortex with time varying circulation [1] [20] while in a more sophisticated approach a continuous vortex sheet is used (see Pullin [17]). This classical problem is a particular case of the more general one where the semi-infinite plate is allowed to move transversely to the flow. In the case in which the plate moves with constant transverse velocity into the fluid the problem represents the two-dimensional unsteady analog of the steady separation off the leading of a delta wing. Furthermore, as we are not constraining the plate velocity to be constant, the present study can be related to the current research on separation control where, for example, dynamical leading edge flaps are used to influence the large vortices on a delta wing (see [8]).

Following the pioneering work of Rott [20], we model the unsteady separation from the transversely moving plate by means of a point vortex whose time-dependent circulation is predicted by

an unsteady Kutta condition. The choice of this model is in part justified by the complexity of the problem and in part supported by the evidence that the model produces satisfactory results when the flow separates from the tip of a zero angle stationary wedge [20]. In the general case of a finite angle wedge the flow is complicated by the occurrence of a secondary separation [18] [20] which cannot be predicted by the present model. Furthermore, in the finite angle wedge case there is some ambiguity concerning the implementation of the Kutta condition [10].

First we investigate power-law starting flows in which the plate also moves with a power-law velocity. Because the equation of motion, which describes the trajectory of the vortex, is singular at the initial time, an analytical solution valid for small time is required and is obtained via perturbation analysis. When the plate is at rest the exact solution proposed by Rott [20] is recovered. In the general case, when the plate is allowed to move, the form of the solution depends on the power law exponents chosen for the free-stream and the plate velocity respectively. In particular, there exists a limiting value for the power law exponent of the plate velocity beyond which separation does not exist in this model. The numerical integration of the equation of motion provides details about the evolution of the flow for large times. We also discuss the potential for controlling the separation process by a prescribed transverse motion of the plate.

Extension of the above results to the case where several vortices are present is obtained by implementing a vortex shedding mechanism first proposed by Graham [9]. In this scheme, a new vortex is introduced into the flow every time the rate of circulation production changes sign. Eventually, Graham abandoned this scheme because it led to divergent results. In the present study further restrictions have been added to the original scheme producing a successful implementation. The set of equations which describe the evolution of the system grow in time, a new equation is added when a new vortex is introduced into the flow. The new equation is singular at the initial time and an approximate solution valid for small times is derived, as before, via perturbation theory. This analysis predicts a limiting value for the plate velocity beyond which the separation process

cannot take place. The numerical integration of the equations of motion provides details about the evolution of the system.

The above results show that the motion of the plate affects sensibly the flow separation and it therefore should be useful for control purposes. The possibility of actively controlling the flow separation is of great interest because, although extremely simple, this basic flow involves several important features common to many unsteady separation processes. In particular, because this flow can be interpreted as the two-dimensional unsteady analog of the three-dimensional steady separation over a delta wing, it could provide deeper insight about vortex management concepts in such three-dimensional flows [19]. Based on the observation that there exists a critical plate velocity beyond which the separation cannot take place in the model, we derive a control strategy which inhibits the production of further circulation when a vortex is present into the flow. Furthermore, we obtain for any time-dependent free-stream velocity the analytical closed form solution of the controller, i.e., the predicted motion of the plate that satisfies the Kutta condition without requiring further shedding of vorticity into the wake. The performance of the controller is then characterized by a dynamical system type of analysis. Finally, we discuss the results provided by two simulations in which the controller is successfully tested.

1.2 Mathematical formulation

In this section we introduce a mathematical model able to represent the phenomenon of two dimensional unsteady separation from the tip of a vertical semi-infinite plate which is allowed to move along the y-axis in the presence of an unsteady free-stream velocity. Let us assume that the regions of vorticity that separate from the boundary layer and are convected away are thin enough to justify a description by means of a vortex sheet. The consequent stretching and rolling up of the vortex sheet, due to the unsteadiness of the flow, suggests a more coarse description via point vortices.

The vortex sheet is not completely lost. It is assumed to consist of a sheet of negligible circulation that connects the feeding point to a point vortex of variable strength which is able to satisfy an unsteady Kutta condition. Mathematically the feeding vortex sheet is just the branch cut due to the logarithmic singularity representing the vortex.

The mathematical formulation of the problem can be simplified by choosing a frame of reference fixed to the plate so that the body can be identified with the negative imaginary axis of the complex plane. In this frame of reference the plate is still and the fluid moves parallel to the y-axis with velocity $-u_p(t)$. Then, the flow of an incompressible irrotational fluid about such a plate can be solved via conformal mapping. The Schwartz-Christoffel technique permits the transformation of the semi-infinite plate in the z-plane onto the real axis in the ζ-plane (see Figure 1.1) with the map:

$$z = -i\zeta^2. \tag{1.1}$$

Since Laplace's equation is linear and the boundary in the mapped plane is simple to treat, we can build the complex potential F by superimposing basic flows. Note that for convenience we are departing from the usual convention and taking the circulation positive when the flow rotates in the clockwise sense. Thus, the complex velocity field $w = \frac{dF}{d\zeta}$ in the mapped plane has the form:

$$\begin{aligned} w(\zeta,t) = U(t) + 2u_p(t)\zeta + \frac{i\Gamma_1(t)}{2\pi}\left(\frac{1}{\zeta-\zeta_1(t)} - \frac{1}{\zeta-\bar{\zeta}_1(t)}\right) \\ + \sum_{n=2}^{N} \frac{i\Gamma_n}{2\pi}\left(\frac{1}{\zeta-\zeta_n(t)} - \frac{1}{\zeta-\bar{\zeta}_n(t)}\right). \end{aligned} \tag{1.2}$$

In the above expression we have the free-stream velocity, U, the velocity of the plate, u_p, and N vortices at $\zeta = \zeta_n$ with their images at the complex conjugate position $\zeta = \bar{\zeta}_n$. Note that U is labeled free-stream velocity for simplicity, in reality, it is the leading order of the expansion of the potential flow past a finite plate about the tip of the plate. We allow the strength of the first vortex to depend on time so that the Kutta condition may be satisfied. We choose the convention that the vortex of variable strength is labeled with the subscript 1, so that any time a vortex is shed all the

others are renumbered.

The need to impose the Kutta condition is a consequence of the fact that the potential flow in the physical plane presents a square root singularity. In the ζ-plane the flow is non-singular since the singularity has been absorbed by the mapping. To remove the singularity in the z-plane the complex velocity (1.2) in the mapped plane has to be zero at the origin all the time. Solving for Γ_1 we obtain:

$$\Gamma_1 = 2\pi i \left(\frac{\zeta_1 \bar{\zeta}_1}{\zeta_1 - \bar{\zeta}_1}\right) \left[U + \sum_{n=2}^{N} \frac{i\Gamma_n}{2\pi} \left(\frac{\zeta_n - \bar{\zeta}_n}{\zeta_n \bar{\zeta}_n}\right)\right]. \tag{1.3}$$

Note Γ_1 does not depend directly on u_p because the motion of the plate reduces in the mapped plane to a stagnation point flow about the origin, in other words, the motion of the plate cannot affect the velocity of the fluid at the origin. However, a change in the position of the plate modifies the relative position of the vortices with respect to the tip and so Γ_1 will be affected indirectly.

To describe the motion of this system of vortices in the physical plane we use the following set of ordinary differential equations:

$$\begin{cases} \dfrac{d\bar{z}_1}{dt} + (\bar{z}_1 - \bar{z}_0)\dfrac{1}{\Gamma_1}\dfrac{d\Gamma_1}{dt} = \lim\limits_{z \to z_1} \left\{ \dfrac{d}{dz} \left[F - \dfrac{i\Gamma_1}{2\pi} \log(z - z_1) \right] \right\} \\ \dfrac{d\bar{z}_r}{dt} = \lim\limits_{z \to z_r} \left\{ \dfrac{d}{dz} \left[F - \dfrac{i\Gamma_r}{2\pi} \log(z - z_r) \right] \right\}, \end{cases} \tag{1.4}$$

with the initial conditions:

$$\begin{cases} z_1(t_s) = z_0 \\ z_r(t_s) = z_{r_s} \qquad r = 2...N, \end{cases} \tag{1.5}$$

where F is the complex potential and z_0 is the separation point. Note z_{r_s} was the final position of the vortex $r-1$ at the shedding time $t = t_s$ which becomes the initial position of the vortex r. Thus the number of equations increases anytime a new vortex is shed. The term containing $\frac{d\Gamma_1}{dt}$ in the first of the above equations is known as Brown and Michael's correction [1]. The motion of vortex of variable strength described by this equation guarantees no net force on the vortex and its connecting cut. The limit on the right hand side, which represents the complex velocity at the vortex location

without the self-induced contribution, has been left indicated to remind the reader that some care has to be taken in its computation. Note that:

$$\begin{aligned} F - \frac{i\Gamma_1}{2\pi}\log(z-z_1) &= F - \frac{i\Gamma_1}{2\pi}\log\left[z(\zeta)-z(\zeta_1)\right] \\ &= F - \frac{i\Gamma_1}{2\pi}\log(\zeta-\zeta_1) - \frac{i\Gamma_1}{4\pi}(\zeta-\zeta_1)\left[\left(\frac{d^2z}{d\zeta^2}\right)\left(\frac{dz}{d\zeta}\right)^{-1}\right]_{\zeta=\zeta_1} + \cdots . \end{aligned} \tag{1.6}$$

Taking the derivative with respect to z and then computing the limit, as z and ζ go to z_1 and ζ_1 respectively, the higher order terms not given go to zero at least fast as $O(\zeta-\zeta_1)$ and the last term in the above expression produces the so called Routh correction [5].

Now we consider if it is more convenient to solve the problem in the physical or in the mapped plane. In both cases we must use complicated transformations, but in the ζ-plane it seems easier to understand and to keep track of the different contributions. Once we have performed the change of variables, substituted for the complex potential and, carried out the limits required in the equations (1.4), we obtain:

$$\begin{cases} \left[2i\bar{\zeta}_1 + \dfrac{i\zeta_1\bar{\zeta}_1}{\zeta_1-\bar{\zeta}_1}\right]\dfrac{d\bar{\zeta}_1}{dt} - \left[\dfrac{i\bar{\zeta}_1^3}{\zeta_1(\zeta_1-\bar{\zeta}_1)}\right]\dfrac{d\zeta_1}{dt} = \\ \qquad \dfrac{i}{2\zeta_1}\left[U + 2u_p\zeta_1 - \dfrac{i\Gamma_1}{2\pi(\zeta_1-\bar{\zeta}_1)} + \displaystyle\sum_{n=2}^{N}\frac{i\Gamma_n}{2\pi}\frac{(\zeta_n-\bar{\zeta}_n)}{(\zeta_1-\zeta_n)(\zeta_1-\bar{\zeta}_n)} - \frac{i\Gamma_1}{4\pi\zeta_1}\right] \\ \qquad -i\bar{\zeta}_1^2\left[\dfrac{dU}{dt} + \displaystyle\sum_{n=2}^{N}\frac{i\Gamma_n}{2\pi}\left(\frac{1}{\zeta_n^2}\frac{d\zeta_n}{dt} - \frac{1}{\bar{\zeta}_n^2}\frac{d\bar{\zeta}_n}{dt}\right)\right]\left[U + \displaystyle\sum_{n=2}^{N}\frac{i\Gamma_n}{2\pi}\frac{\zeta_n-\bar{\zeta}_n}{\zeta_n\bar{\zeta}_n}\right]^{-1} \\ \dfrac{d\bar{\zeta}_r}{dt} = \dfrac{1}{4\zeta_r\bar{\zeta}_r}\left[U + 2u_p\zeta_r - \dfrac{i\Gamma_r}{2\pi(\zeta_r-\bar{\zeta}_r)} + \displaystyle\sum_{n\neq r}^{N}\frac{i\Gamma_n}{2\pi}\frac{(\zeta_n-\bar{\zeta}_n)}{(\zeta_r-\zeta_n)(\zeta_r-\bar{\zeta}_n)} - \frac{i\Gamma_r}{4\pi\zeta_r}\right], \end{cases} \tag{1.7}$$

with the initial conditions:

$$\begin{cases} \zeta_1(t_s) = 0 \\ \zeta_r(t_s) = \zeta_{r_s} \qquad r = 2...N, \end{cases} \tag{1.8}$$

where Γ_1 is given by (1.3). Note because of Brown and Michael's correction [1] the equations are coupled not just through the position of all the vortices but also through their velocities. The size and complexity of the problem is such to discourage any attempt of an analytical solution.

1.3 Starting vortex

In this section we will consider the problem of shedding the first vortex only. The starting vortex is of particular interest because it must handle the singularity of the potential flow. The equation of motion is:

$$\left[2i\bar{\zeta}_1 + \frac{i\zeta_1\bar{\zeta}_1}{\zeta_1 - \bar{\zeta}_1}\right]\frac{d\bar{\zeta}_1}{dt} - \left[\frac{i\bar{\zeta}_1^3}{\zeta_1(\zeta_1 - \bar{\zeta}_1)}\right]\frac{d\zeta_1}{dt} = \frac{i}{2\zeta_1}\left[U + 2u_p\zeta_1 - \frac{i\Gamma_1}{2\pi(\zeta_1 - \bar{\zeta}_1)} - \frac{i\Gamma_1}{4\pi\zeta_1}\right] - \frac{i\bar{\zeta}_1^2}{U}\frac{dU}{dt}, \tag{1.9}$$

where

$$\Gamma_1 = 2\pi i\left(\frac{\zeta_1\bar{\zeta}_1}{\zeta_1 - \bar{\zeta}_1}\right)U, \tag{1.10}$$

and the initial condition is

$$\zeta_1(0) = 0. \tag{1.11}$$

The second and third term on the left hand side and the last term on the right hand side of the equation of motion are the contributions due to Brown and Michael's correction [1]. Consequently, the velocity of the vortex depends not only on the local velocity but also on the free-stream acceleration. The term before the last on the right hand side is Routh's correction [5] which is consequence of the limiting process. Note if $u_p = 0$ and U has the form of a power-law then the problem can be solved analytically in close form (see Rott [20]), but in the general case is necessary to integrate the equations numerically.

Algorithms for the solution of the ordinary differential equations are well known and basically well behaved if the solution is smooth and, if the integration is carried out carefully, the results can be very precise. A singularity can be a source of trouble, in general, but if it affects the initial condition it can be particularly annoying because many algorithms cannot even start. This is exactly our case since the problem is singular at $t = 0$. To overcome this difficulty is necessary to produce an approximate analytical solution valid for small time so that the integrator can start from a well

behaved point.

To find a valid expansion we stretch the time about $t = 0$ defining a new time

$$\tilde{t} = \frac{t}{\epsilon}, \tag{1.12}$$

and expand in ϵ all the quantities which depend on time. We set:

$$\zeta_1(t) = \epsilon^{\alpha} \left(\zeta_{1_1}(\tilde{t}) + \epsilon^{\beta} \zeta_{1_2}(\tilde{t}) + \cdots \right) \tag{1.13}$$

and,

$$U(t) = V t^m = \epsilon^m V \tilde{t}^m \tag{1.14}$$

$$u_p(t) = v_p t^n = \epsilon^n v_p \tilde{t}^n, \tag{1.15}$$

where α and β have to be determined balancing the different terms of the equation and, m and n are positive real numbers. Substituting these relationship into the equations (1.9–1.11), at the first order we have:

$$\begin{aligned} &\left[2i\bar{\zeta}_{1_1} + \frac{i\zeta_{1_1}\bar{\zeta}_{1_1}}{\zeta_{1_1} - \bar{\zeta}_{1_1}} \right] \epsilon^{2\alpha-1} \frac{d\bar{\zeta}_{1_1}}{d\tilde{t}} - \left[\frac{i\bar{\zeta}_{1_1}^3}{\zeta_{1_1}(\zeta_{1_1} - \bar{\zeta}_{1_1})} \right] \epsilon^{2\alpha-1} \frac{d\zeta_{1_1}}{d\tilde{t}} = \\ &\qquad \frac{i}{2\zeta_{1_1}} \epsilon^{-\alpha} \left[2U + 2u_p \zeta_{1_1} \epsilon^{\alpha} - \frac{i\Gamma_1}{2\pi(\zeta_{1_1} - \bar{\zeta}_{1_1})} \epsilon^{-\alpha} - \frac{i\Gamma_1}{4\pi\zeta_{1_1}} \epsilon^{-\alpha} \right] - \frac{i\bar{\zeta}_{1_1}^2}{U} \epsilon^{2\alpha-1} \frac{dU}{d\tilde{t}}, \end{aligned} \tag{1.16}$$

where

$$\Gamma_1 = 2\pi i \epsilon^{\alpha} \left(\frac{\zeta_{1_1}\bar{\zeta}_{1_1}}{\zeta_{1_1} - \bar{\zeta}_{1_1}} \right) U, \tag{1.17}$$

and the initial condition is

$$\zeta_{1_1}(0) = 0. \tag{1.18}$$

Note $\Gamma_1 \sim O(\epsilon^{m+\alpha})$ which is consistent with the fact that the strength of the vortex has to be zero at time $t = 0$. By inspection we can see that the terms related with the vortex velocity or with the rate of circulation production are $\sim O(\epsilon^{2\alpha-1})$, the terms depending of U are $\sim O(\epsilon^{m-\alpha})$ and, the term containing u_p is $\sim O(\epsilon^n)$. Hence, in general, is not possible to find an α which balances all the

first order terms. Since it is difficult to predict which terms should be kept, let us proceed blindly by computing $\alpha = \alpha_m$ when the term containing u_p is assumed to be negligible and $\alpha = \alpha_n$ when the terms depending on U are supposedly negligibles. Then, the leading order is obtained in the following way:

$$\alpha = \min\{\alpha_m = \frac{m+1}{3}, \alpha_n = \frac{n+1}{2}\}, \tag{1.19}$$

Now, the second order is obtained by balancing all the terms of the equations and, of course, it is direct consequence of the choice made at the first order. Hence if

$$\alpha = \alpha_m \qquad \Rightarrow \qquad \beta_m = \frac{3(n+1) - 2(m+1)}{3}, \tag{1.20}$$

otherwise

$$\alpha = \alpha_n \qquad \Rightarrow \qquad \beta_n = \frac{2(m+1) - 3(n+1)}{2}. \tag{1.21}$$

Figure 1.2 shows in which domain the terms depending on U are dominant and where, instead, the term containing u_p is dominant. The common boundary identifies the (m, n) pairs for which all the terms in the equation balance at the same time. It is interesting to observe that the case of the two-dimensional unsteady analog of the steady separation over a delta wing is within the region where U is dominant.

With this information about the order of the expansion we can proceed to compute the approximate solution. Note both the time derivatives of ζ_1 and $\bar{\zeta}_1$ appear in the equation (1.9), thus it becomes necessary to take the complex conjugate of the equation and solve for one of the derivatives. However it is more convenient to separate real and imaginary parts and to switch to polar coordinates. Equation (1.9) becomes:

$$\begin{cases} \dfrac{d\rho_1}{dt} = \dfrac{U \sin\theta_1}{12\rho_1^2} - \dfrac{\rho_1}{3U}\dfrac{dU}{dt} - \dfrac{u_p \cos^2\theta_1}{3\rho_1} \\ \dfrac{d\theta_1}{dt} = \dfrac{U \cos 2\theta_1}{8\rho_1^3 \cos\theta_1} + \dfrac{u_p \sin 2\theta_1}{2\rho_1^2}, \end{cases} \tag{1.22}$$

with the initial conditions:

$$\begin{cases} \rho_1(0) = 0 \\ \theta_1(0) = \theta_0. \end{cases} \tag{1.23}$$

The initial condition for θ_1 will be derived below because we do not know a priori the initial direction of the vortex.

Although, the following results are valid for any m and n real positive, we are limiting our discussion to $m, n = 0, 1, 2$, i.e., only step, ramp and parabolic trends are considered. The following results represent the approximate trajectory of the vortex in the mapped plane. One should keep in mind that inverting the map implies doubling the angles and squaring the radii.

Let us consider first the case where the terms depending on U are dominant, i.e., $\alpha = \alpha_m < \alpha_n$ and $\beta = \beta_m$. Then the approximate solution up to second order valid for $0 \leq t \ll 1$ is:

$$\begin{cases} \rho_1(t) = \left[\dfrac{|V|}{2^{\frac{5}{2}}(2m+1)}\right]^{\frac{1}{3}} t^{\alpha} - \dfrac{[2^{\frac{5}{2}}(2m+1)]^{\frac{1}{3}}}{2[2(5m+2)+3(n+1)]} \dfrac{v_p}{|V|^{\frac{1}{3}}} t^{\alpha+\beta} \\ \theta_1(t) = sgn(V)\dfrac{\pi}{4} + \dfrac{3[2(2m+1)]^{\frac{2}{3}}}{2(5m+2)+3(n+1)} \dfrac{v_p}{V^{\frac{2}{3}}} t^{\beta}, \end{cases} \tag{1.24}$$

where $\zeta_1 = i\rho_1(\sin\theta_1 + i\cos\theta_1)$ and, the strength of the vortex is:

$$\Gamma_1(t) = \frac{\rho_1(t)}{\cos\theta_1(t)} \pi V t^m. \tag{1.25}$$

Note if the plate is at rest (i.e., $v_p = 0$) the higher order corrections are zero and the first order expression becomes the analytical closed form solution to the problem, first obtained by Rott [20] by taking advantage of the self-similarity of the flow. The exact analytical solution of the problem for an arbitrary free-stream velocity is presented in the appendix.

Figures 1.3–1.6 show the results for this case when $m = 0, 1, 2$. The vortex takes off and moves on a trajectory always perpendicular to the plate since $\theta_1(t) = \frac{\pi}{4}$ satisfies identically the second equation of the set (1.22) for all m. Figure 1.4 shows how the rate of circulation production depends on the free-stream acceleration. For the impulsively started case $\frac{dU}{dt}$ is a delta function and $\frac{d\Gamma_1}{dt}$

is initially infinite while for the ramp case $\frac{dU}{dt}$ is a step function and $\frac{d\Gamma_1}{dt}$ starts with an infinite derivative. Figures 1.5 and 1.6 show the instantaneous streamlines for $m = 0, 1$.

We can also make a comparison with Pullin's computation [17] in which the problem has been solved numerically using a full vortex sheet. Because of the lack of data it is not possible to compute the locus of the center of vorticity of the spiral and compare it with the trajectory of our vortex, but we find good agreement between the time dependent circulations: the power laws are exactly the same, only the multiplicative constants are slightly different.

$\diamond$	$-Pullin$	$-Current\ \ Results$
$m = 0$	$\Gamma_1 = \left(\frac{3}{4}\right)^{\frac{1}{3}} J_0 V^{\frac{4}{3}} t^{\frac{1}{3}}$	$\Gamma_1 = \left(\frac{1}{2}\right)^{\frac{1}{3}} \pi V^{\frac{4}{3}} t^{\frac{1}{3}}$
	$J_0 = 2.640$	$J_0^* = 2.744$
$m = 1$	$\Gamma_1 = \left(\frac{3}{8}\right)^{\frac{1}{3}} J_1 V^{\frac{4}{3}} t^{\frac{5}{3}}$	$\Gamma_1 = \left(\frac{1}{6}\right)^{\frac{1}{3}} \pi V^{\frac{4}{3}} t^{\frac{5}{3}}$
	$J_1 = 2.185$	$J_1^* = 2.397$
$m = 2$	$\Gamma_1 = \left(\frac{1}{4}\right)^{\frac{1}{3}} J_2 V^{\frac{4}{3}} t^3$	$\Gamma_1 = \left(\frac{1}{10}\right)^{\frac{1}{3}} \pi V^{\frac{4}{3}} t^3$
	$J_2 = 2.079$	$J_2^* = 2.315$

The constant J_m are computed numerically in Pullin's work [17]. To compute the effective J_m^* for our results we equate the two circulations for the same m. Note how the disagreement increases as m becomes large, i.e., when the circulation at later times becomes more and more important. Furthermore, because of the self-similarity, a qualitative comparison is possible between the instantaneous streamlines showed in Figure 1.5 and those presented by Pullin [17].

Figures 1.7–1.12 show how the motion of the plate, when $n = 1$, modifies the previous results for $m = 1$. When $v_p > 0$ the plate is moving into the fluid and the angle of the initial trajectory

and the circulation increase while the radius decreases with respect to the unforced case. In this case the fluid has a "harder time" going around the tip so a higher circulation is required to satisfy the Kutta condition, see Figures 1.9 and 1.10. In addition the vortex is carried downward along the plate so the angle increases but, at the same time, it also feels its image which pushes it upstream thus the radius increases more slowly (see Figure 1.8). If $v_p < 0$ the plate is pulled out of the fluid and the above arguments can be reversed, see Figures 1.8–1.10. The fluid can go around the tip more easily, requiring less circulation, while the plate moves away from the vortex, decreasing the angle. The effect of the image is reduced hence the vortex is convected away, increasing the radius. Figures 1.11–1.12 show the instantaneous streamlines for the forced cases.

Now let us see what happens when the term containing u_p becomes dominant, i.e., $\alpha = \alpha_n < \alpha_m$ and $\beta = \beta_n$. It is worth remembering that, because of our assumption, if $U(t) = 0$ then the plate can slip back and forth through the fluid without shedding any vorticity. Physically when the plate starts to move forward and $U(t) = 0$ there is no separation, the boundary layer builds up uniformly on both sides starting from the leading edge. If we start the motion in reverse the boundary layer is released into the fluid creating a thin wake. Now if we add a cross flow and $v_p > 0$ our semi-infinite plate flow can be viewed as blowing near the leading edge of a flat wing at angle of attack, for $v_p < 0$ it represents a trailing edge flow. The approximate solution up to second order valid for $0 \leq t \ll 1$ has the following form:

$$\begin{cases} \rho_1(t) = \sqrt{\dfrac{2}{2(m+1)+3n+1}}\sqrt{-v_p}\,t^{\alpha} \\ \theta_1(t) = \dfrac{V}{v_p}\dfrac{\sqrt{2[2(m+1)+3n+1]^3}}{32(2m+1)}\dfrac{t^{\beta}}{\sqrt{-v_p}}, \end{cases} \tag{1.26}$$

and the strength of the vortex is:

$$\Gamma_1(t) = \frac{\rho_1(t)}{\cos\theta_1(t)}\pi V t^m. \tag{1.27}$$

Note the term $\sqrt{-v_p}$ which makes the solution imaginary if $v_p > 0$. A possible interpretation is that

the model does not know, in this case, on which side of the plate to put the vortex. The connection with the physics is the following: at early times the cross flow is so weak in comparison to the speed of the plate that only the boundary layer can be recognized. When $v_p < 0$ there are no such difficulties and a weak vortex leaves the plate along the imaginary axis. It is worth observing that the second order correction to the radius ρ_1 is in this case identically zero.

Figures 1.13–1.18 show the results of the simulation when $m = 1$ and $n = 0$. Note in this case the plate moves initially with infinite acceleration which gives more insight about the term $\sqrt{-v_p}$. The vortex leaves parallel to the plate, then the trajectory bends because of the cross flow, see Figure 1.14. The rate of circulation production and the total circulation are very similar to those presented for the unforced case, see Figures 1.15 and 1.16. Nevertheless, the instantaneous streamline pattern is completely different, see Figure 1.17 and 1.18.

Let us see now if there is any choice of the parameters so that $\alpha = \alpha_m = \alpha_n$ and $\beta = \beta_m = \beta_n$. We find that the combination $m = 2$ and $n = 1$ satisfies these conditions. In this case all the terms in the equation (1.16) are of the same importance and consequently it becomes more difficult to find an approximate solution. However, it is possible to derive the leading order when the ratio between the magnitudes of the free-stream and the plate velocities is very large or very small with respect to unity.

If $\left|\frac{V}{v_p}\right| \gg 1$ then the terms depending on U are dominant and the leading order solution valid for $0 \leq t \ll 1$ is:

$$\begin{cases} \rho_1(t) = \left[\dfrac{|V|}{2^{\frac{5}{2}}(2m+1)}\right]^{\frac{1}{3}} t^{\alpha} \\ \theta_1(t) = sgn(V)\dfrac{\pi}{4} + \dfrac{v_p}{V}\left(\dfrac{V}{2(2m+1)}\right)^{\frac{1}{3}}. \end{cases} \tag{1.28}$$

Note this result is just the leading order of the solution (1.24) with the departure angle modified. Figures 1.19–1.24 show the results of the numerical integration when $m = 2$ and $n = 1$. From the comparison with the unforced case we see that the vortex no longer takes off in a direction

perpendicular to the plate, instead its departure angle is corrected in agreement with the sign of the large parameter, see Figure 1.20. The motion of the plate affects slightly the rate of circulation production and the total circulation, see Figures 1.21 and 1.22. When $v_p > 0$ a larger amount of circulation is necessary to satisfy the Kutta condition. Figures 1.23 and 1.24 permit comparison of the instantaneous streamline patterns when the plate velocity is positive and negative respectively. It is interesting to observe that the closeness of the solutions for early times (see (1.24) and (1.28)) is reflected in the similarity existing between this simulation and that presented in Figures 1.8–1.12.

When $\left|\frac{V}{v_p}\right| \ll 1$ and $v_p > 0$ the flow resembles the separation at the leading edge of a plate at angle of attack. The leading order solution valid for $0 \leq t \ll 1$ has the form:

$$\begin{cases} \rho_1(t) = \frac{1}{2}\left[\left(\frac{|V|}{2m+1}\right)^{\frac{1}{3}} + \frac{1}{24}\frac{|V|}{v_p}\right] t^{\alpha} \\ \theta_1(t) = sgn(V)\left(\frac{\pi}{2} - \frac{1}{2}\sqrt{\left[\left(\frac{|V|}{2m+1}\right)^{\frac{1}{3}} + \frac{1}{24}\frac{|V|}{v_p}\right]^{-1}\frac{|V|}{v_p}}\right). \end{cases} \tag{1.29}$$

The vortex takes off almost tangent to the imaginary axis, (see Figure 1.26) and it is convected downstream along the plate forming a little separation bubble, see Figure 1.29.

Finally, if $\left|\frac{V}{v_p}\right| \ll 1$ and $v_p < 0$ the flow is similar to the separation from the trailing edge of a plate at angle of attack. The leading order solution valid for $0 \leq t \ll 1$ is:

$$\begin{cases} \rho_1(t) = \sqrt{\frac{-v_p}{2m+1}}\, t^{\alpha} \\ \theta_1(t) = -\frac{1}{8}\frac{V}{v_p}\sqrt{\frac{2m+1}{-v_p}}. \end{cases} \tag{1.30}$$

In this case the vortex is left behind on a trajectory which makes a small angle with respect to the direction identified by the plate, see Figure 1.26 and 1.30. Note how the ratio between the magnitudes of the two velocities is always present in the correction of the departure angle. Based on this observation we can conclude that if the effects of the free-stream and those due to the motion of the plate are of the same order then the starting vortex can leave the plate with any angle. This

seems to be physically acceptable and naturally complements the results obtained for the other two more radical situations. Figures 1.25–1.30 show a comparison between the last two cases and the unforced solution. In contrast with the previous simulation (see Figures 1.20–1.24) the motion of the plate strongly affects the evolution of the system in this case. This effect is particularly evident in the trends of the rate of circulation production and total circulation where more than a factor two separates the case where $v_p > 0$ from those where the plate velocity is negative.

From the results presented in this investigation it follows that the motion of the plate is a strong candidate for the active control of the separation process. A careful choice of the motion of the plate in relation with the free-stream condition can produce results that vary from a large modification of the flow structure to fine tuning of the production of circulation.

1.4 Code validation

As pointed out in section 1.3, setting $u_p(t) = 0$ in equation (1.24) recovers the exact solution of equation (1.22) for $U(t) = Vt^m$. With this result we can check and validate the numerical integration carried out with a modified Runge-Kutta-Feldberg fourth-fifth order scheme [2]. Below are some data obtained running the code in double precision on a VAX station 3100, setting the local error tolerance at 10^{-8} and using the approximate solution (1.24) up to time $t = 10^{-5}$:

m	t_{final}	$error$	$CPU(sec)$
0	1.0093	5.72×10^{-10}	11.42
1	1.0058	3.65×10^{-10}	13.09
2	1.0019	1.69×10^{-16}	5.18

where the relative error has been computed as

$$error = \left| \frac{Sol_{ex}(t_{final}) - Sol_{num}(t_{final})}{Sol_{ex}(t_{final})} \right|.$$

It is very encouraging to observe that the total error at $t_{final} \approx 1$ is two orders of magnitude smaller than the local error threshold.

1.5 New vortex

In this section we will consider the problem of shedding a new vortex when $N-1$ other vortices are already present in the flow. If t_s is the shedding time then it is crucial to analyze the transition from t_s^- to t_s^+. Up to the time t_s^- vortex 1 has variable strength such that the Kutta condition is satisfied. At time $t = t_s$ this vortex has its strength frozen and, all the vortices renumbered. Finally at t_s^+ a new vortex 1 is introduced into the flow to remove the square root singularity. If we restrict our simulation to the case where the shed vortices have alternate sign, then we can model the vortex shedding making the assumption that the time $t = t_s$ is determined by the condition:

$$\left. \frac{d\Gamma_1}{dt} \right|_{t=t_s} = 0. \tag{1.31}$$

Assuming

$$\left. \frac{d\Gamma_1}{dt} \right|_{t=t_s^-} = - \left. \frac{d\Gamma_1}{dt} \right|_{t=t_s^+}, \tag{1.32}$$

the circulation produced before t_s is of opposite sign of that produced after t_s , so that t_s is the proper time to freeze the former vortex and introduce a new one. Any other choice for the shedding time implies the arbitrary production of more than one vortex of the same sign or the existence of a vortex which strength decreases in time. The latter situation is physically unacceptable. This procedure has been implemented by Graham [9] to simulate the flow induced by an oscillating diamond shaped cylinder. Eventually he abandoned this strategy because of a divergence in his calculation. We

do not have enough information to understand this negative result but in our simulations such a divergence is not present.

The quality of the simulation with many vortices depends in large part on the shedding mechanism. To avoid any ambiguity we have to restrict ourselves to cases in which the rate of circulation production presents only one peak or trough between two consecutive zero crossing or, equivalently, that $\frac{d^2\Gamma_1}{dt^2}$ does not change sign between two zero crossing. For example, let us assume that in a particular interval of time $\frac{d\Gamma_1}{dt}$ is positive and has two peaks. Then it is not clear whether one or two vortices will be shed. It probably depends on the deepness of the trough separating the peaks. If the trough is very deep it seems reasonable to shed two vortices otherwise just one. Although these restrictions limit the applicability of our model there still are numerous flows we can simulate.

With this in mind let us start the analysis of the equation of motion of the new vortex. The equation has the following form:

$$\left[2i\bar{\zeta}_1 + \frac{i\zeta_1\bar{\zeta}_1}{\zeta_1 - \bar{\zeta}_1}\right]\frac{d\bar{\zeta}_1}{dt} - \left[\frac{i\bar{\zeta}_1^3}{\zeta_1(\zeta_1 - \bar{\zeta}_1)}\right]\frac{d\zeta_1}{dt} =$$
$$\frac{i}{2\zeta_1}\left[U + 2u_p\zeta_1 - \frac{i\Gamma_1}{2\pi(\zeta_1 - \bar{\zeta}_1)} + \sum_{n=2}^{N}\frac{i\Gamma_n}{2\pi}\frac{(\zeta_n - \bar{\zeta}_n)}{(\zeta_1 - \zeta_n)(\zeta_1 - \bar{\zeta}_n)} - \frac{i\Gamma_1}{4\pi\zeta_1}\right] \tag{1.33}$$
$$-i\bar{\zeta}_1^2\left[\frac{dU}{dt} + \sum_{n=2}^{N}\frac{i\Gamma_n}{2\pi}\left(\frac{1}{\zeta_n^2}\frac{d\zeta_n}{dt} - \frac{1}{\bar{\zeta}_n^2}\frac{d\bar{\zeta}_n}{dt}\right)\right]\left[U + \sum_{n=2}^{N}\frac{i\Gamma_n}{2\pi}\frac{\zeta_n - \bar{\zeta}_n}{\zeta_n\bar{\zeta}_n}\right]^{-1},$$

where

$$\Gamma_1 = 2\pi i\left(\frac{\zeta_1\bar{\zeta}_1}{\zeta_1 - \bar{\zeta}_1}\right)\left[U + \sum_{n=2}^{N}\frac{i\Gamma_n}{2\pi}\left(\frac{\zeta_n - \bar{\zeta}_n}{\zeta_n\bar{\zeta}_n}\right)\right], \tag{1.34}$$

with the initial condition

$$\zeta_1(t_s) = 0. \tag{1.35}$$

Note that this equation, although much more complicated in appearance, has exactly the same structure as that for the starting vortex (see 1.9). It is singular at the initial time also, except that up through time $t = t_s^-$ there is another vortex which satisfies the Kutta condition. Consequently it is reasonable to expect a different time behavior for $0 \leq (t - t_s) \ll 1$. Once again it is necessary to

find an approximate analytical solution so that the numerical integration can start smoothly. Let us stretch the time about $t = t_s$ defining a new time

$$\tilde{t} = \frac{t - t_s}{\epsilon}, \tag{1.36}$$

and then set

$$\zeta_1(t) = \epsilon^{\alpha} \left(\zeta_{1_1}(\tilde{t}) + \epsilon^{\beta} \zeta_{1_2}(\tilde{t}) + \cdots \right). \tag{1.37}$$

All the other quantities which depend on time can be expanded in Taylor's series, i.e., we can write:

$$\begin{aligned} f(t) &= f(0) + \epsilon \left. \frac{df}{dt} \right|_{\tilde{t}=0} \tilde{t} + \cdots \\ &= f_s + \epsilon \left. \frac{df}{dt} \right|_s \tilde{t} + \cdots . \end{aligned} \tag{1.38}$$

Note we can expand in this way the positions of the other vortices as well, as can be verified substituting the above expansions into their equations of motion. Substituting these relationship into the equation of motion (1.33), we have to first order:

$$\begin{aligned} &\left[2i\bar{\zeta}_{1_1} + \frac{i\zeta_{1_1}\bar{\zeta}_{1_1}}{\zeta_{1_1} - \bar{\zeta}_{1_1}} \right] \epsilon^{2\alpha-1} \frac{d\bar{\zeta}_{1_1}}{d\tilde{t}} - \left[\frac{i\bar{\zeta}_{1_1}^3}{\zeta_{1_1}(\zeta_{1_1} - \bar{\zeta}_{1_1})} \right] \epsilon^{2\alpha-1} \frac{d\zeta_{1_1}}{d\tilde{t}} = \\ &\qquad \frac{i}{2} \Bigg\{ -U_s \left(\frac{\zeta_{2_s} + \bar{\zeta}_{2_s}}{\zeta_{2_s}\bar{\zeta}_{2_s}} \right) + 2u_{p_s} \\ &\qquad\quad + \sum_{n=3}^{N} \frac{i\Gamma_n}{2\pi} \left(\frac{\zeta_{n_s} - \bar{\zeta}_{n_s}}{\zeta_{n_s}\bar{\zeta}_{n_s}} \right) \left[\frac{\zeta_{n_s} + \bar{\zeta}_{n_s}}{\zeta_{n_s}\bar{\zeta}_{n_s}} - \frac{\zeta_{2_s} + \bar{\zeta}_{2_s}}{\zeta_{2_s}\bar{\zeta}_{2_s}} \right] \Bigg\} - \frac{i\bar{\zeta}_{1_1}^2}{\tilde{t}} \epsilon^{2\alpha-1}, \end{aligned} \tag{1.39}$$

with the initial condition

$$\zeta_{1_1}(0) = 0. \tag{1.40}$$

Since $\Gamma_1 \sim O(\epsilon^{1+\alpha})$ the desingularized velocity is independent of ζ_{1_1} and the strength of the vortex at time $t = t_s$ vanishes. By inspection we can see that the terms related with the vortex velocity or with the rate of circulation production are $\sim O(\epsilon^{2\alpha-1})$ while the term due to the desingularized velocity are $\sim O(\epsilon^0)$. In this case there is no ambiguity and the leading order is $\sim O(\sqrt{\epsilon})$.

Proceeding as before, we find that the leading solution valid for $0 \leq (t - t_s) \ll 1$ has the form:

$$\begin{cases} \rho_1(t) = \sqrt{\dfrac{2}{5}\left[U_s \dfrac{\sin\theta_{2_s}}{\rho_{2_s}} - u_{p_s} + \displaystyle\sum_{n=3}^{N} \frac{\Gamma_n}{\pi}\left(\frac{\sin\theta_{n_s}}{\rho_{n_s}} - \frac{\sin\theta_{2_s}}{\rho_{2_s}}\right)\frac{\cos\theta_{n_s}}{\rho_{n_s}}\right](t - t_s)} \\ \\ \theta_1(t) = 0, \end{cases} \tag{1.41}$$

where the quantity between square brackets is just the value of the desingularized velocity field near to the tip of the plate at the shedding time. Analyzing the argument of the square root it follows that a solution exists if, at the shedding time,

$$u_{p_s} < U_s \frac{\sin\theta_{2_s}}{\rho_{2_s}} + \sum_{n=3}^{N} \frac{\Gamma_n}{\pi}\left(\frac{\sin\theta_{n_s}}{\rho_{n_s}} - \frac{\sin\theta_{2_s}}{\rho_{2_s}}\right)\frac{\cos\theta_{n_s}}{\rho_{n_s}}, \tag{1.42}$$

i.e., if the velocity of the plate is less of the velocity with which the new vortex is convected away. This result supports Rott's prediction of the existence of a limiting value of the plate velocity beyond which the separation process cannot take place, see [20]. Furthermore, the above inequality suggests that a particular value of u_p which inhibits the separation may exist.

The above result provides a valuable test for the validity of the numerical simulation because the sign of the argument of the square root depends on the history of the flow. When the sign is negative, an error was made during the integration or the assumed shedding time was not compatible with the evolution of the system.

We are now able to run simulations with many vortices. A great deal of experimental work has been done concerning the starting vortex produced by a flow impinging on a thin wedge or towing a thin plate in a fluid at rest at infinity. Photographs show (see [25]) that as time increases the vortex sheet which leaves the edge presents some secondary spiral. The vibrations of the experimental apparatus could account for such a behavior. In our numerical simulation the free-stream is accelerated from rest to a peak value and then starts to oscillate about a nonzero mean (see Figure 1.31). In other words we are in the frame of reference fixed with a plate which vibrates parallel to

the free-stream. Figure 1.33 shows that the rate of circulation production is strongly affected by the oscillation, to the point that a small amount of negative circulation is necessary every period to maintain the Kutta condition. On the other hand, it is interesting to observe that the total circulation (see Figure 1.34) includes just some waviness in its behavior. Figures 1.35–1.36 show instantaneous streamlines. The waviness of the zero streamline coming off the tip of the plate closely resembles the secondary roll up present in the photographs.

1.6 Active circulation control

In section 1.3 we have seen how the motion of the plate can modify the flow, in particular how it can affect the rate of circulation production. In section 1.5 the approximate solution (1.41) suggests that there may exist a particular $u_p(t)$ which inhibits the shedding of vorticity. Now it seems legitimate to ask: once the starting vortex has been shed, i.e., $t \geq t_s$, is it possible to move the plate in such a clever way that the Kutta condition remains satisfied without requiring a new vortex ?

First let us recall the equations of motion in polar form for the starting vortex:

$$\begin{cases} \dfrac{d\rho_1}{dt} = \dfrac{U \sin\theta_1}{12\rho_1^2} - \dfrac{\rho_1}{3U}\dfrac{dU}{dt} - \dfrac{u_p \cos^2\theta_1}{3\rho_1} \\ \dfrac{d\theta_1}{dt} = \dfrac{U \cos 2\theta_1}{8\rho_1^3 \cos\theta_1} + \dfrac{u_p \sin 2\theta_1}{2\rho_1^2}, \end{cases} \tag{1.43}$$

with the initial conditions:

$$\begin{cases} \rho_1(0) = 0 \\ \theta_1(0) = \theta_0. \end{cases} \tag{1.44}$$

Now if we assume, as we have before, that a reasonable criterion to shed a vortex is when the rate of circulation production goes to zero, i.e., at $t = t_s$, then is important to analyze the expression for $\frac{d\Gamma_1}{dt}$. Taking the time derivative of the Kutta condition (1.10) in polar form, we get:

$$\frac{d\Gamma_1}{dt} = \frac{\pi}{\cos\theta_1}\left[U\frac{d\rho_1}{dt} + U\rho_1 \tan\theta_1 \frac{d\theta_1}{dt} + \rho_1 \frac{dU}{dt}\right]. \tag{1.45}$$

Using the equations of motion (1.43) we can rewrite the right hand side of the above expression in terms of $U, \frac{dU}{dt}$ and u_p. Equating it to zero and solving for u_p we have:

$$u_{p_s} = \frac{1}{(4\cos^2\theta_{1_s} - 3)} \left[\frac{(8\cos^2\theta_{1_s} - 3)\sin\theta_{1_s}}{8\rho_{1_s}\cos^2\theta_{1_s}} U_s + \frac{2\rho_{1_s}^2}{U_s} \left.\frac{dU}{dt}\right|_{t=t_s} \right]. \tag{1.46}$$

Hence for this choice of u_p the rate of circulation production is zero. At this point then we have a technique to discontinue feeding the starting vortex and to create a new vortex.

Let us assume for the moment that as long as one vortex of fixed circulation is present in the flow it is possible to move the plate in such a way that the Kutta condition is satisfied for all time. Then, from (1.4) without the Brown and Michael correction, this vortex of fixed strength Γ_{1_s} moves in accordance with the following equations:

$$\begin{cases} \dfrac{d\rho_1}{dt} = \dfrac{U\sin\theta_1}{4\rho_1^2} - \dfrac{\Gamma_{1_s}\sin\theta_1}{16\pi\rho_1^3\cos\theta_1} - \dfrac{u_p\cos 2\theta_1}{2\rho_1} \\ \dfrac{d\theta_1}{dt} = \dfrac{U\cos\theta_1}{4\rho_1^3} - \dfrac{\Gamma_{1_s}}{8\pi\rho_1^4} + \dfrac{u_p\sin 2\theta_1}{2\rho_1^2}, \end{cases} \tag{1.47}$$

with the initial conditions:

$$\begin{cases} \rho_1(t_s) = \rho_{1_s} \\ \theta_1(t_s) = \theta_{1_s}, \end{cases} \tag{1.48}$$

where ρ_{1_s}, θ_{1_s} and,

$$\Gamma_{1_s} = \pi \frac{\rho_{1_s}}{\cos\theta_{1_s}} U_s \tag{1.49}$$

are the values at the shedding time. From the Kutta condition or the requirement that the complex velocity be zero at the origin, we obtain the relationship:

$$\frac{\Gamma_{1_s}}{\pi}\frac{\cos\theta_1}{\rho_1} - U = 0. \tag{1.50}$$

If this constraint on the trajectory of the vortex is satisfied for all time after the shedding time, t_s, then the Kutta condition is satisfied. We must now impose this constraint on the equations of motion (1.47). To do so we take the time derivative of (1.50) to obtain:

$$\frac{\pi}{\cos\theta_1}\left[U\frac{d\rho_1}{dt} + U\rho_1\tan\theta_1\frac{d\theta_1}{dt} + \rho_1\frac{dU}{dt}\right] = 0. \tag{1.51}$$

As before, using the equations of motion (1.47), we can rewrite the above expression in terms of U, $\frac{dU}{dt}$ and, u_p. Then solving for u_p we obtain:

$$u_p = \left[\frac{2\pi^2 \rho_1^2 U^2 \sin 2\theta_1 + \pi \rho_1 U \Gamma_{1_s} \left(4\cos^2\theta_1 - 1\right) \sin\theta_1 - \Gamma_{1_s}^2 \sin 2\theta_1}{8\pi\rho_1^2 \left(\pi\rho_1 U \cos 2\theta_1 - \Gamma_{1_s} \sin 2\theta_1 \sin\theta_1\right) \cos\theta_1} + \frac{2\pi\rho_1^3}{\left(\pi\rho_1 U \cos 2\theta_1 - \Gamma_{1_s} \sin 2\theta_1 \sin\theta_1\right)} \frac{dU}{dt} \right]. \tag{1.52}$$

This then is the speed that the plate has to assume for $t \geq t_s$ to take advantage of the presence of the starting vortex now with constant circulation and keep the Kutta condition satisfied without forming a new vortex. Before verifying this result by different means let us check the compatability of the two parts of the argument computing the following limit:

$$\lim_{t \to t_s} u_p = \frac{1}{\left(4\cos^2\theta_{1_s} - 3\right)} \left[\frac{\left(8\cos^2\theta_{1_s} - 3\right) \sin\theta_{1_s}}{8\rho_{1_s} \cos^2\theta_{1_s}} U_s + \frac{2\rho_{1_s}^2}{U_s} \left. \frac{dU}{dt} \right|_{t=t_s} \right]. \tag{1.53}$$

Note the result is equal to the right hand side of (1.46), i.e., the value of u_p which forces to zero the rate of circulation production, and this verifies the continuity of the plate speed. Substituting the plate velocity (1.52) in the equation of motion (1.47) we obtain:

$$\begin{cases} \dfrac{d\rho_1}{dt} = \dfrac{\left(\Gamma_{1_s} \cos\theta_1 - 2\pi\rho_1 U\right) \Gamma_{1_s} \sin\theta_1 \cos\theta_1 + 8\pi^2 \rho_1^5 \dfrac{dU}{dt} \cos 2\theta_1}{8\pi\rho_1^3 \left(\Gamma_{1_s} \sin 2\theta_1 \cos\theta_1 - \pi\rho_1 U \cos 2\theta_1\right)} \\ \dfrac{d\theta_1}{dt} = \dfrac{\left(\Gamma_{1_s} \cos\theta_1 - 2\pi\rho_1 U\right) U \cos\theta_1 - 8\pi\rho_1^4 \dfrac{dU}{dt} \sin 2\theta_1}{8\rho_1^3 \left(\Gamma_{1_s} \sin 2\theta_1 \cos\theta_1 - \pi\rho_1 U \cos 2\theta_1\right)}. \end{cases} \tag{1.54}$$

These are the equations of motion of the vortex in the controlled case. The trajectory of the vortex is intelligently affected by the displacement of the plate which keeps the Kutta condition satisfied.

Since the above equations implicitly satisfy the constraint (1.50), we can use such a relationship to decouple the equations of motion. After the simplification (1.54) reduces to:

$$\frac{d\theta_1}{dt} = \frac{1}{\left(4\cos^2\theta_1 - 3\right)} \left[\frac{\pi^3}{8\Gamma_{1_s}^3 \cos^2\theta_1} U^4 + \frac{\sin 2\theta_1}{U} \frac{dU}{dt} \right], \tag{1.55}$$

with the initial condition

$$\theta_1(t_s) = \theta_{1_s}, \tag{1.56}$$

where the radius is

$$\rho_1 = \frac{\Gamma_{1_s}}{\pi}\frac{\cos\theta_1}{U}, \tag{1.57}$$

and the plate velocity is

$$u_p = \frac{1}{(4\cos^2\theta_1 - 3)}\left[\frac{\pi(8\cos^2\theta_1 - 3)\sin\theta_1}{8\Gamma_{1_s}\cos^3\theta_1}U^2 + \frac{2\Gamma_{1_s}^2\cos^2\theta_1}{\pi^2 U^3}\frac{dU}{dt}\right]. \tag{1.58}$$

Analyzing the denominator of the above expressions we can see that in general, $\frac{d\theta_1}{dt}$ and u_p become singular for:

$$U = 0, \qquad \theta_1 = \begin{cases} \pm\frac{\pi}{6} \\ \pm\frac{\pi}{2} \end{cases}. \tag{1.59}$$

Let us consider the source of these singularities. The constraint on U means that it is not possible to reverse the direction of the free stream and at the same time maintain the Kutta condition satisfied without further production of circulation. In other words, when $U = 0$ the plate prefers not to have a vortex in the flow because the singularity caused by the vortex cannot be balanced, hence the plate takes on an infinite velocity leaving the vortex behind. When $\theta_1 = \pm\frac{\pi}{2}$ the vortex touches the wall of the plate, to avoid this situation the plate has to take infinite speed. Finally, the first constraint on θ_1 is particularly curious because it divides the physical plane in three sectors of angle $\frac{2\pi}{3}$ each and the vortex is not allowed to move from one to another without having the plate take on infinite velocity.

1.7 Dynamical behavior of the controlled system

In the previous section we have been able to find a controller which inhibits the production of circulation when a vortex is present in the flow. Now, we are interested to know if it is possible to control the system for infinite time and, if so, how this might be done. If it is not possible, then we would like to understand how to maintain control as long as possible. Hence, this section is devoted

to the analysis of the dynamical behavior of the controlled system.

Let us start this investigation by determining the fixed points of the unperturbed and uncontrolled system. The set of equations describing this case can be obtained imposing $U(t) = U_s$ and $u_p(t) = 0$ on (1.47). The result is:

$$\begin{cases} \dfrac{d\rho_1}{dt} = \dfrac{U_s \sin\theta_1}{4\rho_1^2} - \dfrac{\Gamma_{1_s} \sin\theta_1}{16\pi\rho_1^3 \cos\theta_1} \\ \dfrac{d\theta_1}{dt} = \dfrac{U_s \cos\theta_1}{4\rho_1^3} - \dfrac{\Gamma_{1_s}}{8\pi\rho_1^4}. \end{cases} \tag{1.60}$$

It is easy to prove that there does not exist any pair (ρ_1, θ_1) such that the right hand sides of the above equations are simultaneously zero. Physically this means that, given a fixed free-stream U_s it is not possible to find a vortex of necessary strength that at the same time does not move and satisfies the Kutta condition.

The lack of fixed points for the unperturbed system makes the search for periodic orbits of the perturbed one much more complicated. It also suggests the possibility of the total lack of such orbits. Hence, the best way to conduct this search is to investigate the global structure of the flow field.

The equations of motion for the perturbed and controlled case (1.54) can be simplified by the use of the trajectory constraint (1.50). The form of the simplified equations can be crucial for the analysis of the dynamics of the system. At first, it seems natural to eliminate one of the equations using the constraint. The result of such simplification (1.55) is numerically very useful because it reduces the computation time and improves the accuracy but does not aid in the analysis. The right hand side of (1.55) is singular which violates the required Lipschitz-continuity to apply averaging methods. Also the use of the singular perturbation theory is very difficult in the case of periodic forcing, the one of interest, because at each cycle we have to match inner and outer solutions. A better way to use this constraint is to eliminate Γ_{1_s} from the equations (1.54). Substituting and

simplifying we obtain:

$$\begin{cases} \dfrac{d\rho_1}{dt} = -\dfrac{1}{8\rho_1^2 U(4\cos^2\theta_1 - 3)}\left[U^2 \sin\theta_1 + 8\rho_1^3 \dfrac{dU}{dt}\cos 2\theta_1\right] \\ \dfrac{d\theta_1}{dt} = \dfrac{1}{8\rho_1^3 U(4\cos^2\theta_1 - 3)}\left[U^2 \cos\theta_1 + 8\rho_1^3 \dfrac{dU}{dt}\sin 2\theta_1\right]. \end{cases} \tag{1.61}$$

Note that we recover the same singularities as defined by (1.59), but the right hand sides present an interesting symmetry. Such a symmetry suggests the use of a Liapunov type stability argument [26] to determine the global behavior of the system. In other words, we attempt to determine a function $V(\rho_1, \theta_1)$ such that its total derivative with respect to time has a definite sign. We limit the free-stream velocity so that it will not change sign because of the above singularity in U and if we assume for the moment that $\theta_1 \in [0, \frac{\pi}{2}]$ or $\theta_1 \in [-\frac{\pi}{2}, 0]$ depending on whether U is positive or negative, then the free-stream acceleration is the only quantity that can change sign without constraint. Hence, the total derivative of V with respect to time should not contain the term $\frac{dU}{dt}$. Helped by the symmetry of the equations we are able to find such a function as follows:

$$V(\rho_1, \theta_1) = \rho_1^2 \sin 2\theta - A, \tag{1.62}$$

for $A \in [0, \infty)$ describes a family of hyperbolas which cover the entire first quadrant (see Figure 1.37). Now taking the total derivative with respect to time we obtain:

$$\frac{dV}{dt} = \nabla V \cdot \frac{d\mathbf{x}}{dt} = \frac{\partial V}{\partial \rho_1}\frac{d\rho_1}{dt} + \frac{\partial V}{\partial \theta_1}\frac{d\theta_1}{dt} = \frac{U\cos\theta_1}{4\rho_1} > 0 \qquad \forall t > t_s \tag{1.63}$$

if

$$U(t) > 0 \qquad \forall t > t_s, \tag{1.64}$$

the converse is also true. Strictly speaking the function $V(\rho_1, \theta_1)$ cannot be called a Liapunov function because it does not have a definite sign [26].

From now on let us restrict our discussion to the case where $U(t) > 0$ for all $t > t_s$ and we leave to the reader the trivial extension to the other case. To interpret the above result let us assume

that at time $t = t_*$ the position of the vortex is identified by the pair $(\rho_{1_*}, \theta_{1_*})$ then the hyperbola which passes through this point is

$$V(\rho_1, \theta_1) = \rho_1^2 \sin 2\theta_1 - \rho_{1_*}^2 \sin 2\theta_{1_*}. \tag{1.65}$$

Now (1.63) proofs that the vortex moves away from this curve to another with a higher value of A and so on, i.e., the vortex drifts irreversibly away from the origin in this sense. This result gains greater physical meaning if we map the function V onto the physical plane. Let us first write (1.62) in complex form, i.e.:

$$V(\zeta, \bar{\zeta}) = \frac{1}{2}(\zeta^2 - \bar{\zeta}^2) - A = 2\Re(\zeta)\Im(\zeta) - A, \tag{1.66}$$

then using the map (1.1) we obtain:

$$V(z, \bar{z}) = \frac{i}{2}(z + \bar{z}) - A = i\Re(z) - A. \tag{1.67}$$

For $A \in [0, \infty)$ this function describes a family of straight vertical lines which cover the entire right half plane (see Figure 1.38). Note for $A = 0$ the function V coincides with the imaginary axis. Finally, we can conclude that the relationship (1.63) excludes the existence of any periodic orbit and consequently the controller cannot trap the vortex near to the plate, it may only slow down the drifting motion.

We can gain further insight about the behavior of the controlled system changing variables and describing the motion of the vortex in terms of a new pair (A, θ_1) where θ_1 is the original angular variable and A is defined as:

$$A = \rho_1^2 \sin 2\theta_1. \tag{1.68}$$

Under this transformation the equations of motion (1.61) take the following form:

$$\begin{cases} \dfrac{dA}{dt} = \dfrac{U\sqrt{\sin\theta_1 \cos^3\theta_1}}{2\sqrt{2A}} \\ \dfrac{d\theta_1}{dt} = \dfrac{U \sin 2\theta_1}{4\sqrt{2A^3}(4\cos^2\theta_1 - 3)} \left[\sqrt{\sin\theta_1 \cos^3\theta_1} + \dfrac{4\sqrt{2A^3}}{U^2} \dfrac{dU}{dt} \right]. \end{cases} \tag{1.69}$$

Note how the first equation above basically restates the previous result (see 1.63). Performing the same operation on (1.52) we obtain the following expression for the plate velocity:

$$u_p = \frac{U}{4\sqrt{2A}(4\cos^2\theta_1 - 3)\sin\theta_1\cos\theta_1}\left[\frac{(8\cos^2\theta_1 - 3)\sqrt{\sin^5\theta_1}}{\sqrt{\cos\theta_1}} + \frac{4\sqrt{2A^3}}{U^2}\frac{dU}{dt}\right]. \tag{1.70}$$

We now wish to determine how the singularity at $\theta_1 = \frac{\pi}{6}$ affects the evolution of the controlled system. The second term between square brackets in the last two equations above is common to both expressions. If we set:

$$P = \frac{4\sqrt{2A^3}}{U^2}\frac{dU}{dt}, \tag{1.71}$$

then P has the same sign of $\frac{dU}{dt}$. Using this term as parameter we can plot $\frac{d\theta_1}{dt}$ and u_p versus θ_1 (see Figures 1.39 and 1.40). The presence of the singularity is clearly shown in both plots by the vertical line at $\theta_1 = \frac{\pi}{6}$ which divides the domain $(0, \frac{\pi}{2})$ in two parts. The plate velocity becomes infinite as the vortex approaches the values $\theta_1 = 0, \frac{\pi}{6}, \frac{\pi}{2}$, consequently the motion of the vortex is confined in the sub-domains $(0, \frac{\pi}{6})$ or $(\frac{\pi}{6}, \frac{\pi}{2})$ depending on the initial conditions. Note how the behavior of the singularity depends on the sign and magnitude of P: for $P > 0$ the vortex is attracted by $\theta_1 = \frac{\pi}{6}$ while for $P < 0$ it approaches or drifts away from the singularity depending on the initial condition and on the value of P. Figure 1.41 presents a phase portrait which gives a condensed view of such behavior.

To better understand how the system evolves let us consider the following four basic scenarios:

1. $\frac{dU}{dt} = 0, \qquad \forall t > t_s.$

   In this case the free-stream velocity is constant and the equation for the vortex trajectory can be obtained by taking the ratio of the equations (1.61). We have:

$$\frac{d\rho_1}{d\theta_1} = -\rho_1\tan\theta_1, \tag{1.72}$$

   with the initial condition:

$$\rho_1(\theta_{1_s}) = \rho_{1_s}. \tag{1.73}$$

Performing the integration we obtain:

$$\rho_1 = \rho_{1_s} \frac{\cos\theta_1}{\cos\theta_{1_s}}. \tag{1.74}$$

The trajectories are plotted in Figure 1.42. Note all the trajectories, independently of the initial condition, end up at $\theta_1 = \frac{\pi}{6}$. This is consequence of the fact that $P = 0$ and hence the singularity behaves as an attractor (see Figure 1.41). As the vortex moves along one of these trajectories the plate picks up speed which tends to infinity as the vortex approaches the singularity (see Figure 1.40).

2. $\frac{dU}{dt} > 0, \qquad \forall t > t_s.$

In this case the free-stream velocity increases monotonically. Note for the particular choice:

$$\frac{1}{U^2}\frac{dU}{dt} = B, \tag{1.75}$$

where B is a constant, it is possible to find the equation for the trajectory. Taking the ratio of the equations (1.61) we have:

$$\frac{d\rho_1}{d\theta_1} = -\frac{\rho_1(\sin\theta_1 + 8\rho_1^3 B\cos 2\theta_1)}{\cos\theta_1 + 8\rho_1^3 B\sin 2\theta_1}, \tag{1.76}$$

and the initial condition is:

$$\rho_1(\theta_{1_s}) = \rho_{1_s}. \tag{1.77}$$

This equation can be integrated analytically and the vortex trajectory is given in implicit form by the following expression:

$$\frac{4B\rho_1^3\sin 2\theta_1 - \cos\theta_1}{\rho_1} = \frac{4B\rho_{1_s}^3\sin 2\theta_{1_s} - \cos\theta_{1_s}}{\rho_{1_s}}, \tag{1.78}$$

when the free-stream velocity has the form:

$$U(t) = \frac{U_s}{1 - BU_s(t - t_s)} \qquad \forall B > 0 \qquad \forall t \in [t_s, t_s + \frac{1}{BU_s}). \tag{1.79}$$

Figure 1.43 shows the vortex trajectories for this case. As in the previous case all the curves, independently of the initial condition, end up at $\theta_1 = \frac{\pi}{6}$. The singularity behaves, again, as an attractor because $P > 0$ (see Figure 1.41), but its strength is greater than before (see Figure 1.39), explaining why the trajectories approach more directly the singularity. The plate velocity has the same trend as before but its magnitude is larger (see Figure 1.40).

3. $\frac{dU}{dt} < 0, \qquad \forall t > t_s.$

In this case the free-stream decreases monotonically and if it satisfies the constraint (1.75) for $B < 0$ then the vortex trajectory has the form

$$\frac{4B\rho_1^3 \sin 2\theta_1 - \cos\theta_1}{\rho_1} = \frac{4B\rho_{1_s}^3 \sin 2\theta_{1_s} - \cos\theta_{1_s}}{\rho_{1_s}}, \tag{1.80}$$

when the free-stream velocity has the form:

$$U(t) = \frac{U_s}{1 - BU_s(t - t_s)} \qquad \forall B < 0 \qquad \forall t > t_s. \tag{1.81}$$

The trajectories are plotted in Figure 1.44. The complexity of the pattern is due to the fact that the singularity at $\theta_1 = \frac{\pi}{6}$ behaves as an attractor or as a repulsor depending on the vortex position and on the value of P. The dashed curve in Figure 1.44 identifies the solution of the following equation:

$$\sqrt{\sin\theta_1 \cos^3\theta_1} + P = 0, \tag{1.82}$$

which determines when $\frac{d\theta_1}{dt}$ changes sign (see 1.69). When the vortex moves within the area defined by the imaginary axis and the dashed line its angular position is attracted by the singularity. Outside this region the singularity switches behavior and the vortex drifts away from the dashed line $\theta_1 = \frac{\pi}{6}$. Note there are trajectories which are crossing the dashed curve. In these cases the attractor is not strong enough to keep the vortex inside the region. Thus when it crosses the dashed curve the singularity starts to repel the vortex which moves irreversibly away.

4. $\frac{dU}{dt} = \sin(\omega t + \phi)$.

   This is a case of simple periodic forcing but in each period we satisfy the condition of one or the other of the two previous cases. Note the upper bound on the acceleration amplitude is given by the free-stream magnitude which we restrict not to go to zero nor change sign. In this case a comprehensive quantitative analysis is possible using the Poincaré map. As an alternative to this computationally intensive technique the evolution of the system will be described qualitatively. The parameter P swings from positive to negative values in accord with the free-stream acceleration and consequently the singularity acts as attractor or as a repulsor in agreement with it (see Figure 1.41). It is important to observe that over an entire period the singularity behaves as an attractor for more than half a period, hence we speculate the vortex drifts down-stream fatally attracted by it. Figures 1.39–1.40 suggest that the evolution of the system is largely affected by the initial condition and that an unlikely escape to infinity is still possible.

From the above analysis it follows that the performance of the controller can be greatly improved by an appropriate choice of the initial condition. Since the vortex eventually ends up on $\theta_1 = \frac{\pi}{6}$ then the best initial condition is that one which forces the time necessary to reach the singularity to be as large as possible. This time can be formally expressed as:

$$t_{tot} = \int_{\theta_{1_s}}^{\frac{\pi}{6}} \left(\frac{dt}{d\theta_1} \right) d\theta_1. \tag{1.83}$$

Then, it would seem that t_{tot} can be made larger choosing the initial condition so that the integrand is singular at $t = t_s$. It follows that the best θ_{1_s} is the one for which:

$$\left. \frac{d\theta_1}{dt} \right|_{t=t_s} = 0, \tag{1.84}$$

and consequently

$$\sqrt{\sin\theta_{1_s} \cos^3\theta_{1_s}} + P(t_s) = 0. \tag{1.85}$$

Note the above equation has a solution only if $P < 0$, i.e., when the free-stream decelerates. In case of uncontrolled periodic forcing, see Figures 1.31 and 1.33, the first vortex is cut away when $\frac{dU}{dt} < 0$ hence the optimal θ_{1_s} can be determined.

1.8 Results

In section 1.5 we presented a simulation where the free-stream at time zero suddenly rose and then oscillated about a nonzero mean. In that case we kept the plate stationary and a sequence of vortices was produced. Based on the results of the last two sections we can run the same numerical experiment moving the plate to inhibit the production of circulation. Here, we want to present and to compare two cases, one when the motion of the vortex is confined in the third sector and another which evolves within the second. As we have noticed previously the formulation (1.55–1.58) is the most convenient for a numerical integration.

We want to start with the active circulation control in the third sector because in the uncontrolled case (see Figure 1.32) the first vortex is naturally shed in this region. Figures 1.45–1.52 illustrate the growth of the starting vortex and then the evolution of the controlled system. Note the velocity of the plate up to the shedding time has been chosen to provide a reasonable distance between the vortex location and the sector divider. Figures 1.47–1.48 show that up to time $t_s \approx .32$ the starting vortex grows in circulation. When the rate of circulation production goes to zero the strength of vortex is frozen, triggering the active control for the rest of the simulation ($t_{final} \approx 6.75$). From Figures 1.45–1.46 we can see that as the vortex is convected farther downstream the plate velocity must increase to maintain control. Also as the trajectory becomes closer to the sector divider the speed of the plate becomes larger making the situation progressively more critical with a complete lose of control for $t > t_{final}$. Figures 1.49–1.52 are snap shots of the streamlines during the controlled period, giving insight into the behavior of the flow near the tip of the plate.

An example of active shedding control within the second sector is given by the Figures 1.53–1.60. Note the free-stream velocity is the same as before and the plate velocity up to the shedding time is basically the same but with opposite sign to provide the necessary initial condition. Figures 1.53–1.54 show that as soon as the controller takes over it imposes large oscillations on the plate motion but the amplitudes grow only slowly in time. Roughly speaking the plate moves as close or as far away from the vortex as necessary to maintain the Kutta condition. Figures 1.57–1.60 show the instantaneous streamlines during the controlled period.

The different behavior of the controller in the two cases is direct consequence of the position and strength of the vortex at the shedding time. In the first case (vortex in the third sector) the plate at the beginning is moving into the flow and a strong vortex is trapped in the recirculating bubble near to the leading edge. Initially, slight movements of the plate are enough to satisfy the Kutta condition, then as the vortex drifts downstream larger oscillations are required. Of great help in this case is the fluid flowing around the edge which "keeps" the vortex away from the attractor and the vortex strength which maintains smooth flow even if the vortex is quite far downstream. In the second case (vortex in the second sector) these factors become handicaps, the vortex is convected toward the sector divider and its strength is almost half of the previous case reducing the controllability of the system. Note the strength of the vortex is the result of the compromise between having a strong vortex too close to the singularity and a weak one too far away from the tip of the plate. The controller is left with a very delicate task and its performance is not as good as the first case.

1.9 Conclusions

An irrotational model has been used to simulate the unsteady separated flow past a semi-infinite plate with transverse motion. The analysis of the power-law starting flow when the plate moves with a power-law also showed that the motion of the plate strongly affects the separation process.

The flow separates in a different fashion depending on the relative strength of the free-stream flow and plate motion. When the free-stream velocity is dominant the motion of the plate introduces a second order correction to the similarity solution proposed by Rott [20] for the motionless plate. When the flow produced by the motion of the plate is dominant, separation is predicted only if the plate is retracting from the flow. In other words, there is a limiting value for the plate velocity time exponent beyond which the separation is not allowed in the present model. Finally, when these two effects balance the separation process depends on the ratio of their magnitudes.

The irrotational model has been extended to the case where several vortices are present in the flow by implementing a suitable vortex shedding mechanism. The separation of the flow in the presence of other vortices was then analyzed. In this case the trajectory of the new vortex is always parallel to the plate but there exists a limiting value of the plate velocity beyond which the separation is not allowed in the present model. This result gives mathematical evidence for Rott's prediction of such a limiting value [20].

Within this model we derived a control strategy which inhibits the production of additional circulation when a vortex is present in the flow. Because of the mathematical simplicity of the model we obtained the analytical closed form solution of the controller for any time-dependent free-stream velocity. Subsequently, the performance of the controller was characterized with a dynamical system type of analysis. This investigation showed that the time over which the system is controllable is finite as a consequence of the drifting motion which convects the vortex downstream but it can be maximized by an intelligent choice of the separation conditions. Finally, we successfully tested the controller when the free-stream oscillates about a nonzero mean and showed that the motion of the plate, before the shedding time, can initiate the controlled system in two totally different controllable states. The robustness issue was not addressed in the present work because in general it is strictly related to the final application.

Figures

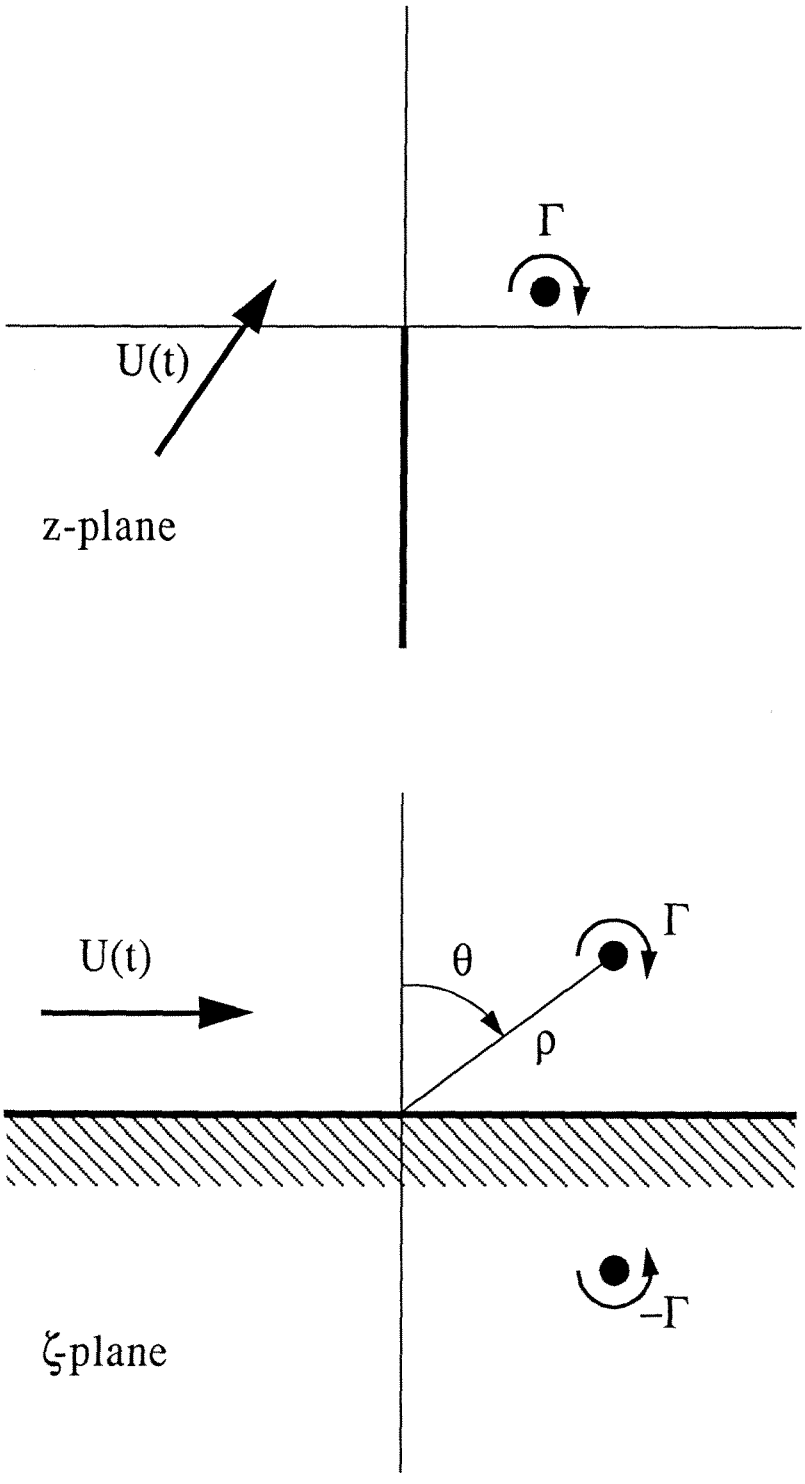

Figure 1.1: Physical and mapped planes.

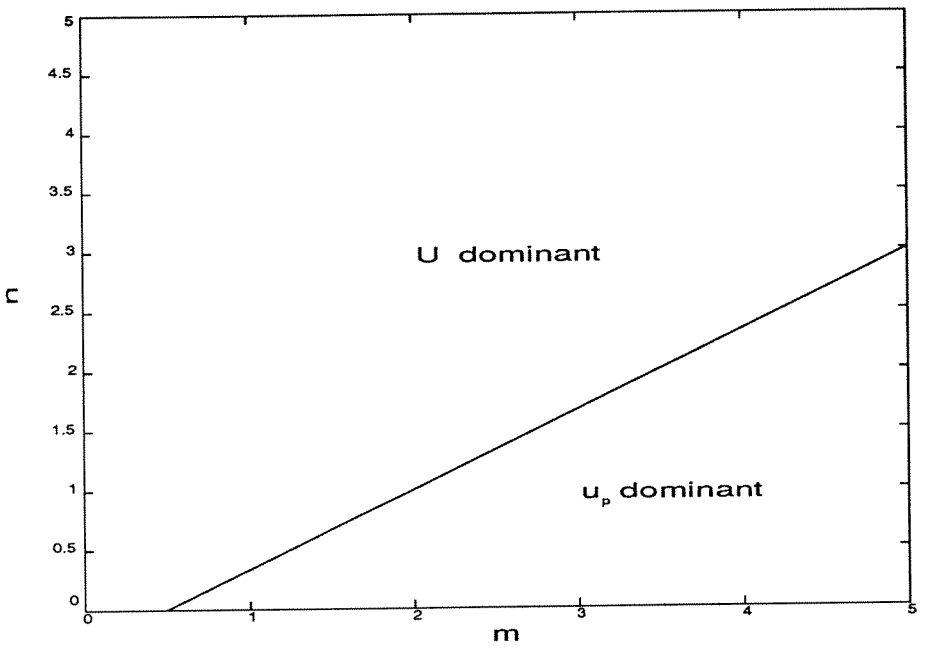

Figure 1.2: Parameters space.

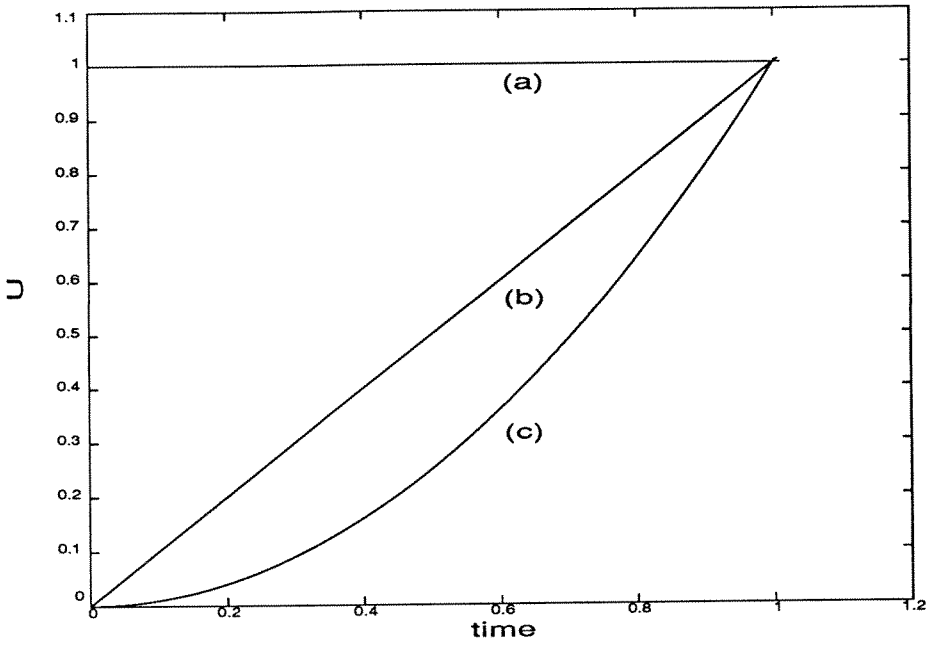

Figure 1.3: Free-stream velocity: $U(t) = Vt^m$ ($m = 0, 1, 2$).

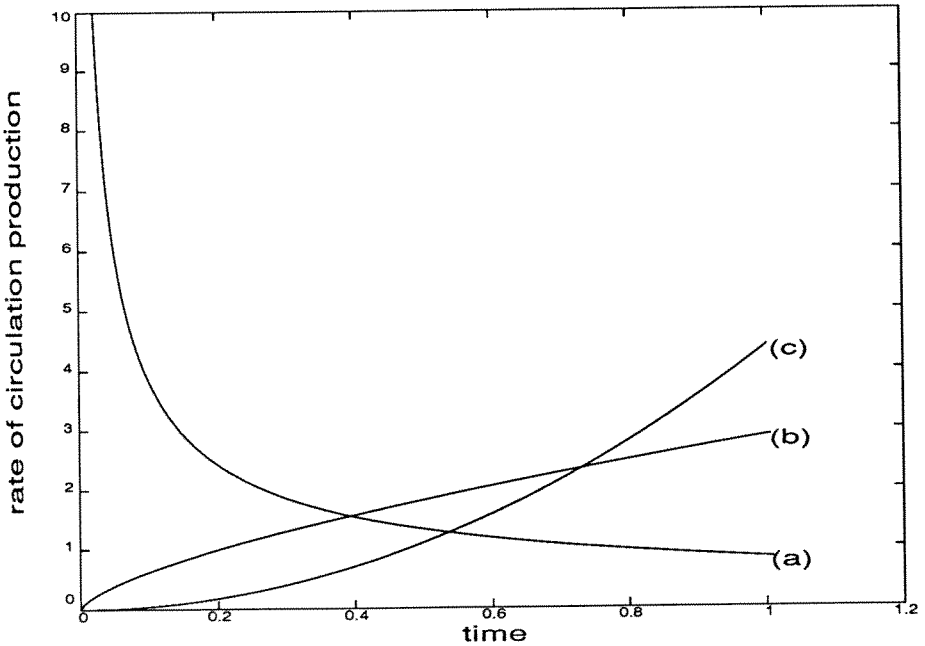

Figure 1.4: Rate of circulation production ($m = 0, 1, 2$).

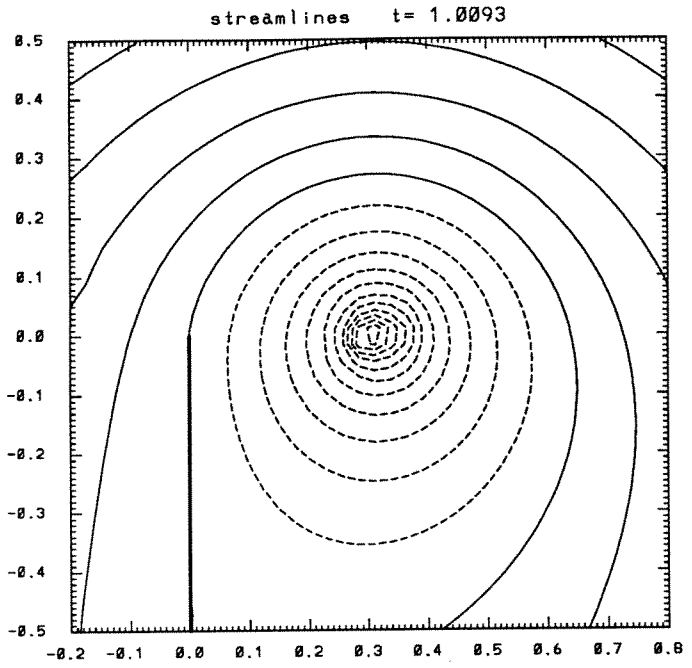

Figure 1.5: Starting vortex ($t = 1.0093$, $m = 0$).

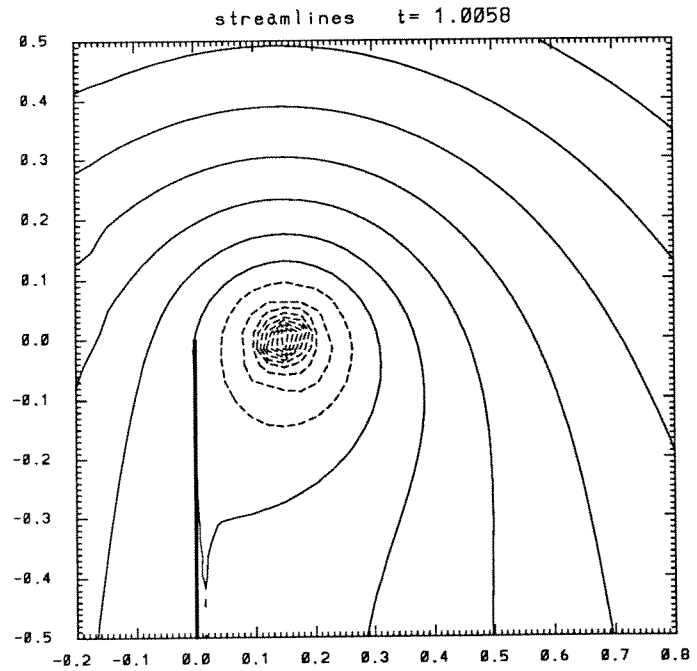

Figure 1.6: Starting vortex ($t = 1.0058$, $m = 1$).

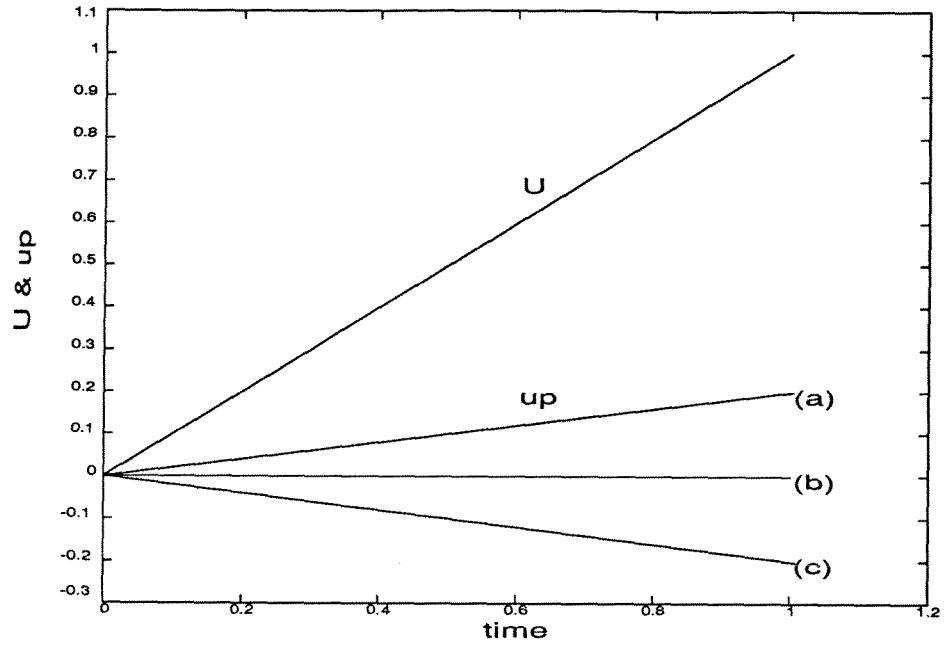

Figure 1.7: Free-stream and plate velocities: $U(t) = Vt^m, u_p = v_p t^n$ ($m = 1$, $n = 1$).

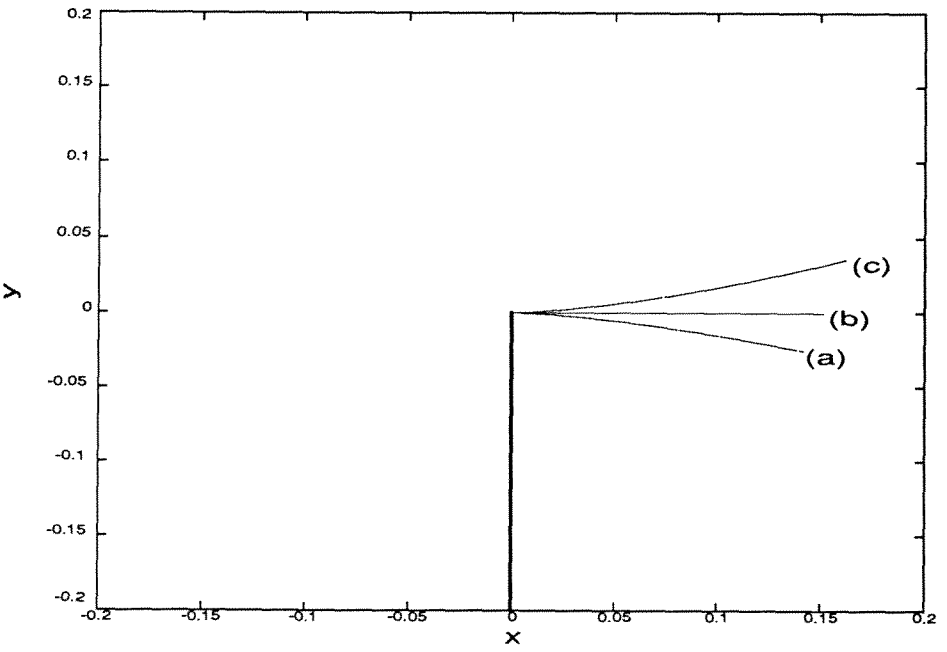

Figure 1.8: Starting vortex trajectories ($m = 1$, $n = 1$).

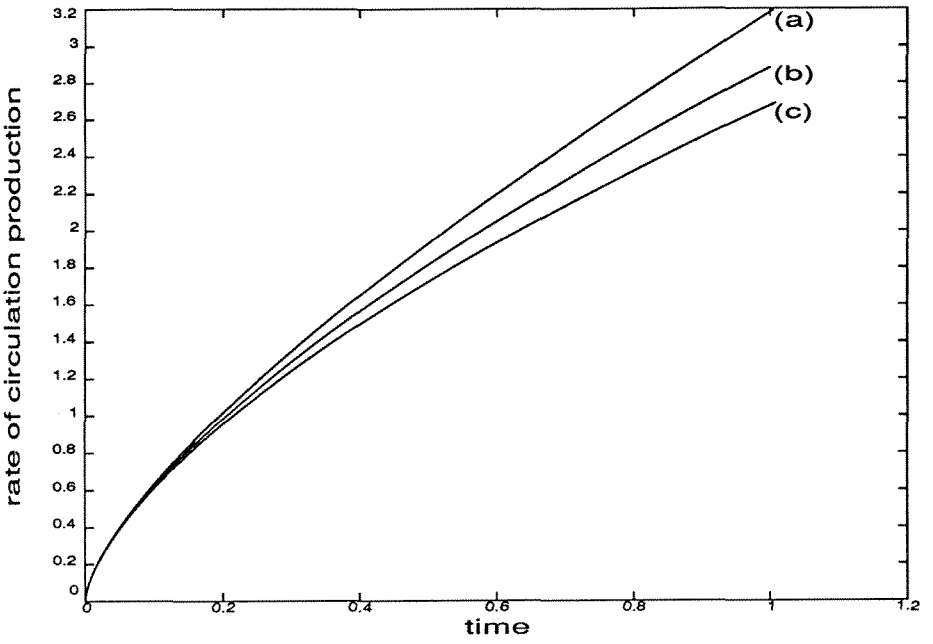

Figure 1.9: Rate of circulation production ($m = 1$, $n = 1$).

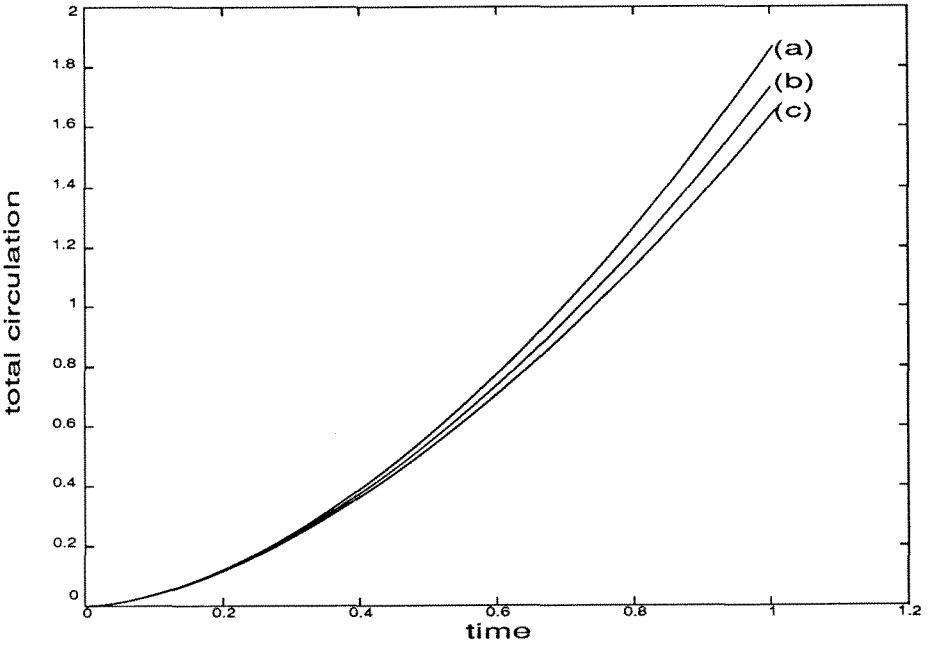

Figure 1.10: Total circulation ($m = 1$, $n = 1$).

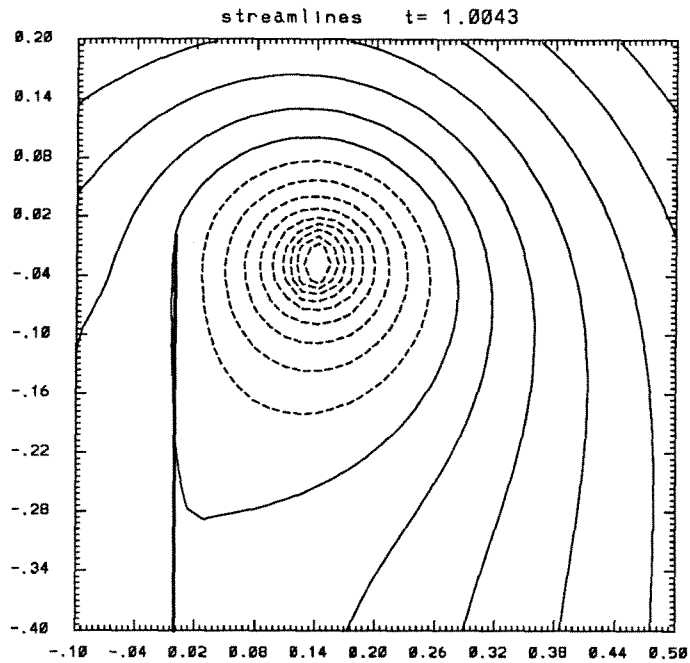

Figure 1.11: Starting vortex: case (a) ($m = 1$, $n = 1$, $v_p > 0$).

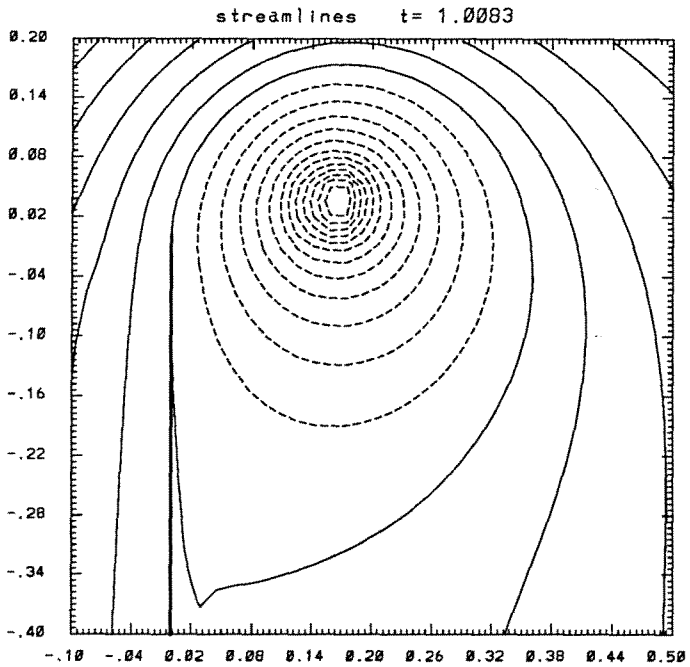

Figure 1.12: Starting vortex: case (c) ($m = 1$, $n = 1$, $v_p < 0$).

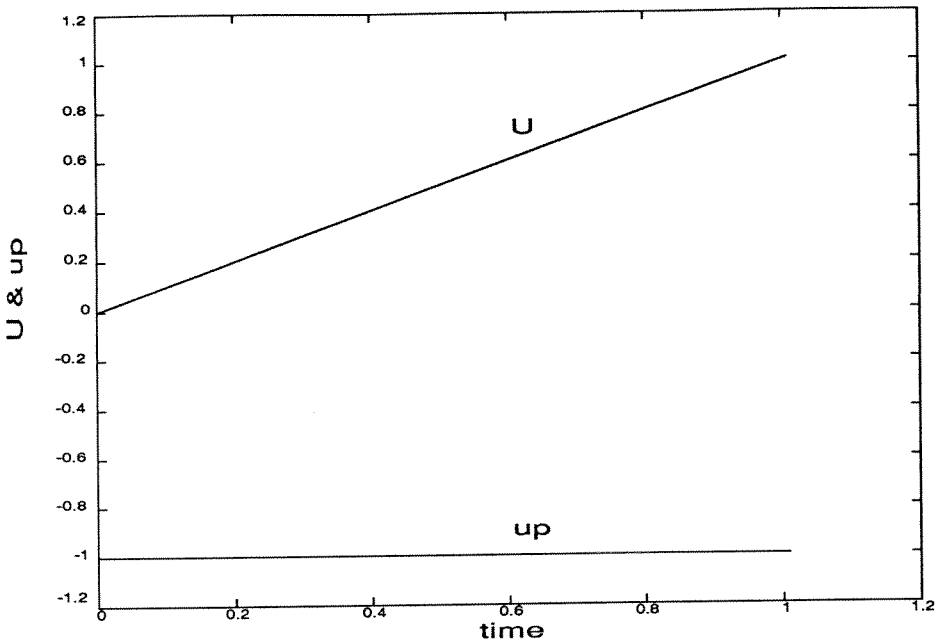

Figure 1.13: Free-stream and plate velocities: $U(t) = Vt^m, u_p = v_p t^n$ ($m = 1$, $n = 0$, $v_p < 0$).

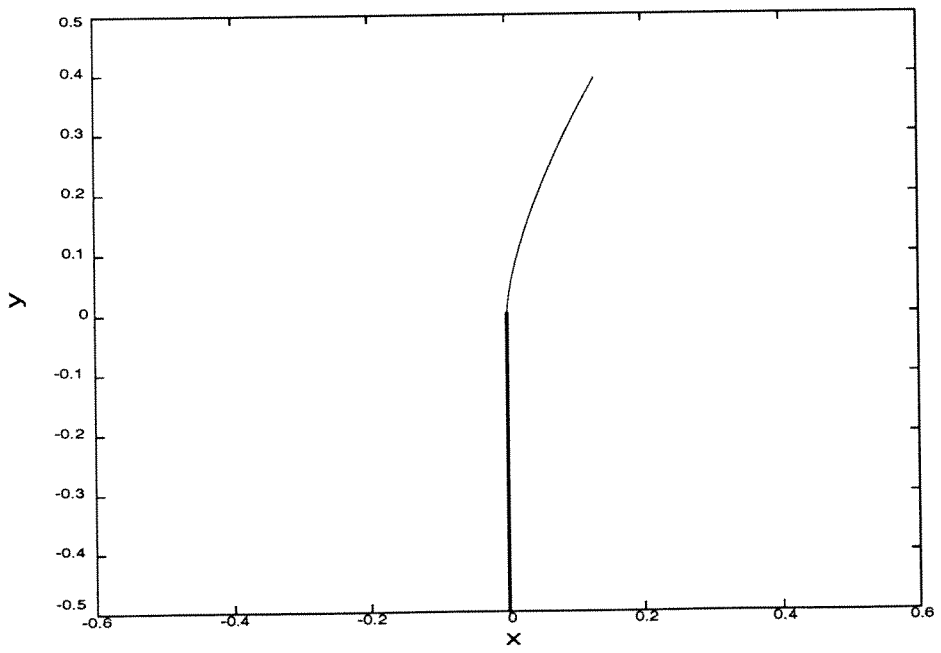

Figure 1.14: Starting vortex trajectory ($m = 1$, $n = 0$, $v_p < 0$).

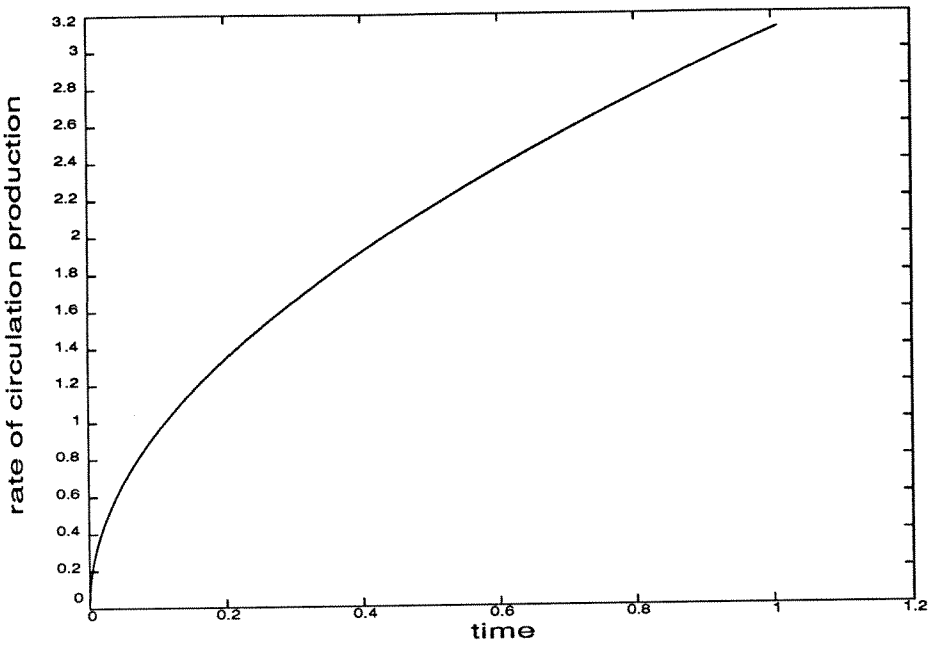

Figure 1.15: Rate of circulation production ($m = 1$, $n = 0$, $v_p < 0$).

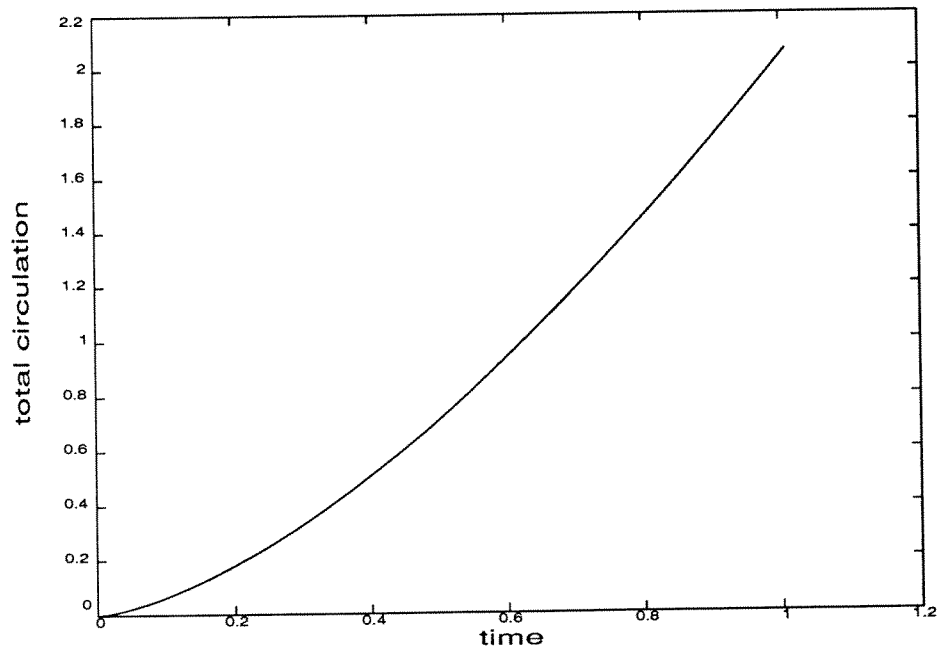

Figure 1.16: Total circulation ($m = 1$, $n = 0$, $v_p < 0$).

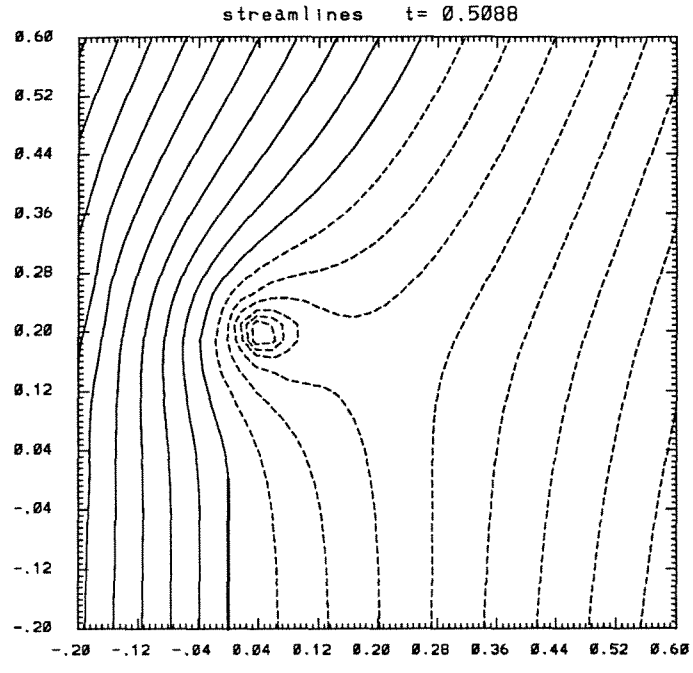

Figure 1.17: Starting vortex ($t = .5088$, $m = 1$, $n = 0$, $v_p < 0$).

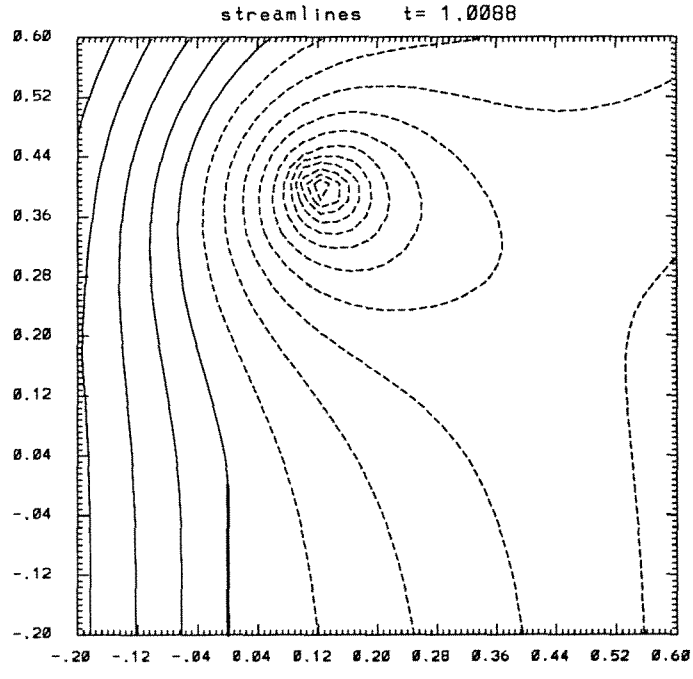

Figure 1.18: Starting vortex ($t = 1.0088$, $m = 1$, $n = 0$, $v_p < 0$).

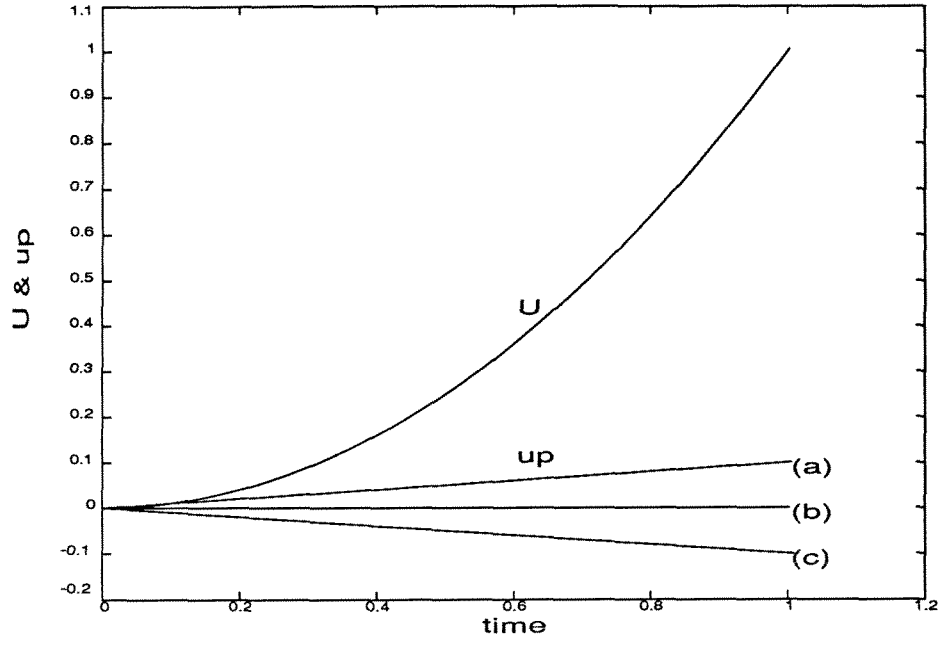

Figure 1.19: Free-stream and plate velocities: $U(t) = Vt^m, u_p = v_p t^n$ ($m = 2$, $n = 1$, $\left|\frac{V}{v_p}\right| \gg 1$).

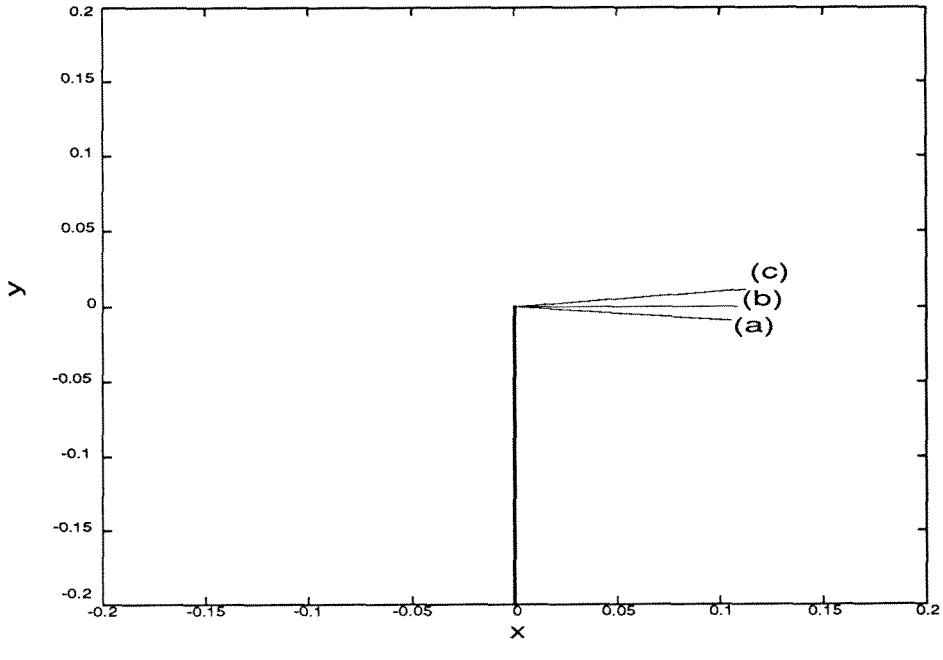

Figure 1.20: Starting vortex trajectories ($m = 2$, $n = 1$, $\left|\frac{V}{v_p}\right| \gg 1$).

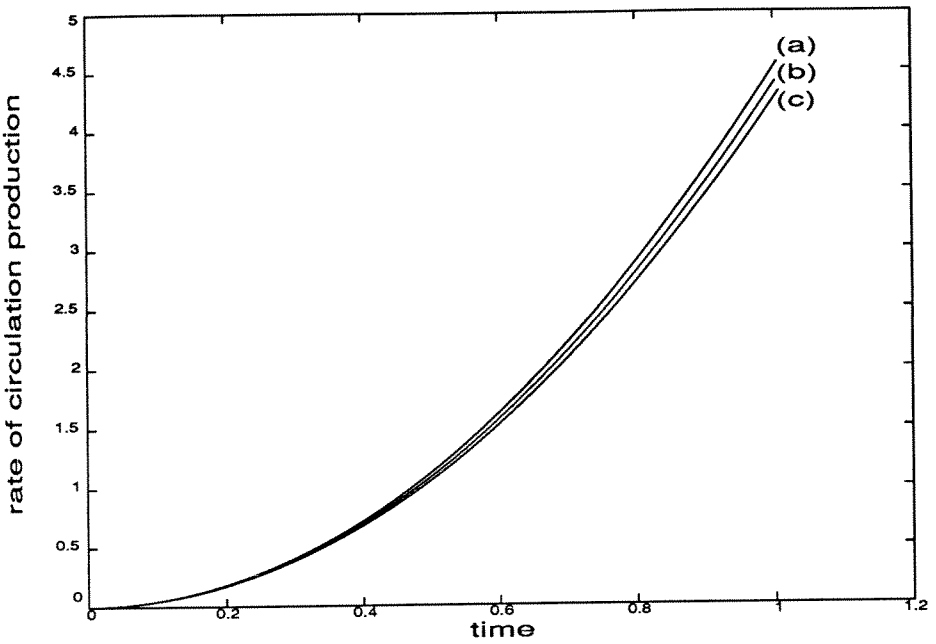

Figure 1.21: Rate of circulation production ($m = 2$, $n = 1$, $\left|\frac{V}{v_p}\right| \gg 1$).

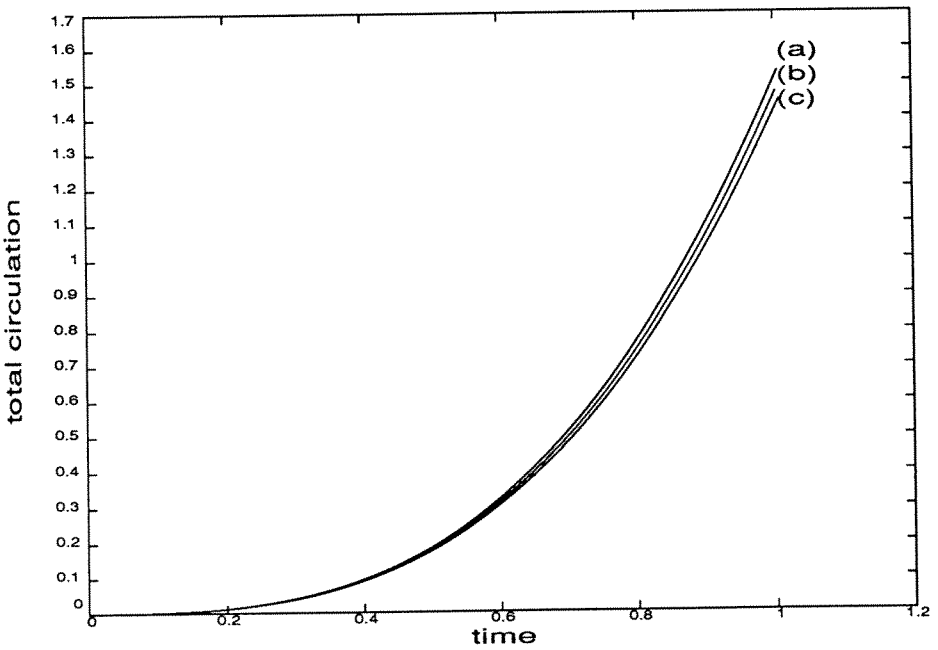

Figure 1.22: Total circulation ($m = 2$, $n = 1$, $\left|\frac{V}{v_p}\right| \gg 1$).

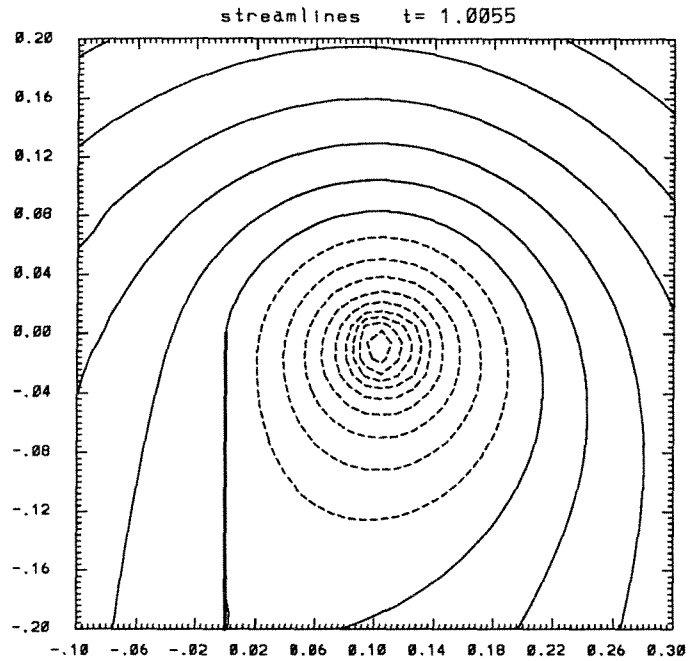

Figure 1.23: Starting vortex: case (a) ($t = 1.0055$, $m = 2$, $n = 1$, $\left|\frac{V}{v_p}\right| \gg 1$, $v_p > 0$).

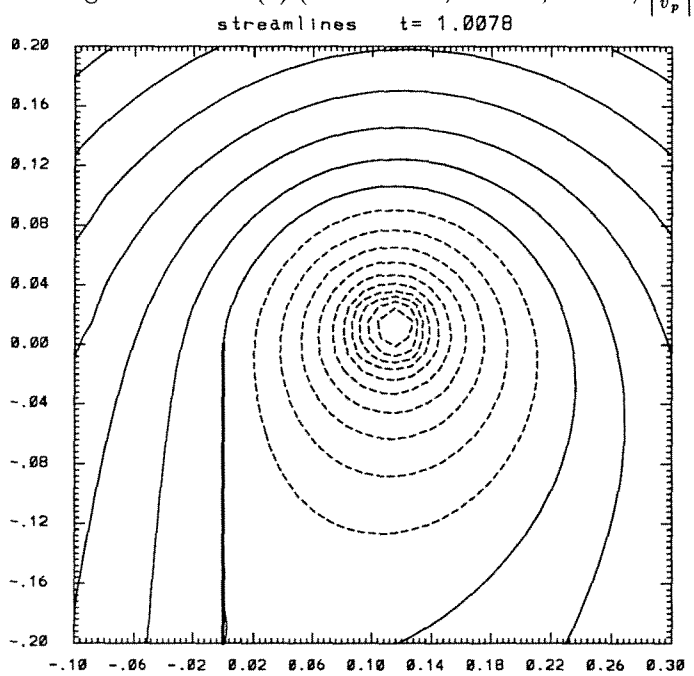

Figure 1.24: Starting vortex: case (c) ($t = 1.0078$, $m = 2$, $n = 1$, $\left|\frac{V}{v_p}\right| \gg 1$, $v_p < 0$).

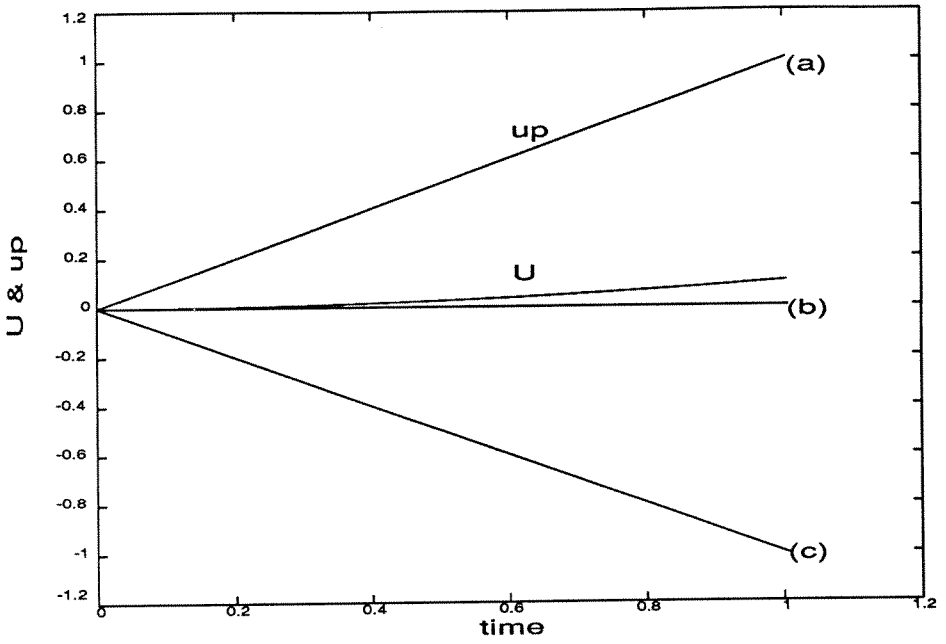

Figure 1.25: Free-stream and plate velocities: $U(t) = Vt^m, u_p = v_p t^n$ ($m = 2$, $n = 1$, $\left|\frac{V}{v_p}\right| \ll 1$).

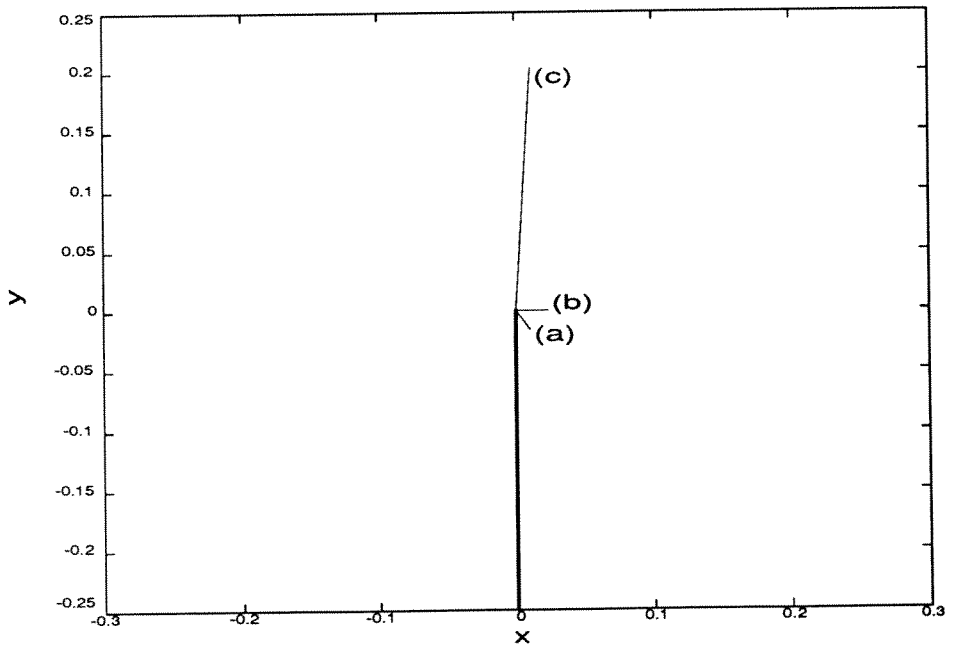

Figure 1.26: Starting vortex trajectories ($m = 2$, $n = 1$, $\left|\frac{V}{v_p}\right| \ll 1$).

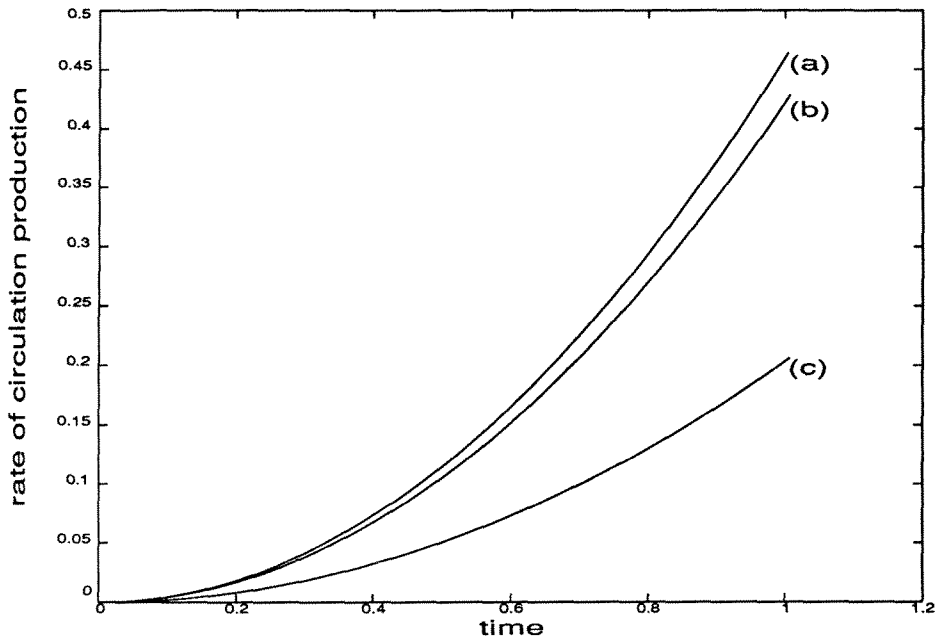

Figure 1.27: Rate of circulation production ($m = 2$, $n = 1$, $\left|\frac{V}{v_p}\right| \ll 1$).

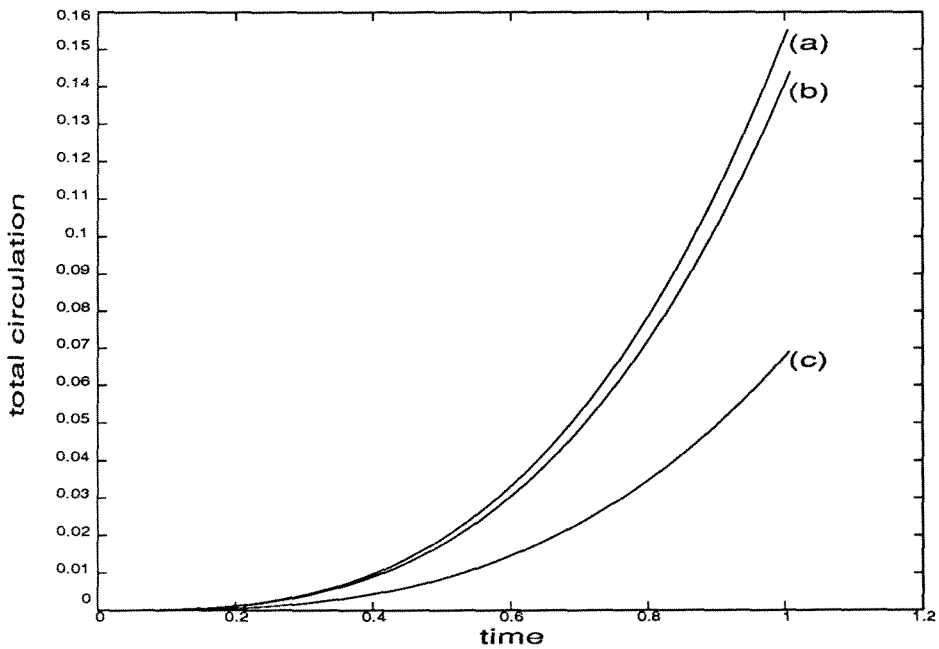

Figure 1.28: Total circulation ($m = 2$, $n = 1$, $\left|\frac{V}{v_p}\right| \ll 1$).

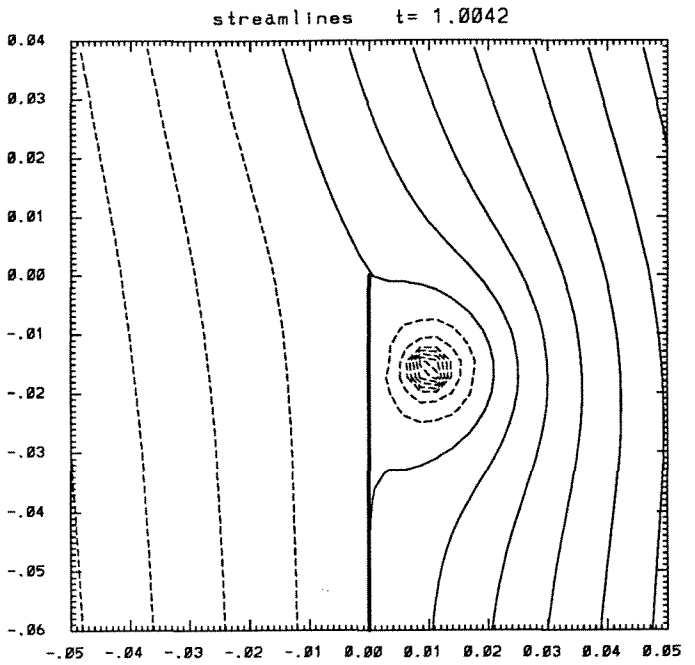

Figure 1.29: Starting vortex: case (a) ($t = 1.0042$, $m = 2$, $n = 1$, $\left|\frac{V}{v_p}\right| \ll 1$, $v_p > 0$).

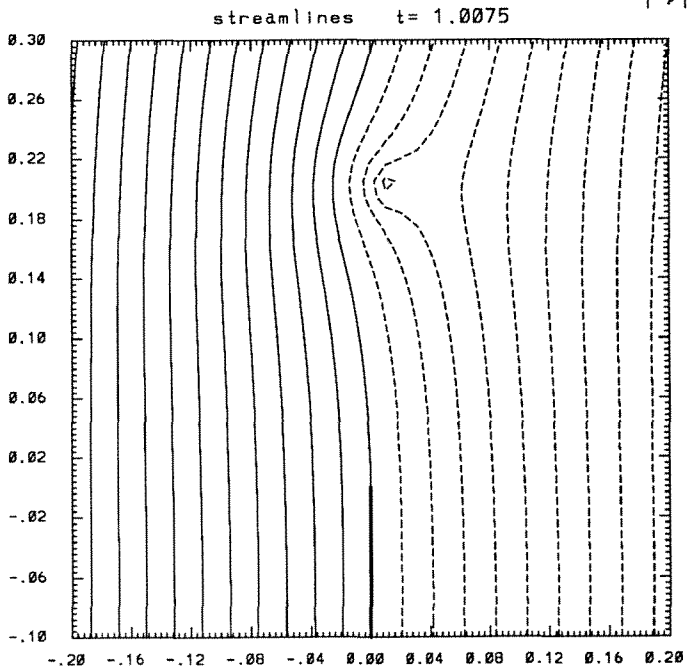

Figure 1.30: Starting vortex: case (c) ($t = 1.0075$, $m = 2$, $n = 1$, $\left|\frac{V}{v_p}\right| \ll 1$, $v_p < 0$).

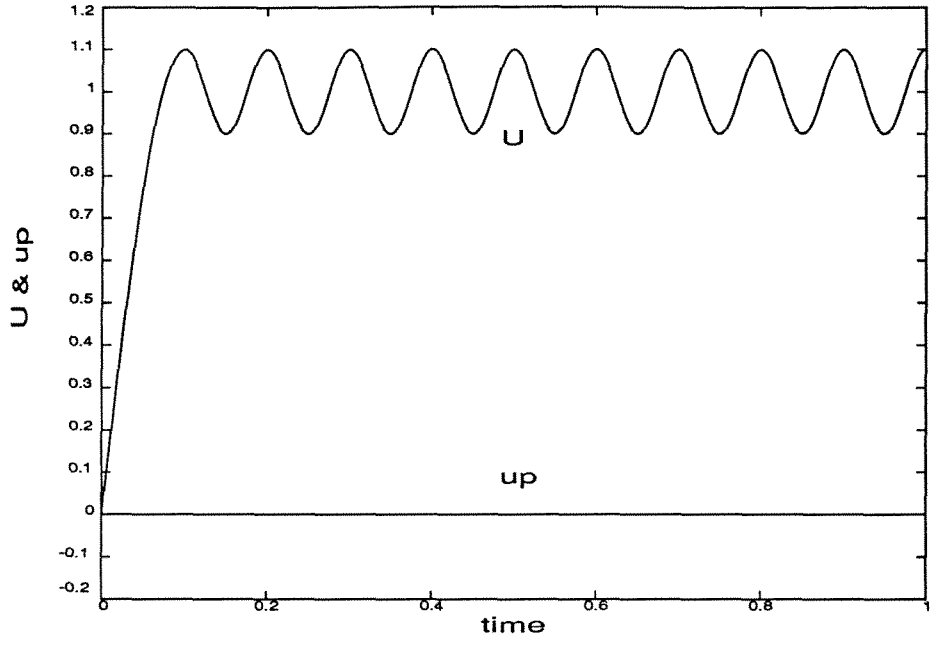

Figure 1.31: Free-stream and plate velocities.

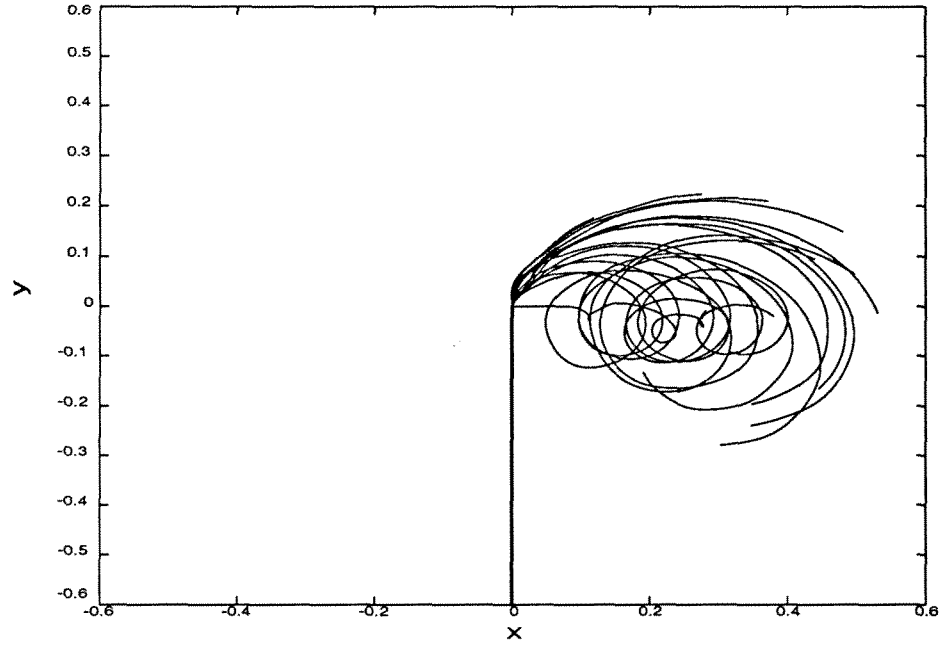

Figure 1.32: Vortices trajectory.

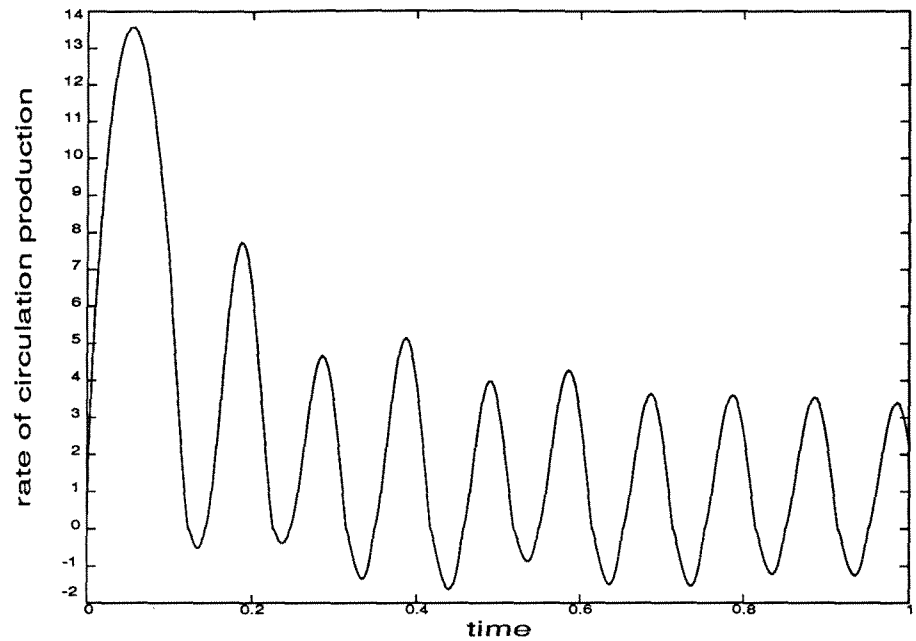

Figure 1.33: Rate of circulation production.

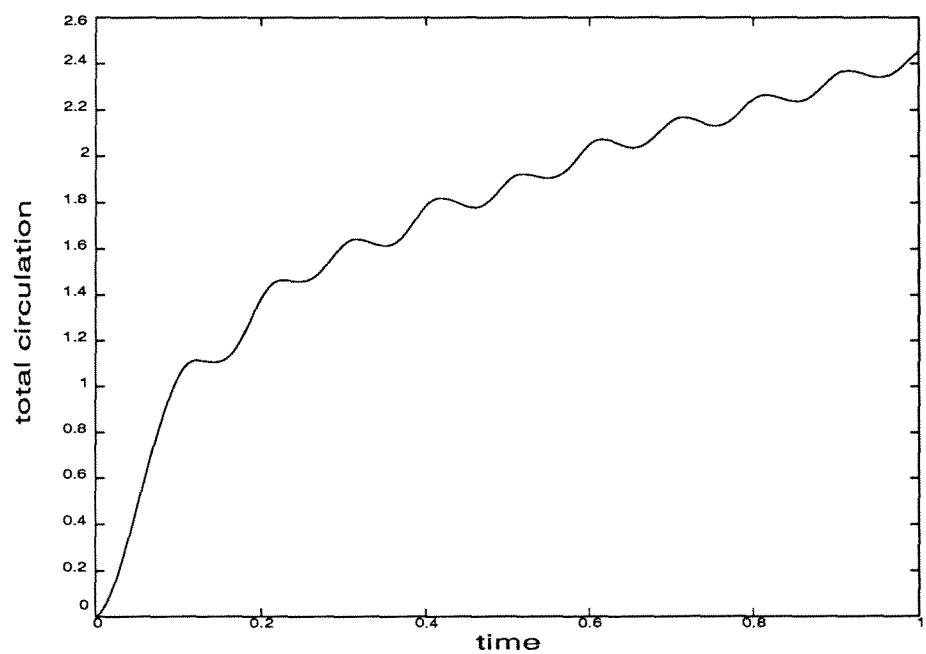

Figure 1.34: Total circulation.

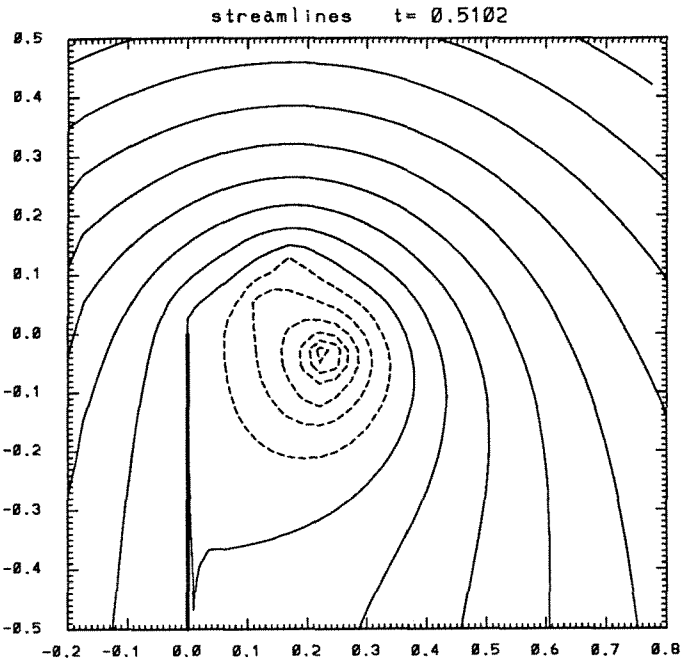

Figure 1.35: Streamlines ($t = 0.5025$).

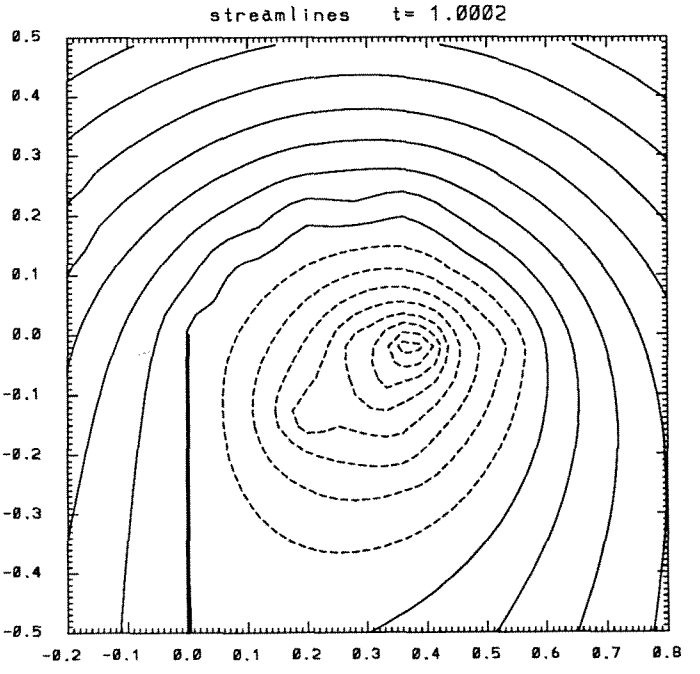

Figure 1.36: Streamlines ($t = 1.0002$).

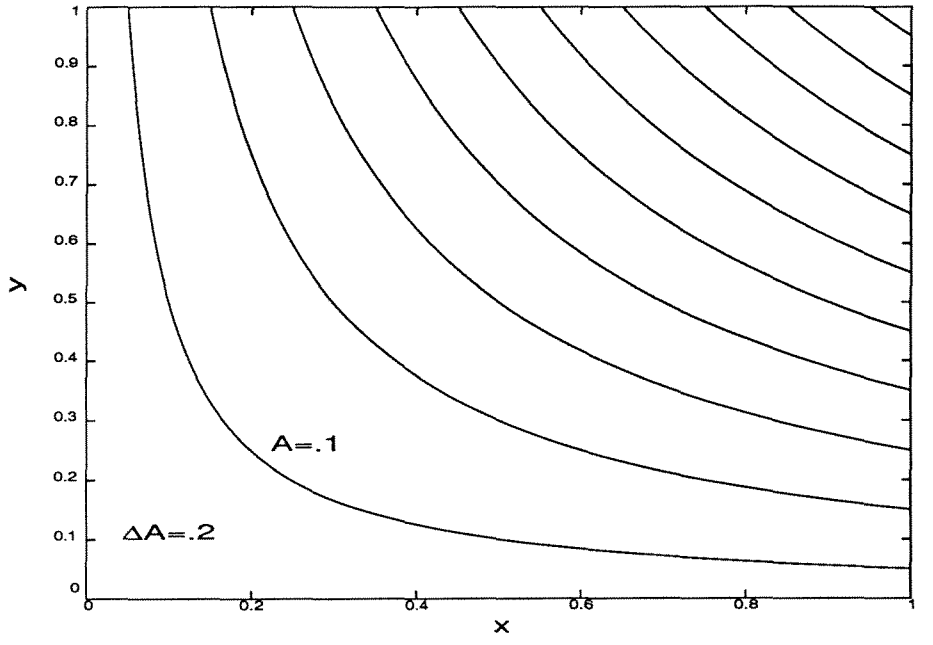

Figure 1.37: Function V in the mapped plane ($U(t) > 0, \forall t > t_s$).

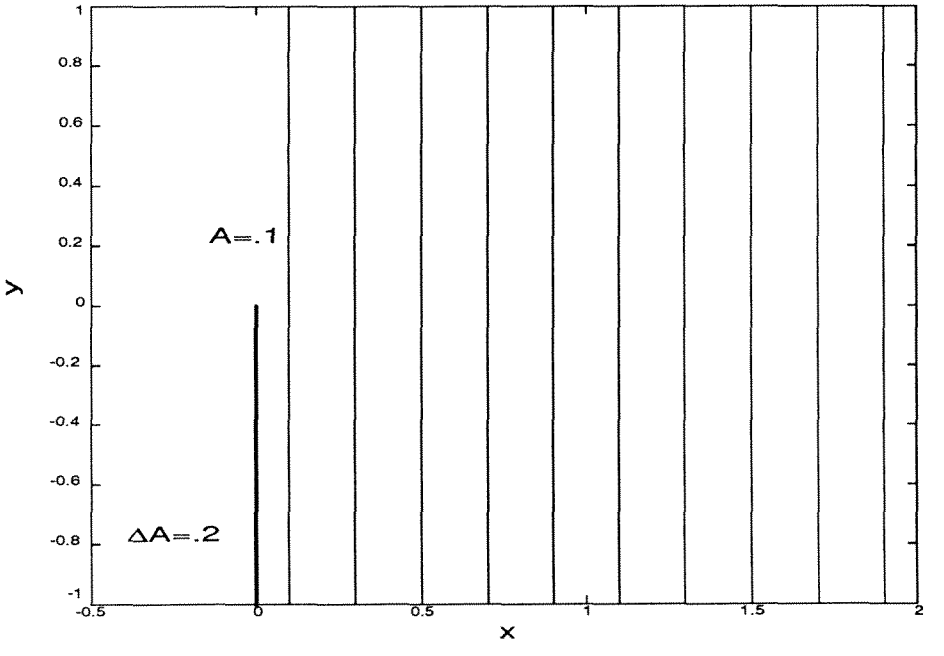

Figure 1.38: Function V in the physical plane ($U(t) > 0, \forall t > t_s$).

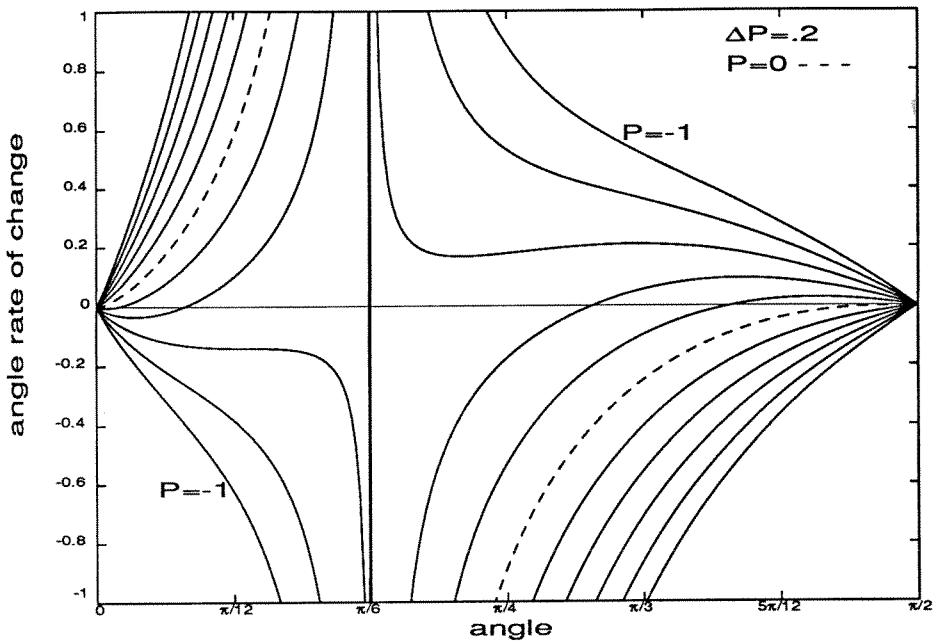

Figure 1.39: Qualitative behavior of $\frac{d\theta_1}{dt}$ with respect to θ_1.

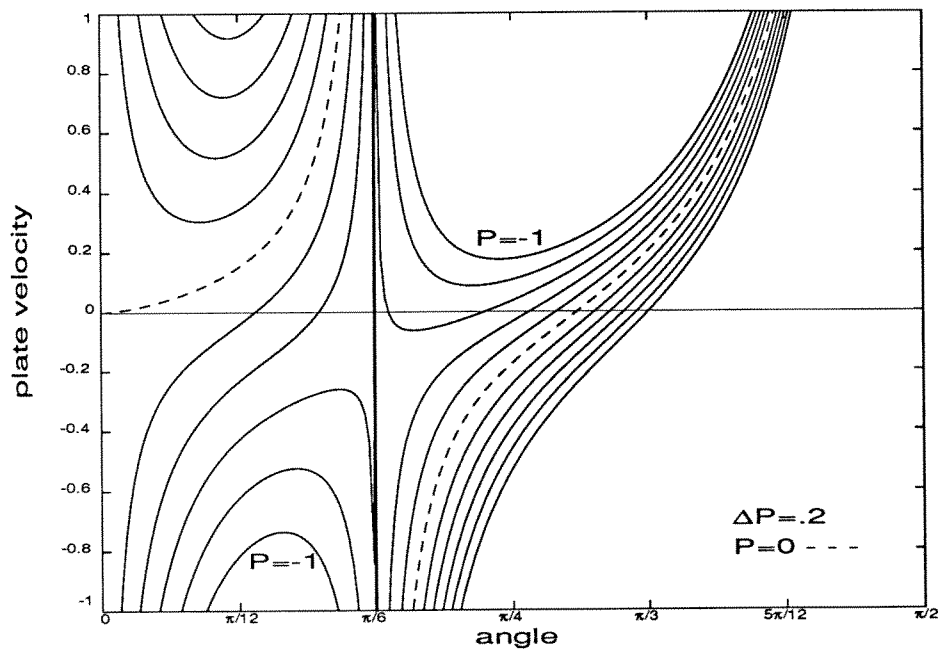

Figure 1.40: Qualitative behavior of the plate velocity u_p with respect to θ_1.

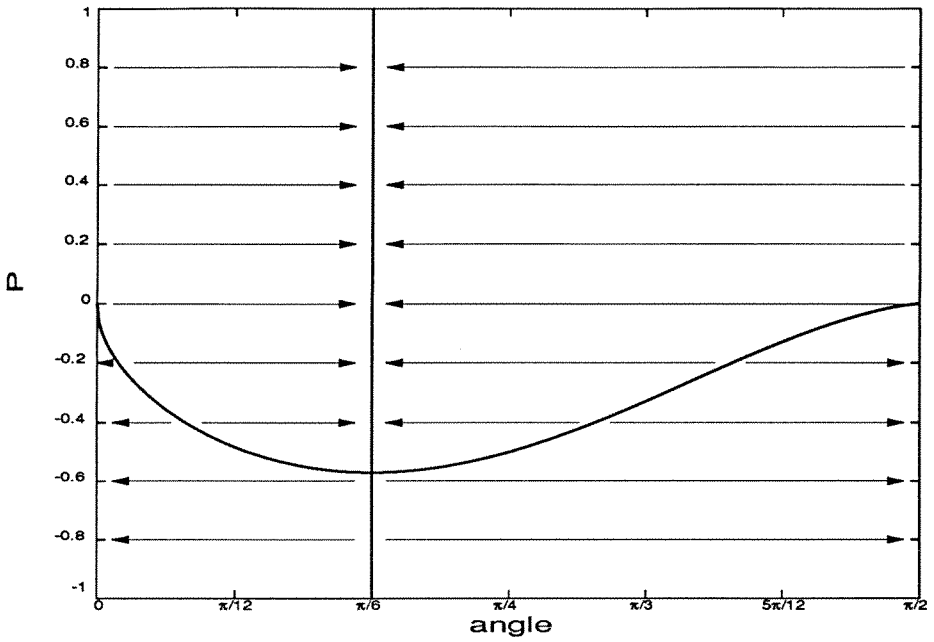

Figure 1.41: Phase portrait.

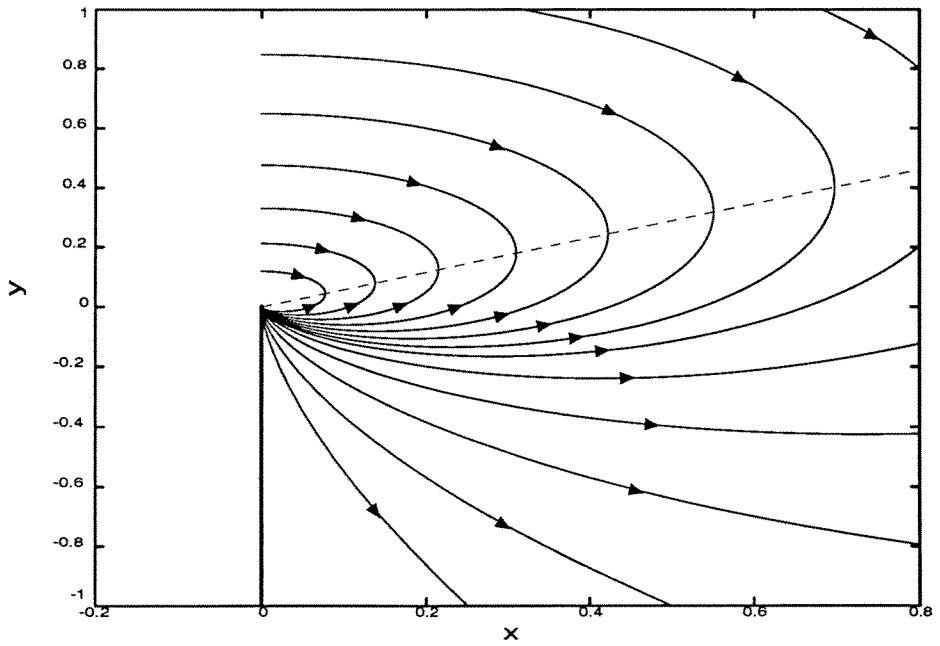

Figure 1.42: Vortex trajectories ($U(t) = const.$).

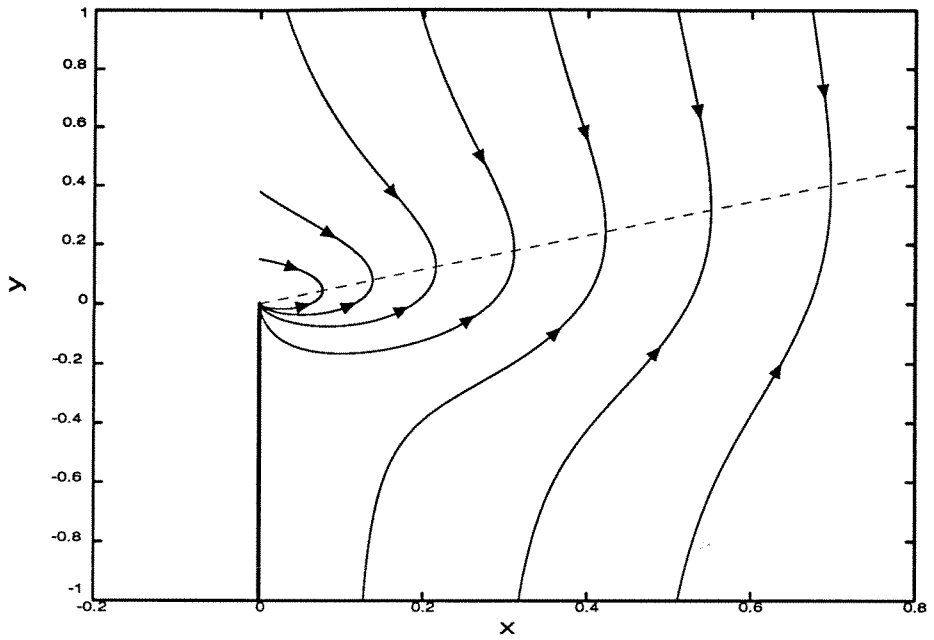

Figure 1.43: Vortex trajectories ($\frac{dU}{dt} = U^2$).

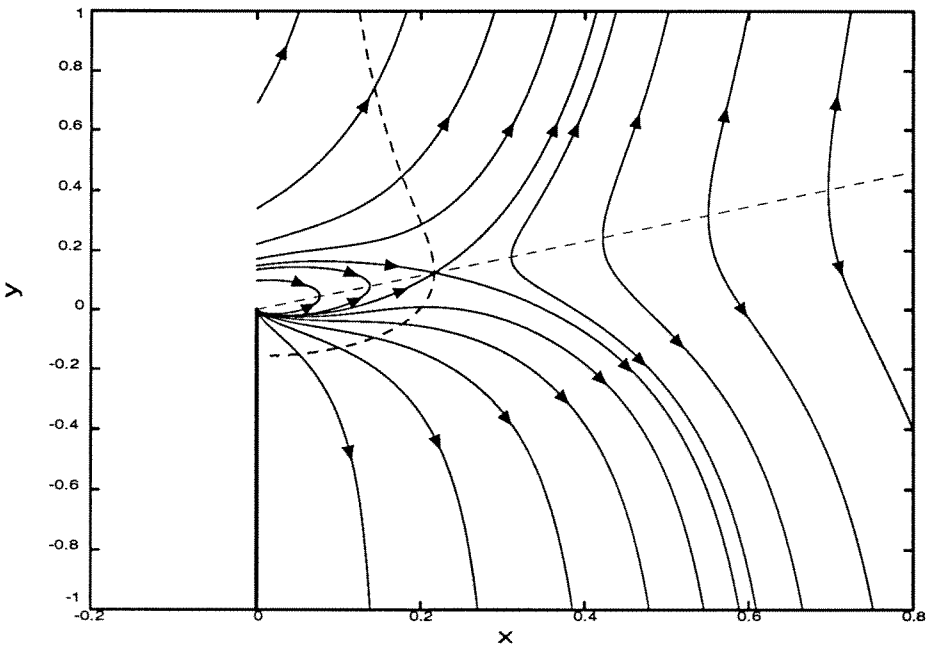

Figure 1.44: Vortex trajectories ($\frac{dU}{dt} = -U^2$).

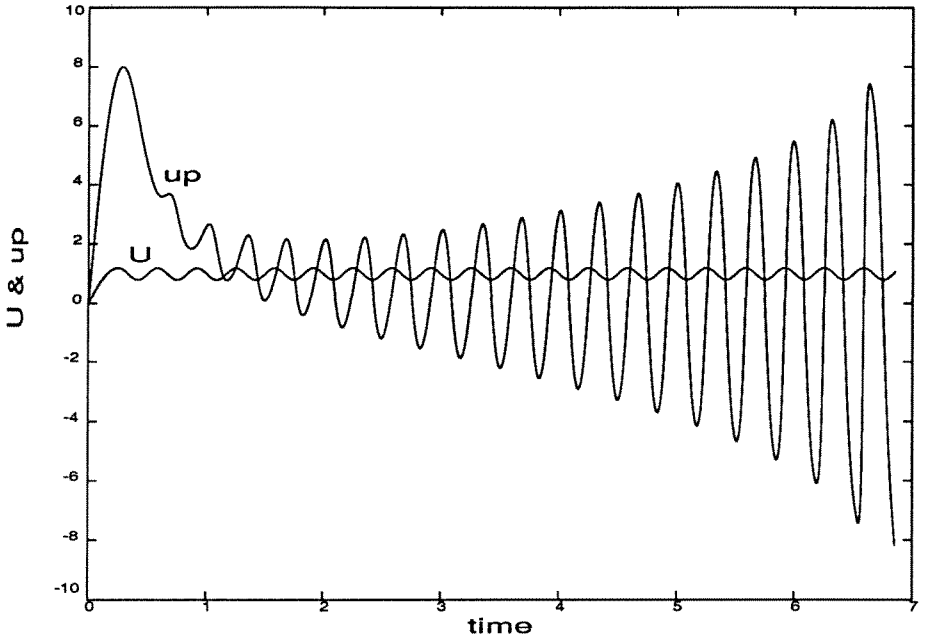

Figure 1.45: Free-stream and plate velocities.

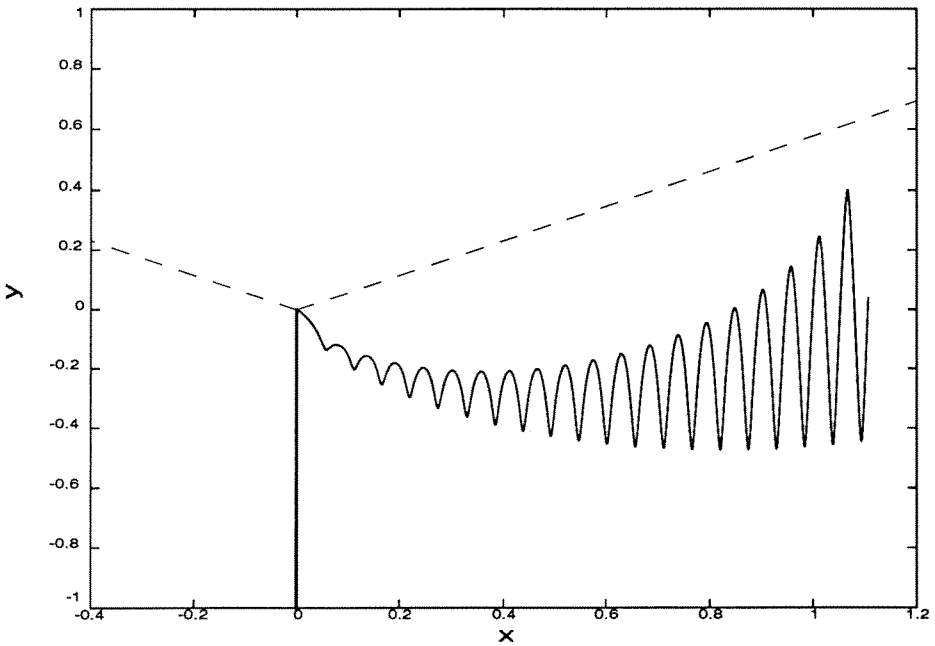

Figure 1.46: Starting vortex trajectory.

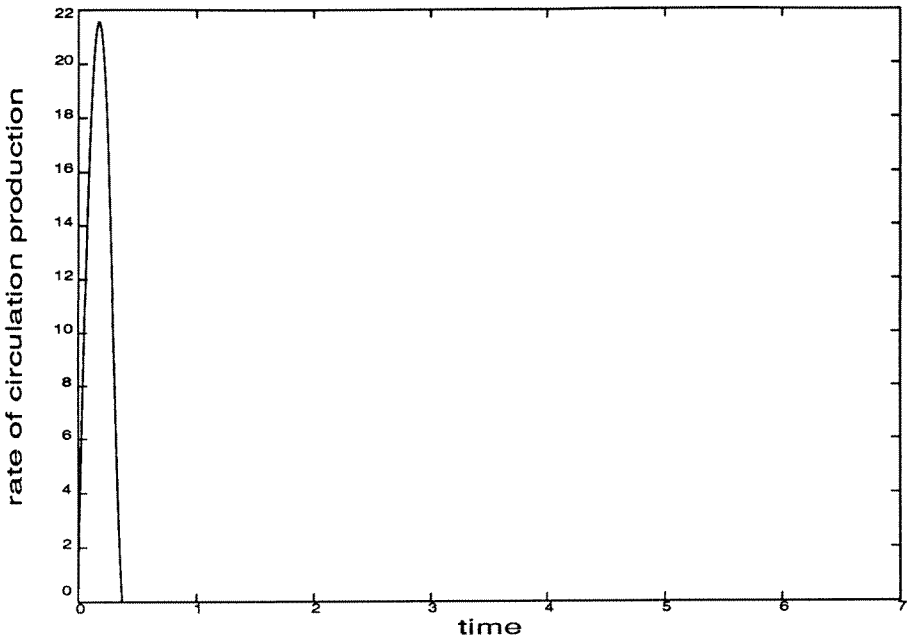

Figure 1.47: Rate of circulation production.

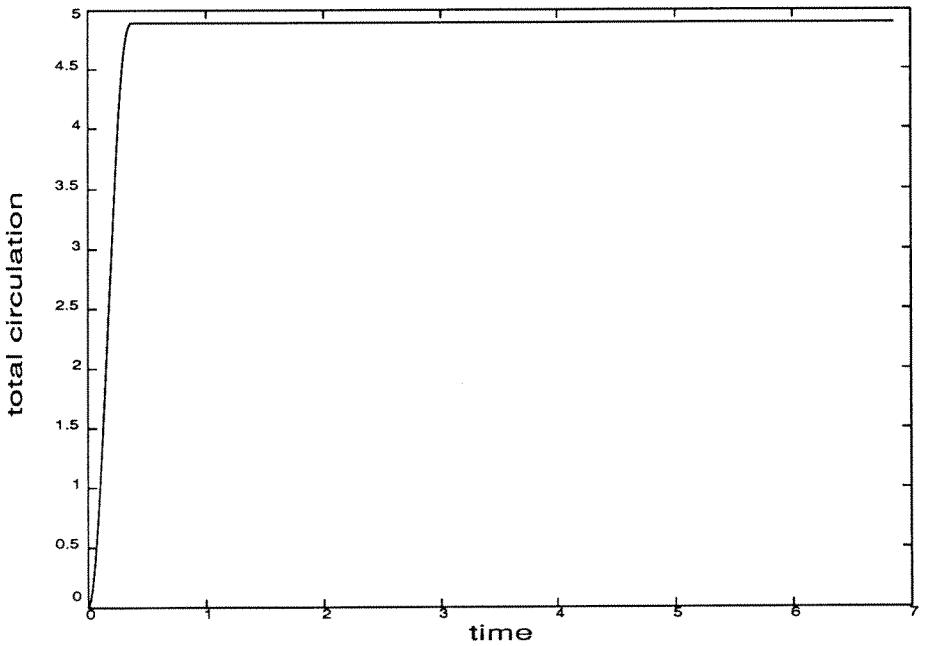

Figure 1.48: Total circulation.

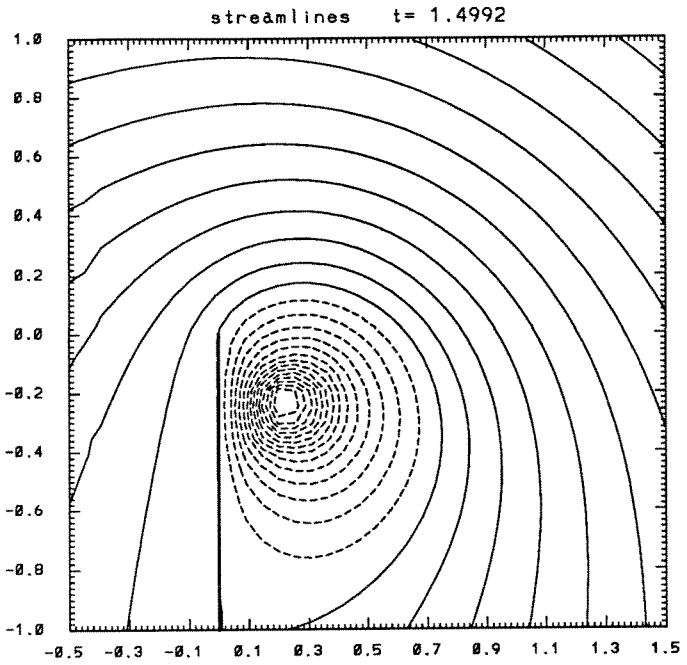

Figure 1.49: Shedding control ($t = 1.4992$).

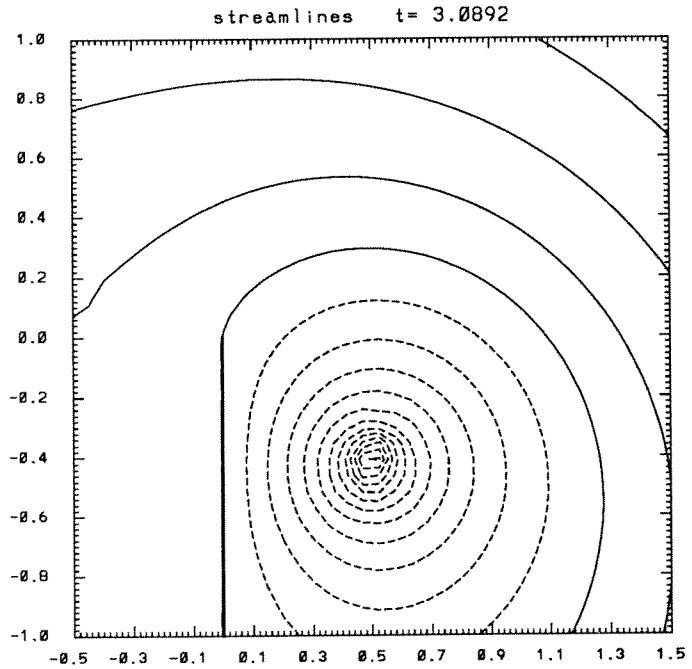

Figure 1.50: Shedding control ($t = 3.0892$).

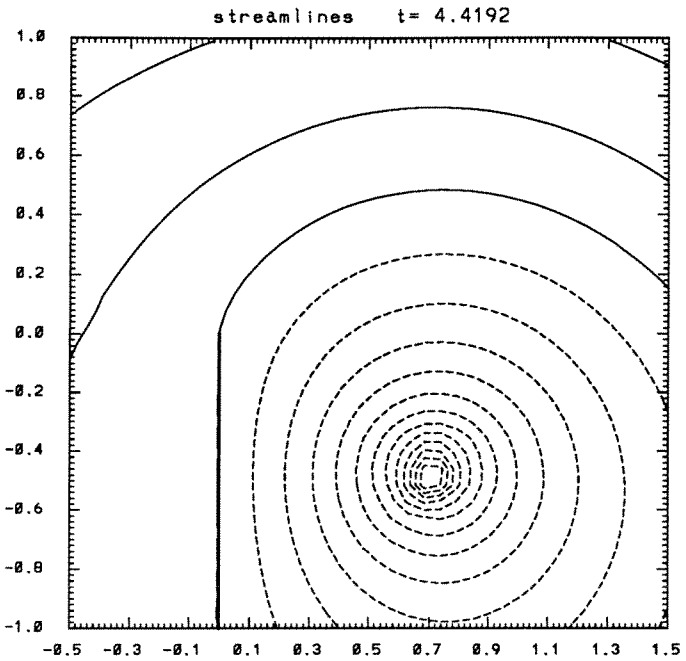

Figure 1.51: Shedding control ($t = 4.4192$).

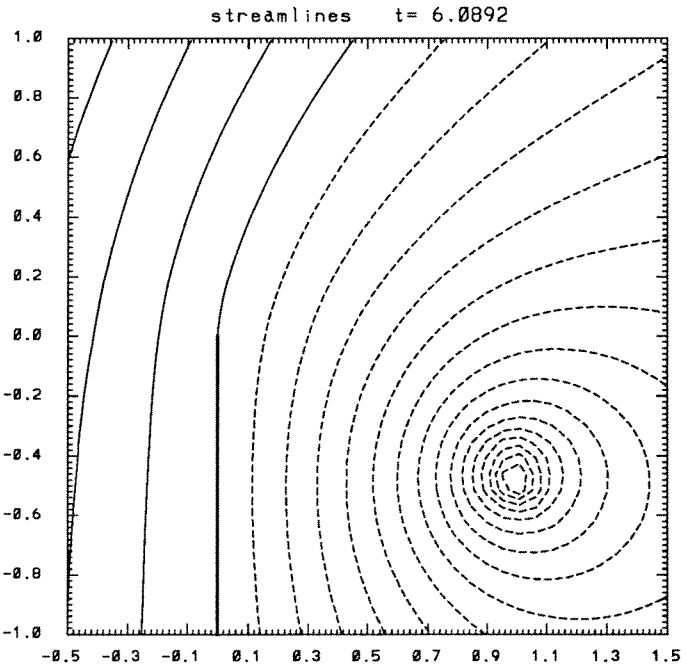

Figure 1.52: Shedding control ($t = 6.0892$).

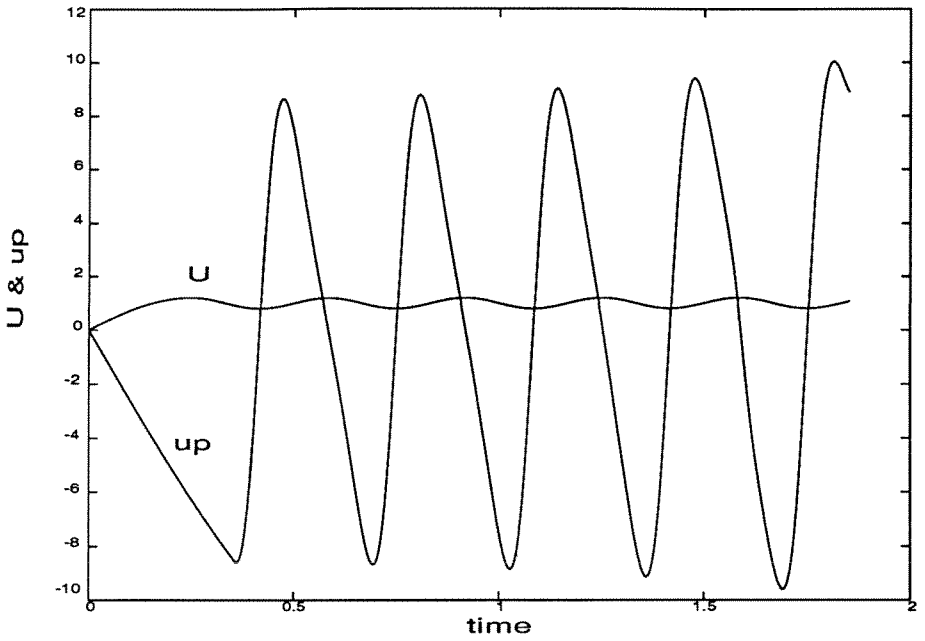

Figure 1.53: Free-stream and plate velocities.

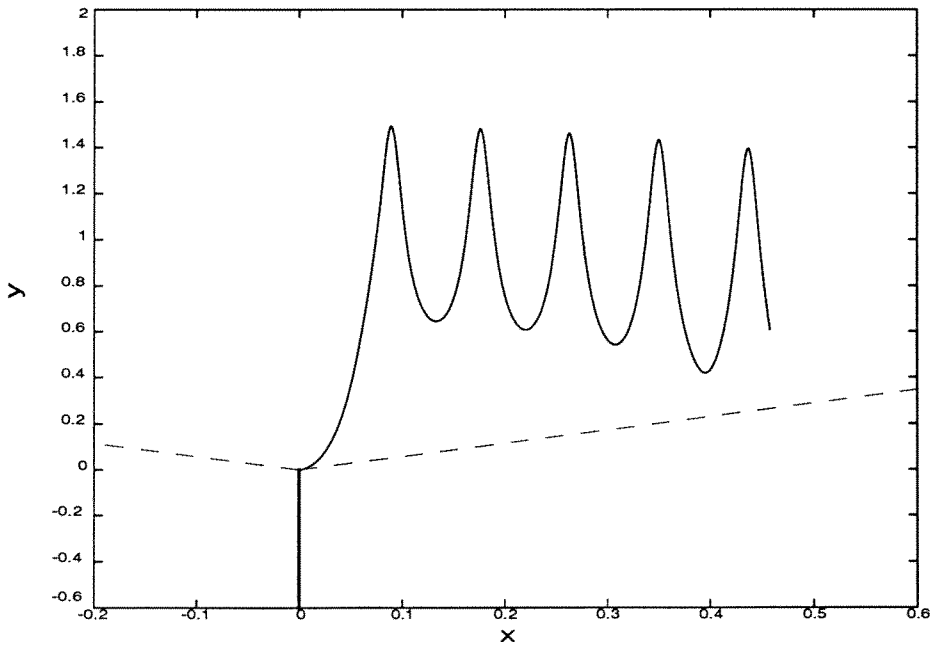

Figure 1.54: Starting vortex trajectory.

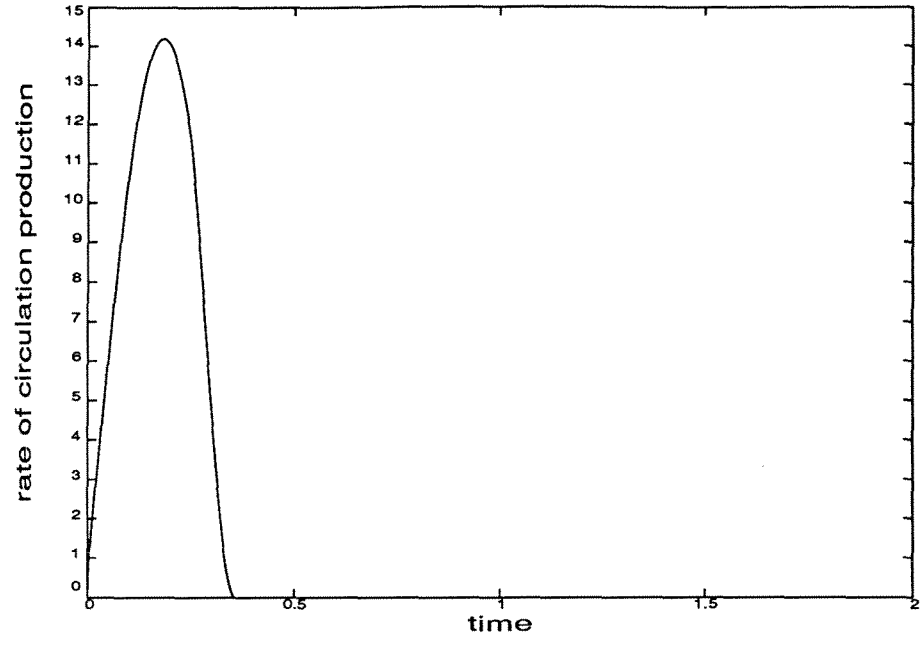

Figure 1.55: Rate of circulation production.

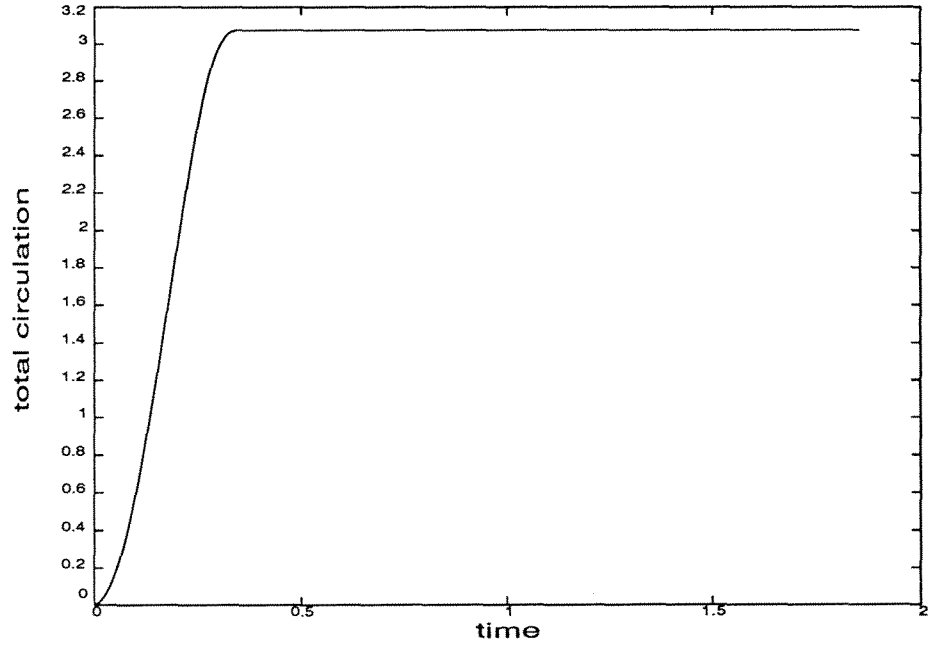

Figure 1.56: Total circulation.

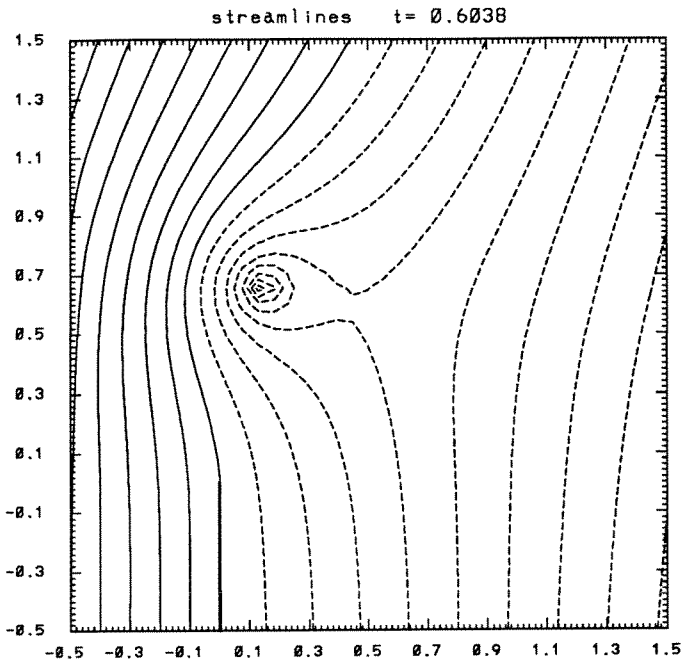

Figure 1.57: Shedding control ($t = 0.6038$).

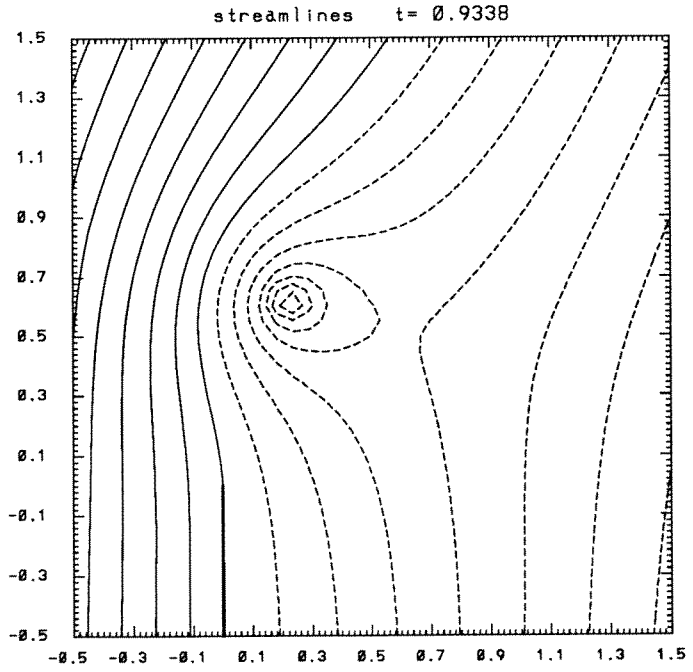

Figure 1.58: Shedding control ($t = .9338$).

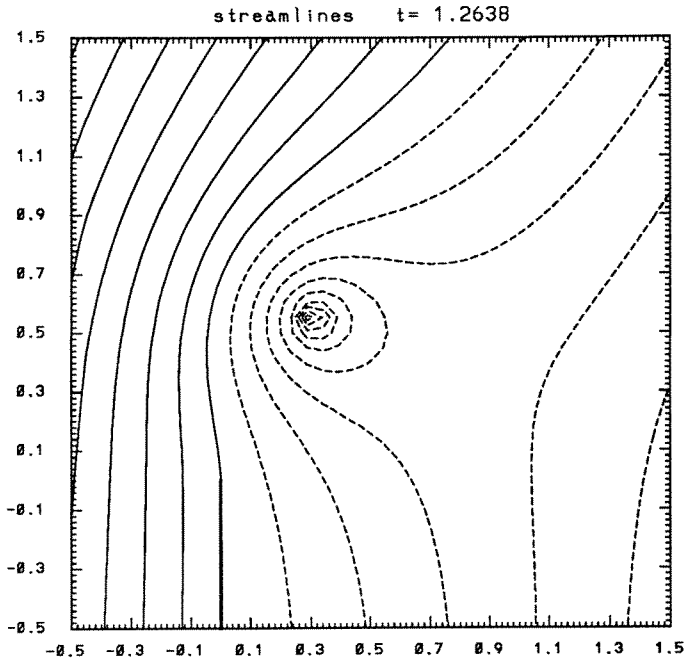

Figure 1.59: Shedding control ($t = 1.2638$).

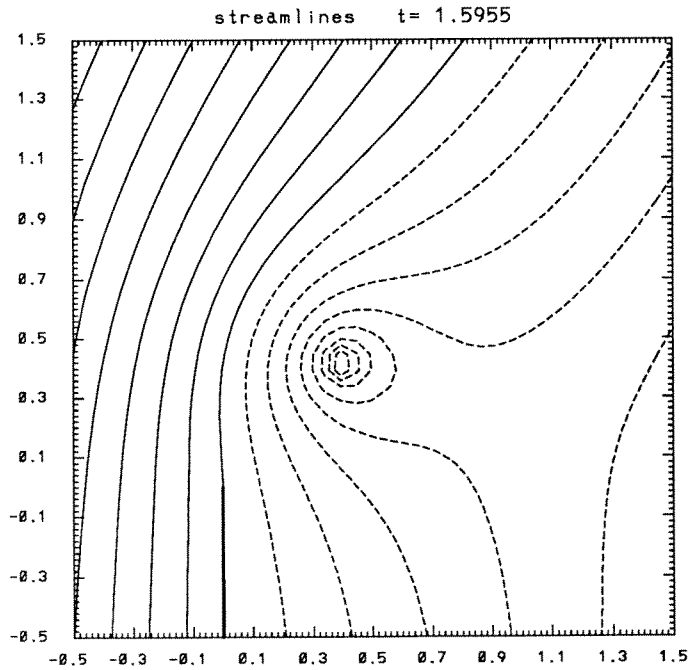

Figure 1.60: Shedding control ($t = 1.5955$).

Appendix

In this appendix we derive the exact solution of the equations of motion for the starting vortex, under the Brown and Michael approximation, for an arbitrary free-stream velocity when the plate is stationary. Let us assume the free-stream velocity finite and positive semi-definite, i.e., $U(t) \geq 0$ $\forall t \geq 0$. These restrictions do not violate the generality of the solution because in the first case an infinite velocity is unphysical and in the second case when the flow reverses the solution cannot be given in terms of only one vortex. We obtain the equations of motion in polar form by setting $u_p = 0$ in (1.22). We have:

$$\begin{cases} \dfrac{d\rho_1}{dt} = \dfrac{U \sin\theta_1}{12\rho_1^2} - \dfrac{\rho_1}{3U}\dfrac{dU}{dt} \\ \dfrac{d\theta_1}{dt} = \dfrac{U\cos 2\theta_1}{8\rho_1^3 \cos\theta_1}, \end{cases} \tag{1.86}$$

with the initial conditions:

$$\begin{cases} \rho_1(0) = 0 \\ \theta_1(0) = \theta_0, \qquad\qquad \theta_0 \in (-\frac{\pi}{2}, \frac{\pi}{2}). \end{cases} \tag{1.87}$$

The initial condition for θ_1 will be derived below because we do not know a priori the initial direction of the vortex.

We multiply the first equation by $3U\rho_1^2$ and the second equation by $\sin\theta_1$. Then, we combine the left hand side of the first equation with the last term on the other side by using a basic differentiation rule. After the manipulation the equations have the following form:

$$\begin{cases} \dfrac{d(U\rho_1^3)}{dt} = \dfrac{U^2 \sin\theta_1}{4} \\ \dfrac{d(\sin\theta_1)}{dt} = \dfrac{U(1-2\sin^2\theta_1)}{8\rho_1^3}. \end{cases} \tag{1.88}$$

Let us now divide both equations by U^2 and introduce the following new variables:

$$\alpha = U\rho_1^3, \qquad\qquad \beta = \sin\theta_1, \tag{1.89}$$

and

$$\tilde{t} = \int_0^t U^2(t')dt'. \tag{1.90}$$

Rewriting the above equations of motion in terms of these new variables we obtain:

$$\begin{cases} \dfrac{d\alpha}{d\tilde{t}} = \dfrac{\beta}{4} \\ \dfrac{d\beta}{d\tilde{t}} = \dfrac{1-2\beta^2}{8\alpha} \end{cases} \tag{1.91}$$

with the initial conditions:

$$\begin{cases} \alpha(0) = 0 \\ \beta(0) = \beta_0, \qquad\qquad \beta_0 \in (-1,1). \end{cases} \tag{1.92}$$

Note the set of equations is independent of the free-stream velocity and hence autonomous.

Combining together the above equations we obtain a second order equation for α only, which has the following form:

$$4\frac{d^2\alpha}{d\tilde{t}^2} + \frac{4}{\alpha}\left(\frac{d\alpha}{d\tilde{t}}\right)^2 - \frac{1}{8\alpha} = 0. \tag{1.93}$$

We multiply this equation by $\alpha/4$ and then we combine the first two terms together by using, again, a basic differentiation rule. We have:

$$\frac{d}{d\tilde{t}}\left(\alpha\frac{d\alpha}{d\tilde{t}}\right) = \frac{1}{32}. \tag{1.94}$$

The integration of this equation is now trivial and the solution is:

$$\alpha = \pm\sqrt{\frac{\tilde{t}^2}{32} + C_1\tilde{t} + C_2}, \tag{1.95}$$

The solution for β is only matter of a differentiation (see 1.91) and we obtain:

$$\beta = \pm 2\left(\frac{\tilde{t}}{16} + C_1\right)\left(\frac{\tilde{t}^2}{32} + C_1\tilde{t} + C_2\right)^{-\frac{1}{2}}. \tag{1.96}$$

Let us determine the constants of integration by imposing the initial conditions. From the condition on α we have:

$$\alpha(0) = 0 \qquad \Rightarrow \qquad C_2 = 0. \tag{1.97}$$

From the condition on β it follows:

$$\beta(0) = \beta_0 \qquad \beta_0 \in (-1, 1) \qquad \Rightarrow \qquad C_1 = 0. \tag{1.98}$$

Finally, the solution is:

$$\alpha = \pm\frac{\tilde{t}}{2^{\frac{5}{2}}}, \qquad \beta = \pm\frac{\sqrt{2}}{2}, \tag{1.99}$$

where the signs have to be taken positive if the flow is from left to right and negative in the opposite direction. Since we assumed initially $U(t) \geq 0\ \forall t \geq 0$, we choose the positive signs. The solution for ρ_1 and θ_1 is recovered simply by inverting the relationships (1.89). We obtain:

$$\rho_1 = \left[\frac{1}{2^{\frac{5}{2}}U}\int_0^t U^2(t')dt'\right]^{\frac{1}{3}}, \qquad \theta_1 = \frac{\pi}{4}. \tag{1.100}$$

Note that $\theta_1 = \frac{\pi}{4}$ is the universal departure angle, i.e., within this model the starting vortex leaves the tip of the plate and moves on a trajectory always perpendicular to the plate for any free-stream condition. We derive the circulation associated with the vortex converting the expression (1.10) in polar coordinate and then substituting for ρ_1 and θ_1 the above expressions. We obtain:

$$\Gamma_1 = \pi U\left[\frac{1}{2U}\int_0^t U^2(t')dt'\right]^{\frac{1}{3}}. \tag{1.101}$$

The rate of circulation production is the time derivative of the above expression and has the following form:

$$\frac{d\Gamma_1}{dt} = \frac{\pi}{3}U\left[\frac{dU}{dt}\int_0^t U^2(t')dt' + \frac{U^3}{2}\right]\left[\frac{U^2}{2}\int_0^t U^2(t')dt'\right]^{-\frac{2}{3}}. \tag{1.102}$$

The last two results permit us to define the range of validity of the solution. The solution is physically valid $\forall t \geq 0$ only if the free-stream velocity is a monotonically increasing function of time. Otherwise, if the flow is allowed to decelerate then the rate of circulation production might change sign and hence the solution is valid only up to time t_s when $\frac{d\Gamma_1}{dt} = 0$. To analyze this situation let us assume that the free-stream velocity is a monotonically increasing function of time up to t_{max} where it reaches its maximum and then it becomes a monotonically decreasing function of time up

to t_{final} when it becomes zero. In other words, $U(t)$ is such that:

$$\begin{aligned} \frac{dU}{dt} &> 0 \qquad && 0 < t < t_{max}, \\ \frac{dU}{dt} &= 0 \qquad && t = t_{max}, \\ \frac{dU}{dt} &< 0 \qquad && t_{max} < t < t_{final}. \end{aligned}$$

For such a free-stream velocity the above solution is mathematically, but not physically, well defined. In fact, from the expression for Γ_1 it follows that the sign of the circulation agrees with the sign of the free-stream velocity and it goes to zero at t_{final}. Consequently, the the strength of the vortex increases at the beginning, then it reaches a maximum, then starts to decrease and finally the vortex vanishes. This behavior is unphysical but the solution is valid up to time t_s when the circulation has its maximum. In other words, at time t_s, when the rate of circulation production changes sign, the simulation should be stopped and a new vortex introduced in the flow as assumed in Section 1.5. It is interesting to predict when this happens. The expression (1.102) shows that the sign of the rate of circulation production depends on the sign of the free-stream acceleration. Since $\frac{d\Gamma_1}{dt}$ is positive up to time t_{max}, because $\frac{dU}{dt} \geq 0$, and negative at time t_{final}, because $\Gamma_1 = 0$, it follows that $t_{max} < t_s < t_{final}$. Hence, the rate of circulation production changes sign always during the flow deceleration or, in other words, the system starts to produce circulation of opposite sign before the flow is actually reversed. The time t_s when the rate of circulation production goes to zero depends on free-stream velocity and in principle can always be computed by solving the following equation:

$$\left.\frac{dU}{dt}\right|_{t=t_s} = -\frac{U^3(t_s)}{2}\left[\int_0^{t_s} U^2(t')dt'\right]^{-1}. \tag{1.103}$$

The case where the free-stream velocity has more than one maximum is physically ambiguous because we do not know how many vortices are actually created. The solution is mathematically well defined but its physical meaning depends on the particular situation under investigation.

The form of the above solutions (1.100–1.101) suggests scaling the problem in the following way:

$$\rho_1^* = \rho_1, \qquad \theta_1^* = \theta_1, \qquad t^* = \frac{1}{U}\int_0^t U^2(t')dt', \tag{1.104}$$

and

$$U^* = \frac{U}{U} = 1, \qquad \Gamma_1^* = \frac{\Gamma_1}{U}. \tag{1.105}$$

Note the scaled rate of circulation production is related to the physical quantities in a rather unusual and complex form:

$$\frac{d\Gamma_1^*}{dt^*} = \left[\frac{d\Gamma_1}{dt} - \frac{\Gamma_1}{U}\frac{dU}{dt}\right]\left[U^2 - \frac{1}{U}\frac{dU}{dt}\int_0^t U^2(t')dt'\right]^{-1}. \tag{1.106}$$

Rewriting the solution in terms of the above quantities we obtain:

$$\rho_1^* = \frac{t^{*\frac{1}{3}}}{2^{\frac{1}{6}}}, \qquad \theta_1^* = \frac{\pi}{4}, \tag{1.107}$$

and the circulation and its rate of production become:

$$\Gamma_1^* = \pi\left(\frac{t^*}{2}\right)^{\frac{1}{3}}, \qquad \frac{d\Gamma_1^*}{dt^*} = \frac{\pi}{3}\frac{1}{(2t^{*2})^{\frac{1}{3}}}. \tag{1.108}$$

It is worth to underline that the scaled solution is, within the model, the universal solution of the problem and coincides with the solution for the impulsively started case when $U(t) = 1$. Consequently, the knowledge of the behavior of the system for the impulsively started case is sufficient to produce complete information about any other case.

Chapter 2

The finite plate of variable length

2.1 Introduction

In recent years, the efforts to actively control unsteady separated fluid flows in a broad range of applications have become more intense, see [8] for a discussion and references. In particular the control of the flow past bluff bodies is receiving a great amount of attention because of the large variety of applications: lift enhancement, drag reduction, noise and vibration control, mixing improvement, etc.. It is worth recalling that most of these studies are of an experimental nature while numerical contributions have increased in the past few years. Theoretical work is almost nonexistent probably because of the high complexity of the equations governing the flow.

The description of the flow through the full Navier-Stokes equations might be preferable for accuracy but would be dependent on large-scale computation and would not necessarily lead to any insights that would guide to the derivation of a control strategy. Consequently, this route will unlikely produce a controller which can be applied to an experimental situation in the near future. The approach we are taking in the present study is to derive a simpler fluid model which is able to capture the major features of the flow. With a simpler mathematical description it might be

possible to solve theoretically a class of interesting control problems and to produce fast numerical algorithms. All the secondary details neglected by the model and the further uncertainty introduced by the final application can be accounted for by making the controller robust [6] [7].

Recently, efforts to control certain features of the wake behind bluff and slender bodies, such as reduction or magnification of the wake thickness [24], vortex cancellation [11] and pattern reproduction [15] [16] have been successful. In all these experiments the free-stream velocity was kept constant and quasi-steady results were achieved, in general, by moving the body with a frequency scaled by the shedding frequency. In a more general situation in which the free-stream velocity is time dependent this approach is generally not sufficient to control the flow and a feedback control strategy is necessary.

In the present study we investigate active circulation control of a two-dimensional separated flow past a flat plate of variable length. Based on the successful results obtained in Chapter 1 we extend the model and the control strategy derived for the semi-infinite plate to the finite geometry. At first, we give a general formulation of the model but subsequently, due to the complexity of the problem, we impose symmetry respect to the x-axis. In other words, we restrict ourselves to study symmetric wakes only and, consequently, the only degree of freedom left to control the flow is the length of the plate. This restriction is not that severe because there is experimental evidence [13] that the near wake is almost symmetric when the free-stream acceleration is nonzero. The well known symmetry of the starting wake is an example. Furthermore, the plate of variable length can be regarded as the two-dimensional analog of a delta wing of variable sweep angle and therefore these studies could provide deeper insight about vortex management concepts in such three-dimensional flows [19].

Following our previous work we model the unsteady separation from the finite plate by means of a vortex pair whose time-dependent circulation is predicted by an unsteady Kutta condition. The expansion of the equation of motion about the tip of the plate recovers, at the leading order, the equation of motion obtained for the semi-infinite plate. Therefore, the small times approximate

solutions derived in Chapter 1 can be used to start the numerical integration of the present problem. To validate the model we compare the results regarding the drag experienced by the plate and the length of the recirculating bubble during a power-law starting flow with those provided by experiments and a full numerical simulation (see [4], [13] and [23]).

The analysis of the results obtained for the power-law starting flow also suggests a new approach in scaling the flow. When the problem is scaled with a suitable function of time the hidden universality is revealed, i.e., all the results nearly collapse on to a set of universal functions. During the evolution of the flow we can recognize two distinct regimes, at early times there are two small recirculating bubbles while at later times only a large bubble is present in the flow. Consequently, two time-dependent scaling functions are proposed which unveiled the universality of the phenomenon for small and large times.

The vortex shedding mechanism proposed and tested in Chapter 1 is extended to the present problem to allow the simulation of flows involving multiple vortices. Because our final goal is to derive a fast numerical algorithm, a highly conservative vortex merging scheme is proposed to recombine vortices and improve the computational time. A new approach is taken with respect to the conventional merging schemes [22] and the vortices are recombined in such a way that the velocity at the separation point remains unchanged and the impulse is identically conserved. Furthermore for a proposed merge to take place, the change in the rate of circulation production and in the drag must be below certain limits.

From the expansion of the equation of motion for the first vortex when other vortices are present in the flow we obtain an expression which is closely related with that derived in Chapter 1 for the semi-infinite plate. As before there exists a critical rate of change of the plate length beyond which the separation cannot take place in the model. Based on this observation we derive a control strategy which inhibits the production of further circulation when a vortex pair is present in the flow. Furthermore, we obtain for any time-dependent free-stream velocity an ordinary differential

equation which predicts the length of the plate that satisfies the Kutta condition without requiring further shedding of vorticity into the wake. The performance of the controller is then characterized by a dynamical system type of analysis. Finally, we discuss the results provided by two simulations in which the controller is successfully tested.

2.2 Mathematical formulation

In this section we introduce a mathematical model able to represent the phenomenon of the two dimensional unsteady separation from the tips of a finite plate of variable span in the presence of an unsteady free-stream velocity. Let us assume that the regions of vorticity that separate from the boundary layer and are convected away are thin enough to justify a description by means of a vortex sheet. The consequent stretching and rolling up of the vortex sheet, due to the unsteadiness of the flow, suggests a more coarse description via point vortices. The vortex sheet is not completely lost, it is assumed of negligible circulation that connects the feeding point to a point vortex of variable strength which is able to satisfy an unsteady Kutta condition. Mathematically the feeding vortex sheet is just the branch cut due to the logarithmic singularity representing the vortex.

The mathematical formulation of the problem can be simplified by choosing a frame of reference fixed to the plate so that the body can be identified with the segment $[-2ia(t), 2ia(t)]$. In this frame of reference the plate is still and the fluid moves parallel to the x-axis with free-stream velocity $U(t)$. Then, the flow of an incompressible irrotational fluid about such a body can be solved via conformal mapping. The Joukowski transformation maps a finite plate of semi-span $2a$ in the z-plane onto the circle of radius a in the ζ-plane (see Figure 2.1) preserving the characteristic of the flow at infinity. If the span of the plate changes on time then the mapping has to depend on time too, so we have:

$$z = \zeta - \frac{a^2(t)}{\zeta}. \tag{2.1}$$

Since Laplace's equation is linear and the boundary conditions in the mapped plane can be treated

using the circle theorem [14], we can build the complex potential F superimposing basic flows. Note that for convenience we are departing from the usual convention and taking the circulation positive when in the clockwise sense. Thus, the complex velocity field $w = \frac{dF}{d\zeta}$ has the form:

$$\begin{aligned} w(\zeta,t) = U(t)\left(1-\frac{a^2(t)}{\zeta^2}\right) + \frac{i\Gamma_1^t(t)}{2\pi}\left(\frac{1}{\zeta-\zeta_1^t(t)} + \frac{\bar{\zeta}_1^t(t)}{a^2(t)-\zeta\bar{\zeta}_1^t(t)} + \frac{1}{\zeta}\right) + \\ + \sum_{n=2}^{N_t}\frac{i\Gamma_n^t}{2\pi}\left(\frac{1}{\zeta-\zeta_n^t(t)} + \frac{\bar{\zeta}_n^t(t)}{a^2(t)-\zeta\bar{\zeta}_n^t(t)} + \frac{1}{\zeta}\right) + \\ + \frac{i\Gamma_1^b(t)}{2\pi}\left(\frac{1}{\zeta-\zeta_1^b(t)} + \frac{\bar{\zeta}_1^b(t)}{a^2(t)-\zeta\bar{\zeta}_1^b(t)} + \frac{1}{\zeta}\right) + \\ + \sum_{n=2}^{N_b}\frac{i\Gamma_n^b}{2\pi}\left(\frac{1}{\zeta-\zeta_n^b(t)} + \frac{\bar{\zeta}_n^b(t)}{a^2(t)-\zeta\bar{\zeta}_n^b(t)} + \frac{1}{\zeta}\right). \end{aligned} \tag{2.2}$$

In the above expression we have the free-stream velocity, U, the radius of the circle, a, N_t vortices shed by the top tip at $\zeta = \zeta_n^t$ with their images within the circle, and N_b vortices shed by the bottom tip at $\zeta = \zeta_n^b$ and their images. We allow the strength of the first top and bottom vortex to depend on time so that the Kutta condition at the two tips of the plate may be satisfied. We choose the convention that the vortex of variable strength is labeled with the subscript 1, so that any time a vortex is shed all the others are renumbered.

To describe the motion of this system of vortices in the physical plane we use the following set of ordinary differential equations:

$$\begin{cases} \dfrac{d\bar{z}_1^t}{dt} + (\bar{z}_1^t - \bar{z}_0^t)\dfrac{1}{\Gamma_1^t}\dfrac{d\Gamma_1^t}{dt} = \lim\limits_{z\to z_1^t}\left\{\dfrac{d}{dz}\left[F - \dfrac{i\Gamma_1^t}{2\pi}\log(z-z_1^t)\right]\right\} \\ \dfrac{d\bar{z}_r^t}{dt} = \lim\limits_{z\to z_r^t}\left\{\dfrac{d}{dz}\left[F - \dfrac{i\Gamma_r^t}{2\pi}\log(z-z_r^t)\right]\right\} \\ \dfrac{d\bar{z}_1^b}{dt} + (\bar{z}_1^b - \bar{z}_0^b)\dfrac{1}{\Gamma_1^b}\dfrac{d\Gamma_1^b}{dt} = \lim\limits_{z\to z_1^b}\left\{\dfrac{d}{dz}\left[F - \dfrac{i\Gamma_1^b}{2\pi}\log(z-z_1^b)\right]\right\} \\ \dfrac{d\bar{z}_r^b}{dt} = \lim\limits_{z\to z_r^b}\left\{\dfrac{d}{dz}\left[F - \dfrac{i\Gamma_r^b}{2\pi}\log(z-z_r^b)\right]\right\}, \end{cases} \tag{2.3}$$

with the initial conditions:

$$\begin{cases} z_1^t(t_s) = z_0^t \\ z_r^t(t_s) = z_{r_s}^t \qquad r = 2...N_t \\ z_1^b(t_s) = z_0^b \\ z_r^b(t_s) = z_{r_s}^b \qquad r = 2...N_b, \end{cases} \tag{2.4}$$

where F is the complex potential and z_0^t and z_0^b are the top and bottom separation points. Note, for example, $z_{r_s}^t$ was the final position of the top vortex $r-1$ at the shedding time $t = t_s$ which becomes the initial position of the top vortex r. Thus the number of equations increases anytime a new vortex is shed.

There is experimental evidence [13] that the near wake is nearly two dimensional and symmetric about the x-axis if the plate moves with a non-zero acceleration. Under these circumstances the problem can be simplified through the following constraints:

$$\begin{cases} \Gamma_n^t = \Gamma_n \\ \zeta_n^t = \zeta_n \\ \bar{\zeta}_n^t = \bar{\zeta}_n, \end{cases} \qquad \begin{cases} \Gamma_n^b = -\Gamma_n \\ \zeta_n^b = \bar{\zeta}_n \\ \bar{\zeta}_n^b = \zeta_n, \end{cases} \qquad n = 1...N. \tag{2.5}$$

Imposing these conditions on the complex velocity field (2.2) it reduces to:

$$\begin{aligned} w(\zeta,t) = U\left(1-\frac{a^2}{\zeta^2}\right) + \frac{i\Gamma_1}{2\pi}\left(\frac{1}{\zeta-\zeta_1} + \frac{\bar{\zeta}_1}{a^2-\zeta\bar{\zeta}_1} - \frac{1}{\zeta-\bar{\zeta}_1} - \frac{\zeta_1}{a^2-\zeta\zeta_1}\right) + \\ + \sum_{n=2}^{N} \frac{i\Gamma_n}{2\pi}\left(\frac{1}{\zeta-\zeta_n} + \frac{\bar{\zeta}_n}{a^2-\zeta\bar{\zeta}_n} - \frac{1}{\zeta-\bar{\zeta}_n} - \frac{\zeta_n}{a^2-\zeta\zeta_n}\right). \end{aligned} \tag{2.6}$$

The need to impose the Kutta condition is consequence of the fact that the potential flow in the physical plane presents a square root singularity at the tips of the plate. In the ζ-plane the flow is non-singular since the singularity has been absorbed by the mapping. To remove the singularity in

the z-plane the complex velocity (2.6) in the mapped plane has to be zero at the top and bottom of the circle, i.e., at $\zeta = \pm ia$. Solving for Γ_1 we obtain:

$$\Gamma_1 = -\pi i \frac{(a^2+\zeta_1^2)(a^2+\bar{\zeta}_1^2)}{(\zeta_1-\bar{\zeta}_1)(a^2-\zeta_1\bar{\zeta}_1)} \left[2U - \sum_{n=2}^{N} \frac{i\Gamma_n}{\pi} \frac{(\zeta_n-\bar{\zeta}_n)(a^2-\zeta_n\bar{\zeta}_n)}{(a^2+\zeta_n^2)(a^2+\bar{\zeta}_n^2)} \right]. \tag{2.7}$$

From the comparison of this expression with that obtained for the semi-infinite plate (1.3) we can see that the structure, although more complicated, is basically the same. Note, also, the strong dependency of Γ_1 from the radius a of the circle, i.e., from the length of the plate. Let us see now how the symmetry constraints affect the equations of motion (2.3). They collapse to:

$$\begin{cases} \dfrac{d\bar{z}_1}{dt} + (\bar{z}_1 - \bar{z}_0)\dfrac{1}{\Gamma_1}\dfrac{d\Gamma_1}{dt} = \lim\limits_{z\to z_1} \left\{ \dfrac{d}{dz} \left[F - \dfrac{i\Gamma_1}{2\pi} \log(z-z_1) \right] \right\} \\ \dfrac{d\bar{z}_r}{dt} = \lim\limits_{z\to z_r} \left\{ \dfrac{d}{dz} \left[F - \dfrac{i\Gamma_r}{2\pi} \log(z-z_r) \right] \right\}, \end{cases} \tag{2.8}$$

with the initial conditions:

$$\begin{cases} z_1(t_s) = z_0 \\ z_r(t_s) = z_{r_s} \qquad r = 2...N. \end{cases} \tag{2.9}$$

Hence, formally, the problem reduces to the same one we have solved for the semi-infinite plate (1.4), all the differences are due to the more complicated form of the complex velocity field w, compare (2.6) with (1.2).

Now we consider if it is more convenient to solve the problem in the physical or in the mapped plane. In both cases we must use complicated transformations, but in the ζ-plane it seems easier to understand and keep track of the different contributions. Once we have performed the change of variables, substituted for the complex potential and, carried out the limits required in the equations

(2.8), we obtain:

$$
\begin{cases}
\left[\dfrac{\bar{\zeta}_1^2+a^2}{\bar{\zeta}_1^2}+\dfrac{(\bar{\zeta}_1+ia)^2}{\bar{\zeta}_1}\dfrac{(a^2+\zeta_1^2)(a^2-\bar{\zeta}_1^2)}{(a^2+\bar{\zeta}_1^2)(\zeta_1-\bar{\zeta}_1)(a^2-\zeta_1\bar{\zeta}_1)}\right]\dfrac{d\bar{\zeta}_1}{dt}+ \\
\qquad -\left[\dfrac{(\bar{\zeta}_1+ia)^2}{\bar{\zeta}_1}\dfrac{(a^2-\zeta_1^2)(a^2+\bar{\zeta}_1^2)}{(a^2+\zeta_1^2)(\zeta_1-\bar{\zeta}_1)(a^2-\zeta_1\bar{\zeta}_1)}\right]\dfrac{d\zeta_1}{dt}= \\
\dfrac{2a}{\bar{\zeta}_1}\dfrac{da}{dt}+\left(\dfrac{\zeta_1^2}{a^2+\zeta_1^2}\right)\left\{U\left(1-\dfrac{a^2}{\zeta_1^2}\right)+\dfrac{i\Gamma_1}{2\pi}\left[\dfrac{\bar{\zeta}_1}{a^2-\zeta_1\bar{\zeta}_1}-\dfrac{1}{\zeta_1-\bar{\zeta}_1}-\dfrac{\zeta_1}{a^2-\zeta_1^2}\right]+\right. \\
\qquad \left.+\sum_{n=2}^{N}\dfrac{i\Gamma_n}{2\pi}\dfrac{(a^2-\zeta_1^2)(\zeta_n-\bar{\zeta}_n)(a^2-\zeta_n\bar{\zeta}_n)}{(\zeta_1-\zeta_n)(\zeta_1-\bar{\zeta}_n)(a^2-\zeta_1\zeta_n)(a^2-\zeta_1\bar{\zeta}_n)}+\dfrac{i\Gamma_1}{2\pi}\dfrac{a^2}{\zeta_1(a^2+\zeta_1^2)}\right\}+ \\
-\dfrac{(\bar{\zeta}_1+ia)^2}{\bar{\zeta}_1}\left\{\dfrac{[(a^2-\zeta_1\bar{\zeta}_1)^2-\zeta_1\bar{\zeta}_1(\zeta_1+\bar{\zeta}_1)^2]}{(a^2+\zeta_1^2)(a^2+\bar{\zeta}_1^2)(a^2-\zeta_1\bar{\zeta}_1)}2a\dfrac{da}{dt}+\right. \\
+\left[2\dfrac{dU}{dt}-\sum_{n=2}^{N}\dfrac{i\Gamma_n}{\pi}\left[\dfrac{a^2-\zeta_n^2}{(a^2+\zeta_n^2)^2}\dfrac{d\zeta_n}{dt}-\dfrac{a^2-\bar{\zeta}_n^2}{(a^2+\bar{\zeta}_n^2)^2}\dfrac{d\bar{\zeta}_n}{dt}\right]+\right. \\
\qquad \left.\left.+\sum_{n=2}^{N}\dfrac{i\Gamma_n}{\pi}(\zeta_n-\bar{\zeta}_n)\dfrac{[(a^2-\zeta_n\bar{\zeta}_n)^2-\zeta_n\bar{\zeta}_n(\zeta_n+\bar{\zeta}_n)^2]}{(a^2+\zeta_n^2)^2(a^2+\bar{\zeta}_n^2)^2}2a\dfrac{da}{dt}\right]\right. \\
\qquad \left.\left[2U-\sum_{n=2}^{N}\dfrac{i\Gamma_n}{\pi}\dfrac{(\zeta_n-\bar{\zeta}_n)(a^2-\zeta_n\bar{\zeta}_n)}{(a^2+\zeta_n^2)(a^2+\bar{\zeta}_n^2)}\right]^{-1}\right\} \\
\dfrac{d\bar{\zeta}_r}{dt}=\dfrac{2a\bar{\zeta}_r}{(a^2+\bar{\zeta}_r^2)}\dfrac{da}{dt}+ \\
+\left[\dfrac{\zeta_r^2\bar{\zeta}_r^2}{(a^2+\zeta_r^2)(a^2+\bar{\zeta}_r^2)}\right]\left\{U\left(1-\dfrac{a^2}{\zeta_r^2}\right)+\dfrac{i\Gamma_r}{2\pi}\left[\dfrac{\bar{\zeta}_r}{a^2-\zeta_r\bar{\zeta}_r}-\dfrac{1}{\zeta_r-\bar{\zeta}_r}-\dfrac{\zeta_r}{a^2-\zeta_r^2}\right]+\right. \\
\qquad \left.+\sum_{n\neq r}^{N}\dfrac{i\Gamma_n}{2\pi}\dfrac{(a^2-\zeta_r^2)(\zeta_n-\bar{\zeta}_n)(a^2-\zeta_n\bar{\zeta}_n)}{(\zeta_r-\zeta_n)(\zeta_r-\bar{\zeta}_n)(a^2-\zeta_r\zeta_n)(a^2-\zeta_r\bar{\zeta}_n)}+\dfrac{i\Gamma_r}{2\pi}\dfrac{a^2}{\zeta_r(a^2+\zeta_r^2)}\right\},
\end{cases}
\tag{2.10}
$$

with the initial conditions:

$$
\begin{cases}
\zeta_1(t_s)=ia \\
\zeta_r(t_s)=\zeta_{r_s} \qquad r=2...N,
\end{cases}
\tag{2.11}
$$

where Γ_1 is given by (2.7). Note because of Brown and Michael's correction [1] the equations are coupled not just through the position of all the vortices but also through their velocities.

To make the problem dimensionless we have to define a characteristic length and time scale. For

this purpose we write the free-stream velocity and the radius of the circle as follows:

$$U(t) = U_\infty + U_1(t) \qquad\qquad a(t) = a_0 + a_1(t), \tag{2.12}$$

where U_∞ is the unperturbed free-stream velocity and a_0 is the initial radius of the circle. If we choose a_0 as characteristic length and $\frac{a_0}{U_\infty}$ as characteristic time of the problem then we can define the following dimensionless quantities:

$$\begin{gathered} z^* = \frac{z}{a_0}, \qquad\qquad \zeta^* = \frac{\zeta}{a_0}, \\ t^* = \frac{U_\infty t}{a_0}, \\ U^* = \frac{U}{U_\infty} = 1 + \epsilon_U, \qquad\qquad a^* = \frac{a}{a_0} = 1 + \epsilon_a, \\ \Gamma^* = \frac{\Gamma}{U_\infty a_0}, \end{gathered} \tag{2.13}$$

where ϵ_U and ϵ_a contain the unsteadiness of the free-stream velocity and of the span of the plate, not necessarily small compared with the steady terms. Note the advantage of this choice is that after substituting these quantities into the equations of motion (2.10), simplifying them and dropping the asterisks, the resulting equations are identical to the former ones with the only convention that the starting radius of the circle and the mean free-stream velocity are unity.

Because of the size and complexity of the problem we are not attempting an analytical solution of it but we will show in the next sections how it can be integrated numerically taking advantage of the analytical work done for the semi-infinite plate (see Chp. 1).

2.3 Drag calculation

The forces acting on the plate are of particular interest because they are the crucial quantities in any problem involving the interaction between fluids and structures. Furthermore, since these quantities can be measured experimentally we have the opportunity to validate our model and further extend

the experimental results. The forces acting on the plate can be computed by means of the Blasius theorem [14]:

$$X - iY = \frac{1}{2} i\rho \oint_C \left(\frac{dF}{dz}\right)^2 dz - i\rho \frac{\partial}{\partial t} \oint_C \bar{F} d\bar{z}. \tag{2.14}$$

The evaluation of these integrals can made easier by a smart choice of the integration path C. Since by construction the vortices cannot sustain any force then the forces acting on the plate are the same as the forces acting on the entire system constituted by plate plus vortices and the contour C can be taken around the all system. Now, all the singularities are inside the integration path, while outside C the integrands are analytic function, hence the contour can be stretched to a circle of infinite radius by means of the Cauchy theorem [14]. Finally, the forces can be computed using the theorem of the residues [14].

Since all the quantities are known in the mapped plane it is necessary to rewrite the above formula in the following way:

$$X - iY = \frac{1}{2} i\rho \oint_C \left(\frac{dF}{d\zeta}\right)^2 \frac{d\zeta}{dz} d\zeta - i\rho \frac{\partial}{\partial t} \oint_C \left(\bar{F} \frac{d\bar{z}}{d\bar{\zeta}}\right) d\bar{\zeta}. \tag{2.15}$$

Substituting the expressions for the complex potential and the mapping, the integration can be carried out successfully and the drag has the following form:

$$\begin{aligned} X = 4\pi\rho \frac{d}{dt}\left(a^2 U\right) + i\rho \frac{d}{dt}\left[\frac{\Gamma_1 (a^2 - \zeta_1 \bar{\zeta}_1)(\zeta_1 - \bar{\zeta}_1)}{\zeta_1 \bar{\zeta}_1}\right] + \\ + i\rho \sum_{n=2}^{N} \Gamma_n \frac{d}{dt}\left[\frac{(a^2 - \zeta_n \bar{\zeta}_n)(\zeta_n - \bar{\zeta}_n)}{\zeta_n \bar{\zeta}_n}\right]. \end{aligned} \tag{2.16}$$

Note the component of the force along the imaginary axis is zero because of the imposed symmetry. This result agrees with those obtained by Graham [9] and Cheers [3], both of whom used slightly different and more complicated arguments. The first term on the right hand side is the force due to added mass, i.e., is the inertia of the attached flow. If we expand this term we have:

$$4\pi\rho \frac{d}{dt}\left(a^2 U\right) = 4\pi\rho a^2 \frac{dU}{dt} + 8\pi\rho a U \frac{da}{dt}, \tag{2.17}$$

where $4\pi\rho a^2$ is the added mass for a flat plate of length $4a$, see [21]. The first contribution is the force necessary to accelerate a plate of fixed length, while the second is the force necessary to tow at constant velocity a plate which length changes in time.

It is possible to write the drag as the time derivative of the total impulse, see [12]:

$$X = \frac{dI}{dt}, \tag{2.18}$$

where

$$I = 4\pi\rho a^2 U + i\rho\left[\frac{\Gamma_1(a^2-\zeta_1\bar{\zeta}_1)(\zeta_1-\bar{\zeta}_1)}{\zeta_1\bar{\zeta}_1}\right] + i\rho\sum_{n=2}^{N}\Gamma_n\left[\frac{(a^2-\zeta_n\bar{\zeta}_n)(\zeta_n-\bar{\zeta}_n)}{\zeta_n\bar{\zeta}_n}\right]. \tag{2.19}$$

The last expression represents the impulse required to set up the irrotational flow instantaneously from rest.

2.4 Starting flow

In this section we will consider the initial evolution of the flow, i.e., we will restrict the problem to the shedding of the first pair of vortices only. This transient is interesting because both experiments and full numerical simulations often are unable to capture the early stages of the separation process. The equation of motion is:

$$\begin{aligned}
&\left[\frac{\bar{\zeta}_1^2+a^2}{\bar{\zeta}_1^2}+\frac{(\bar{\zeta}_1+ia)^2}{\bar{\zeta}_1}\frac{(a^2+\zeta_1^2)(a^2-\bar{\zeta}_1^2)}{(a^2+\bar{\zeta}_1^2)(\zeta_1-\bar{\zeta}_1)(a^2-\zeta_1\bar{\zeta}_1)}\right]\frac{d\bar{\zeta}_1}{dt}+\\
&\qquad -\left[\frac{(\bar{\zeta}_1+ia)^2}{\bar{\zeta}_1}\frac{(a^2-\zeta_1^2)(a^2+\bar{\zeta}_1^2)}{(a^2+\zeta_1^2)(\zeta_1-\bar{\zeta}_1)(a^2-\zeta_1\bar{\zeta}_1)}\right]\frac{d\zeta_1}{dt} =\\
&\left(\frac{\zeta_1^2}{a^2+\zeta_1^2}\right)\left\{U\left(1-\frac{a^2}{\zeta_1^2}\right)+\frac{i\Gamma_1}{2\pi}\left[\frac{\bar{\zeta}_1}{a^2-\zeta_1\bar{\zeta}_1}-\frac{1}{\zeta_1-\bar{\zeta}_1}-\frac{\zeta_1}{a^2-\zeta_1^2}\right]+\frac{i\Gamma_1}{2\pi}\frac{a^2}{\zeta_1(a^2+\zeta_1^2)}\right\}+\\
&\qquad -\frac{(\bar{\zeta}_1+ia)^2}{\bar{\zeta}_1}\left\{\frac{[(a^2-\zeta_1\bar{\zeta}_1)^2-\zeta_1\bar{\zeta}_1(\zeta_1+\bar{\zeta}_1)^2]}{(a^2+\zeta_1^2)(a^2+\bar{\zeta}_1^2)(a^2-\zeta_1\bar{\zeta}_1)}2a\frac{da}{dt}+\frac{1}{U}\frac{dU}{dt}\right\}+\frac{2a}{\bar{\zeta}_1}\frac{da}{dt},
\end{aligned} \tag{2.20}$$

where

$$\Gamma_1 = -2\pi i\left[\frac{(a^2+\zeta_1^2)(a^2+\bar{\zeta}_1^2)}{(\zeta_1-\bar{\zeta}_1)(a^2-\zeta_1\bar{\zeta}_1)}\right]U, \tag{2.21}$$

and the initial condition is

$$\zeta_1(0) = ia. \tag{2.22}$$

The second term within the first pair of square brackets and third term on the left hand side and the term before the last on the right hand side of the equation of motion are the contribution due to Brown and Michael's correction [1]. Routh's correction [5] can be recognized as the last term within the first pair of curly brackets on the right hand side. The last term on the right hand side is the contribution due to the unsteadiness of the mapping. Note how the trajectory of the pair strongly depends on the free-stream velocity and acceleration and on the plate span and its rate of change.

The numerical integration of this equation is complicated by the fact that the problem is singular at $t = 0$, but the kind of singularity is the same as that we were able to overcome in section 1.3. To find an approximate solution valid for small time let us then use the same approach and stretch the time about $t = 0$ defining a new time

$$\tilde{t} = \frac{t}{\epsilon}, \tag{2.23}$$

and expand in ϵ all the quantities which depend on time. We set:

$$\zeta_1(t) = ia + \epsilon^{\alpha}\left(\zeta_{1_1}(\tilde{t}) + \epsilon^{\beta}\zeta_{1_2}(\tilde{t}) + \cdots\right) \tag{2.24}$$

and,

$$\begin{aligned} U(t) &= Vt^m = \epsilon^m V\tilde{t}^m && m \geq 0 \\ a(t) &= 1 + At^p = 1 + \epsilon^p A\tilde{t}^p && p \geq 1 \end{aligned} \tag{2.25}$$

where α and β have to be determined balancing the different terms of the equation and, m and p are positive real numbers. Substituting these relationships into the equation of motion (2.20), at the first order we have:

$$\begin{aligned} &\left[2i\bar{\zeta}_{1_1} + \frac{i\zeta_{1_1}\bar{\zeta}_{1_1}}{\zeta_{1_1} - \bar{\zeta}_{1_1}}\right]\epsilon^{2\alpha-1}\frac{d\bar{\zeta}_{1_1}}{d\tilde{t}} - \left[\frac{i\bar{\zeta}_{1_1}^3}{\zeta_{1_1}(\zeta_{1_1} - \bar{\zeta}_{1_1})}\right]\epsilon^{2\alpha-1}\frac{d\zeta_{1_1}}{d\tilde{t}} = \\ &\qquad \frac{i}{2\zeta_{1_1}}\epsilon^{-\alpha}\left[2U + 4\zeta_{1_1}\epsilon^{\alpha}\frac{da}{d\tilde{t}} - \frac{i\Gamma_1}{2\pi(\zeta_{1_1} - \bar{\zeta}_{1_1})}\epsilon^{-\alpha} - \frac{i\Gamma_1}{4\pi\zeta_{1_1}}\epsilon^{-\alpha}\right] - \frac{i\bar{\zeta}_{1_1}^2}{U}\epsilon^{2\alpha-1}\frac{dU}{d\tilde{t}}, \end{aligned} \tag{2.26}$$

where

$$\Gamma_1 = 4\pi i \epsilon^{\alpha} \left(\frac{\zeta_{1_1} \bar{\zeta}_{1_1}}{\zeta_{1_1} - \bar{\zeta}_{1_1}} \right) U, \tag{2.27}$$

and the initial condition is

$$\zeta_{1_1}(0) = 0. \tag{2.28}$$

Now if we set:

$$\hat{U} = 2U, \qquad \hat{u}_p = 2\frac{da}{d\tilde{t}}, \qquad n = p - 1, \tag{2.29}$$

we can see that (2.26-2.28) coincide exactly with the leading order equations (1.16-1.18) obtained for the semi-infinite plate. This is not surprising because, at early stages, when the small vortex is very close to the tip of the plate it sees the plate as semi-infinite and it cannot feel the presence of the other vortex. The factor two of difference is due to the fact that the fluid velocity at the top of the circle is twice the free-stream velocity. Hence we can use as leading order approximate solutions those obtained in section 1.3.

An opportunity to validate this model is given by the experiment done by Taneda and Honji [23]. In this experiment they measured the length of the symmetric wake bubble behind a flat plate impulsively started or constantly accelerated, i.e., when $U(t) = Vt^m$ with $m = 0, 1$. The main result is that the growth of the bubble is independent of the Reynolds number and for the impulsively started plate the time law is:

$$\frac{L_{bbl}}{L} = 0.89 \left[\frac{Vt}{L} \right]^{\frac{2}{3}}, \tag{2.30}$$

while for the constantly accelerated case is:

$$\frac{L_{bbl}}{L} = 0.48 \left[\frac{Vt^2}{L} \right]^{\frac{2}{3}}, \tag{2.31}$$

where L_{bbl} is the length of the bubble, L is the length of the plate.

We can basically repeat step by step this experiment and determine the length of the bubble. Furthermore, because of the simplicity of our model, we can also compute the position of the

stagnation points to obtain a complete characterization of the flow. At early time the flow presents two small recirculating bubbles close to the tips of the plate and three stagnation points can be recognized on the back face of the body (see Figures 2.10 and 2.11). The stagnation point on the front face of the plate is always present and it coincides with the origin because of the imposed symmetry. Later on, as the two recirculating bubbles grow the two stagnation points move away from the tips until they meet at the origin. At this point the two bubbles start to merge together and a new stagnation point is created and moves away from the origin along the positive x-axis (see Figures 2.12 and 2.13). The merging process is rather quick and soon a large recirculating bubble dominates the flow (see Figures 2.14 and 2.15). In all phases of the flow the length of the bubble is defined as the streamwise length of the recirculating domain.

Because of the mathematical formulation it is easier to compute these quantities in the mapped plane. A further simplification is consequence of the fact that the experiment has been performed with a plate of fixed length. If we assume $a = a_0$ and use the scaling (2.13) the equation of motion (2.20) becomes:

$$\begin{aligned}
&\left[\frac{\bar{\zeta}_1^2+1}{\bar{\zeta}_1^2}+\frac{(\bar{\zeta}_1+i)^2}{\bar{\zeta}_1}\frac{(1+\zeta_1^2)(1-\bar{\zeta}_1^2)}{(1+\bar{\zeta}_1^2)(\zeta_1-\bar{\zeta}_1)(1-\zeta_1\bar{\zeta}_1)}\right]\frac{d\bar{\zeta}_1}{dt}+\\
&\qquad -\left[\frac{(\bar{\zeta}_1+i)^2}{\bar{\zeta}_1}\frac{(1-\zeta_1^2)(1+\bar{\zeta}_1^2)}{(1+\zeta_1^2)(\zeta_1-\bar{\zeta}_1)(1-\zeta_1\bar{\zeta}_1)}\right]\frac{d\zeta_1}{dt}=\\
&\left(\frac{\zeta_1^2}{1+\zeta_1^2}\right)\left\{U\left(1-\frac{1}{\zeta_1^2}\right)+\frac{i\Gamma_1}{2\pi}\left[\frac{\bar{\zeta}_1}{1-\zeta_1\bar{\zeta}_1}-\frac{1}{\zeta_1-\bar{\zeta}_1}-\frac{\zeta_1}{1-\zeta_1^2}\right]+\frac{i\Gamma_1}{2\pi}\frac{1}{\zeta_1(1+\zeta_1^2)}\right\}+\\
&\qquad -\frac{(\bar{\zeta}_1+i)^2}{\bar{\zeta}_1}\frac{1}{U}\frac{dU}{dt},
\end{aligned} \tag{2.32}$$

where

$$\Gamma_1=-2\pi i\left[\frac{(1+\zeta_1^2)(1+\bar{\zeta}_1^2)}{(\zeta_1-\bar{\zeta}_1)(1-\zeta_1\bar{\zeta}_1)}\right]U, \tag{2.33}$$

and the initial condition is

$$\zeta_1(0)=i. \tag{2.34}$$

Let us start with the stagnation points on the back face of the plate. They can be determined by

the points where the complex velocity w is identically zero along the circle. One point is trivially determined by the intersection of the circle with the x-axis, while the other two points are identified in terms of polar coordinates as follow:

$$\rho = 1, \qquad \theta = \pm \arcsin\left[\frac{(\rho_1^2+1)\sin\theta_1}{\rho_1}\right]. \tag{2.35}$$

The position of these points in the physical plane can be determined using the mapping (2.1):

$$x = 0^+, \qquad y = \pm\frac{2}{\rho_1}\sqrt{\rho_1^2 - (\rho_1^2+1)^2\sin^2\theta_1}. \tag{2.36}$$

Let us continue with the computation of the stagnation points on the x-axis. They can be identified with the points where the real part of the complex velocity field is zero. The nontrivial point created by the merging of the two bubbles has the following position in the mapped plane:

$$\xi = \frac{\sqrt{(\rho_1^2+1)^2\sin^2\theta_1 - \rho_1^2} + (\rho_1^2+1)\sin\theta_1}{\rho_1}, \qquad \eta = 0. \tag{2.37}$$

As before, the position of this stagnation point in the physical plane can be determined using the mapping (2.1):

$$x = \frac{2}{\rho_1}\left[\frac{(\rho_1^2+1)\sin\theta_1\sqrt{(\rho_1^2+1)^2\sin^2\theta_1 - \rho_1^2} + (\rho_1^2+1)^2\sin^2\theta_1 - \rho_1^2}{\sqrt{(\rho_1^2+1)^2\sin^2\theta_1 - \rho_1^2} + (\rho_1^2+1)\sin\theta_1}\right], \qquad y = 0. \tag{2.38}$$

Note how the evolution of the flow is determined by the sign of the following expression:

$$(\rho_1^2+1)^2\sin^2\theta_1 - \rho_1^2. \tag{2.39}$$

The above quantity is negative at the early stages of the flow when there are two small recirculating bubbles and consequently the expressions (2.35–2.36) are well defined. Later on, when the bubbles meet at the origin the quantity (2.39) is zero and the stagnation points defined by (2.36) and (2.38) coincide. Finally, as the merging process takes place the above quantity turns positive and the expressions (2.37–2.38) become well defined.

The length of the recirculating bubble can be mathematically identified with the real part of the complex variable z which satisfies at the same time the following two equations:

$$\Im(F) = 0 \qquad \Re(\frac{dF}{dz}) = 0. \tag{2.40}$$

The solution of this set of equations is a point which lies on the zero streamline, the one that separates the recirculating region from the rest of the flow, and the complex velocity field at such a point is parallel to the plate. Note as the merging process is completed this statement becomes trivial and this point is the stagnation point defined by the expression (2.38). At earlier time the solution of this problem is not trivial but it can be obtained numerically.

It is interesting to observe that all the above expressions (2.35–2.39) are independent of the free-stream velocity $U(t)$ and the only important information is the position of the vortex pair. This fact agrees with the result given by Taneda and Honji [23] that the length of the bubble is independent of the Reynolds number ($Re = \frac{UL}{\nu}$). Furthermore, it predicts that the entire geometry of the flow evolves independently of $U(t)$.

The numerical simulation of this experiment is illustrated by Figures 2.2-2.15. These plots permit the comparison of the cases where the plate is impulsively started, constantly accelerated and linearly accelerated, i.e., when $U(t) = Vt^m$ with $m = 0, 1, 2$ (see Figure 2.2). A striking feature is that each vortex moves almost on the same trajectory in all three cases (see Figure 2.3). Figures 2.4 and 2.5 show the total circulation and rate of circulation production for the top vortex. The small window magnifies the trend at small times when it is comparable with the results obtained for the semi-infinite plate (see Figure 1.4). Making this comparison we should remember that there is a factor 2 in the dimensionless free-stream velocity (see 2.29).

Figure 2.7 shows how the length of the recirculating bubble for the impulsively started case compares with that measured by Taneda and Honji [23] and with that obtained by Chua [4]. Note that Chua in his simulation uses a vortex method algorithm able to model the boundary layer on the

plate. The agreement is reasonably good but both numerical simulations show a similar departure from the best fit proposed by Taneda for late times. At small times, we are able to extend Taneda's result down to time $t \sim O(10^{-7})$. We estimate that at very early times ($10^{-7} < t < 10^{-5}$) the bubble grows proportionally to $t^{0.68}$, which is in good agreement with time-law of $t^{\frac{2}{3}}$ derived by Pullin for the semi-infinite plate case (see [17]). This time-law slightly changes with time, as the coupling between top and bottom vortices becomes more important. In fact, during the merging process ($.15 < t < 1.5$) we estimate that the bubble grows as $t^{0.77}$. Later on, the departure from the quasi-linear trend, in the log-log plot, can be clearly identified with the end of the merging process, see the solid diamond symbol. Finally, for large times the deviation from the experiment is not anymore negligible but consistent with the other numerical simulation. This departure could be consequence of the two dimensionality and symmetry imposed in our model. Note that Chua produces a result slightly closer to the experiment without imposing symmetry. It is unclear if the remaining deviation is consequence of the two dimensionality of the simulation or if it is due to the low level of noise present in the numerical environment in comparison with that present in a real experiment.

Figure 2.6 shows the drag coefficient for the three different free-stream conditions. This coefficient is defined as follows:

$$C_D = \frac{D}{\frac{1}{2}\rho U_\infty^2 L}. \tag{2.41}$$

It is important to note that the drag coefficient is well defined for the impulsively started case only, in the other cases, when $m \neq 0$, it is not possible to select a characteristic free-stream velocity. In these cases we selected $U_\infty = 1\ ms^{-1}$, i.e., the velocity reached by the plate after one unit of time.

The forces acting on the plate for the purely impulsively started case cannot be measured experimentally. However, a comparison can be made with the results obtained by Chua [4] in his numerical simulation, see Figure 2.8. The overall agreement is reasonably good. Figure 2.7 shows that the recirculating bubble grows faster in Chua's simulation than in our case and this explains

the difference in drag at early times. At later times our model tends to underestimate the drag probably because of the lack of distributed vorticity and imposed symmetry.

When the plate is constantly accelerated the forces can be measured experimentally. Results for the drag are not available from the Taneda and Honji experiment, but recently Lisoski [13] measured the forces acting on a flat towed at linearly increasing velocity. Figure 2.9 shows the comparison with Lisoski [13] and Chua [4] results. The overall agreement is still reasonably good and the discrepancies can be explained as for the impulsively started case. It is interesting that the experimental data are within the two curves obtained numerically. Note that the drag coefficient, in this case, is based on the final free-stream velocity.

2.5 Universality of the starting flow

In this section we derive a time dependent scaling that will allow us to nearly collapse all the results obtained in the previous section. Clearly the classical scaling (2.13) introduced to make the problem dimensionless fails this purpose. However, if we analyze the plots which describe the starting flow presented in the previous section we can note few striking facts. First, the vortex pair seems to move always on the same trajectory but with a different time law which depends on the free-stream velocity (see Figure 2.3). Furthermore, from the comparison of the instantaneous streamlines taken at two different times for two different free-stream conditions (see Figures 2.10– 2.15), it follows that the geometry of the flow goes through the same states but at different times. Finally, the scaling used by Taneda and Honji [23] seems to be more appropriate for the analysis of this flow.

Based on the above observations it follows that the appropriate choice of a representative time scale would improve the quantitative and qualitative understanding of the phenomenon. One thing which has not been taken into account is how the distance travelled by the plate relates with the

evolution of the flow. Such a distance can be easily computed by integrating the free-stream velocity:

$$x_p = \int_0^t U(t')dt' = \int_0^t Vt'^m dt' = \frac{Vt^{m+1}}{m+1} = \frac{U(t)t}{m+1}. \tag{2.42}$$

Then, the number of radii travelled by the plate is given by:

$$\frac{x_p}{a_0} = \frac{U(t)t}{a_0(m+1)}. \tag{2.43}$$

Thus, if we choose the right hand side as the dimensionless time, then the motion of the plate is synchronized in this new time frame. In other words, the plate travels an equal distance in time for all possible free-stream conditions (i.e.$\forall m \in [0, \infty)$).

Let us start the scaling of the equation (2.20) by observing that it can be made dimensionless dividing it by $U(t)$. Similarly Γ_1 can be made dimensionless dividing by $a_0 U(t)$ (see 2.21). Then, it is natural to introduce the following dimensionless quantities:

$$\begin{aligned} z^* &= \frac{z}{a_0}, & \zeta^* &= \frac{\zeta}{a_0}, \\ & t^* = \frac{U(t)t}{a_0(m+1)}, & & \\ U^* &= \frac{U(t)}{U(t)} = 1, & a^* &= \frac{a}{a_0} = 1, \\ & \Gamma^* = \frac{\Gamma}{U(t)a_0}. & & \end{aligned} \tag{2.44}$$

A consequence of this time dependent scaling is that the quantities which involve time derivatives have a nontrivial and rather unusual form. The rate of circulation production, for example, has the following dimensionless form:

$$\frac{d\Gamma^*}{dt^*} = \frac{1}{U^2}\left(\frac{d\Gamma}{dt} - \frac{m\Gamma}{t}\right), \tag{2.45}$$

while, the forces acting on the plate, which can be computed taking the time derivative of the impulse I, have the form:

$$X^* - iY^* = \frac{dI^*}{dt^*} = \frac{1}{\rho a_0 U^2}\left(\frac{dI}{dt} - \frac{mI}{t}\right). \tag{2.46}$$

Note for $m = 0$ we are recovering the classical scaling (2.13). Rewriting the equation of motion (2.20) in terms of dimensionless quantities and dropping the asterisks, we obtain:

$$\begin{aligned}\left[\frac{\bar{\zeta}_1^2+1}{\bar{\zeta}_1^2}+\frac{(\bar{\zeta}_1+i)^2}{\bar{\zeta}_1}\frac{(1+\zeta_1^2)(1-\bar{\zeta}_1^2)}{(1+\bar{\zeta}_1^2)(\zeta_1-\bar{\zeta}_1)(1-\zeta_1\bar{\zeta}_1)}\right]\frac{d\bar{\zeta}_1}{dt}+ \\ -\left[\frac{(\bar{\zeta}_1+i)^2}{\bar{\zeta}_1}\frac{(1-\zeta_1^2)(1+\bar{\zeta}_1^2)}{(1+\zeta_1^2)(\zeta_1-\bar{\zeta}_1)(1-\zeta_1\bar{\zeta}_1)}\right]\frac{d\zeta_1}{dt}= \\ \left(\frac{\zeta_1^2}{1+\zeta_1^2}\right)\left\{\left(1-\frac{1}{\zeta_1^2}\right)+\frac{i\Gamma_1}{2\pi}\left[\frac{\bar{\zeta}_1}{1-\zeta_1\bar{\zeta}_1}-\frac{1}{\zeta_1-\bar{\zeta}_1}-\frac{\zeta_1}{1-\zeta_1^2}\right]+\frac{i\Gamma_1}{2\pi}\frac{1}{\zeta_1(1+\zeta_1^2)}\right\}+ \\ -\frac{(\bar{\zeta}_1+i)^2}{\bar{\zeta}_1}\frac{m}{(m+1)t},\end{aligned} \tag{2.47}$$

where

$$\Gamma_1 = -2\pi i\left[\frac{(1+\zeta_1^2)(1+\bar{\zeta}_1^2)}{(\zeta_1-\bar{\zeta}_1)(1-\zeta_1\bar{\zeta}_1)}\right], \tag{2.48}$$

and the initial condition is

$$\zeta_1(0) = i. \tag{2.49}$$

The dependency from the free-stream velocity is reduced to the factor $\frac{m}{(m+1)}$ which appears in the last term of the equation of motion. Note the boundness of this term:

$$0 \leq \frac{m}{(m+1)} < 1, \qquad \forall m \in [0,\infty). \tag{2.50}$$

Furthermore, such dependency is completely lost for large time because of the factor t^{-1}. In other words, the scaled equation reduces to the dimensionless equation of motion for the impulsively started case plus a correction which dies out at large time. Consequently, varying the power of time we produce a family of curves which can be compared with the impulsively started case as shown by Figures 2.16–2.29. It is interesting to observe that as a consequence of the boundness of the factor $\frac{m}{m+1}$ all the curves are confined in a narrow strip in the plotting plane and are bounded by the limiting cases $m = 0, \infty$. Furthermore, since the correction dies out as t^{-1}, the scaled system captures the universality of the phenomenon at large times. Indication of universality is that at large times the curves collapse all together, as in the case for the rate of circulation production and

drag (see Figures 2.18 and 2.23), or they become parallel as in the case of total circulation, impulse and bubble length (see Figures 2.19, 2.20 and 2.22).

In this time frame, it becomes meaningful to compare the time evolution of the geometrical quantities which characterize the flow (see Figures 2.20–2.21). The bubble length, at any given time, decreases as m increases. The merging process of the two small recirculating bubbles is delayed also as m becomes larger. The diamond symbols in Figure 2.21 show at which time and bubble length the merging process is completed. Note how this happens always at about the same bubble length. From the comparison of the drag (see Figure 2.23), we can conclude that the optimal way to put a plate in motion is through a smooth acceleration. Furthermore, once the plate is in motion and the recirculating bubble is fully developed, the drag is independent of the free-stream velocity. This universality at large times suggests that it should be possible to obtain excellent aerodynamics performance from a bluff body if one is able to keep the wake symmetric.

As we have seen, the above results are able to capture the universality of the phenomenon at late times. Since during the evolution of the flow we can identify two different trends, one at early time, when there are two distinct recirculating bubbles, and another at large time when the bubble is fully developed, then we should expect to find two different time scales. The time scale at early times is suggested by Figure 2.21. If we synchronize the time when the two small recirculating bubbles meet at the origin, we have to choose the dimensionless time as follows:

$$t^* = \frac{U(t)t}{a_0(2m+1-\epsilon m)}, \qquad 0 < \epsilon \ll 1, \tag{2.51}$$

where ϵ is a parameter which has to be deduced empirically from the data of the unscaled simulation. Note when $\epsilon = 0$ the previous expression reduces to the characteristic time of the first order approximate solution. It is worth recalling that the leading order approximate solution for small time can be written as:

$$\zeta_1^*(t) = \frac{\zeta_1(t)}{a_0} = i + \frac{(1+i)}{2a_0^{\frac{2}{3}}}\left[\frac{U(t)t}{a_0(2m+1)}\right]^{\frac{1}{3}}. \tag{2.52}$$

As time increases, higher order terms should be included and the parameter ϵ has been introduced to account for these higher order corrections. The scaling of the equation of motion (2.20) is carried out similarly to the previous case using the following dimensionless quantities:

$$\begin{aligned} z^* &= \frac{z}{a_0}, & \zeta^* &= \frac{\zeta}{a_0}, \\ & t^* = \frac{U(t)t}{a_0(2m+1-\epsilon m)}, & & \\ U^* &= \frac{U(t)}{U(t)} = 1, & a^* &= \frac{a}{a_0} = 1, \\ & \Gamma^* = \frac{\Gamma}{U(t)a_0}. & & \end{aligned} \tag{2.53}$$

As before, the quantities which involve time derivatives have a nontrivial and rather unusual expression. The rate of circulation production has the following dimensionless form:

$$\frac{d\Gamma^*}{dt^*} = \frac{(2m+1-\epsilon m)}{U^2(m+1)}\left(\frac{d\Gamma}{dt} - \frac{m\Gamma}{t}\right), \tag{2.54}$$

while the forces acting on the plate have the form:

$$X^* - iY^* = \frac{dI^*}{dt^*} = \frac{(2m+1-\epsilon m)}{\rho a_0 U^2(m+1)}\left(\frac{dI}{dt} - \frac{mI}{t}\right). \tag{2.55}$$

As before, for m=0 we are recovering the classical scaling (2.13). Rewriting the equation of motion (2.20) in terms of dimensionless quantities and dropping the asterisks, we obtain:

$$\begin{aligned} &\left[\frac{\bar{\zeta}_1^2+1}{\bar{\zeta}_1^2} + \frac{(\bar{\zeta}_1+i)^2}{\bar{\zeta}_1}\frac{(1+\zeta_1^2)(1-\bar{\zeta}_1^2)}{(1+\bar{\zeta}_1^2)(\zeta_1-\bar{\zeta}_1)(1-\zeta_1\bar{\zeta}_1)}\right]\frac{(m+1)}{(2m+1-\epsilon m)}\frac{d\bar{\zeta}_1}{dt} + \\ &\qquad - \left[\frac{(\bar{\zeta}_1+i)^2}{\bar{\zeta}_1}\frac{(1-\zeta_1^2)(1+\bar{\zeta}_1^2)}{(1+\zeta_1^2)(\zeta_1-\bar{\zeta}_1)(1-\zeta_1\bar{\zeta}_1)}\right]\frac{(m+1)}{(2m+1-\epsilon m)}\frac{d\zeta_1}{dt} = \\ &\left(\frac{\zeta_1^2}{1+\zeta_1^2}\right)\left\{\left(1-\frac{1}{\zeta_1^2}\right) + \frac{i\Gamma_1}{2\pi}\left[\frac{\bar{\zeta}_1}{1-\zeta_1\bar{\zeta}_1} - \frac{1}{\zeta_1-\bar{\zeta}_1} - \frac{\zeta_1}{1-\zeta_1^2}\right] + \frac{i\Gamma_1}{2\pi}\frac{1}{\zeta_1(1+\zeta_1^2)}\right\} + \\ &\qquad - \frac{(\bar{\zeta}_1+i)^2}{\bar{\zeta}_1}\frac{m}{(2m+1-\epsilon m)t}, \end{aligned} \tag{2.56}$$

where

$$\Gamma_1 = -2\pi i\left[\frac{(1+\zeta_1^2)(1+\bar{\zeta}_1^2)}{(\zeta_1-\bar{\zeta}_1)(1-\zeta_1\bar{\zeta}_1)}\right], \tag{2.57}$$

and the initial condition is

$$\zeta_1(0) = i. \tag{2.58}$$

In this case, the dependency from the free-stream velocity is reduced to two factors: one which multiplies the time derivatives and the other which appears in the last term of the equation of motion. Note the boundness of these terms:

$$0 \leq \frac{m}{(2m+1-\epsilon m)} < \frac{1}{2-\epsilon}, \qquad \forall m \in [0,\infty), \tag{2.59}$$

and

$$\frac{1}{2-\epsilon} < \frac{m+1}{(2m+1-\epsilon m)} \leq 1, \qquad \forall m \in [0,\infty). \tag{2.60}$$

Figures 2.30–2.35 show the results of the scaled simulation up to time $t^* = 3$. The overall effect of the scaling is to collapse all the cases on the $m = 0$ curve for $t^* < 1$. The plots of the free-stream velocity and the trajectories of the top vortex have been omitted because they basically coincide with the previous one (see Figure 2.16–2.17).

Figure 2.33 show the loci of the stagnation points on the back face of the plate and on the x-axis. The merging of the two small recirculating bubble has been synchronized choosing $\epsilon = .09065$. The effect of this procedure is to produce the universality of the phenomenon at early times. It is interesting to observe how the curves are generally indistinguishable up to about time $t^* = 1$ although the time scaling has been derived by the leading order of the approximate solution. Only the rate of circulation production and drag show some sensitivity at earlier times (see Figures 2.30 and 2.35).

2.6 New vortex pair

In this section we will consider the problem of shedding a new pair of vortices when $N-1$ other pairs are already present into the flow. We will use the shedding mechanism that has been introduced in

Section 1.5, with the same limitations and constraints. We recall that, if t_s is the shedding time, then up to the time t_s^- the vortex pair 1 has variable strength such that the Kutta condition is satisfied. At time $t = t_s$ this pair has its strength frozen and, all the pairs renumbered. Finally at t_s^+ a new vortex pair 1 is introduced into the flow to remove the square root singularity.

The equation of motion of this new pair is

$$\begin{aligned}
&\left[\frac{\bar{\zeta}_1^2+a^2}{\bar{\zeta}_1^2}+\frac{(\bar{\zeta}_1+ia)^2}{\bar{\zeta}_1}\frac{(a^2+\zeta_1^2)(a^2-\bar{\zeta}_1^2)}{(a^2+\bar{\zeta}_1^2)(\zeta_1-\bar{\zeta}_1)(a^2-\zeta_1\bar{\zeta}_1)}\right]\frac{d\bar{\zeta}_1}{dt}+\\
&\qquad-\left[\frac{(\bar{\zeta}_1+ia)^2}{\bar{\zeta}_1}\frac{(a^2-\zeta_1^2)(a^2+\bar{\zeta}_1^2)}{(a^2+\zeta_1^2)(\zeta_1-\bar{\zeta}_1)(a^2-\zeta_1\bar{\zeta}_1)}\right]\frac{d\zeta_1}{dt}=\\
&\frac{2a}{\bar{\zeta}_1}\frac{da}{dt}+\left(\frac{\zeta_1^2}{a^2+\zeta_1^2}\right)\left\{U\left(1-\frac{a^2}{\zeta_1^2}\right)+\frac{i\Gamma_1}{2\pi}\left[\frac{\bar{\zeta}_1}{a^2-\zeta_1\bar{\zeta}_1}-\frac{1}{\zeta_1-\bar{\zeta}_1}-\frac{\zeta_1}{a^2-\zeta_1^2}\right]+\right.\\
&\qquad\left.+\sum_{n=2}^{N}\frac{i\Gamma_n}{2\pi}\frac{(a^2-\zeta_1^2)(\zeta_n-\bar{\zeta}_n)(a^2-\zeta_n\bar{\zeta}_n)}{(\zeta_1-\zeta_n)(\zeta_1-\bar{\zeta}_n)(a^2-\zeta_1\zeta_n)(a^2-\zeta_1\bar{\zeta}_n)}+\frac{i\Gamma_1}{2\pi}\frac{a^2}{\zeta_1(a^2+\zeta_1^2)}\right\}+\\
&-\frac{(\bar{\zeta}_1+ia)^2}{\bar{\zeta}_1}\left\{\frac{[(a^2-\zeta_1\bar{\zeta}_1)^2-\zeta_1\bar{\zeta}_1(\zeta_1+\bar{\zeta}_1)^2]}{(a^2+\zeta_1^2)(a^2+\bar{\zeta}_1^2)(a^2-\zeta_1\bar{\zeta}_1)}2a\frac{da}{dt}+\right.\\
&+\left[2\frac{dU}{dt}-\sum_{n=2}^{N}\frac{i\Gamma_n}{\pi}\left[\frac{a^2-\zeta_n^2}{(a^2+\zeta_n^2)^2}\frac{d\zeta_n}{dt}-\frac{a^2-\bar{\zeta}_n^2}{(a^2+\bar{\zeta}_n^2)^2}\frac{d\bar{\zeta}_n}{dt}\right]+\right.\\
&\qquad\left.\left.+\sum_{n=2}^{N}\frac{i\Gamma_n}{\pi}(\zeta_n-\bar{\zeta}_n)\frac{[(a^2-\zeta_n\bar{\zeta}_n)^2-\zeta_n\bar{\zeta}_n(\zeta_n+\bar{\zeta}_n)^2]}{(a^2+\zeta_n^2)^2(a^2+\bar{\zeta}_n^2)^2}2a\frac{da}{dt}\right]\right.\\
&\qquad\left.\left[2U-\sum_{n=2}^{N}\frac{i\Gamma_n}{\pi}\frac{(\zeta_n-\bar{\zeta}_n)(a^2-\zeta_n\bar{\zeta}_n)}{(a^2+\zeta_n^2)(a^2+\bar{\zeta}_n^2)}\right]^{-1}\right\},
\end{aligned}\tag{2.61}$$

where

$$\Gamma_1=-\pi i\frac{(a^2+\zeta_1^2)(a^2+\bar{\zeta}_1^2)}{(\zeta_1-\bar{\zeta}_1)(a^2-\zeta_1\bar{\zeta}_1)}\left[2U-\sum_{n=2}^{N}\frac{i\Gamma_n}{\pi}\frac{(\zeta_n-\bar{\zeta}_n)(a^2-\zeta_n\bar{\zeta}_n)}{(a^2+\zeta_n^2)(a^2+\bar{\zeta}_n^2)}\right],\tag{2.62}$$

with the initial condition

$$\zeta_1(t_s)=ia.\tag{2.63}$$

Note that this equation, although much more complicated in appearance, has exactly the same structure of that for the starting pair. It is singular at $t = t_s$ also, except that up through time $t = t_s^-$ there is another vortex pair which satisfies the Kutta condition. Consequently it is reasonable

to expect a different time behavior for $(t-t_s) \ll 1$. Once again it is necessary to find an approximate analytical solution so that the numerical integration can start smoothly. Let us stretch the time about $t = t_s$ defining a new time

$$\tilde{t} = \frac{t - t_s}{\epsilon}, \tag{2.64}$$

and then set

$$\zeta_1(t) = ia + \epsilon^\alpha \left(\zeta_{1_1}(\tilde{t}) + \epsilon^\beta \zeta_{1_2}(\tilde{t}) + \cdots\right). \tag{2.65}$$

All the other quantities which are depending on time can be expanded in Taylor's series, i.e., we can write:

$$\begin{aligned} f(t) &= f(0) + \epsilon \left.\frac{df}{dt}\right|_{\tilde{t}=0} \tilde{t} + \cdots \\ &= f_s + \epsilon \left.\frac{df}{dt}\right|_s \tilde{t} + \cdots. \end{aligned} \tag{2.66}$$

Note we can expand in this way the positions of the other vortex pairs as well, as can be verified substituting the above expansions into their equations of motion. Substituting these relationships into the equation of motion (2.61), at the first order we have:

$$\begin{aligned} &\left[2i\bar{\zeta}_{1_1} + \frac{i\zeta_{1_1}\bar{\zeta}_{1_1}}{\zeta_{1_1} - \bar{\zeta}_{1_1}}\right]\epsilon^{2\alpha-1}\frac{d\bar{\zeta}_{1_1}}{d\tilde{t}} - \left[\frac{i\bar{\zeta}_{1_1}^3}{\zeta_{1_1}(\zeta_{1_1} - \bar{\zeta}_{1_1})}\right]\epsilon^{2\alpha-1}\frac{d\zeta_{1_1}}{d\tilde{t}} = \\ &\frac{i}{2}\Bigg\{-4a_s^2 U_s \frac{[\zeta_{2_s}(a_s^2 + \bar{\zeta}_{2_s}^2) + \bar{\zeta}_{2_s}(a_s^2 + \zeta_{2_s}^2)]}{(a_s^2 + \zeta_{2_s}^2)(a_s^2 + \bar{\zeta}_{2_s}^2)} + 4a_s \left.\frac{da}{dt}\right|_s + \\ &\quad -2a_s^2 \sum_{n=3}^{N} \frac{i\Gamma_n}{\pi} \frac{(\zeta_{n_s} - \bar{\zeta}_{n_s})(a_s^2 - \zeta_{n_s}\bar{\zeta}_{n_s})}{(a_s^2 + \zeta_{n_s}^2)(a_s^2 + \bar{\zeta}_{n_s}^2)} \Bigg[\frac{[\zeta_{n_s}(a_s^2 + \bar{\zeta}_{n_s}^2) + \bar{\zeta}_{n_s}(a_s^2 + \zeta_{n_s}^2)]}{(a_s^2 + \zeta_{n_s}^2)(a_s^2 + \bar{\zeta}_{n_s}^2)} + \\ &\qquad - \frac{[\zeta_{2_s}(a_s^2 + \bar{\zeta}_{2_s}^2) + \bar{\zeta}_{2_s}(a_s^2 + \zeta_{2_s}^2)]}{(a_s^2 + \zeta_{2_s}^2)(a_s^2 + \bar{\zeta}_{2_s}^2)}\Bigg]\Bigg\} - \frac{i\bar{\zeta}_{1_1}^2}{\tilde{t}}\epsilon^{2\alpha-1}, \end{aligned} \tag{2.67}$$

with the initial condition

$$\zeta_{1_1}(0) = 0. \tag{2.68}$$

In this case, at contrary to what happened for the first pair, the leading order does not coincide with the result obtained for the semi-infinite plate (see section 1.5), but it still has the same structure.

When the plate has finite length the new small vortex which is very close to the tip of the plate sees the plate as semi-infinite and the existing vortices as infinitely far away, instead, when the plate is semi-infinite, the existing vortices appear to be located at finite distance from the new vortex. Consequently, the difference between the above equation and equation (1.39) is in the contribution due to the desingularized velocity. Hence, we can write down the approximate solution for this case simply substituting the new contribution into the approximate solution (1.41). Then we have:

$$\begin{cases} \rho_1(t) = a_s + \left\{ \frac{4}{5} a_s \left[2U_s a_s \frac{\rho_{2_s}(\rho_{2_s}^2 + a_s^2)\sin\theta_{2_s}}{a_s^4 - 2a_s^2\rho_{2_s}^2\cos 2\theta_{2_s} + \rho_{2_s}^4} - \left.\frac{da}{dt}\right|_s + \right.\right. \\ \qquad +2a_s \sum_{n=3}^{N} \frac{\Gamma_n}{\pi} \frac{\rho_{n_s}(\rho_{n_s}^2 - a_s^2)\cos\theta_{n_s}}{a_s^4 - 2a_s^2\rho_{n_s}^2\cos 2\theta_{n_s} + \rho_{n_s}^4} \left[\frac{\rho_{n_s}(\rho_{n_s}^2 + a_s^2)\sin\theta_{n_s}}{a_s^4 - 2a_s^2\rho_{n_s}^2\cos 2\theta_{n_s} + \rho_{n_s}^4} + \right. \\ \qquad \left.\left. \left. - \frac{\rho_{2_s}(\rho_{2_s}^2 + a_s^2)\sin\theta_{2_s}}{a_s^4 - 2a_s^2\rho_{2_s}^2\cos 2\theta_{2_s} + \rho_{2_s}^4} \right] \right] \right\}^{\frac{1}{2}} \sqrt{(t - t_s)} \\ \theta_1(t) = 0, \end{cases} \tag{2.69}$$

where the quantity between square brackets is just the value of the desingularized velocity field at the shedding time. Note the argument of the square root is not positive definite but its sign depends on the history of the flow. This provides a test of the validity of the simulation, if the sign is negative an error was made during the integration. We find that a solution exists if, at the shedding time,

$$\begin{aligned} \left.\frac{da}{dt}\right|_s < \Bigg[& 2U_s a_s \frac{\rho_{2_s}(\rho_{2_s}^2 + a_s^2)\sin\theta_{2_s}}{a_s^4 - 2a_s^2\rho_{2_s}^2\cos 2\theta_{2_s} + \rho_{2_s}^4} \\ & +2a_s \sum_{n=3}^{N} \frac{\Gamma_n}{\pi} \frac{\rho_{n_s}(\rho_{n_s}^2 - a_s^2)\cos\theta_{2_s}}{a_s^4 - 2a_s^2\rho_{n_s}^2\cos 2\theta_{n_s} + \rho_{n_s}^4} \left[\frac{\rho_{n_s}(\rho_{n_s}^2 + a_s^2)\sin\theta_{2_s}}{a_s^4 - 2a_s^2\rho_{n_s}^2\cos 2\theta_{n_s} + \rho_{n_s}^4} \right. \\ & \left. - \frac{\rho_{2_s}(\rho_{2_s}^2 + a_s^2)\sin\theta_{2_s}}{a_s^4 - 2a_s^2\rho_{2_s}^2\cos 2\theta_{2_s} + \rho_{2_s}^4} \right] \Bigg], \end{aligned} \tag{2.70}$$

i.e., if the rate of change of the span of the plate is less of the velocity with which the new vortex is convected away.

2.7 Start-stop flow

In this section we present the results obtained from the numerical simulation of a start-stop flow. In other words, the flow generated by a free-stream velocity which starts from rest, then accelerates reaching a maximum speed, and then decelerates in a symmetrical fashion to a final stop. The fluid velocity, of course, will continue to be non zero even after the driving free-stream vanished and we are interested in monitoring the evolution of the quantities which characterize the flow. The goal is to validate our model when more than one vortex pair is present in the flow. As far as we know, there are very few experimental and numerical data available for this type of flow. A qualitative insight about the evolution of the flow can be obtained by the flow visualization of Pullin and Perry [18].

Let us analyze the evolution of the flow when the free-stream velocity has the trend shown in Figure 2.36. At the beginning, when the flow accelerates, a first pair of vortices is created and convected down-stream (see Figures 2.37 and 2.42). This pair satisfies the Kutta condition, not only during the acceleration (up to time $t = 1$), but even at the beginning of the deceleration, due to the balance between the growth of the vortices and their drifting motion away from the plate. This balance fails as the free-stream velocity decreases and the existing pair reverses the flow around the tips of the plate. In fact, at approximatively time $t = 1.1864$, the rate of circulation production changes sign (see Figure 2.38) and a new pair of vortices is introduced into the flow to satisfy the Kutta condition. The strength of the new pair grows very quickly and by time $t = 2$, when the plate stops, it has reached about 69% of the strength of the other pair (see Figure 2.39). As the external forcing stops, the interaction between the vortices drives the flow, and the top and bottom pairs start to move away from the plate on a direction almost parallel to the imaginary axis (see Figure 2.37 and 2.43). This drifting motion continues unperturbed as time goes on (see Figures 2.44 and 2.45) and all the quantities go to zero rather quickly (see Figures 2.38–2.39 and Figure 2.41). Only

the impulse, the time integral of the drag, is left nonzero (see Figure 2.40).

The overall behavior of the model it very reasonable, although, it cannot be compared with any experiment or numerical simulation because of the lack of data. The qualitative agreement with the flow visualization of Pullin and Perry [18] it is extremely encouraging.

2.8 Vortex merging scheme

In this section we present an application of our model to a case where many vortex pairs are produced during the simulation. Furthermore, since one of our goals is to design a computationally fast model able to capture the main features of the flow, we propose a new conservative merging scheme.

As noticed by Sarpkaya [22], the reasons to amalgamate two or more vortices are common to many vortex method schemes. Often is necessary to reduce the unphysically large velocities induced in each other, to limit their propensity to orbit about each other, to simulate more closely some naturally occurring merging, and to reduce computer time. Sarpkaya [22] also underlines the fact that it has been customary to combine two vortices of circulation Γ_p and Γ_q and position ζ_p and ζ_q into a single vortex of strength

$$\Gamma_m = \Gamma_p + \Gamma_q, \tag{2.71}$$

placed at their center of vorticity, given by

$$\zeta_m = \frac{\Gamma_p \zeta_p + \Gamma_q \zeta_q}{\Gamma_p + \Gamma_q}. \tag{2.72}$$

This process conserves total circulation and linear momentum only when the boundary of the problem can be mapped onto a straight line. The error introduced in the complex velocity field by the amalgamation process decays as $\sim \zeta^{-3}$ far from the merging location. In the case of a finite size body, the above scheme conserves only the total circulation while the linear momentum of the system is not conserved in general. Consequently, the error induced on the velocity field decays only

as $\sim \zeta^{-2}$. This fact can be explained by mapping the finite body onto a circle, which in principle can always be done, and considering the image vorticity. From the above formula it follows that the image of the vortex Γ_m is placed at:

$$\frac{a^2}{\bar{\zeta}_m} = \frac{a^2(\Gamma_p + \Gamma_q)}{\Gamma_p \bar{\zeta}_p + \Gamma_q \bar{\zeta}_q}. \tag{2.73}$$

Now, if we actually compute the position of the image of Γ_m merging the images of the vortices Γ_p and Γ_q so that the circulation and linear impulse of the image system is conserved, we obtain:

$$\frac{a^2}{\bar{\zeta}_m} = \frac{a^2(\Gamma_p \bar{\zeta}_q + \Gamma_q \bar{\zeta}_p)}{\bar{\zeta}_p \bar{\zeta}_q (\Gamma_p + \Gamma_q)}, \tag{2.74}$$

which is different from the previous formula.

To conserve both total circulation and linear impulse and to produce an error $\sim \zeta^{-3}$ in the complex velocity field when a body of finite size is present into the flow, it is necessary to consider the contribution of vortices and their images. One way to achieve this result is to take the difference of the expressions of the complex velocity field before and after the merging process and then expand the result in powers of ζ^{-1}. Setting equal to zero the first two leading terms we obtain two equations which predict strength and position of the new vortex. Finally, it is possible to check that the linear impulse is conserved. The formula for the position ζ_m of the new vortex is simplified if we set:

$$I_p = \Gamma_p \left(\zeta_p - \frac{a^2}{\bar{\zeta}_p} \right), \qquad I_q = \Gamma_q \left(\zeta_q - \frac{a^2}{\bar{\zeta}_q} \right), \tag{2.75}$$

and

$$I_{pq} = I_p + I_q. \tag{2.76}$$

Then the vortex resulting from the merging process has to have circulation

$$\Gamma_m = \Gamma_p + \Gamma_q, \tag{2.77}$$

and has to be placed at

$$\zeta_m = \sqrt{\frac{I_{pq}}{\bar{I}_{pq}}} \left[\frac{\sqrt{I_{pq}\bar{I}_{pq} + 4a^2(\Gamma_p + \Gamma_q)^2} + \sqrt{I_{pq}\bar{I}_{pq}}}{2(\Gamma_p + \Gamma_q)} \right], \tag{2.78}$$

where a is the radius of the circle on which the body has been mapped, and $\bar{I}_{pq}$ is the complex conjugate of I_{pq}. To use this scheme effectively the amalgamation process has to take place sufficiently far from the body so that it perturbs only slightly the velocity field near to the body, in particular the velocity field close to the separation points. Unfortunately, because of the reasons stated at the beginning of this section, the merging process has to take place even when the vortices are not that far from the body, and consequently introduces a significant time dependent perturbation in the velocity field near to the separation points. In other words, we find that the effect of the merging process is instantaneously fed back to the body affecting the separation and making the shedding process rather noisy.

To avoid this problem one could propose a completely different amalgamation scheme which does not modify the rate of circulation production, i.e., $\frac{d\Gamma_1}{dt}$. Unfortunately, the mathematics involved discourages any attempt to impose such a condition. A reasonable compromise is to impose the condition that the velocity field at the separation point is not affected by the merging process. In other words, the circulation of the vortex connected to the separation point should not be modified by the amalgamation process. If $t = t_m$ is the time when the merging takes place, then it should be:

$$\Gamma_1(t_m^-) = \Gamma_1(t_m^+). \tag{2.79}$$

Let us assume that at $t = t_m$ we are merging two vortices, Γ_p and Γ_q, then using (2.7) the above condition translates into the following equation:

$$\Gamma_m \frac{(\zeta_m - \bar{\zeta}_m)(a^2 - \zeta_m\bar{\zeta}_m)}{(a^2 + \zeta_m^2)(a^2 + \bar{\zeta}_m^2)} = \Gamma_p \frac{(\zeta_p - \bar{\zeta}_p)(a^2 - \zeta_p\bar{\zeta}_p)}{(a^2 + \zeta_p^2)(a^2 + \bar{\zeta}_p^2)} + \Gamma_q \frac{(\zeta_q - \bar{\zeta}_q)(a^2 - \zeta_q\bar{\zeta}_q)}{(a^2 + \zeta_q^2)(a^2 + \bar{\zeta}_q^2)}. \tag{2.80}$$

Because of the imposed symmetry, this equation is invariant under the complex conjugate operation, hence we need another constraint to determine completely ζ_m. This condition is obtained imposing the conservation of the total impulse of the system (2.19) during the merging process, i.e.:

$$I(t_m^-) = I(t_m^+). \tag{2.81}$$

From this constraint we obtained the second equation necessary to close the problem:

$$\Gamma_m \frac{(\zeta_m - \bar{\zeta}_m)(a^2 - \zeta_m \bar{\zeta}_m)}{\zeta_m \bar{\zeta}_m} = \Gamma_p \frac{(\zeta_p - \bar{\zeta}_p)(a^2 - \zeta_p \bar{\zeta}_p)}{\zeta_p \bar{\zeta}_p} + \Gamma_q \frac{(\zeta_q - \bar{\zeta}_q)(a^2 - \zeta_q \bar{\zeta}_q)}{\zeta_q \bar{\zeta}_q}. \tag{2.82}$$

These two equations plus the conservation of the circulation permit to determine uniquely position and strength of the new vortex.

A possible implementation of this scheme is sketched in Figure 2.46. Let us assume we want to amalgamate two vortices of circulation Γ_p and Γ_q and position ζ_p and ζ_q, then the relative distance between the vortices is:

$$r_{pq} = |\zeta_p - \zeta_q|, \tag{2.83}$$

and the average distance of the vortex pair from the center of the body is:

$$r_{av} = |\zeta_{av}| = \frac{|\zeta_p + \zeta_q|}{2}. \tag{2.84}$$

It is reasonable to assume that the merging is a local process, hence the resulting vortex has to be placed close to the generating pair, let us say within a circle of radius r_{pq} centered in ζ_{av}. This assumption becomes important when we are merging two vortices of opposite sign because the resulting vortex is in general placed outside the circle of diameter r_{pq} which interpolates the generating pair. This constraint translates in the following inequality:

$$|\zeta_m - \zeta_{av}| < r_{pq}. \tag{2.85}$$

At the same time we do not want the amalgamation process to take place too close to the body, hence the merging process has to take place outside some circular region centered at the center of the body. If this circular area has radius $a + \alpha r_{pq}$, then this region would not overlap the previous one if the following inequality is satisfied:

$$\frac{r_{pq}}{r_{av} - a} < \frac{1}{\alpha + 1}, \tag{2.86}$$

where α is a positive parameter. In this way, closer pairs are allowed to merge closer to the body and vice versa. Since our final goal is to perturb only slightly the rate of circulation production

and the pressure field acting on the body, we select between all the potential pairs of vortices which satisfy the previous two constraints, those able to satisfy also the following inequalities:

$$\left| \frac{\frac{d\Gamma_1}{dt}\Big|_{t=t_m^+} - \frac{d\Gamma_1}{dt}\Big|_{t=t_m^-}}{\frac{d\Gamma_1}{dt}\Big|_{t=t_m^-}} \right| < \beta, \tag{2.87}$$

and

$$\left| \frac{X(t_m^+) - X(t_m^-)}{X(t_m^-)} \right| < \gamma, \tag{2.88}$$

where β and γ are positive parameters.

To test the quality of this scheme we ran the same simulation involving the shedding of many vortices twice, with and without the merging scheme activated, and the comparison of the results is shown if Figures 2.47–2.56. In this simulation the free-stream velocity is initially zero, then increases rapidly and finally oscillates about a unit mean (see Figure 2.47). The amplitude and frequency of the oscillation is chosen so that the rate of circulation production changes sign twice for each period (see Figure 2.49), and consequently, two new pairs of vortices are introduced into the flow at each period. To test the scheme we created a "worse scenario" by choosing $\alpha = .5$ and $\beta = \gamma = .01$ and allowing the merging when at least four vortex pairs are present in the flow. In this way, the simulation with the merging activated reaches the final time $t = 10$ with seven vortex pairs when the simulation without amalgamation ends up with twenty pairs. Figures 2.48–2.50 show the comparison for total circulation, rate of circulation production and drag coefficient measured during the two simulations. The agreement is excellent, only a slight deviation at late times is noticeable. The effect of the amalgamation is recognizable in the different streamline pattern as shown in Figures 2.51–2.56. Those figures are the instantaneous streamlines at times $t = 6, 8, 10$ when the system with the merging activated has $5, 6, 7$ vortex pairs, while the one without amalgamation has $12, 16, 20$ pairs. It is interesting to observe that although the small structures are lost, the zero streamlines, which separate the recirculating domain from the free-stream flow, have almost the same geometry. Finally, we want to stress the fact that the simulation with the merging activated saved about 70%

of computing time with respect to the other one.

2.9 Active shedding control

In section 1.6 we have seen that it is possible to actively control the rate of circulation production by moving the semi-infinite plate. In particular we have shown that it is possible to inhibit further production of circulation when a vortex is present in the flow. Furthermore, in sections 2.4 and 2.6 we have seen how the results obtained for the flow past a semi-infinite plate are manifested in the behavior for early times of the flow past a finite plate. For these reasons, we expect to extend the control strategy derived in section 1.6 to the finite plate case. In other words, once the starting vortex pair has been shed, i.e., $t \geq t_s$, we want to determine how to change the length of the plate so that the Kutta condition remains satisfied without requiring a new vortex pair.

Let us write the equations of motion in polar coordinates for the starting vortex pair in the following compact form:

$$\begin{cases} \dfrac{d\rho_1}{dt} = R^b_U(\rho_1,\theta_1,a)U + R^b_{\frac{dU}{dt}}(\rho_1,\theta_1,a)\dfrac{dU}{dt} + R^b_{\frac{da}{dt}}(\rho_1,\theta_1,a)\dfrac{da}{dt} \\ \dfrac{d\theta_1}{dt} = \Theta^b_U(\rho_1,\theta_1,a)U + \Theta^b_{\frac{dU}{dt}}(\rho_1,\theta_1,a)\dfrac{dU}{dt} + \Theta^b_{\frac{da}{dt}}(\rho_1,\theta_1,a)\dfrac{da}{dt}, \end{cases} \tag{2.89}$$

with the initial conditions:

$$\begin{cases} \rho_1(0) = ia_0 \\ \theta_1(0) = \theta_0. \end{cases} \tag{2.90}$$

The super-script b indicates quantities which hold before the shedding time t_s. Now if we assume, as in section 1.5, that a reasonable criterion to shed a vortex pair is when the rate of circulation production goes to zero, i.e., at $t = t_s$, then is important to analyze the expression for $\frac{d\Gamma_1}{dt}$. For this purpose it is convenient to rewrite the Kutta condition (2.21) in polar form:

$$\Gamma_1 = \pi \frac{\rho_1^4 - 2a^2\rho_1^2\cos 2\theta_1 + a^4}{(\rho_1^2 - a^2)\rho_1\cos\theta_1} U = G(\rho_1,\theta_1,a,U). \tag{2.91}$$

Then, the rate of circulation production computed from the previous expression using the chain rule has the following form:

$$\frac{d\Gamma_1}{dt} = \frac{dG}{d\rho_1}\frac{d\rho_1}{dt} + \frac{dG}{d\theta_1}\frac{d\theta_1}{dt} + \frac{dG}{dU}\frac{dU}{dt} + \frac{dG}{da}\frac{da}{dt}. \tag{2.92}$$

Using the equations of motion (2.89) we can rewrite the right hand side of the above expression in terms of $U, \frac{dU}{dt}$ and $\frac{da}{dt}$. Then equating it to zero and solving for $\frac{da}{dt}$ we have:

$$\left.\frac{da}{dt}\right|^{b}_{t=t_s} = -\left\{\left[R^b_U\frac{dG}{d\rho_1} + \Theta^b_U\frac{dG}{d\theta_1}\right]_{t=t_s} U_s + \left[R^b_{\frac{dU}{dt}}\frac{dG}{d\rho_1} + \Theta^b_{\frac{dU}{dt}}\frac{dG}{d\theta_1} + \frac{dG}{dU}\right]_{t=t_s}\left.\frac{dU}{dt}\right|_{t=t_s}\right\} \left[R^b_{\frac{da}{dt}}\frac{dG}{d\rho_1} + \Theta^b_{\frac{da}{dt}}\frac{dG}{d\theta_1} + \frac{dG}{da}\right]^{-1}_{t=t_s}. \tag{2.93}$$

Hence for this choice of $\frac{da}{dt}$ the rate of circulation production goes to zero. At this point then we have a technique to stop feeding the starting vortex pair and to create a new one.

Let us assume for the moment that as long as one vortex pair is present in the flow it is possible to move the plate in such a way that the Kutta condition is satisfied for all time. Then, from (2.8) without the Brown and Michael correction, this vortex of fixed strength Γ_{1_s} moves in accordance with the following equations:

$$\begin{cases} \dfrac{d\rho_1}{dt} = R^a_U(\rho_1,\theta_1,a)U + R^a_{\Gamma_{1_s}}(\rho_1,\theta_1,a)\Gamma_{1_s} + R^a_{\frac{da}{dt}}(\rho_1,\theta_1,a)\dfrac{da}{dt} \\ \dfrac{d\theta_1}{dt} = \Theta^a_U(\rho_1,\theta_1,a)U + \Theta^a_{\Gamma_{1_s}}(\rho_1,\theta_1,a)\Gamma_{1_s} + \Theta^a_{\frac{da}{dt}}(\rho_1,\theta_1,a)\dfrac{da}{dt}, \end{cases} \tag{2.94}$$

with the initial conditions:

$$\begin{cases} \rho_1(t_s) = \rho_{1_s} \\ \theta_1(t_s) = \theta_{1_s}, \end{cases} \tag{2.95}$$

where ρ_{1_s}, θ_{1_s} and,

$$\Gamma_{1_s} = G(\rho_{1_s}, \theta_{1_s}, a_s, U_s) \tag{2.96}$$

are the values at the shedding time. The super-script a indicates quantities which hold after the shedding time t_s. The explicit form of the functions which appear in the above equations is given

in the Appendix. From the Kutta condition or the requirement that the complex velocity be zero at the origin, we obtain the relationship:

$$\Gamma_{1_s} - G(\rho_1, \theta_1, a, U) = 0. \tag{2.97}$$

If this constraint on the trajectory of the vortex is satisfied for all time after the shedding time, t_s, then the Kutta condition is satisfied. Hence, to achieve the control of the system we must embed this constraint into the equations of motion (2.94). As a first step, let us take the time derivative of the above constraint, and obtain:

$$\frac{d\Gamma_1}{d\rho_1}\frac{d\rho_1}{dt} + \frac{d\Gamma_1}{d\theta_1}\frac{d\theta_1}{dt} + \frac{d\Gamma_1}{dU}\frac{dU}{dt} + \frac{d\Gamma_1}{da}\frac{da}{dt} = 0. \tag{2.98}$$

As before, using the equations of motion (2.94), we can rewrite the above expression in terms of U, $\frac{dU}{dt}$ and, $\frac{da}{dt}$. Then solving for $\frac{da}{dt}$ we obtain:

$$\begin{aligned}\frac{da}{dt} = -\left\{\left[R^a_U\frac{dG}{d\rho_1} + \Theta^a_U\frac{dG}{d\theta_1}\right]U + \frac{dG}{dU}\frac{dU}{dt} + \left[R^a_{\Gamma_{1_s}}\frac{dG}{d\rho_1} + \Theta^a_{\Gamma_{1_s}}\frac{dG}{d\theta_1}\right]\Gamma_{1_s}\right\} \\ \left[R^a_{\frac{da}{dt}}\frac{dG}{d\rho_1} + \Theta^a_{\frac{da}{dt}}\frac{dG}{d\theta_1} + \frac{dG}{da}\right]^{-1}.\end{aligned} \tag{2.99}$$

This then is the rate of change of the plate length necessary to take advantage of the presence of the starting pair and keep the Kutta condition satisfied without forming a new pair. Before verifying this result let us check the compatability of the two parts of the argument (see equations 2.93 and 2.99) by computing the following limit:

$$\lim_{t\to t_s}\frac{da}{dt} = \left.\frac{da}{dt}\right|^b_{t=t_s}. \tag{2.100}$$

The above statement is true because at time $t = t_s$ the rate of circulation production is zero, consequently the Brown and Michael correction vanishes and the equations of motion before and after shedding coincide. Furthermore, this result guarantees the continuity of the rate of change of the length of the plate. Substituting (2.99) in the equation of motion (2.94) we obtain the set of

equation for the controlled system as follows:

$$\begin{cases} \dfrac{d\rho_1}{dt} = R^c_U(\rho_1,\theta_1,a)U + R^c_{\Gamma_{1_s}}(\rho_1,\theta_1,a)\Gamma_{1_s} + R^c_{\frac{dU}{dt}}(\rho_1,\theta_1,a)\dfrac{dU}{dt} \\ \dfrac{d\theta_1}{dt} = \Theta^c_U(\rho_1,\theta_1,a)U + \Theta^c_{\Gamma_{1_s}}(\rho_1,\theta_1,a)\Gamma_{1_s} + \Theta^c_{\frac{dU}{dt}}(\rho_1,\theta_1,a)\dfrac{dU}{dt} \\ \dfrac{da}{dt} = A^c_U(\rho_1,\theta_1,a)U + A^c_{\Gamma_{1_s}}(\rho_1,\theta_1,a)\Gamma_{1_s} + A^c_{\frac{dU}{dt}}(\rho_1,\theta_1,a)\dfrac{dU}{dt}, \end{cases} \tag{2.101}$$

with initial conditions:

$$\begin{cases} \rho_1(t_s) = \rho_{1_s} \\ \theta_1(t_s) = \theta_{1_s} \\ a(t_s) = a_s, \end{cases} \tag{2.102}$$

and the circulation associated with the vortex pair is:

$$\Gamma_{1_s} = G(\rho_{1_s},\theta_{1_s},a_s,U_s). \tag{2.103}$$

The super-script c indicates quantities which hold for the controlled system. The explicit form of the functions which appear in the above equation is given in the Appendix. These are the equations of motion of the vortex pair in the controlled case. In essence, the trajectories of the vortices are intelligently affected by the change in the plate length, keeping the Kutta condition satisfied. Analyzing the denominator of the above equations we can see that in general they become singular for:

$$U = 0, \qquad \theta_1 = \pm \arccos\left(\sqrt{\frac{3(\rho_1^2+a^2)^2}{4(\rho_1^4+a^2\rho_1^2+a^4)}}\right). \tag{2.104}$$

These singularities are strictly related to those discovered in section 1.6 for the case of the semi-infinite plate. As before, the constraint on U means that is not possible to reverse the direction of the free-stream and at the same time maintain the Kutta condition without further production of circulation. The singularity in θ_1, instead, reduces to that presented in section 1.6 through an expansion about the tip of the plate. Consequently the semi-plane $y > 0$ is divided into three sectors and the top vortex is not allowed to move from one to the other without a singularity in the rate of

change of the plate length. Because of the imposed symmetry, the same singularity would occur in the negative semi-plane.

Because the equations (2.101) implicitly satisfy the constraint (2.97), we could theoretically use such a relationship to reduce the equations of motion to a set of two. Unfortunately, the mathematics is too involved to allow such a simplification. Nevertheless, this constraint becomes useful during the numerical integration of the above equations.

2.10 Dynamical behavior of the controlled system

In the previous section we have been able to find a controller which inhibits the production of circulation when a vortex pair is present in the flow. This section is devoted to the analysis of the dynamical behavior of the controlled system.

We start this investigation by searching for the fixed points of the unperturbed and uncontrolled system. The set of equations describing this case can be obtained imposing $U(t) = U_s$ and $\frac{da}{dt} = 0$ on (2.94). The result is:

$$\begin{cases} \dfrac{d\rho_1}{dt} = R^a_U(\rho_1, \theta_1, a)U_s + R^a_{\Gamma_{1_s}}(\rho_1, \theta_1, a)\Gamma_{1_s} \\ \dfrac{d\theta_1}{dt} = \Theta^a_U(\rho_1, \theta_1, a)U_s + \Theta^a_{\Gamma_{1_s}}(\rho_1, \theta_1, a)\Gamma_{1_s}. \end{cases} \tag{2.105}$$

The above equations for the fixed points can be reduced to a constraint on the trajectory of the vortex pair, known as the Föppl curve, i.e.:

$$\cos^2\theta_1 = \frac{(\rho_1^2 - a^2)^2}{4(\rho_1^4 - a^2\rho_1^2 + a^4)}, \tag{2.106}$$

and a constraint on the circulation associated with the vortex pair, i.e.:

$$\Gamma_{1_s} = \frac{4\pi U(\rho_1^2 - a^2)[(\rho_1^4 + a^4)^2 - 4a^4\rho_1\cos^2 2\theta_1]\cos\theta_1}{\rho_1[8a^2\rho_1^2(\rho_1^4 - 2a^2\rho_1^2\cos^2\theta_1 + a^4)\cos^2\theta_1 + (\rho_1^2 - a^2)^4]}. \tag{2.107}$$

It is possible to prove mathematically that there does not exist any vortex pair with the above associated circulation which lies on the Föppl curve beside the pathological situations when the circulation is zero or infinite. Figure 2.57 shows that for values of circulation up to 10 there is no intersection between the loci of points where a vortex of fixed circulation can lie satisfying the Kutta condition and the Föppl curve. For higher values of the circulation the two curves intersect each other identifying two points but there is a mismatch between the vortex circulation and that required to lie at those points of the Föppl curve. Physically this means that, given any fixed free-stream velocity U_s it is not possible to find a vortex pair of any finite strength that simultaneously does not move and satisfies the Kutta condition. This is an interesting result in that it predicts that for any free-stream velocity a flow, which separates from the tips of a flat plate cannot reach a steady-state solution. As far as our knowledge there is not any experimental evidence which contradicts this prediction. An analogous result which shows, instead, the existence of a steady-state solution as been proved by Milne-Thomson [14] for a circular cylinder. Note for a circular cylinder the flow separates from the back stagnation point.

Let us first analyze the restrictions that the trajectory constraint (2.97) imposes on the motion of the vortex pair. It is convenient to rewrite the constraint as follows:

$$\frac{\Gamma_{1_s}(\rho_1^2 - a^2)\rho_1 \cos\theta_1 - \pi(\rho_1^4 - 2a^2\rho_1^2 \cos 2\theta_1 + a^4)U}{(\rho_1^2 - a^2)\rho_1 \cos\theta_1} = 0. \tag{2.108}$$

The numerator can be regarded as a biquadratic algebraic equation in a which can be easily solved. Then, we have to select from all the possible solutions those for which $a \in (0, \rho_1)$. The result of this analysis is to determine areas of the domain within which the vortex pair is allowed to move. If we assume that $U > 0$, $\Gamma_{1_s} > 0$ and $\theta_1 \in (0, \frac{\pi}{2})$ then the following results hold in the $x, y > 0$ quadrant. We have two real positive solutions if:

$$\frac{\Gamma_{1_s} \cos\theta_1}{\pi U} < \rho_1 < \frac{\Gamma_{1_s}(1 + \sin\theta_1)}{2\pi U \sin 2\theta_1} \qquad 0 < \theta_1 < \frac{\pi}{6} \tag{2.109}$$

while, we have one real positive solution if:

$$a < \rho_1 < \frac{\Gamma_{1_s} \cos\theta_1}{\pi U} \qquad 0 < \theta_1 < \frac{\pi}{2}. \tag{2.110}$$

Figure 2.58 shows the regions within which one or two real positive roots exist when a vortex pair of circulation $\Gamma_{1_s} = \pm 10$ is at $\rho_1 = 1.45$ and $\theta_1 = \pm\frac{\pi}{5}$. As the vortex pair drifts downstream the boundaries of these regions move also, depending on the position of the vortex pair, the magnitude of the free-stream velocity and the plate length. When the vortex pair reaches the boundary of the region where the roots are not real positive the length of the plate goes to zero. This possibility represents a strong constraint on the controllability of the system which was not present in the semi-infinite plate case.

The existence of a finite controllability region restricts the search for periodic orbits to the region itself, but the lack of fixed points for the unperturbed system suggests the absence of such orbits. Because of the remarkable similarity with the results obtained for the semi-infinite plate in sections 1.6 and 1.7 we proceed to investigate the global structure of the flow field in the same fashion. The set equations of motion for the perturbed and controlled case (2.101) can be, in principle, decoupled and reduced to a set of two equations by means of the trajectory constraint (2.97) but the complexity of the equations discourages such attempts. Nevertheless, this constraint can be used to eliminate Γ_{1_s} from the equations (2.101). Substituting and simplifying we obtain:

$$\begin{cases} \dfrac{da}{dt} = \mathbf{A}^c_U(\rho_1,\theta_1,a)U + \mathbf{A}^c_{\frac{dU}{dt}}(\rho_1,\theta_1,a)\dfrac{dU}{dt} \\ \dfrac{d\rho_1}{dt} = \mathbf{R}^c_U(\rho_1,\theta_1,a)U + \mathbf{R}^c_{\frac{dU}{dt}}(\rho_1,\theta_1,a)\dfrac{dU}{dt} \\ \dfrac{d\theta_1}{dt} = \mathbf{\Theta}^c_U(\rho_1,\theta_1,a)U + \mathbf{\Theta}^c_{\frac{dU}{dt}}(\rho_1,\theta_1,a)\dfrac{dU}{dt}. \end{cases} \tag{2.111}$$

The super-script c indicates quantities which hold for the controlled system. The size and complexity of these equations together with the presence of moving boundaries makes the search of a Liapunov like function extremely difficult. However, because the results obtained for the semi-infinite plate

hold, at least at early times, around the tips of the plate, there is good reason to believe that they might hold over the entire controllability region for larger times. The numerical simulations presented in the next section adds credence to this conjecture.

2.11 Results

In section 2.8 we presented a simulation in which the free-stream at time zero suddenly rises and then oscillates about a nonzero mean. In that case we kept the length of the plate constant and a cloud of vortices was produced. Based on the results of the last two sections we can run the same numerical experiment changing the length of the plate to inhibit the production of circulation.

We start with a quite simpler situation in which the free-stream velocity after an initial sharp acceleration decelerates to a constant nonzero value (see Figure 2.59). Figures 2.60–2.66 illustrate the growth of the starting pair and the evolution of the controlled system. Note the length of the plate up to the shedding time has been chosen to position the vortices at some distance from the sector dividers. Figures 2.61–2.62 show that up to time $t_s \approx .37$ the starting pair grows. When the rate of circulation production goes to zero the strength of the vortices is frozen, triggering the active control for the rest of the simulation ($t_{final} \approx 2.5$). From Figures 2.59 and 2.60 we can see that as the vortex pair is convected downstream the plate length increases during the first half of the simulation then decreases during the second part to maintain control and finally drops almost instantaneously to zero. Figures 2.60 shows that the control is lost when the vortex reaches simultaneously the sector divider (dotted line) and the border of the domain of controllability (dashed line). Figure 2.63 shows the trend of the drag coefficient which has been computed using the instantaneous length of the plate. At early times we observe large oscillations due to the added mass term then, when the free-stream acceleration go to zero, the drag coefficient decreases slowly as the recirculating bubble becomes more streamlined. Figures 2.64–2.66 are the instantaneous streamlines during the

controlled period. It is worth observing that at early times, when a strong free-stream acceleration drives the flow, the plate changes length to delay the formation of a large recirculating bubble. At later times however, when the free-stream velocity is constant, the plate allows the bubble to grow and takes advantage of the streamlined shape to satisfy the Kutta condition.

In the second set of results we present the active shedding control of a flow similar to that used in section 2.8. Figures 2.67–2.74 illustrate the growth of the starting pair and the evolution of the controlled system. As before, the length of the plate up to the shedding time has been chosen to locate the vortices away from the sector dividers. The starting pair grows up to time $t_s \approx .27$ when the rate of circulation production drops to zero (see Figures 2.69 and 2.70). Then, the controller takes over and predicts the length of the plate for the rest of the simulation ($t_{final} \approx 1$). As the vortex pair drifts downstream the plate length increases during the first part of the simulation then oscillates about a constant value and finally undergoes a sudden contraction. In this case the control is lost because the vortex reaches the sector divider (dotted line in Figure 2.68) while still well inside the domain of controllability (dashed line). The drag coefficient has large oscillations for the entire simulation because of the added mass contribution while its mean value slowly goes to zero (see Figure 2.71). Figures 2.72–2.74 are the instantaneous streamlines during the controlled period. In this case the free-stream acceleration drives the entire simulation and the two small recirculating bubbles never merge to create the larger one.

2.12 Conclusions

An irrotational model has been used to simulate the unsteady separated flow past a finite plate of variable length. The analysis of the evolution of the system at early times recovers, at first order, the result obtained for the semi-infinite plate. Consequently, this result validates the model for small times and, furthermore, provides the approximate solutions necessary to start the numerical

integration of the equations of motion. The simulation of the power-law starting flow when the plate length is fixed provides further insight about the validity of the model. The length of the recirculating bubble and the drag experienced by the plate compare well with the results obtained experimentally and numerically by other researchers. Finally, a time-dependent scaling was proposed to make the problem dimensionless. This approach unveils the universality hidden in the phenomenon and nearly collapses the results for any power-law.

The irrotational model has been extended to the case where several vortices are present in the flow by implementing the vortex shedding mechanism used for the semi-infinite plate. The separation of the flow in the presence of other vortices was then analyzed. The approximate solution for early times has the same structure of that obtained for the semi-infinite plate. Consequently, the trajectory of the new vortex is always parallel to the plate but there exists a limiting value of the rate of change of the plate length beyond which the separation is not allowed in the present model. This result gives further mathematical evidence for Rott's prediction of such a limiting value [20] even for finite geometries. Finally, to further improve the computational time an highly conservative merging scheme was presented and successfully tested.

Within this model we derived a control strategy which inhibits the production of additional circulation when a vortex pair is present in the flow. Because of the mathematical simplicity of the model we obtained the exact solution of the controller, for any time-dependent free-stream velocity, in the form of a ordinary differential equation. Subsequently, the performance of the controller was characterized with a dynamical system type of analysis. This investigation showed that the time over which the system is controllable is finite as a consequence of the conflicting effects of the drifting motion which convects the vortex downstream and the existence of a controllability region within which the vortex should move. Nevertheless, this time can be maximized by an intelligent choice of the separation conditions. Finally, we successfully tested the controller for two different types of free-stream conditions. The robustness issue was not addressed in the present work because in

general it is strictly related to the final application.

2.13 Recommendations for further investigations

The results of our investigation showed that the Brown and Michael [1] model is accurate enough to capture the main features of the flow past a flat plate and simple enough to permit the analytical derivation of a controller. For the particular control problem we chose, the controller performed satisfactorily only over a finite lapse of time. The control was eventually lost because the vortices were irreversibly convected down-stream. This fact is probably a direct consequence of the lack of fixed points for the unperturbed flow.

The logical continuation of this research is to explore other geometries like cambered or v-shaped plates, lens or diamond-shaped cylinders in both bounded an unbounded domains searching for the fixed points of the unperturbed flow. The existence of such a critical points and their stability properties should provide a criterion for selecting the preferred geometry and the desired control strategy. Following the approach presented in our investigation, it should then be possible to derive a controller able to stabilize the fixed points with respect to a perturbated free-stream velocity. If this result can be achieved for infinite time then the robustness issue should be addressed. Robustness is in fact a necessary condition for a possible use of the controller in a real situation.

The implementation of the derived controller to a real experiment will be difficult and has to be carried out step by step. The first step would be to embed the controller into a more sophisticated CFD code which can simulate the flow under investigation by integrating, for example, the full Navier-Stokes equations. There are several advantages in undertaking this intermediate step. The two codes, solver and controller, can be synchronized, all the necessary quantities computed and robustness tested in a quite simple way. During this process, time series theory should produce further information about the actual complexity of the associated dynamical system and provide

an indication about the robustness required to maintain control. A success at this stage will open possibilities for the active control of large-scale coherent turbulence.

There are at least three potential directions for the use of this work. First is the application of this model to the unsteady, separated flow past a flat plate with a forward-facing dynamical flap (casper wing) at high angles of attack. In this case, the control strategy has to predict the movement of the flap so that a vortex is trapped and kept trapped above the wing increasing the lift and reducing the drag. Eventual results can contribute to the advance of VSTOL technology and give good insight as to how to handle dynamic stalls. The second possibility is the addition of some elasticity to the plate to model the fluid structure interaction for basic motions such as flapping and pitching. The solution of this problem can contribute to several areas of research such as: biofluidmechanics, flow induced vibrations, structural engineering and material fatigue. The third possibility is to apply this model to reacting flows, for example to study the dynamics of a simplified combustion chamber by first developing a model to reproduce combustion instabilities and then determining a strategy for control them.

Figures

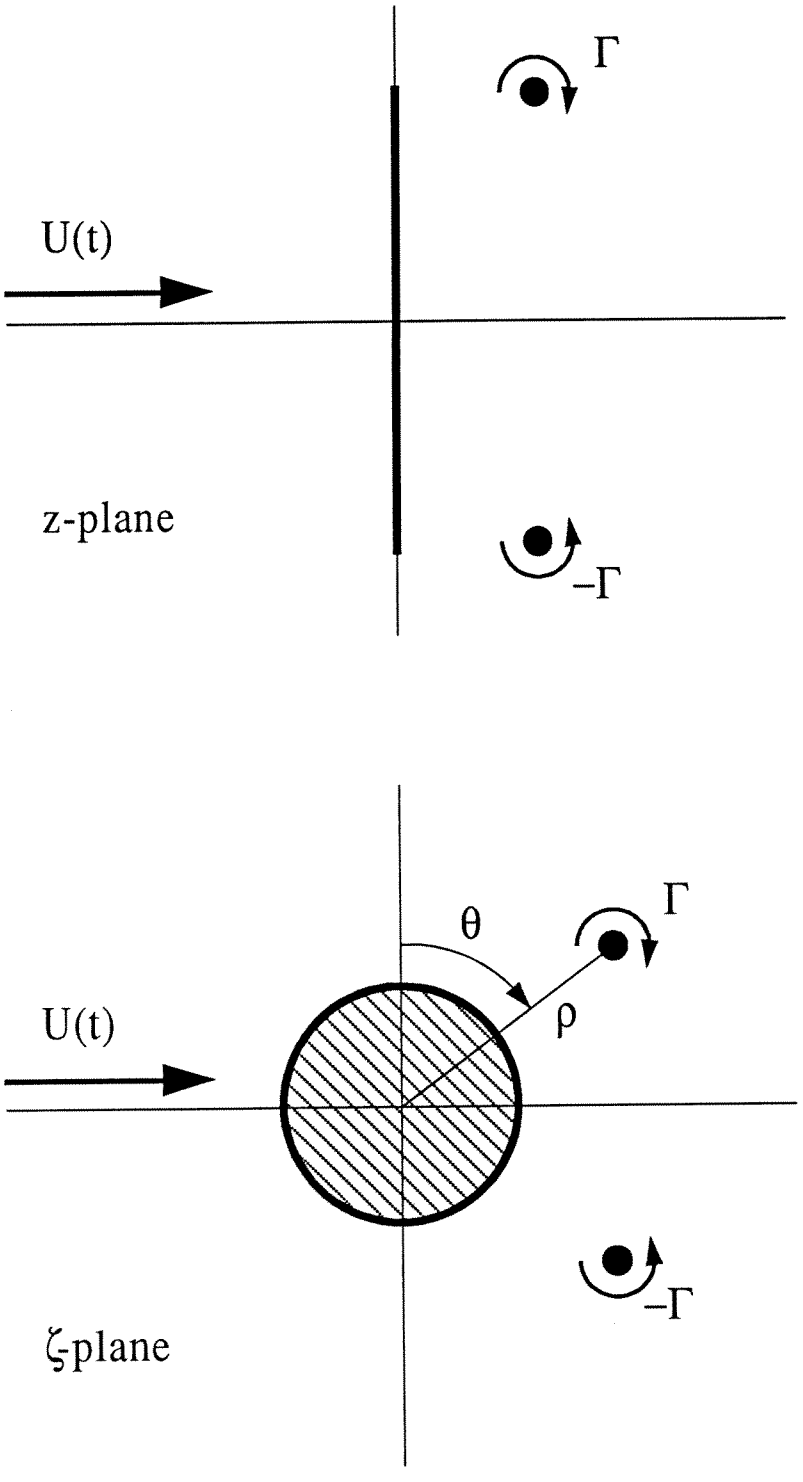

Figure 2.1: Physical and mapped planes.

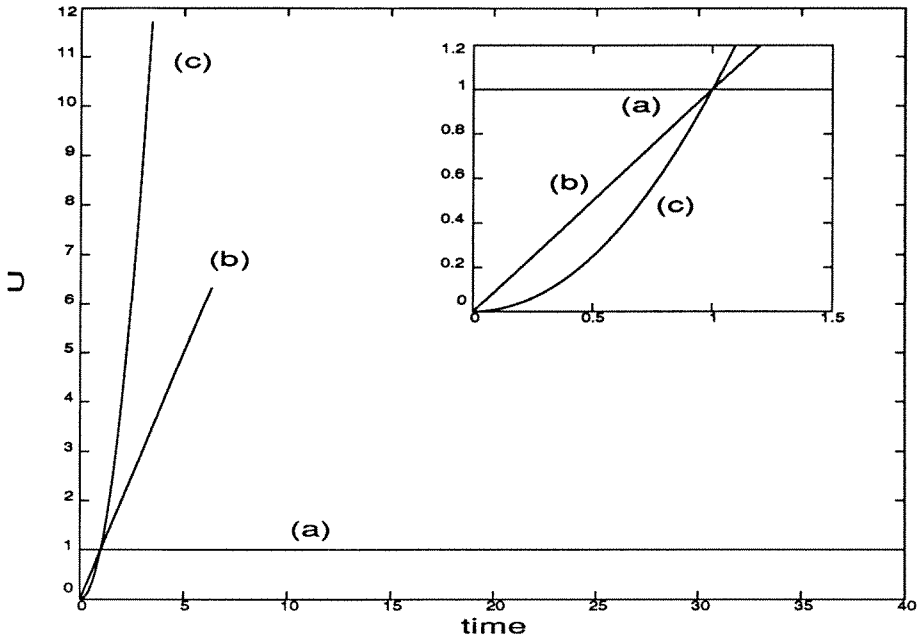

Figure 2.2: Free-stream velocity: $U(t) = Vt^m$ ($m = 0, 1, 2$).

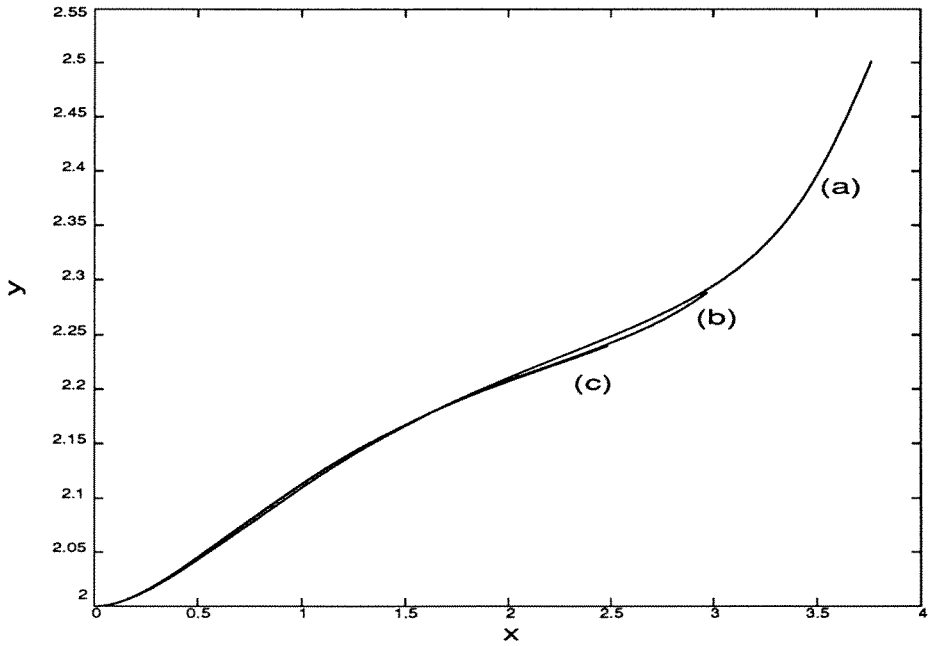

Figure 2.3: Trajectories of the top vortex ($m = 0, 1, 2$).

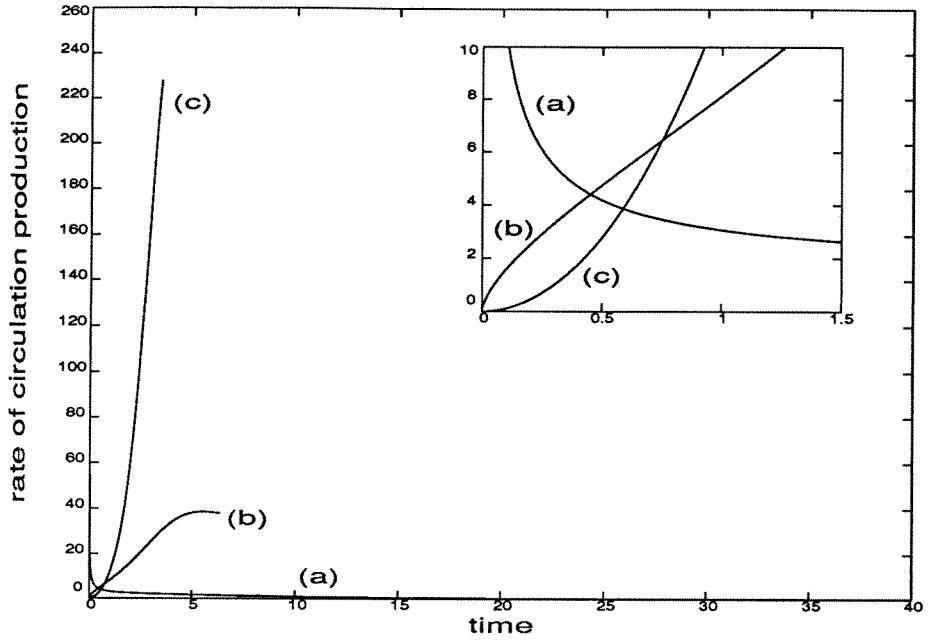

Figure 2.4: Rate of circulation production for the top vortex ($m = 0, 1, 2$).

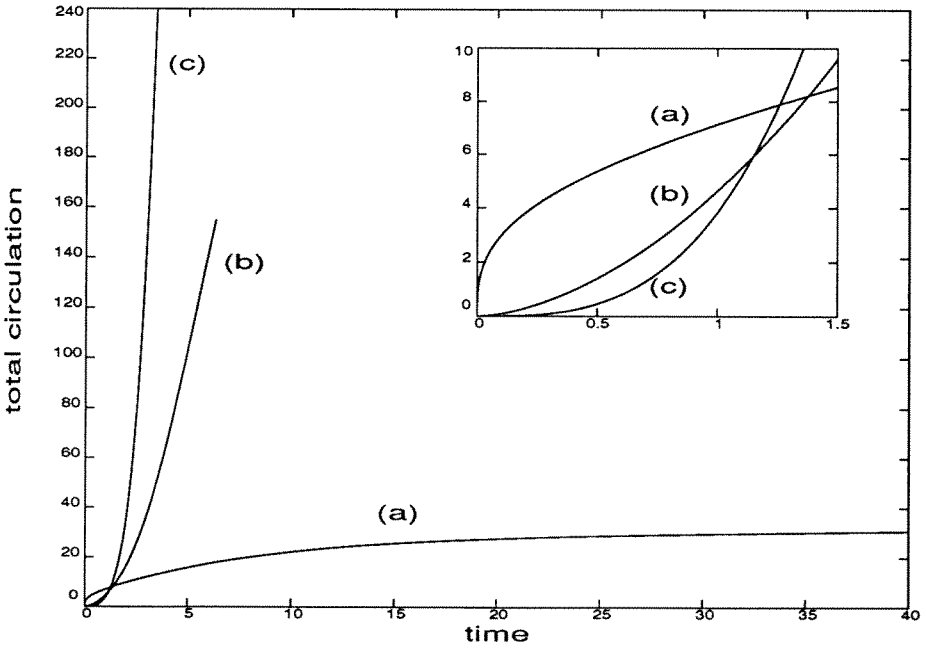

Figure 2.5: Total circulation of the top vortex ($m = 0, 1, 2$).

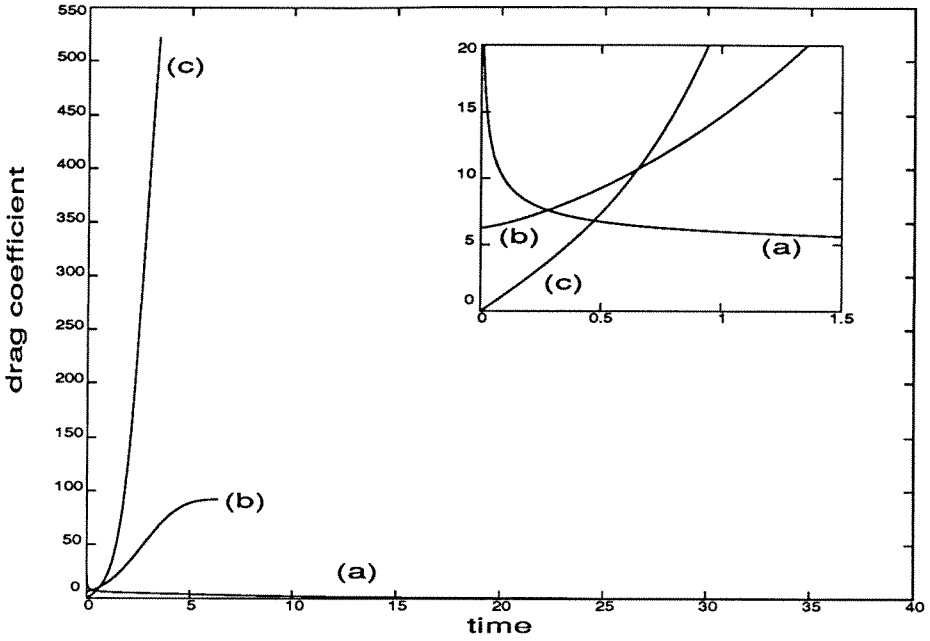

Figure 2.6: Drag coefficient ($m = 0, 1, 2$).

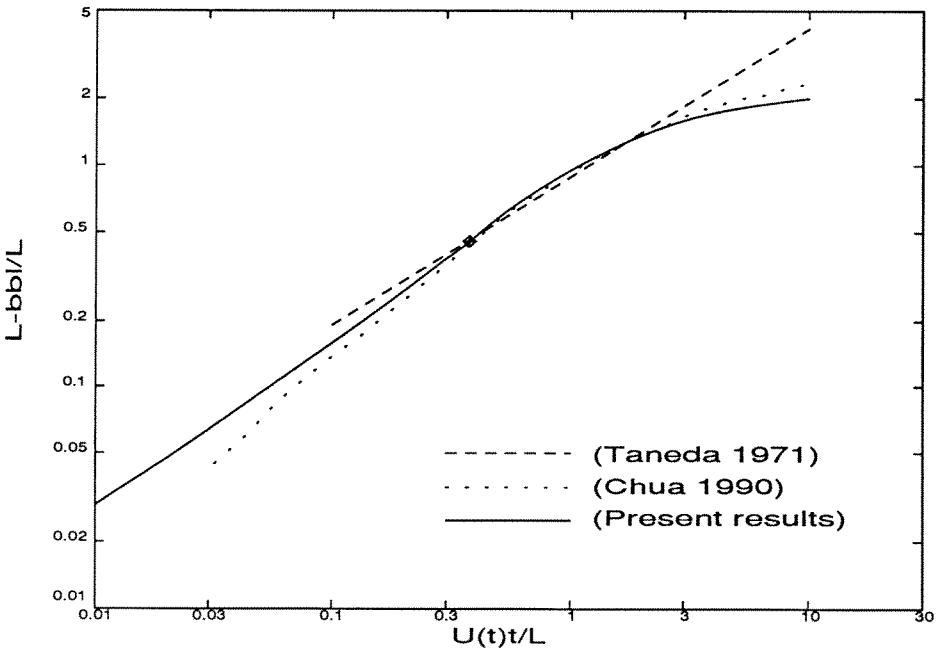

Figure 2.7: Length of the recirculating bubble, a comparison.

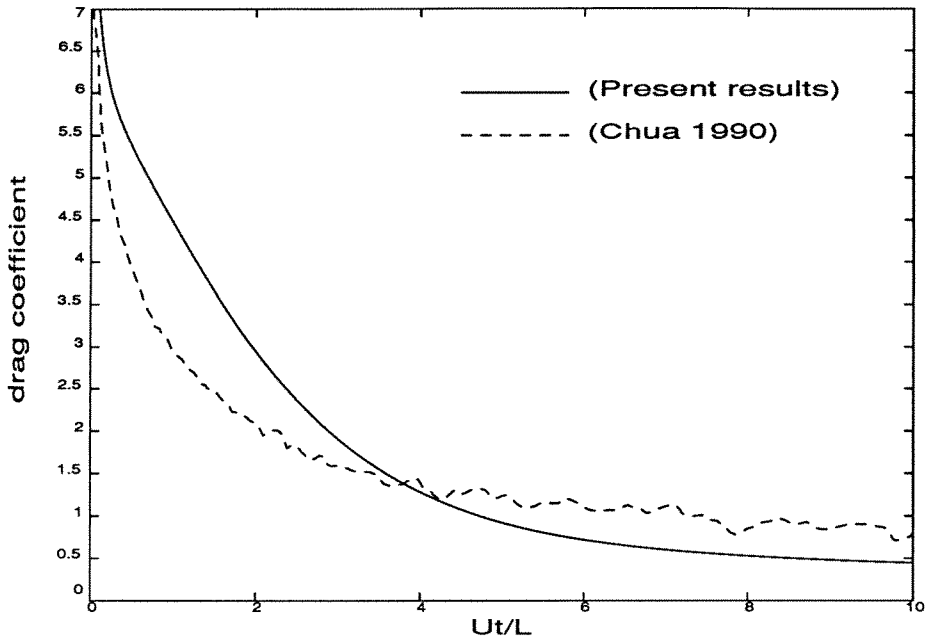

Figure 2.8: Drag coefficient comparison for the impulsively started plate ($m = 0$).

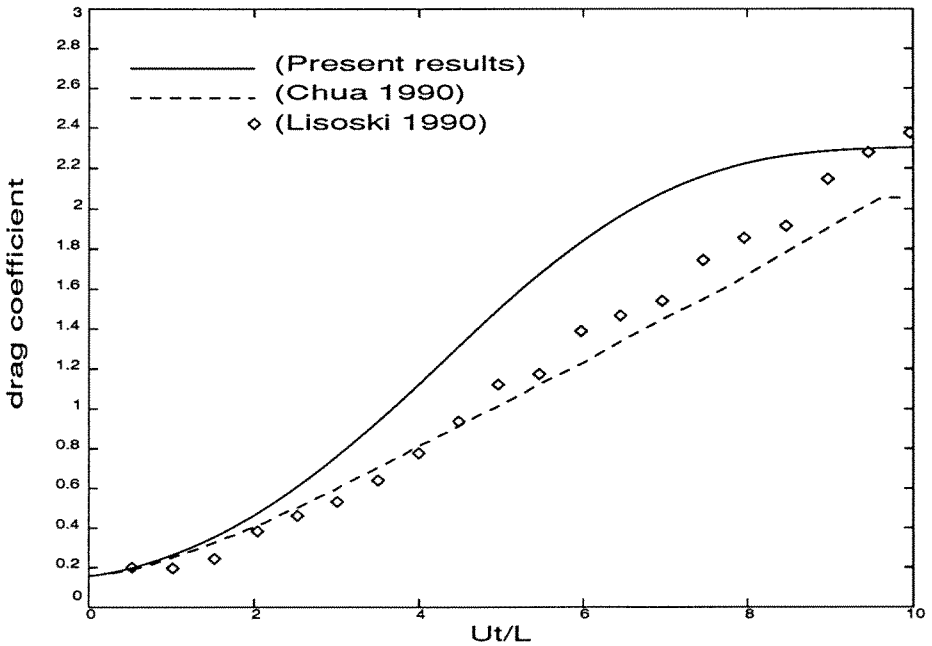

Figure 2.9: Drag coefficient comparison for the constantly accelerated plate ($m = 1$).

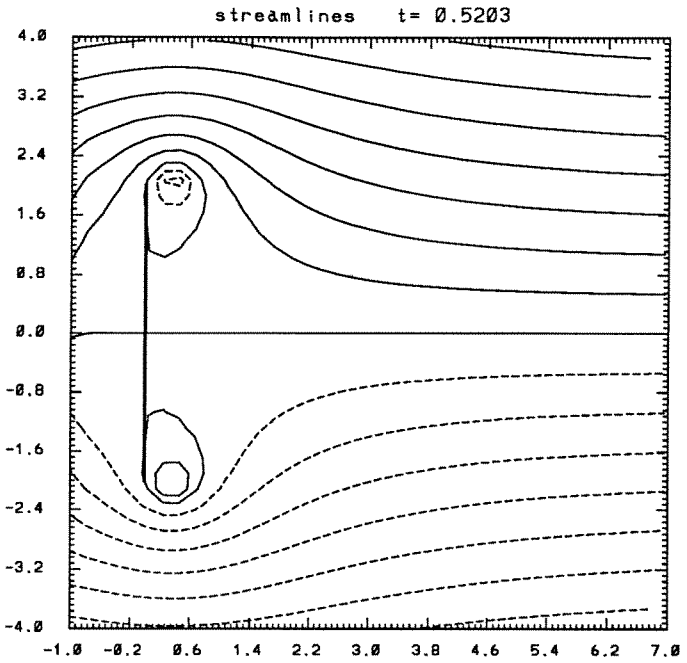

Figure 2.10: Recirculating bubbles: case (a) ($t = .5203, m = 0$).

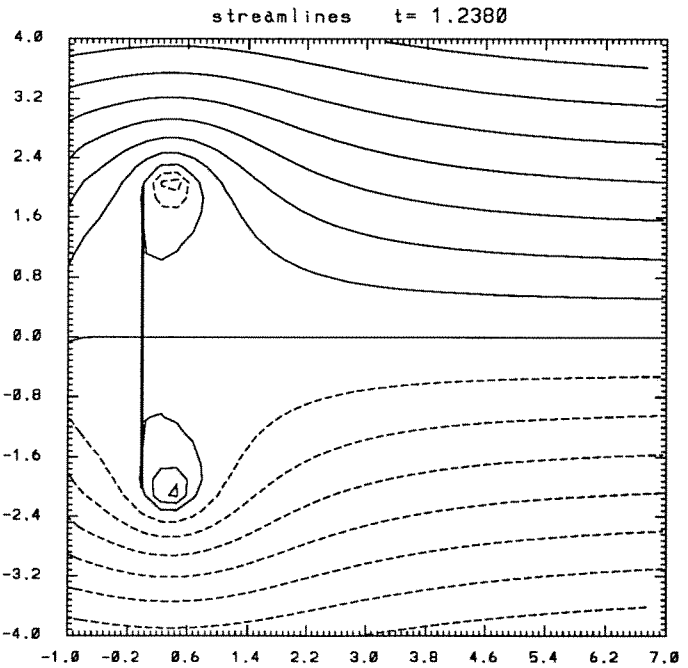

Figure 2.11: Recirculating bubbles: case (b) ($t = 1.2380, m = 1$).

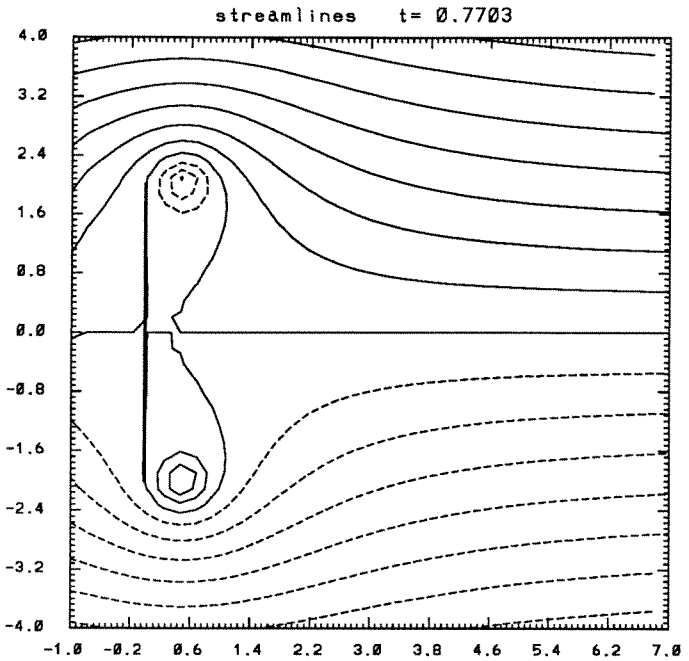

Figure 2.12: Recirculating bubble: case (a) ($t = .7703, m = 0$).

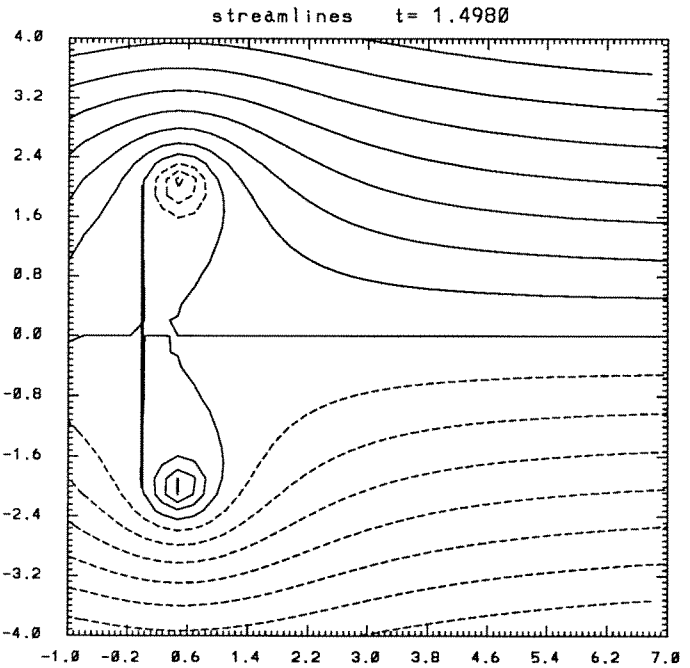

Figure 2.13: Recirculating bubble: case (b) ($t = 1.4980, m = 1$).

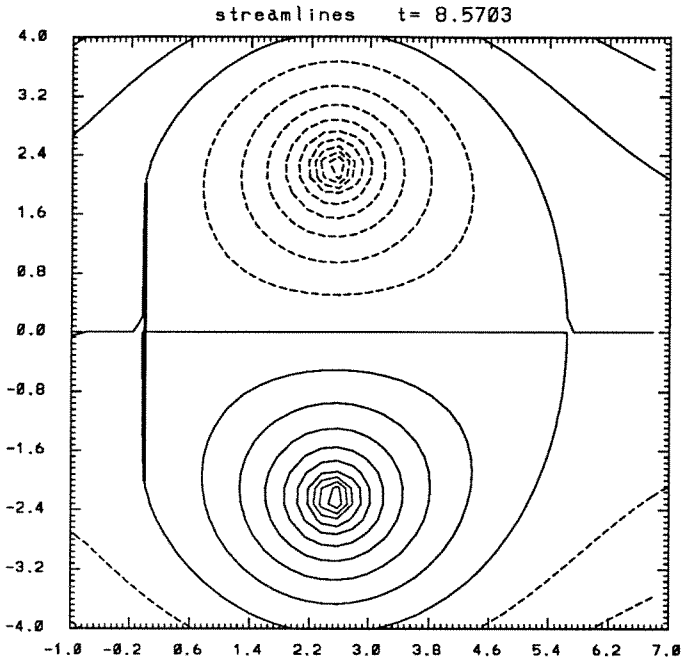

Figure 2.14: Recirculating bubble: case (a) ($t = 8.5703, m = 0$).

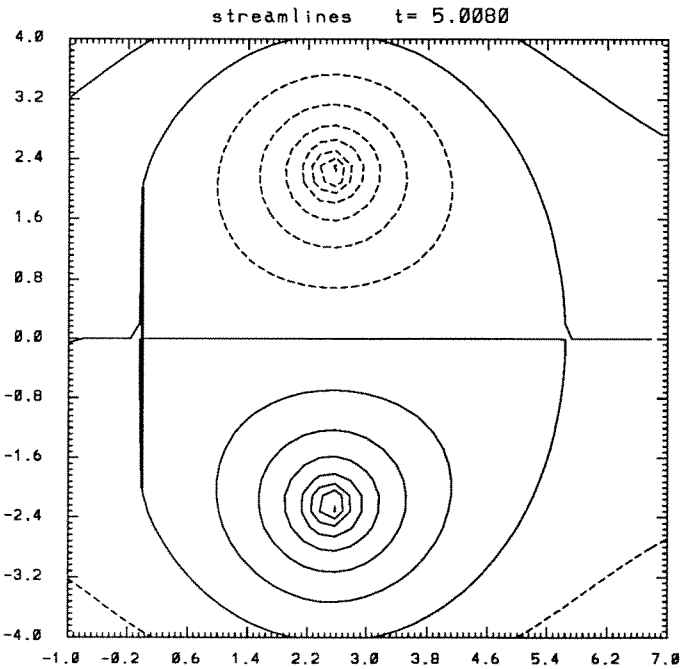

Figure 2.15: Recirculating bubble: case (b) ($t = 5.0080, m = 1$).

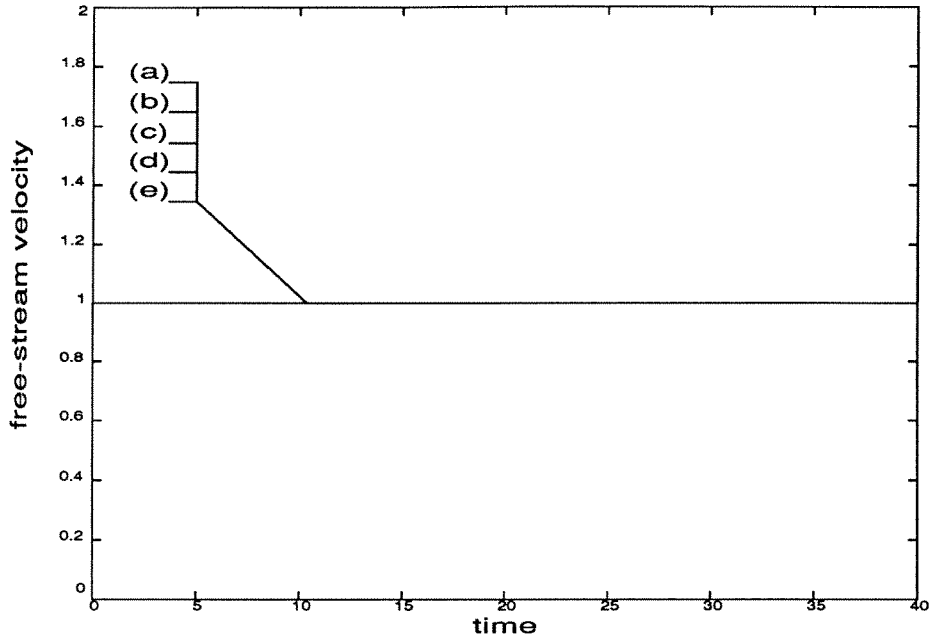

Figure 2.16: Free-stream velocity ($m = 0, 1, 2, 5, 10$).

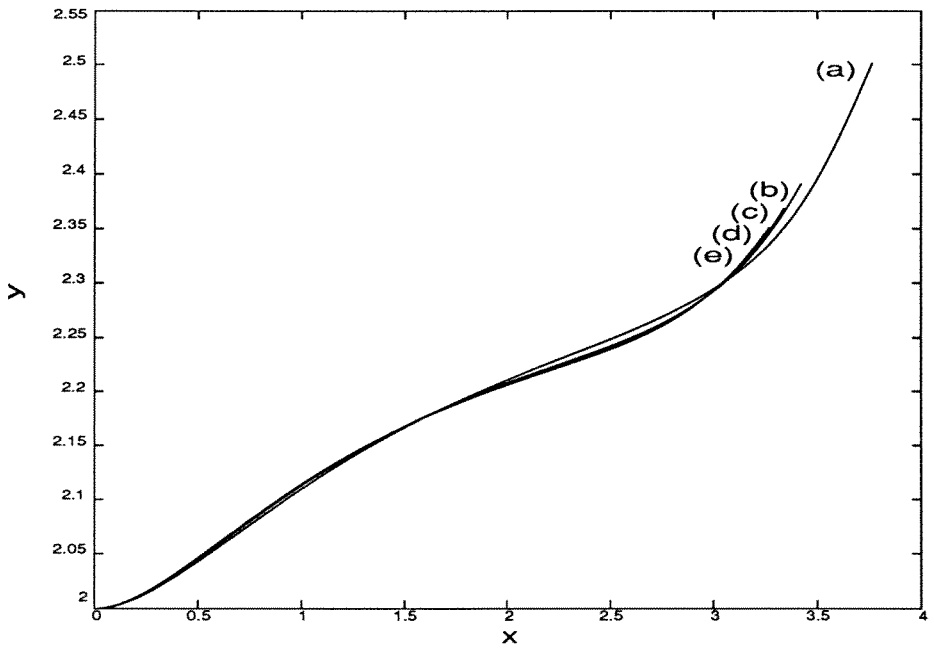

Figure 2.17: Trajectories of the top vortex ($m = 0, 1, 2, 5, 10$).

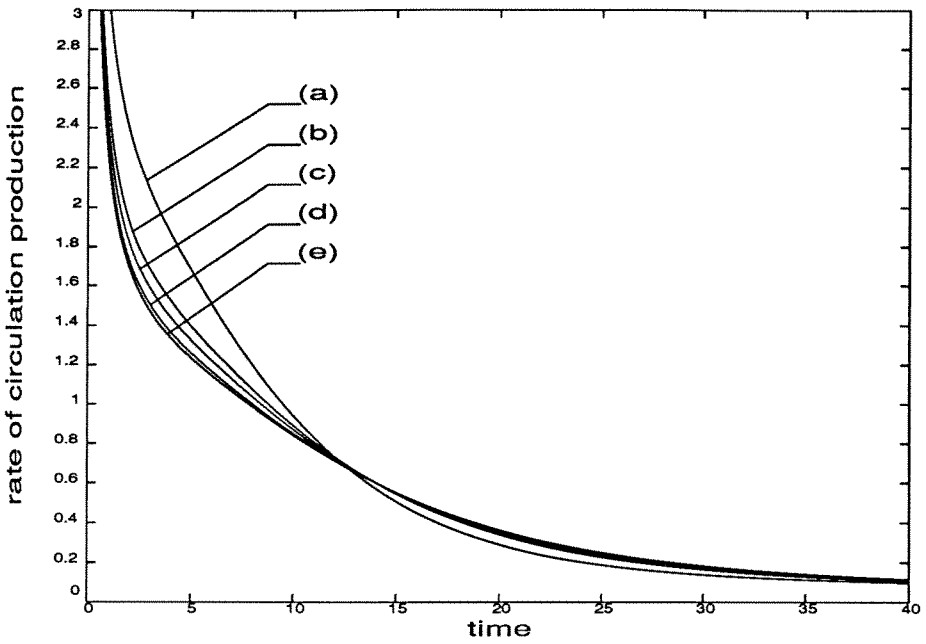

Figure 2.18: Rate of circulation production for the top vortex ($m = 0, 1, 2, 5, 10$).

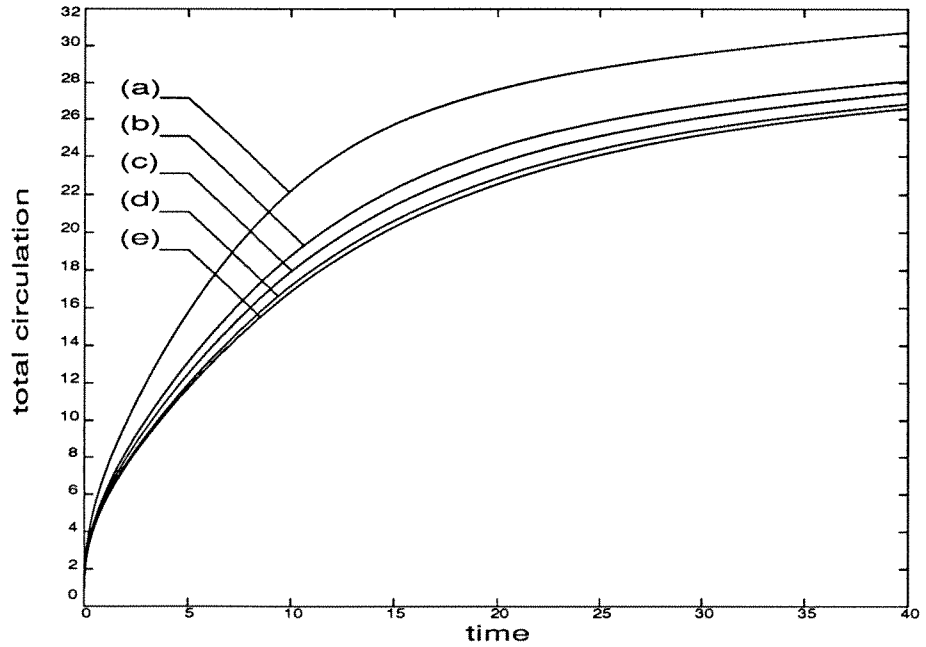

Figure 2.19: Total circulation of the top vortex ($m = 0, 1, 2, 5, 10$).

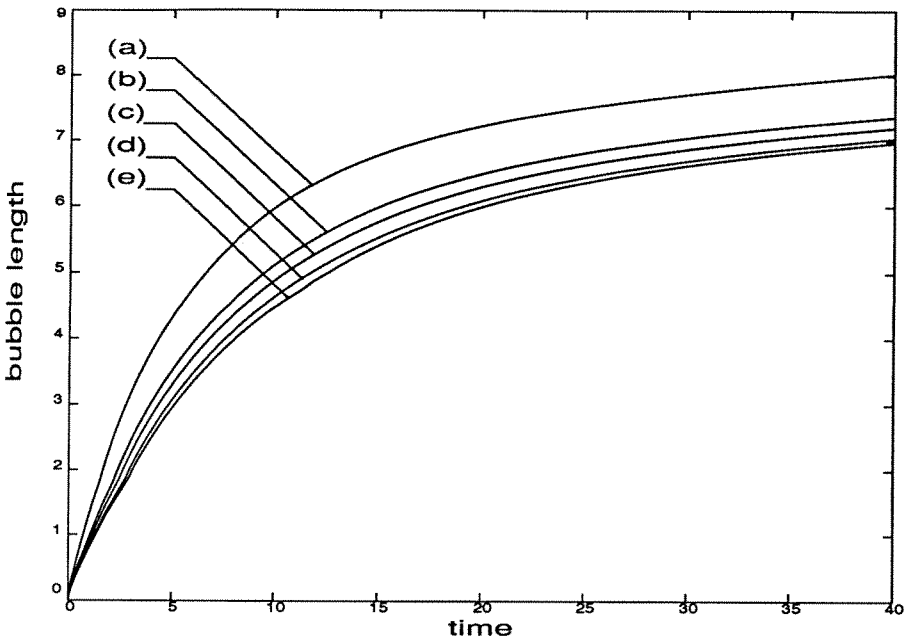

Figure 2.20: Length of the recirculating bubble ($m = 0, 1, 2, 5, 10$).

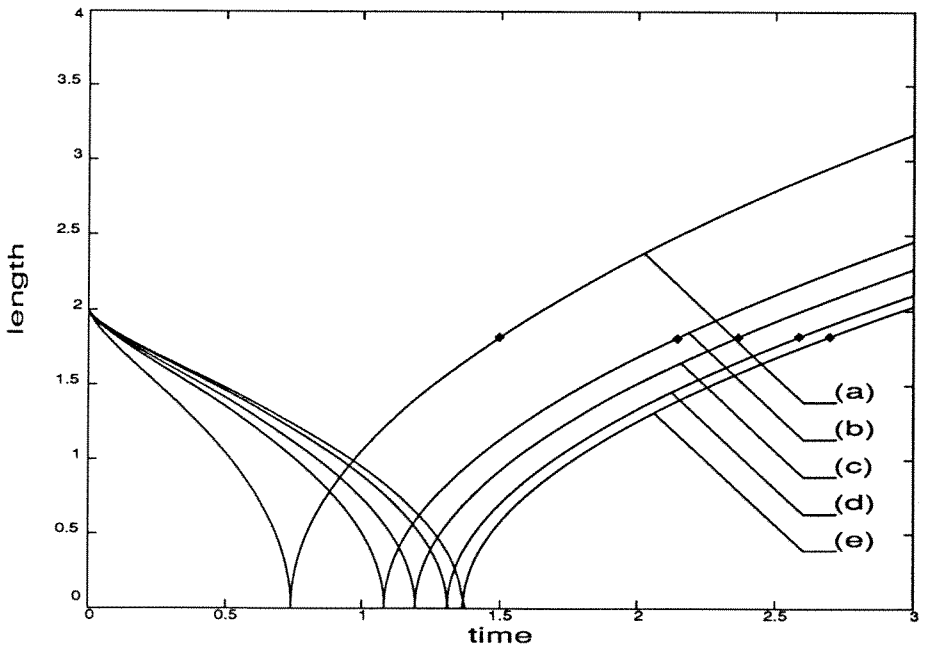

Figure 2.21: Loci of the stagnation points ($m = 0, 1, 2, 5, 10$).

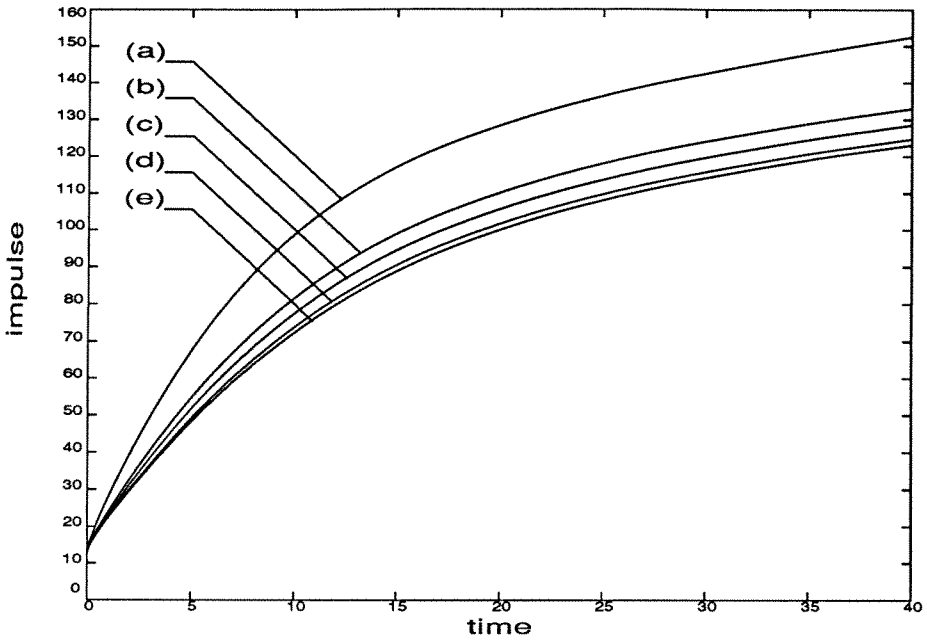

Figure 2.22: Total impulse ($m = 0, 1, 2, 5, 10$).

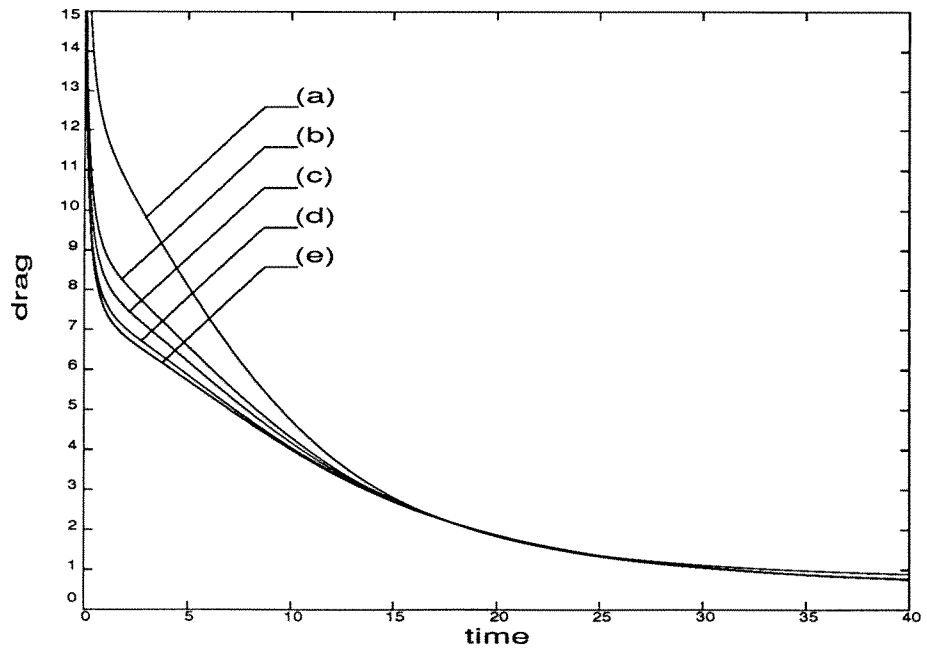

Figure 2.23: Drag ($m = 0, 1, 2, 5, 10$).

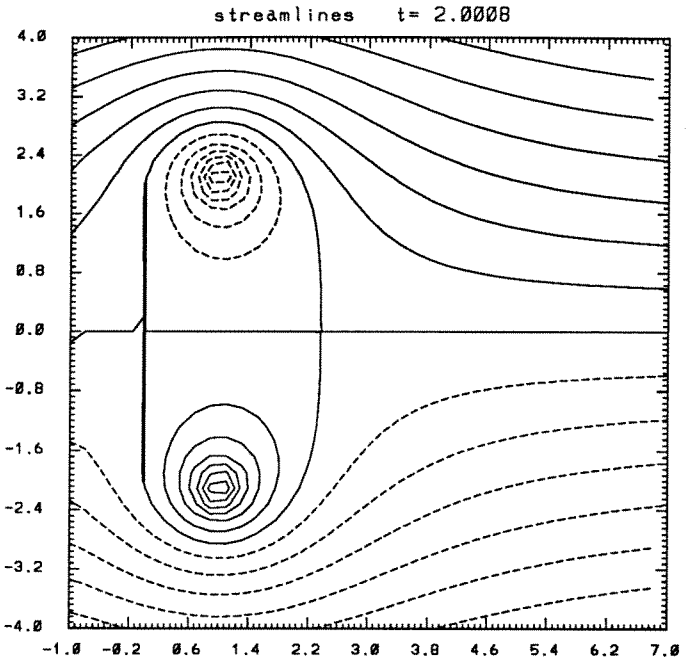

Figure 2.24: Recirculating bubble: case (a) ($t = 2.0008, m = 0$).

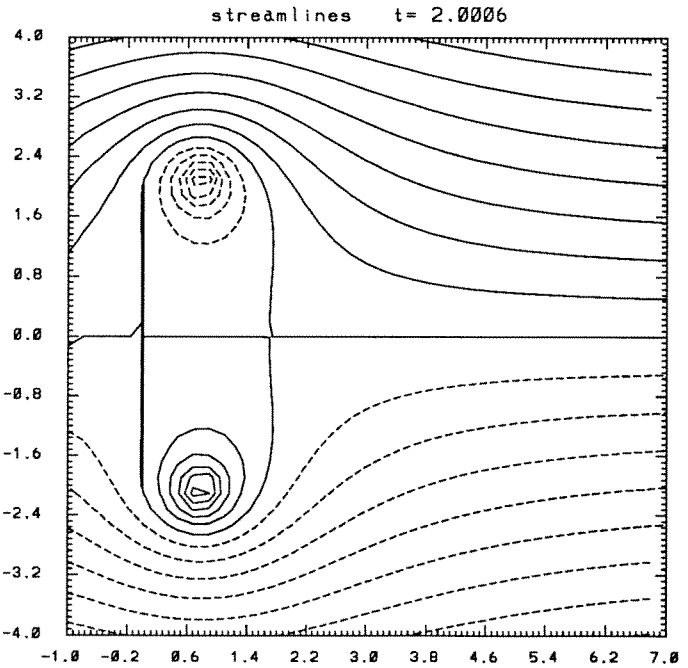

Figure 2.25: Recirculating bubble: case (b) ($t = 2.0006, m = 1$).

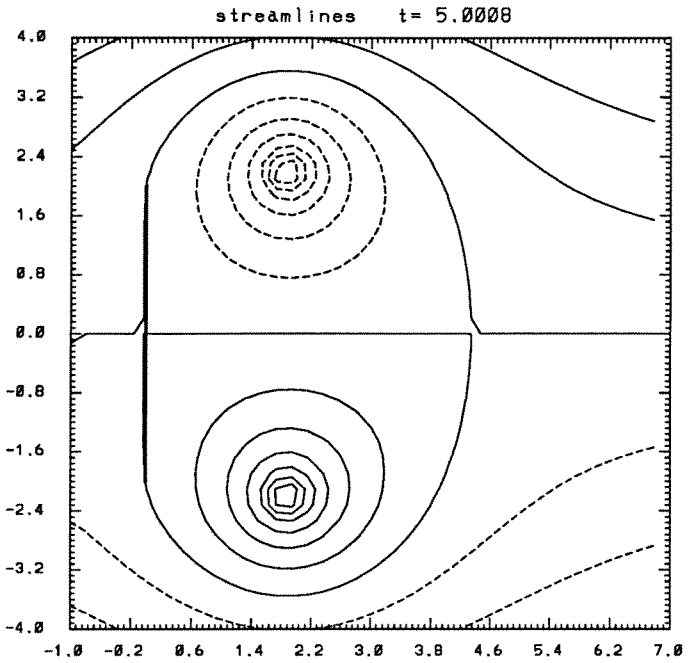

Figure 2.26: Recirculating bubble: case (a) ($t = 5.0008, m = 0$).

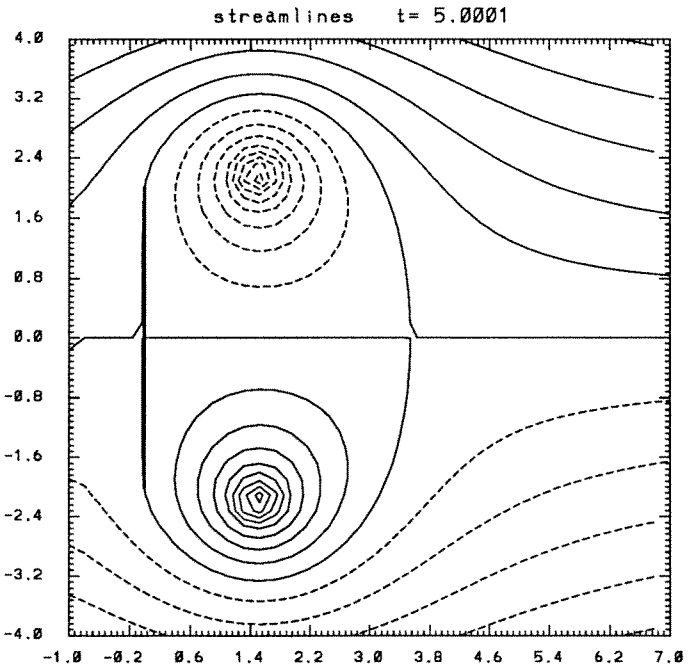

Figure 2.27: Recirculating bubble: case (b) ($t = 5.0001, m = 1$).

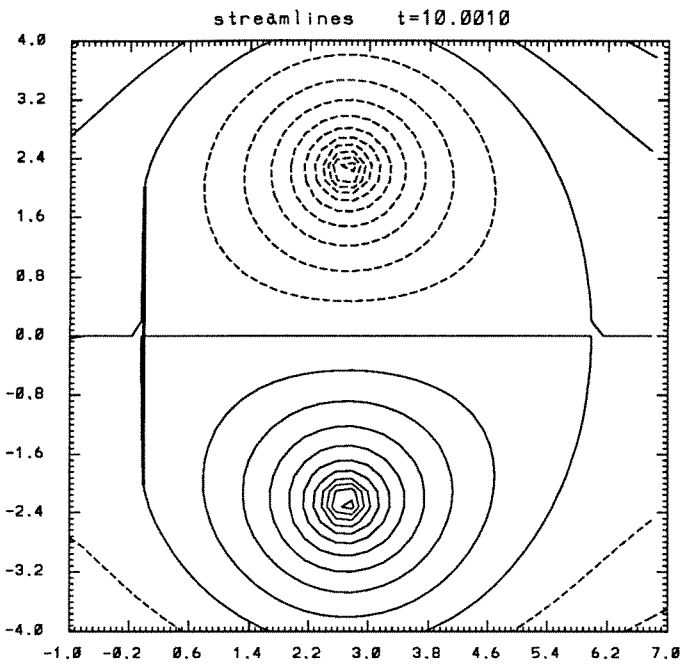

Figure 2.28: Recirculating bubble: case (a) ($t = 10.0010, m = 0$).

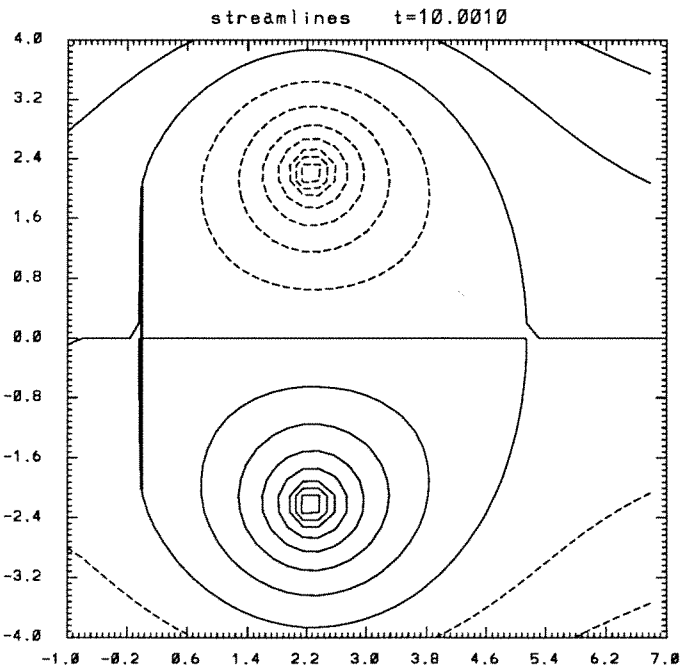

Figure 2.29: Recirculating bubble: case (b) ($t = 10.0010, m = 1$).

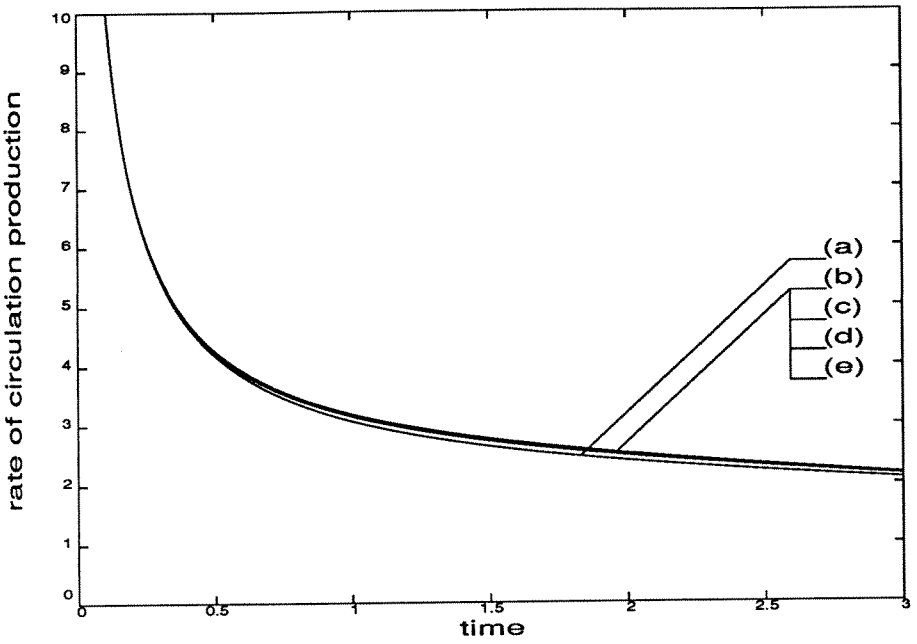

Figure 2.30: Rate of circulation production for the top vortex ($m = 0, 1, 2, 5, 10$).

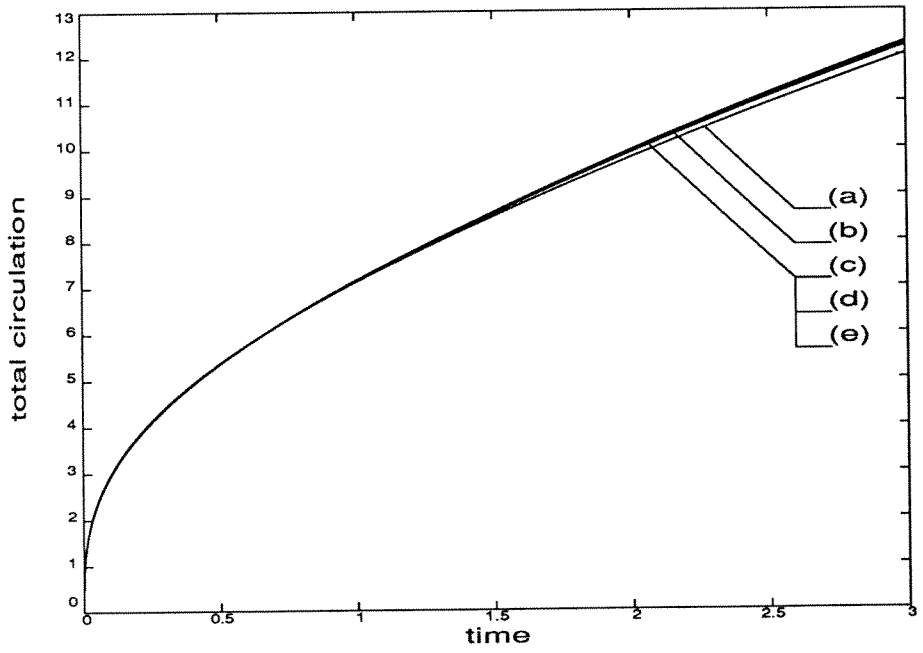

Figure 2.31: Total circulation of the top vortex ($m = 0, 1, 2, 5, 10$).

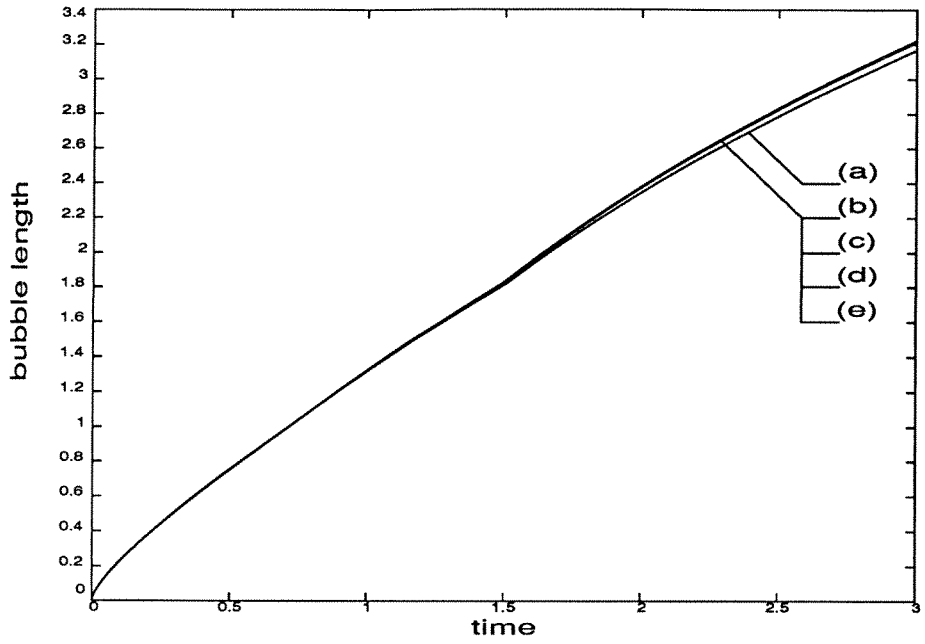

Figure 2.32: Length of the recirculating bubble ($m = 0, 1, 2, 5, 10$).

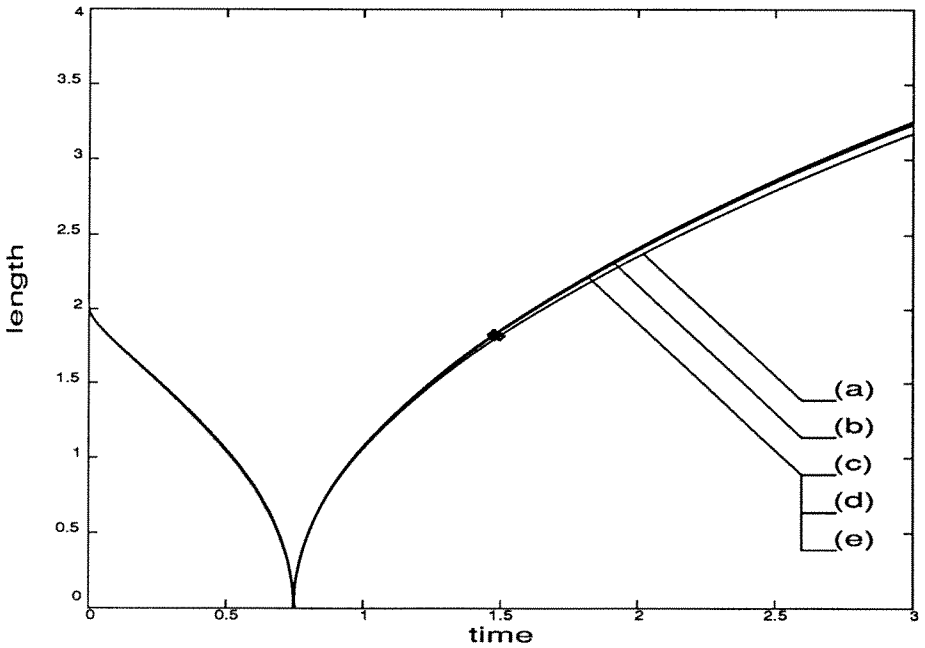

Figure 2.33: Loci of the stagnation points ($m = 0, 1, 2, 5, 10$).

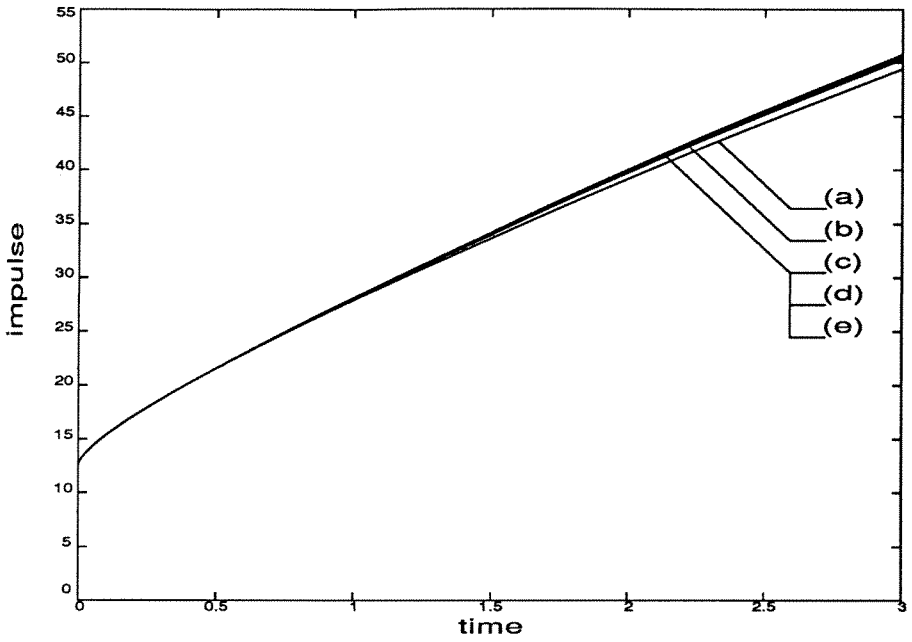

Figure 2.34: Total impulse ($m = 0, 1, 2, 5, 10$).

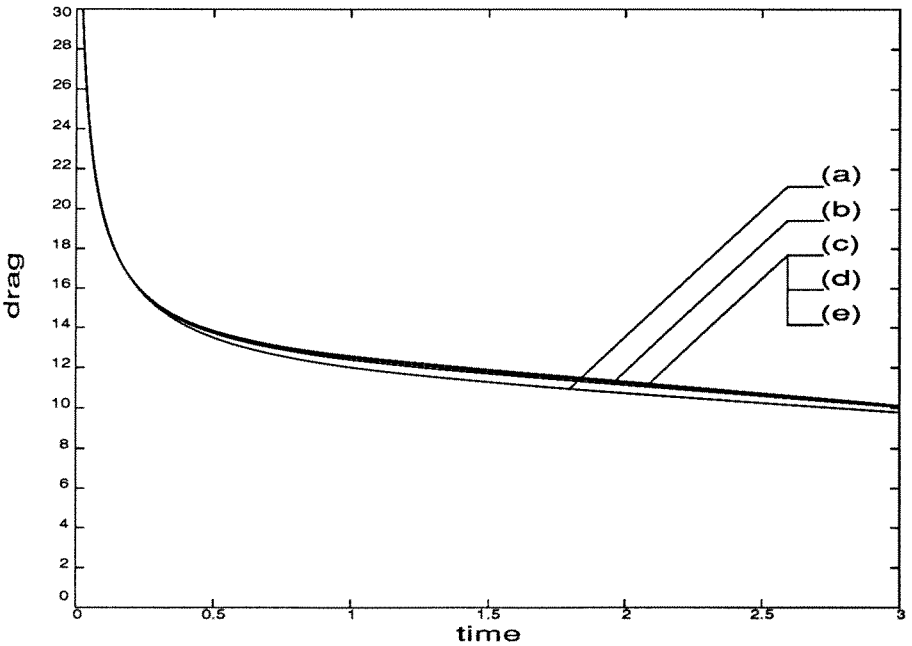

Figure 2.35: Drag ($m = 0, 1, 2, 5, 10$).

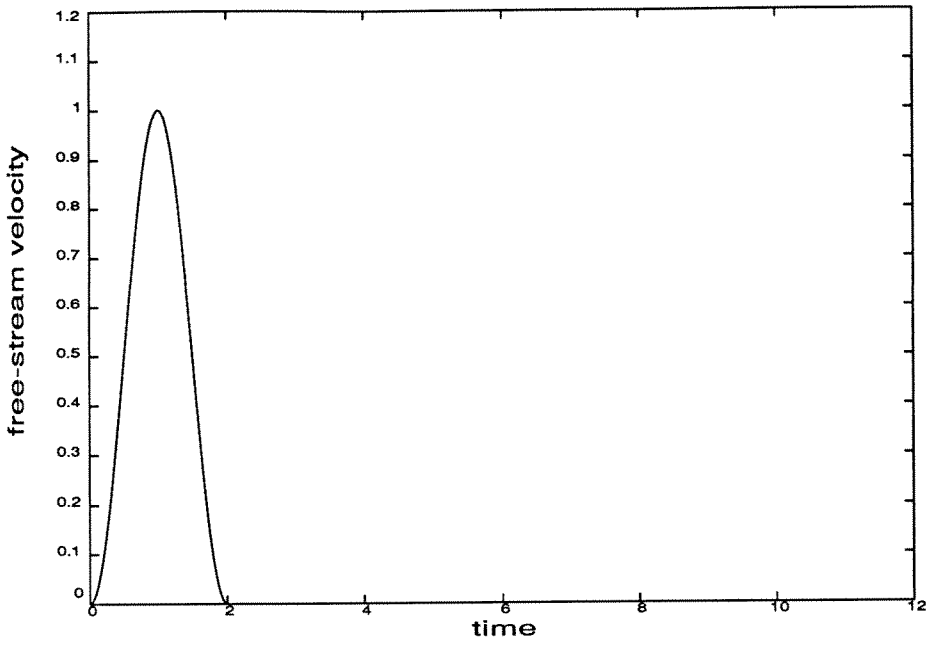

Figure 2.36: Free-stream velocity.

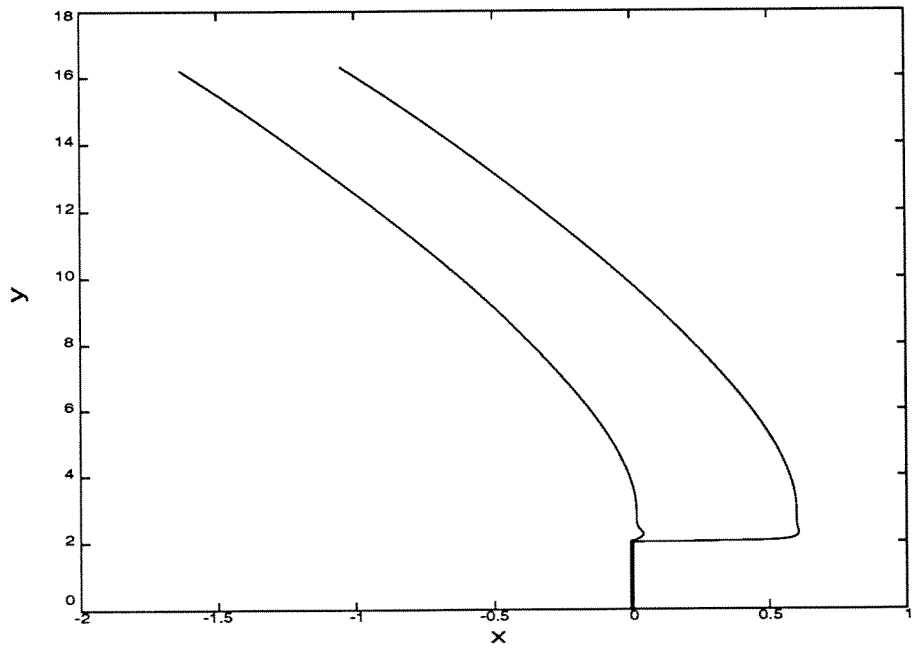

Figure 2.37: Trajectories of the top vortices.

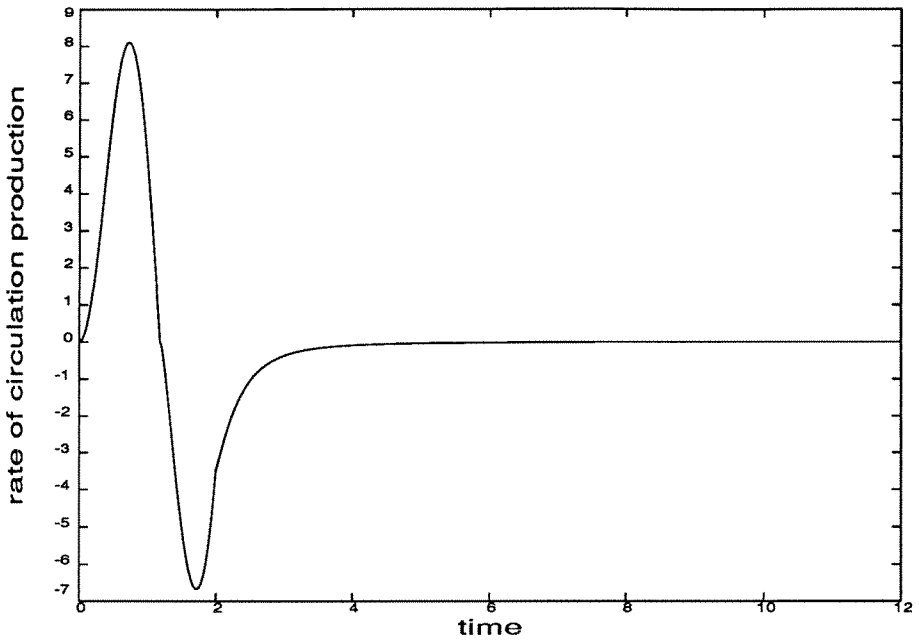

Figure 2.38: Rate of circulation production for the top vortices.

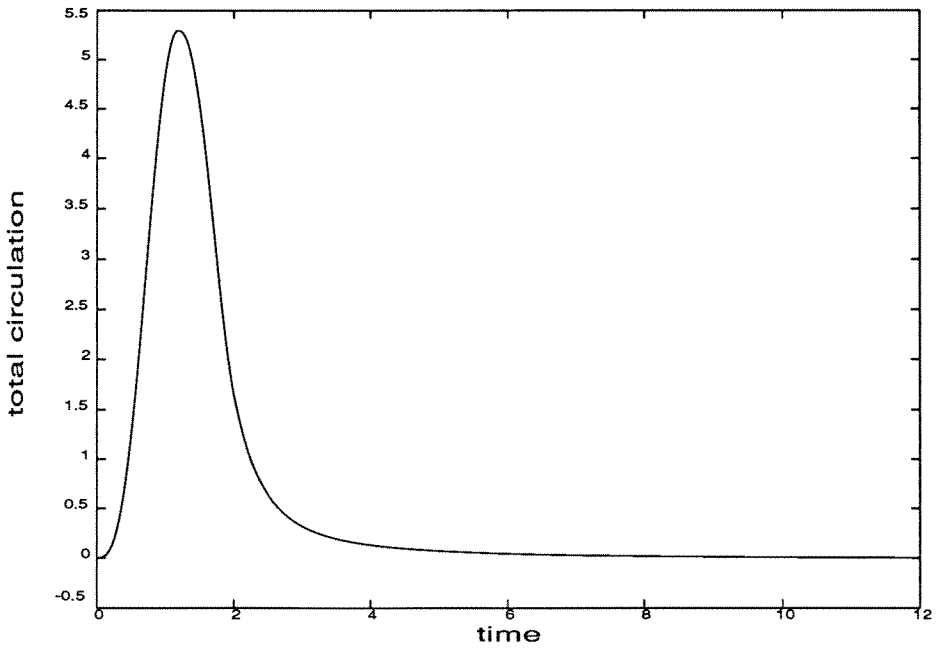

Figure 2.39: Total circulation of the top vortices.

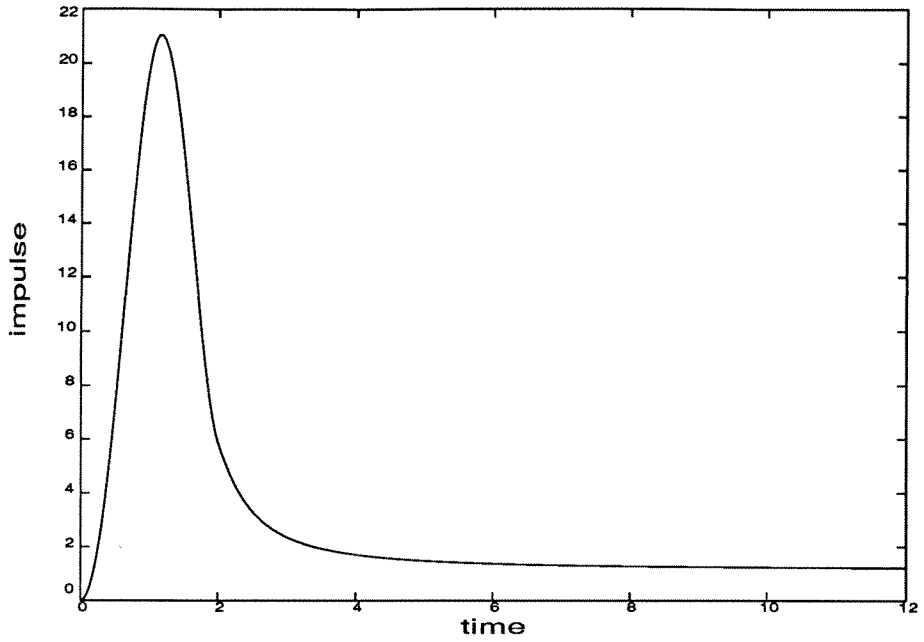

Figure 2.40: Impulse.

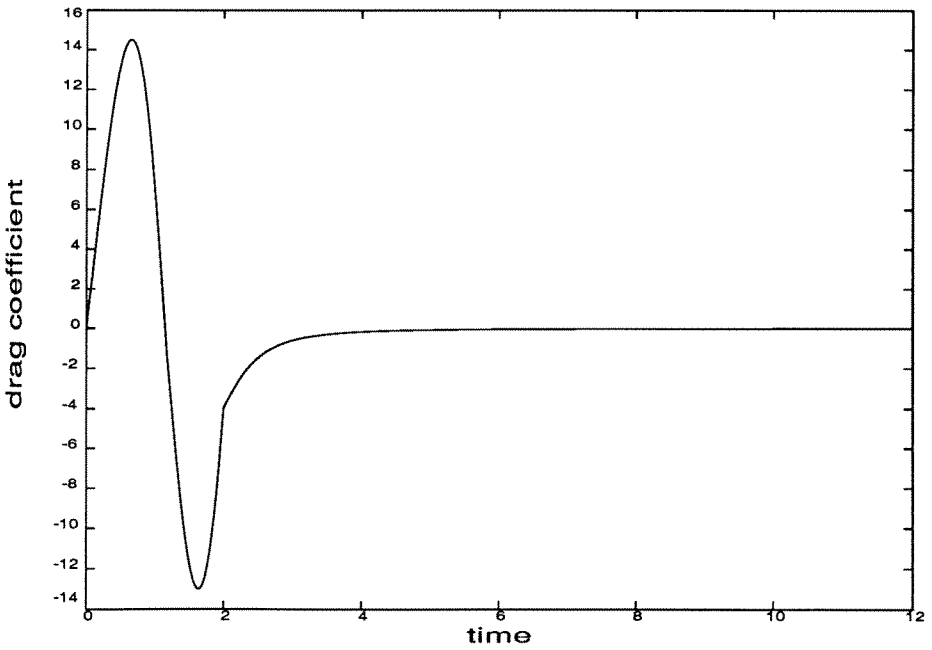

Figure 2.41: Drag coefficient.

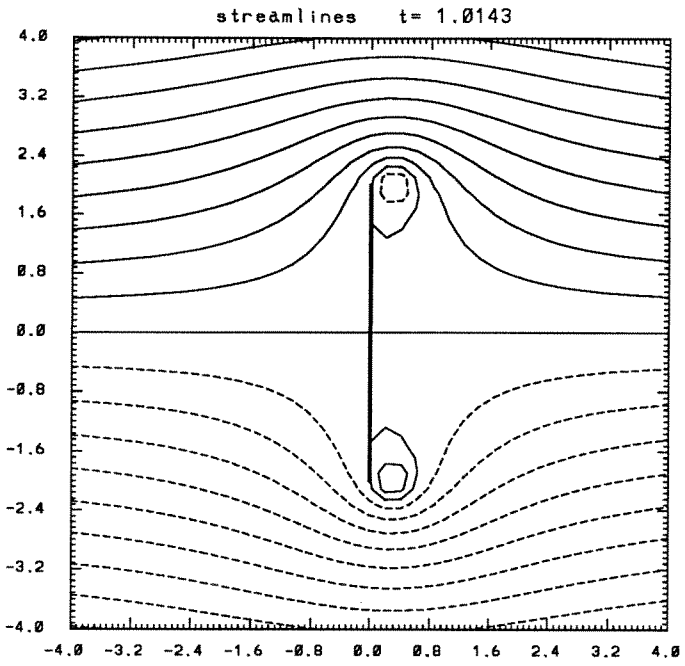

Figure 2.42: Instantaneous streamlines ($t = 1.0143$).

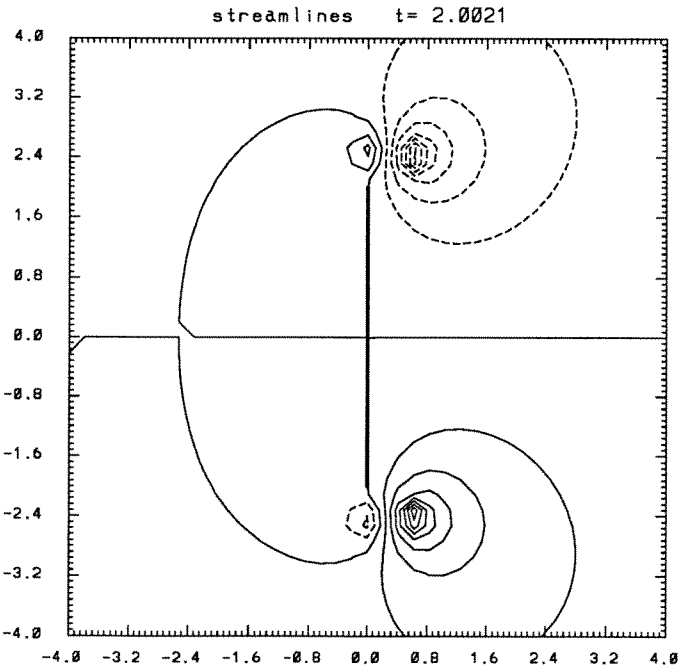

Figure 2.43: Instantaneous streamlines ($t = 2.0021$).

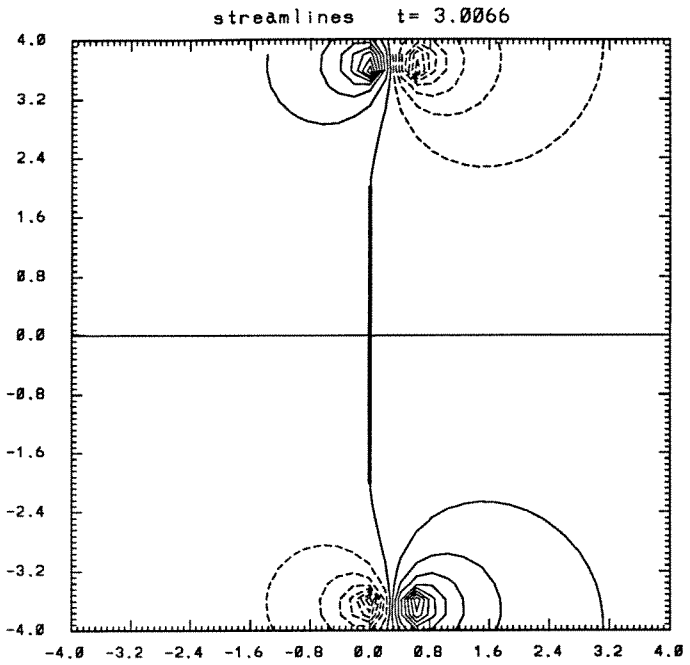

Figure 2.44: Instantaneous streamlines ($t = 3.0066$).

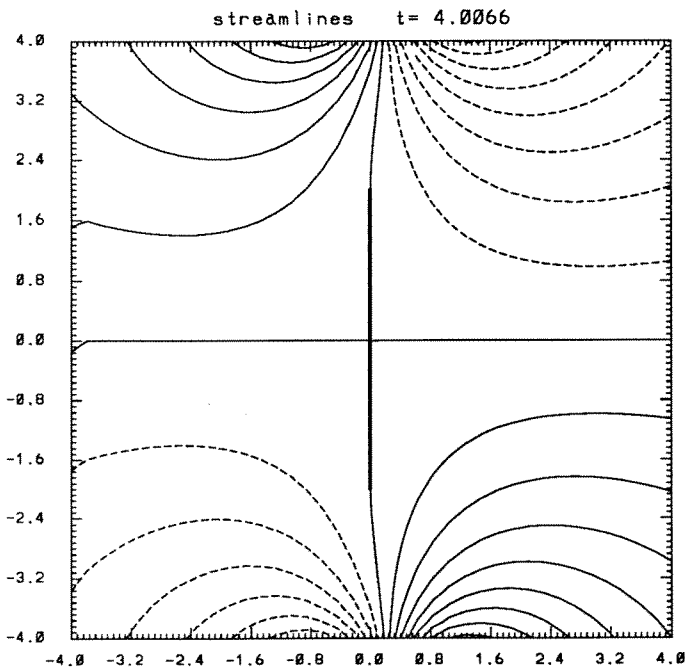

Figure 2.45: Instantaneous streamlines ($t = 4.0066$).

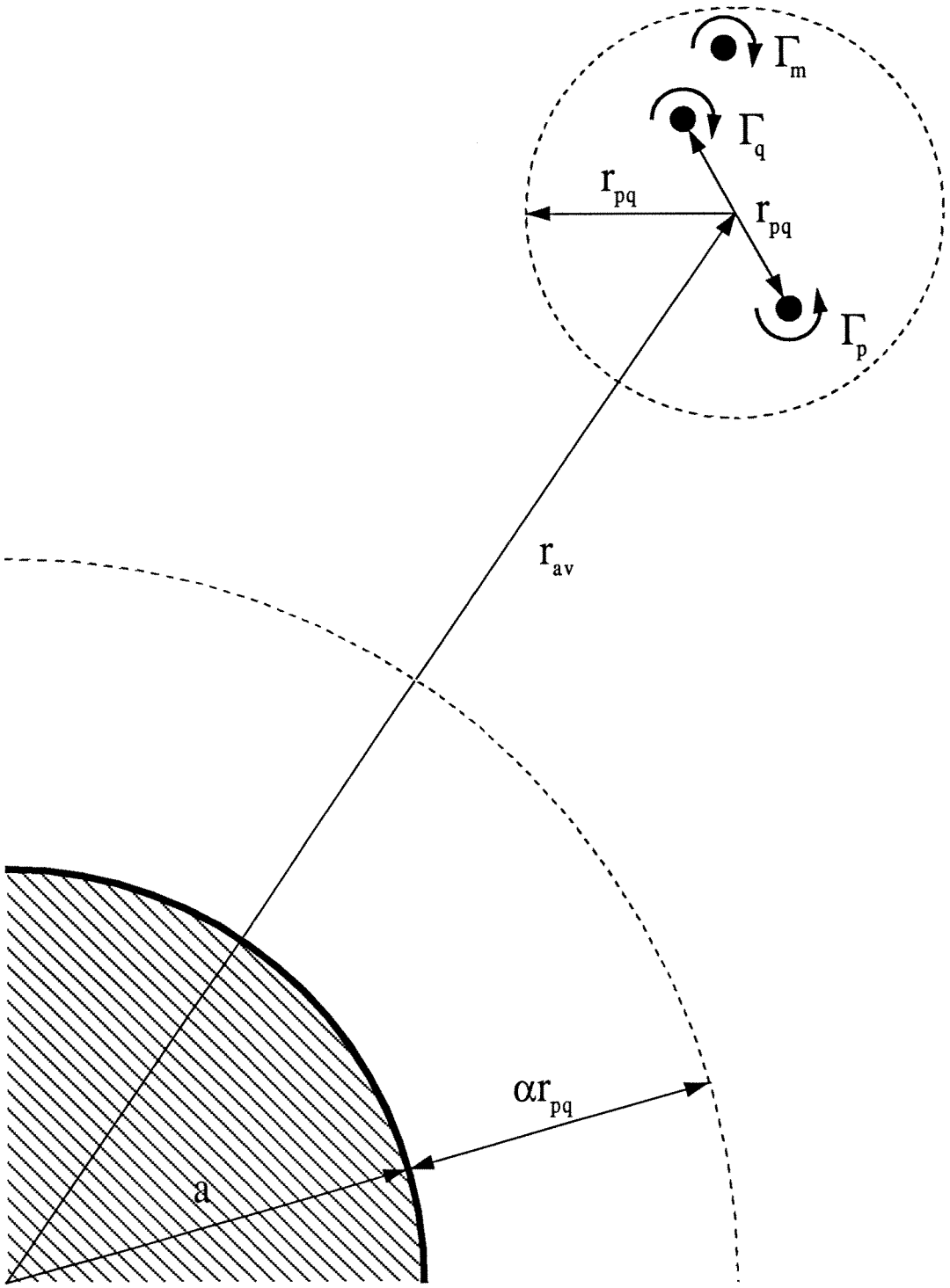

Figure 2.46: Vortex merging.

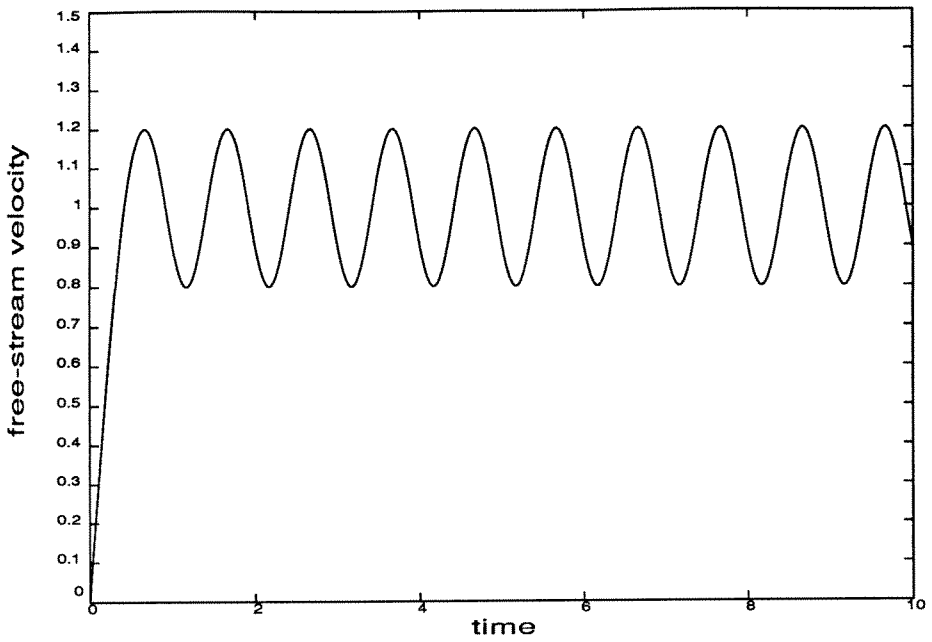

Figure 2.47: Free-stream velocity.

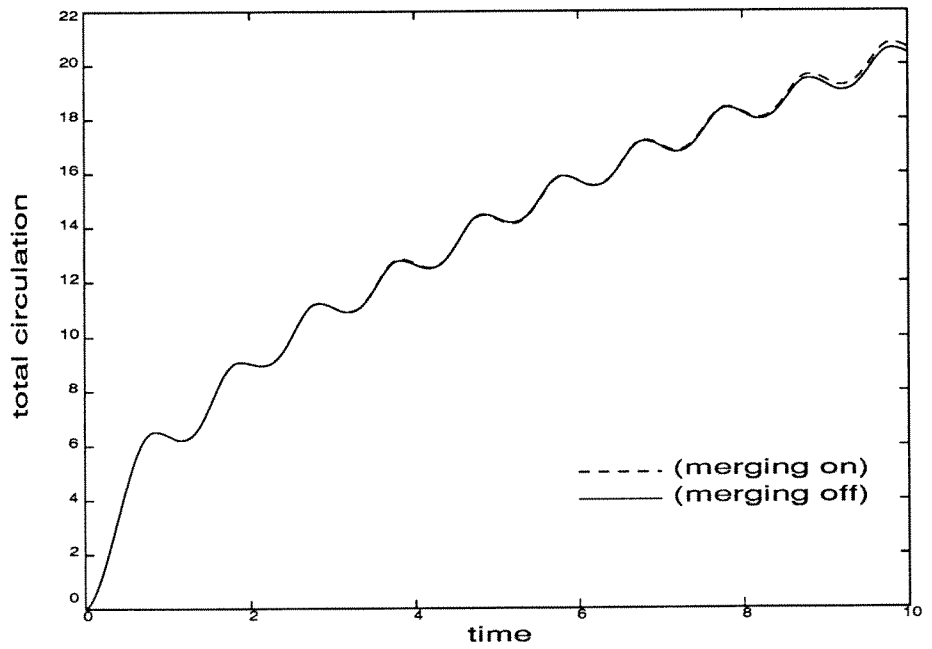

Figure 2.48: Total circulation of the top vortices.

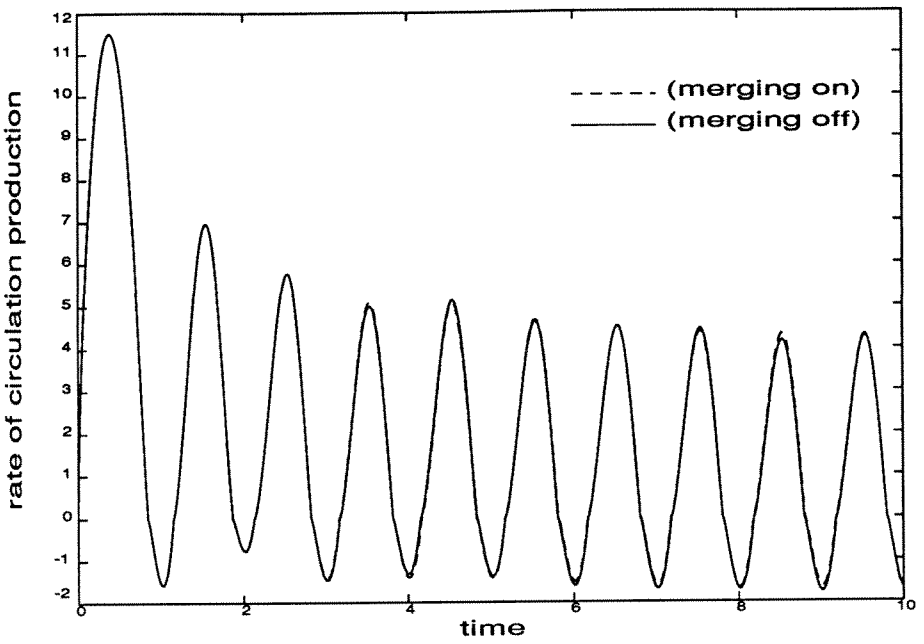

Figure 2.49: Rate of circulation production for the top vortices.

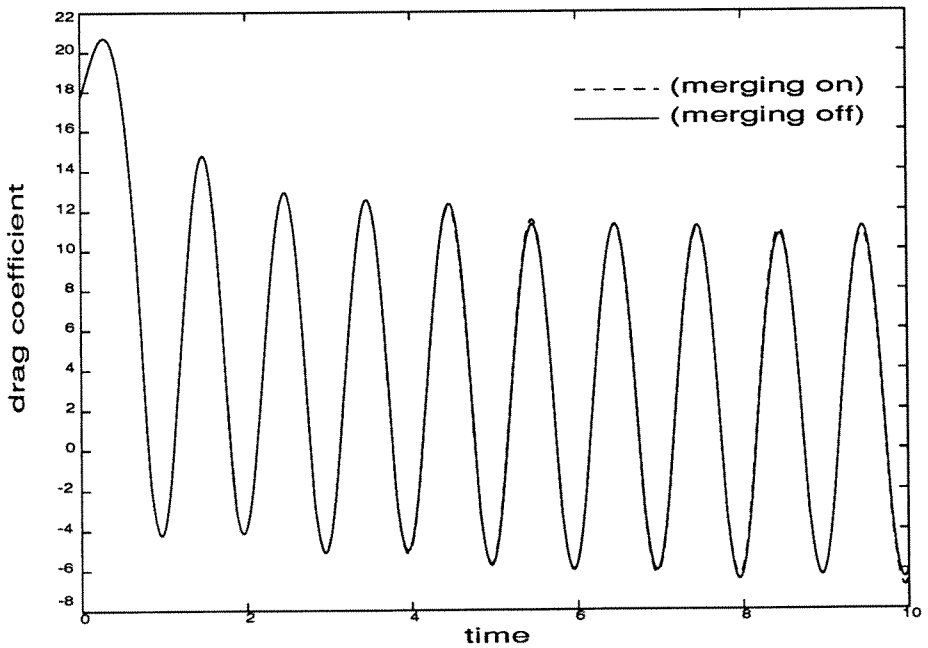

Figure 2.50: Drag coefficient.

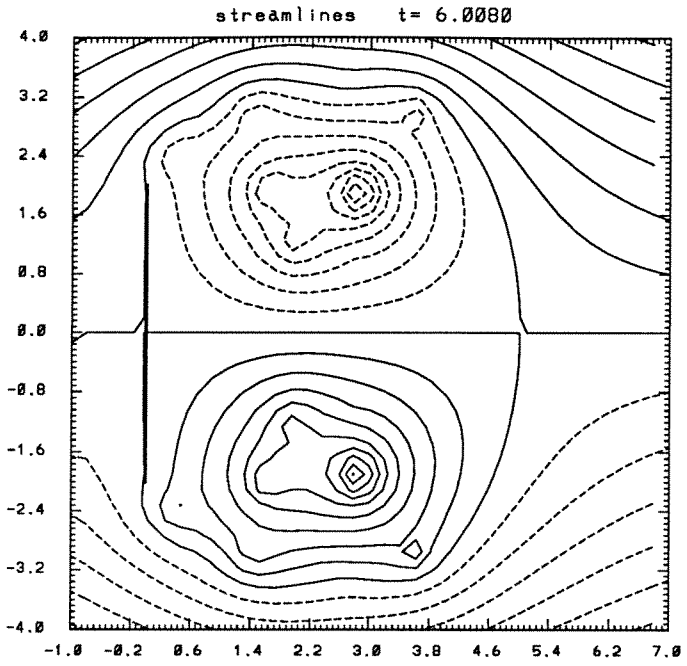

Figure 2.51: Instantaneous streamlines: vortex merging off ($t = 6.0080$).

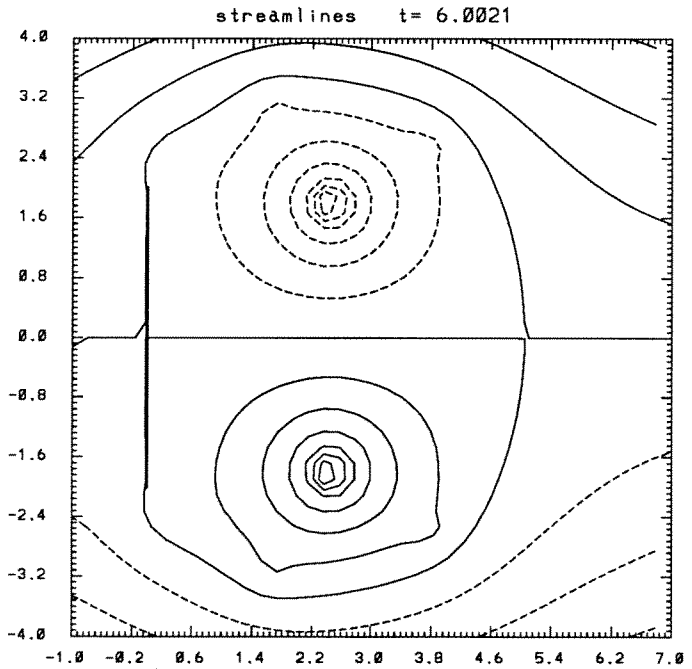

Figure 2.52: Instantaneous streamlines: vortex merging on ($t = 6.0021$).

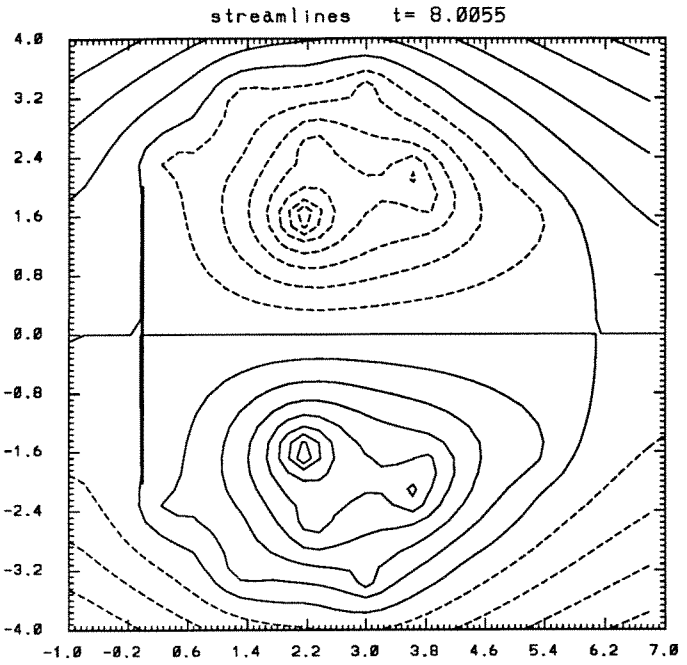

Figure 2.53: Instantaneous streamlines: vortex merging off ($t = 8.0055$).

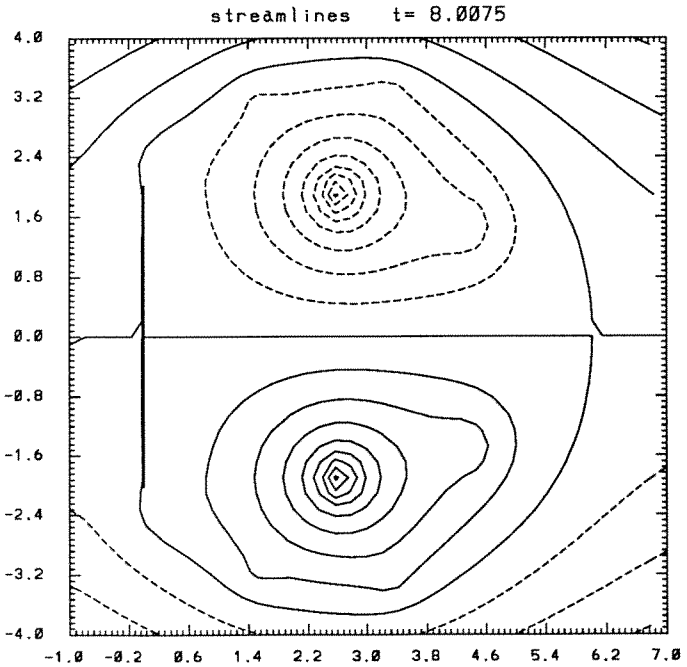

Figure 2.54: Instantaneous streamlines: vortex merging on ($t = 8.0075$).

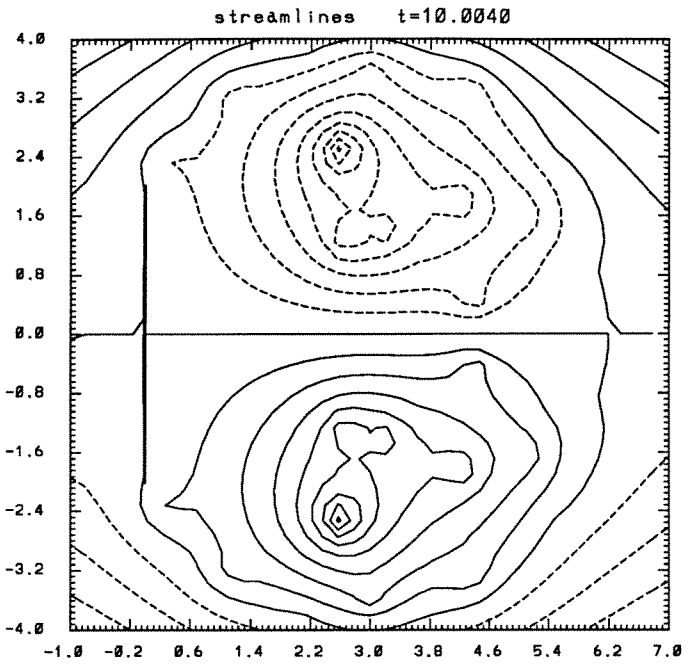

Figure 2.55: Instantaneous streamlines: vortex merging off ($t = 10.0040$).

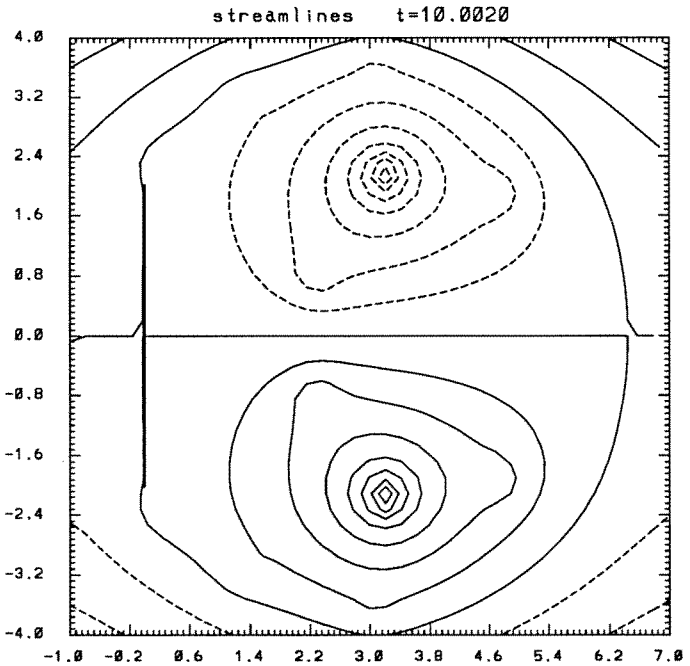

Figure 2.56: Instantaneous streamlines: vortex merging on ($t = 10.0020$).

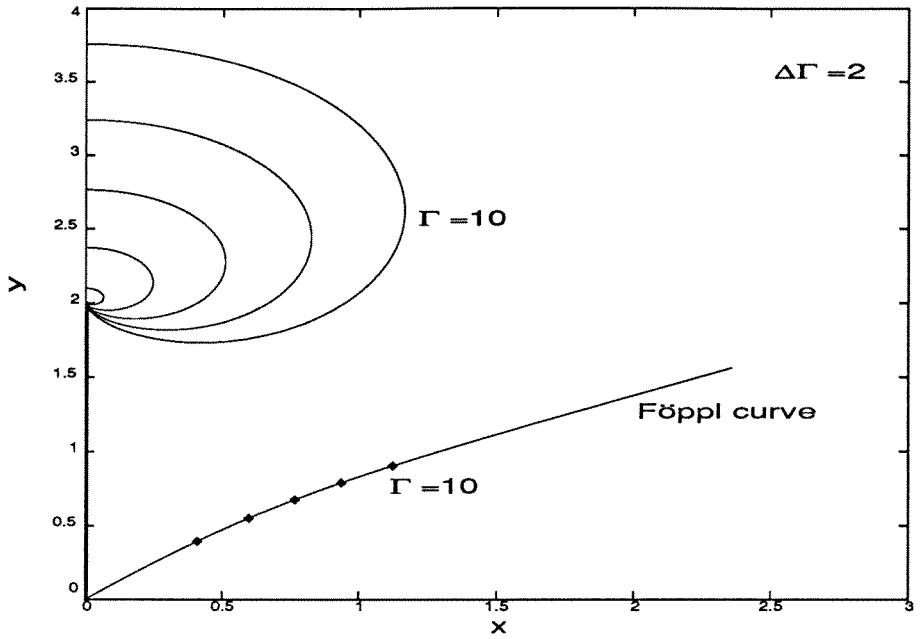

Figure 2.57: Föppl's and constant circulation curves.

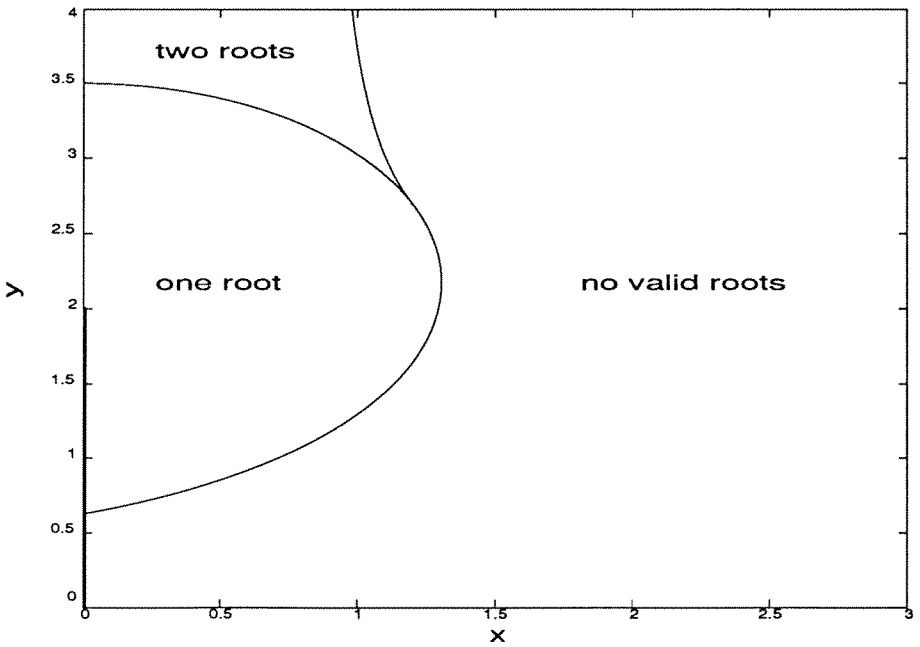

Figure 2.58: Roots map.

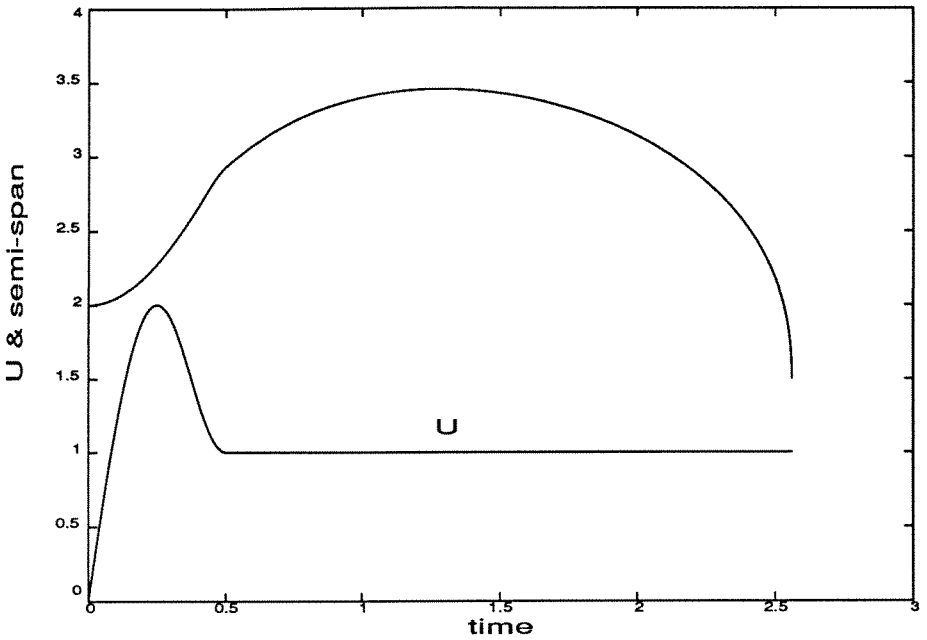

Figure 2.59: Free-stream velocity and plate semi-span.

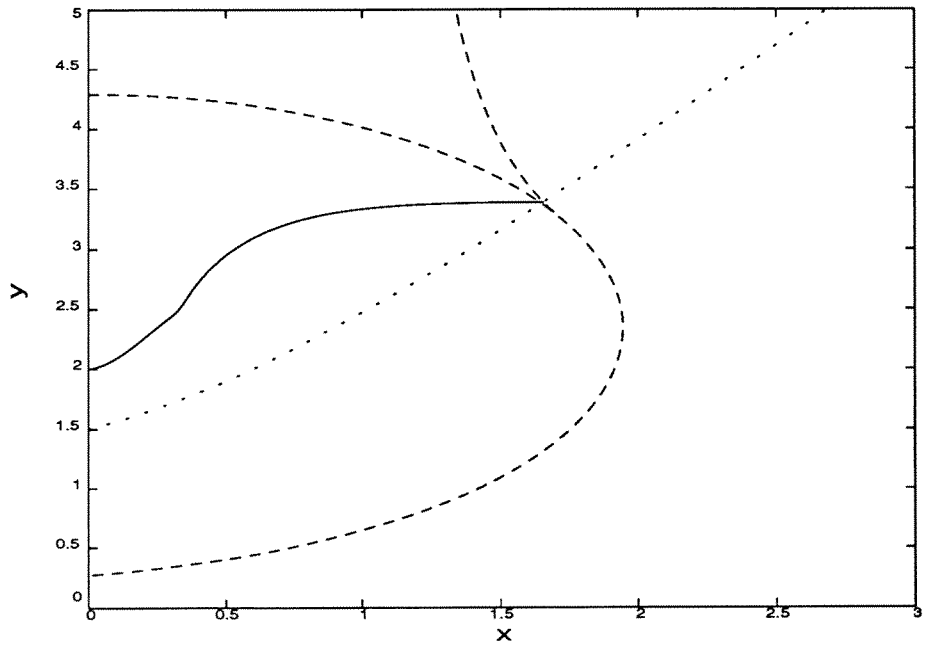

Figure 2.60: Trajectory of the top vortex.

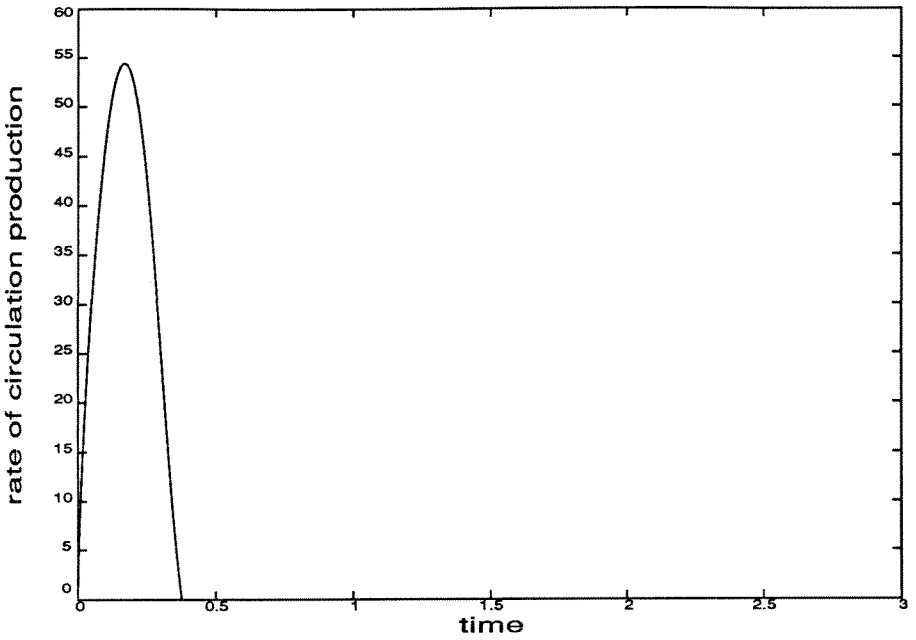

Figure 2.61: Rate of circulation production for the top vortex.

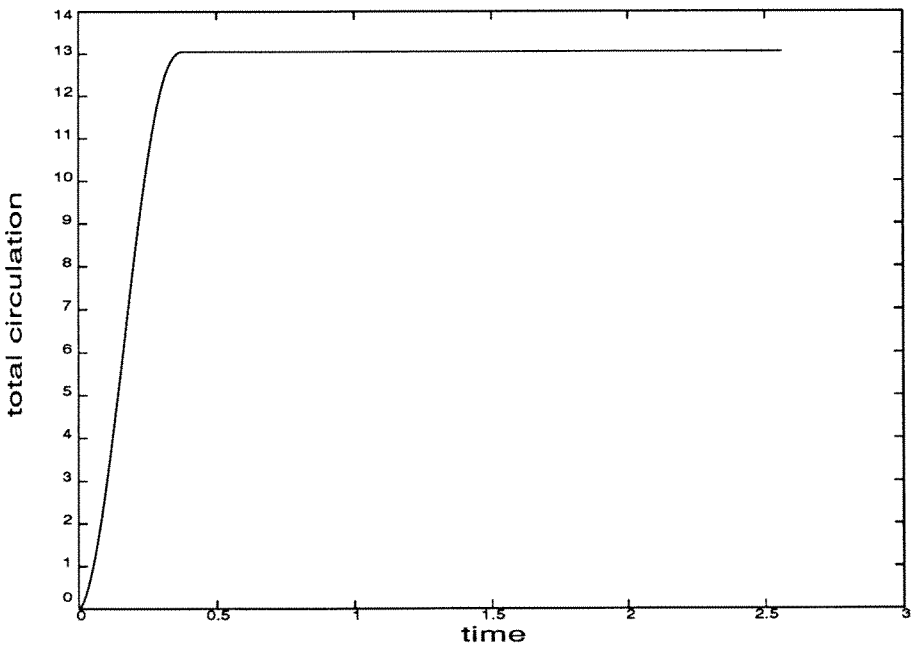

Figure 2.62: Total circulation of the top vortex.

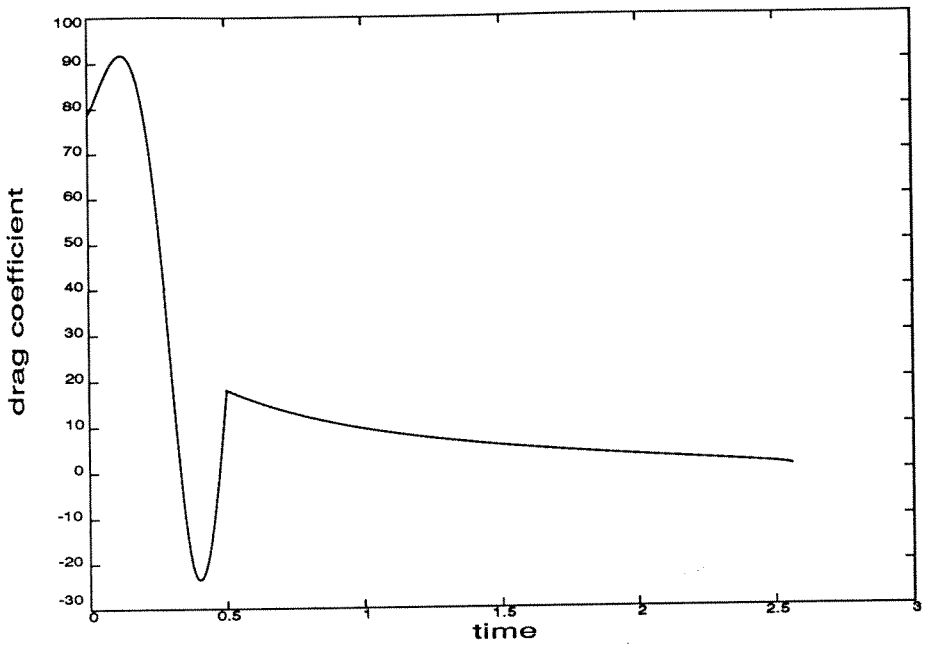

Figure 2.63: Drag coefficient.

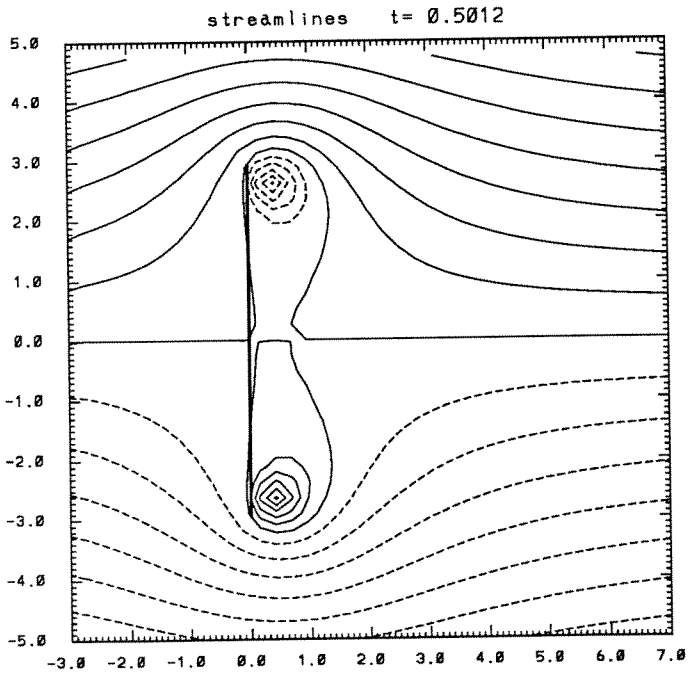

Figure 2.64: Shedding control ($t = .5012$).

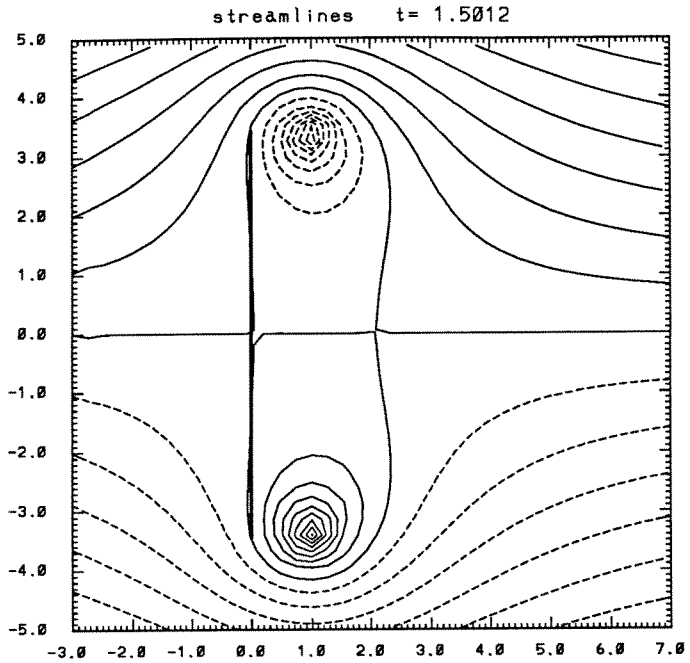

Figure 2.65: Shedding control ($t = 1.5012$).

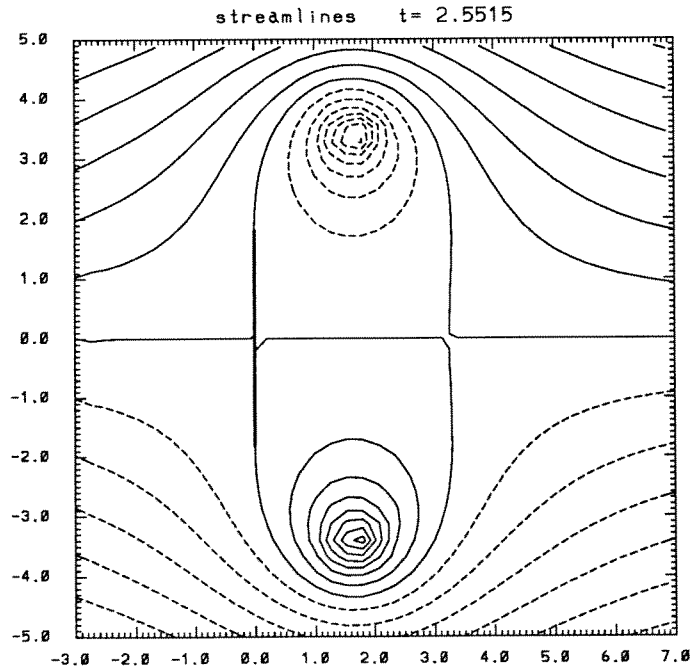

Figure 2.66: Shedding control ($t = 2.5515$).

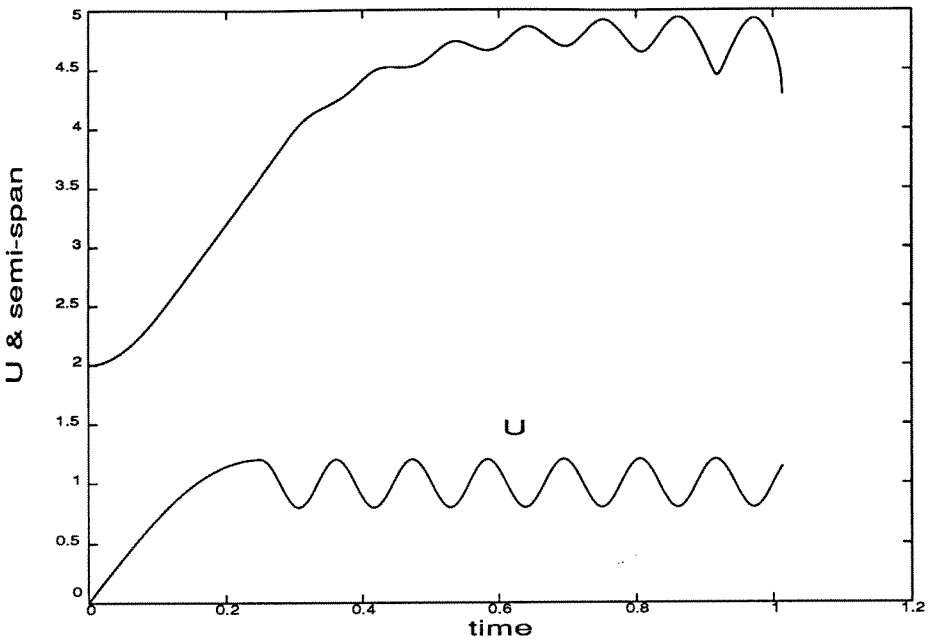

Figure 2.67: Free-stream velocity and plate semi-span.

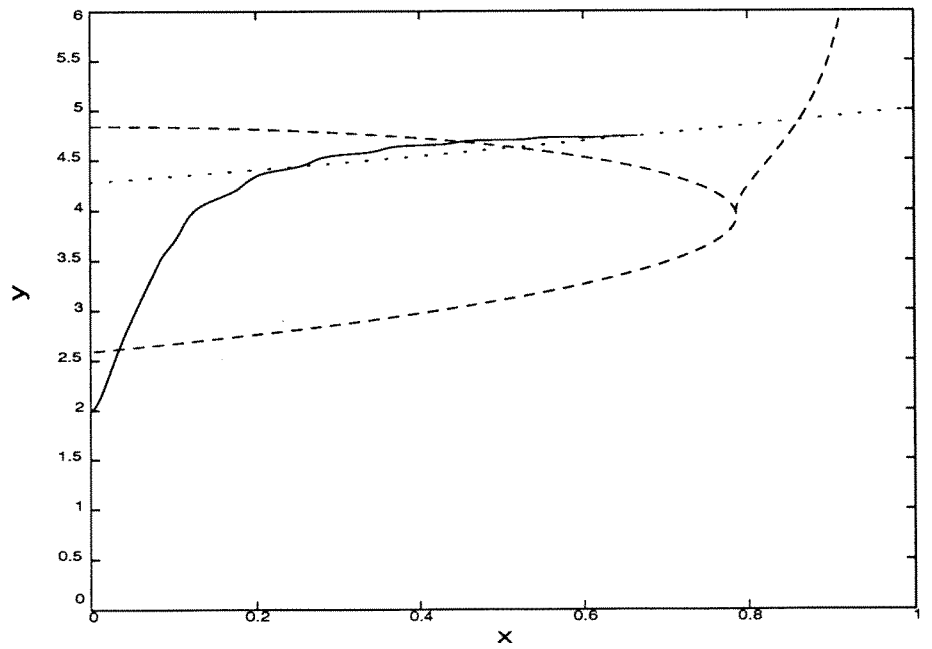

Figure 2.68: Trajectory of the top vortex.

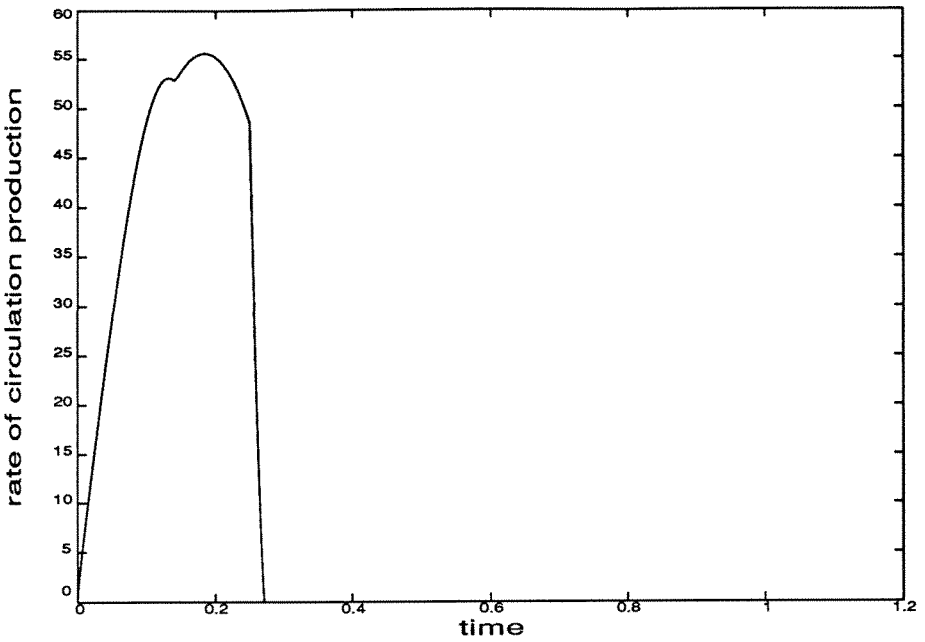

Figure 2.69: Rate of circulation production for the top vortex.

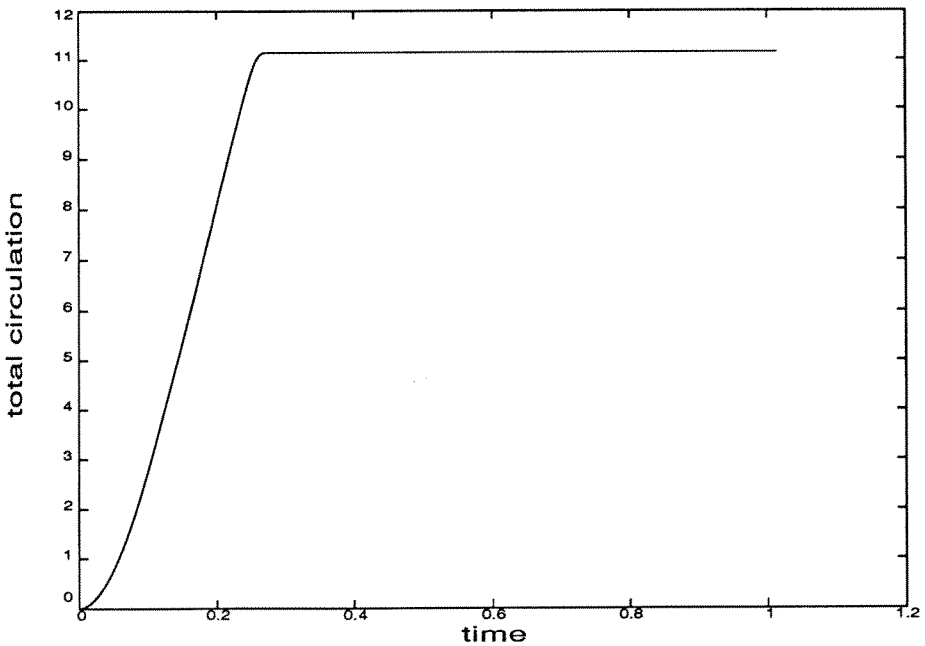

Figure 2.70: Total circulation of the top vortex.

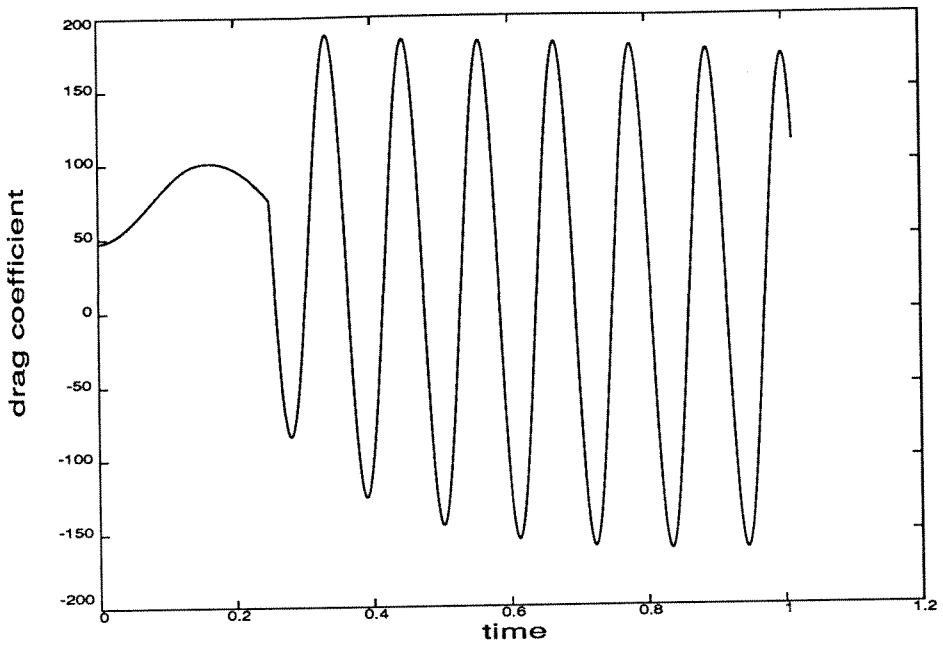

Figure 2.71: Drag coefficient.

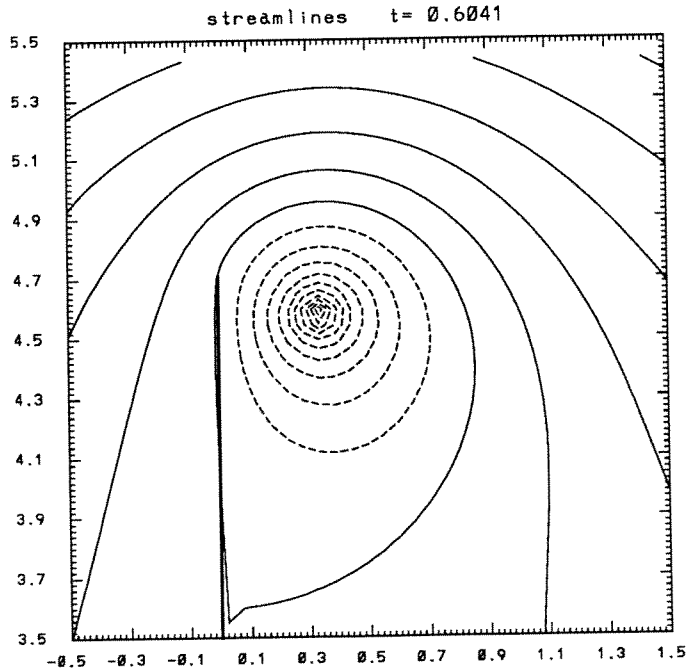

Figure 2.72: Shedding control ($t = .6041$).

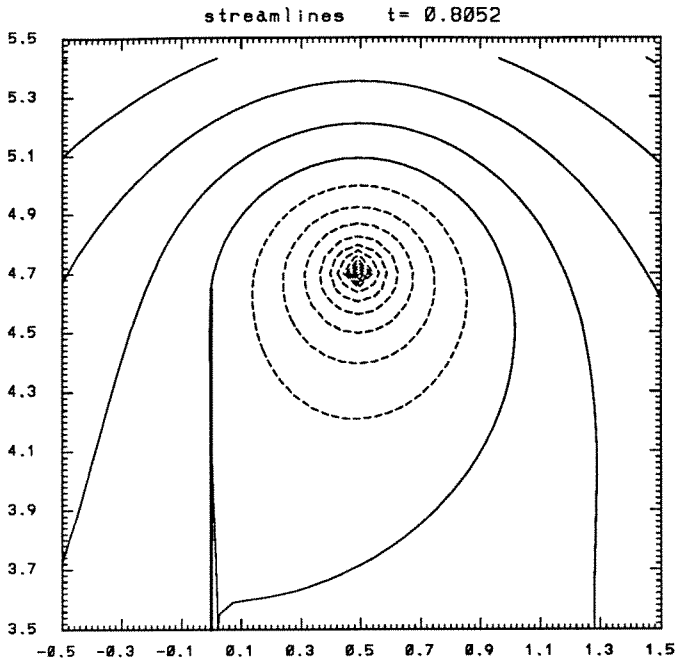

Figure 2.73: Shedding control ($t = .8052$).

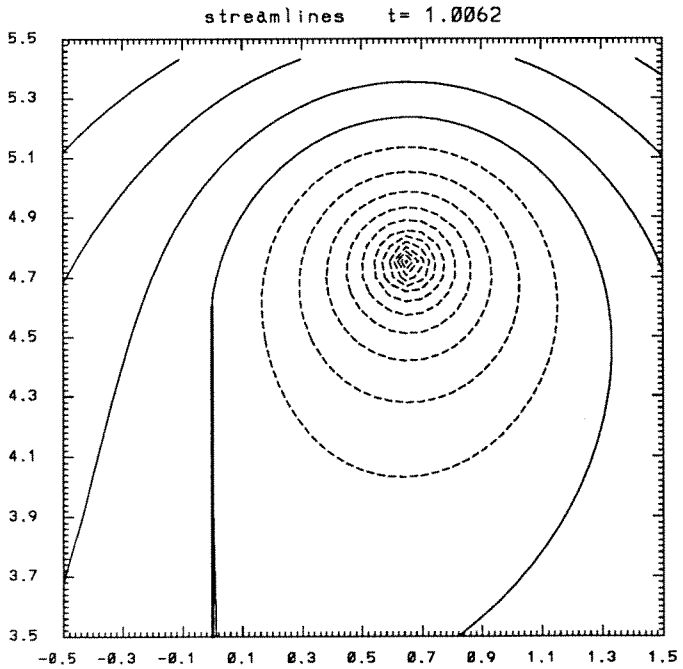

Figure 2.74: Shedding control ($t = 1.0062$).

Appendix

The explicit form of the functions which appear in the equation of motion (2.94) is the following:

$$R^a_U(\rho_1,\theta_1,a)=\frac{\rho_1^2(\rho_1^2-a^2)\sin\theta_1}{\rho_1^4-2a^2\rho_1^2\cos 2\theta_1+a^4},$$

$$R^a_{\Gamma_{1_s}}(\rho_1,\theta_1,a)=\frac{\rho_1^3[8a^2\rho_1^2(\rho_1^4-2a^2\rho_1^2\sin^2\theta_1+a^4)\cos^2\theta_1-(\rho_1^4-a^4)^2]\sin\theta_1}{4\pi[(\rho_1^4+a^4)^2-4a^4\rho_1^4\cos^2 2\theta_1](\rho_1^4-2a^2\rho_1^2\cos 2\theta_1+a^4)\cos\theta_1},$$

$$R^a_{\frac{da}{dt}}(\rho_1,\theta_1,a)=-\frac{2a\rho_1(\rho_1^2\cos 2\theta_1-a^2)}{\rho_1^4-2a^2\rho_1^2\cos 2\theta_1+a^4},$$

$$\Theta^a_U(\rho_1,\theta_1,a)=\frac{\rho_1^2(\rho_1^2+a^2)\cos\theta_1}{\rho_1^4-2a^2\rho_1^2\cos 2\theta_1+a^4},$$

$$\Theta^a_{\Gamma_{1_s}}(\rho_1,\theta_1,a)=-\frac{\rho_1^2(\rho_1^2+a^2)[8a^2\rho_1^2(2a^2\rho_1^2\cos^2\theta_1-\rho_1^4-a^4)\cos^2\theta_1-(\rho_1^2-a^2)^4]}{4\pi(\rho_1^2-a^2)[(\rho_1^4+a^4)^2-4a^4\rho_1^4\cos^2 2\theta_1](\rho_1^4-2a^2\rho_1^2\cos 2\theta_1+a^4)},$$

$$\Theta^a_{\frac{da}{dt}}(\rho_1,\theta_1,a)=\frac{2a\rho_1^2\sin 2\theta_1}{\rho_1^4-2a^2\rho_1^2\cos 2\theta_1+a^4}.$$

The explicit form for the functions which appear in the equation of motion for the controlled system (2.101) is the following:

$$R^c_U=R^a_U+R^a_{\frac{da}{dt}}A^c_U,$$

$$R^c_{\frac{dU}{dt}}=R^a_{\frac{da}{dt}}A^c_{\frac{dU}{dt}},$$

$$R^c_{\Gamma_{1_s}}=R^a_{\Gamma_{1_s}}+R^a_{\frac{da}{dt}}A^c_{\Gamma_{1_s}},$$

$$\Theta^c_U=\Theta^a_U+\Theta^a_{\frac{da}{dt}}A^c_U,$$

$$\Theta^c_{\frac{dU}{dt}}=\Theta^a_{\frac{da}{dt}}A^c_{\frac{dU}{dt}},$$

$$\Theta^c_{\Gamma_{1_s}}=\Theta^a_{\Gamma_{1_s}}+\Theta^a_{\frac{da}{dt}}A^c_{\Gamma_{1_s}},$$

$$A^c_U=-\left[R^a_U\frac{dG}{d\rho_1}+\Theta^a_U\frac{dG}{d\theta_1}\right]\left[R^a_{\frac{da}{dt}}\frac{dG}{d\rho_1}+\Theta^a_{\frac{da}{dt}}\frac{dG}{d\theta_1}+\frac{dG}{da}\right]^{-1},$$

$$A^c_{\frac{dU}{dt}}=-\frac{dG}{dU}\left[R^a_{\frac{da}{dt}}\frac{dG}{d\rho_1}+\Theta^a_{\frac{da}{dt}}\frac{dG}{d\theta_1}+\frac{dG}{da}\right]^{-1},$$

$$A^c_{\Gamma_{1_s}}=-\left[R^a_{\Gamma_{1_s}}\frac{dG}{d\rho_1}+\Theta^a_{\Gamma_{1_s}}\frac{dG}{d\theta_1}\right]\left[R^a_{\frac{da}{dt}}\frac{dG}{d\rho_1}+\Theta^a_{\frac{da}{dt}}\frac{dG}{d\theta_1}+\frac{dG}{da}\right]^{-1}.$$

Bibliography

[1] Brown, C.E. & Michael, W.H. 1959

Effect of the leading-edge separation on the lift of a delta wing.

J. Aero. Sci. **21**, 690–694.

[2] Butcher, J.C. 1987

The numerical analysis of ordinary differential equations

Runge-Kutta and general linear methods.

John Wiley & Sons

[3] Cheers, A.Y. 1979

A study of incompressible 2-d vortex flow past a circular cylinder.

Lawrence Berkeley Laboratory LBL-9950.

[4] Chua, K. 1990

Vortex simulation of separated flows in two and three dimensions.

Ph.D. Thesis, California Institute of Technology.

[5] Clements, R.R. 1973

An inviscid model of two-dimensional vortex shedding.

J. Fluid Mech. **57**, 321–336.

[6] Doyle, J.C. Francis, B.A. & Tannenbaum, A.R. 1992

Feedback control theory.

The Macmillan Company, New York

[7] Fan, M.K.H. Tits, A.L. & Doyle, J.C. 1991

Robustness in the presence of mixed parametric uncertainty and unmodeled dynamics.

IEEE Auto. C. **36**, 25–38.

[8] Gad-el-Hak, M. & Bushnell, D.M. 1991

Separation control: review.

ASME J. Fluids Eng. **113**, 5–30.

[9] Graham, J.M.R. 1980

The forces on the sharp-edged cylinders in oscillatory flow at low Keulegan-Carpenter numbers.

J. Fluid Mech. **97**, 331–346.

[10] Graham, J.M.R. 1983

The lift on an aerofoil in starting flow.

J. Fluid Mech. **133**, 413–425.

[11] Koochesfahani, M.M. & Dimotakis, P.E. 1988

A cancellation experiment in a forced turbulent shear layer.

First National Fluid Dynamics Congress July 25-28, 1988/Cincinnati, Ohio

AIAA Paper No.88-3713-CP.

[12] Lighthill, J. 1986

An informal introduction to theoretical fluid mechanics

Clarendon Press, Oxford

[13] Lisoski, D.L. & Roshko, A. 1991

Private communication.

California Institute of Technology

[14] Milne-Thomson, L.M. 1968

Theoretical hydrodynamics. 5^{th} ed.

The Macmillan Company, New York

[15] Ongoren A. & Rockwell, D. 1988

Flow structure from an oscillating cylinder

Part 1. Mechanisms of phase shift and recovery in the near wake.

J. Fluid Mech. **191**, 197–223.

[16] Ongoren A. & Rockwell, D. 1988

Flow structure from an oscillating cylinder

Part 2. Mode competition in the near wake.

J. Fluid Mech. **191**, 225–245.

[17] Pullin, D.I. 1978

The large-scale structure of unsteady self-similar rolled-up vortex-sheets.

J. Fluid Mech. **88**, 401–430.

[18] Pullin, D.I. & Perry, A.E. 1980

Some flow visualization experiments on the starting vortex.

J. Fluid Mech. **97**, 239–255.

[19] Rao D.M. 1987

Vortical flow management techniques.

Prog. Aerospace Sci. **24**, 173–224.

[20] Rott, N. 1956

Diffraction of a weak shock with vortex generation.

J. Fluid Mech. **1**, 111–128.

[21] Sarpkaya, T. & Isaacson, M. 1981

Mechanics of wave forces on offshore structures

Van Nostrand Reinhold Company, New York

[22] Sarpkaya, T. 1989

Computational methods with vortices – The 1988 Freeman Scholar Lecture.

ASME J. Fluids Eng. **111**, 5–52.

[23] Taneda, S. & Honji, H. 1971

Unsteady flow past a flat plate normal to the direction of motion.

J. Phys. Soc. of Japan **30**, 263–272.

[24] Tokumaru, P.T. & Dimotakis, P.E. 1991

Rotary oscillation control of a cylinder wake.

J. Fluid Mech. **224**, 77–90.

[25] Van Dyke M. 1982

An album of fluid motion.

The Parabolic Press

[26] Wiggins, S. 1990

Introduction to applied nonlinear dynamical systems and chaos.

Springer-Verlag, New York